VNIVERSITAT DE VALÈNCIA

Phenomenology of low-scale Seesaw Models

PhD thesis

Marija Kekić

IFIC - Universitat de València - CSIC
Departament de Física Teòrica

Programa de Doctorat en Física

Director: Pilar Hernández Gamazo

Valencia, Noviembre 2016

Pilar Hernández Gamazo,
catedrático de la Universidad de Valencia,

CERTIFICA:

Que la presente memoria "Phenomenology of low-scale Seesaw Models" ha sido realizada bajo su dirección en el Instituto de Física Corpuscular, centro mixto de la Universidad de Valencia y del CSIC, por Marija Kekic y constituye su Tesis para optar al grado de Doctor en Física.

Y para que así conste, en cumplimiento de la legislación vigente, presenta en el Departamento de Física Teórica de la Universidad de Valencia la referida Tesis Doctoral, y firma el presente certificado.

Valencia, a 09 de Noviembre de 2016.

Pilar Hernández Gamazo

List of publications

This PhD thesis is based on the following publifications:

- *Low-scale seesaw models versus N_{eff}* [1]
  P. Hernández, M. Kekic and J. López-Pavón
  Phys.Rev. D89 (2014) no.7, 073009
- *N_{eff} in low-scale seesaw model versus the lightest neutrino mass* [2]
  P. Hernández, M. Kekic and J. López-Pavón.
  Phys.Rev. D90 (2014) no.6, 065033
- *Leptogenesis in GeV scale seesaw models* [3]
  P. Hernández , M. Kekic , J. López-Pavón , J. Racker and N. Rius .
  JHEP 1510 (2015) 067
- *Testable Baryogenesis in Seesaw Models* [4]
  P. Hernández , M. Kekic , J. López-Pavón , J. Racker and J. Salvadó .
  JHEP 1608 (2016) 157

Preface

In this doctoral thesis we have focused on the phenomenology of the minimal extensions of the Standard Model (SM) that can explain neutrino masses and are potentially testable in the next generation experiments, the so called low-scale Seesaw Models. These models add two or three extra singlet (sterile) fermions to the SM, with masses below the electroweak scale. The main goal of this thesis is to study the impact of these extra states in the Early Universe.

The thesis is divided in two parts, the first one covers a lengthy introduction and background material for understanding the original results of this work, that have been published in [1–4].

The plan of this thesis is as follows: In Chapter 1 we motivate the need for new physics (NP) beyond the SM. In Chapter 2 we give a brief review of the SM, the theory that has been experimentally confirmed at the highest energies probed by current collider experiments. On the other hand, neutrinos were assumed massless in the SM while oscillation experiments have demonstrated that neutrinos have non vanishing masses. In Chapter 3 we give a list of the most popular extensions of the SM that can explain light neutrino masses. In Chapter 4, we summarize what is known about the lepton flavor sector of the SM, focusing particularly on the phenomenology of the low-scale Seesaw Models. In Chapter 5 we give the motivation for the mass scale of the extra fermions in these models, the parametrization of the models and the current and future experimental constraints on the model parameters. In Chapter 6 we give a brief review of the Standard Cosmological Model (ΛCDM), and in Chapter 7 we discuss the thermodynamics of the Early Universe plasma. In Chapter 8 we focus on the sterile neutrino evolution before the electroweak phase transition (EWPT), where they can seed the observed matter-antimatter asymmetry in the Universe. The evolution of the sterile neutrinos after the EWPT and their impact on the cosmological parameters is given in Chapter 9. Finally, in Chapter 10 we summarize the main scientific results in this work, divided in four publications, that are reproduced in full in Part II of the thesis.

Acknowledgment

Firstly, I would like to thank my supervisor Pilar for giving me the opportunity to learn from her, for her guidance and for being available whenever I needed help or motivation to continue with my progress.

Secondly, I thank my collaborators Jacobo, Nuria and Juan without whose expertise and dedication none of the work could be accomplished, and to all the present and past members of my group. Special thanks to Carlos and Nuria for helping me deal with the Spanish bureaucracy.

Many thanks to the whole Invisibles network for providing all the seminars, conferences, schools, research stays and lasting friendships.

Thanks to all the friends that filled my procrastination time with discussions, laugh, motivational conversations and coffees. Thanks to Javi, Sandrine, Marc, Victor, Astrid, Laura, Antonio, Pablo, Javi, Damian, Mehran and many others.

Finally, I would like to thank my whole family, especially my parents Miodrag and Dragoslava and my sister Ana without whose support I would have never even started this journey. Double thanks to my Jordi for not only being a supportive partner especially in my moments of despair but also for all fruitful and inspiring physics discussions and collaborations.

Contents

Part I

Introduction and background material

Chapter 1

Introduction

The belief that matter is made of smaller components goes back to the VIth century B.C., while the term "atom" was firstly used by Democritus, as the smallest indivisible particle. More than 20 centuries later, the first elementary particle, the electron, was detected, which launched an avalanche of progress both in theoretical and experimental sub-atomic physics. Quantum mechanics and special relativity emerged as the theory ruling the microscopic word, and a zoo of particles was discovered.

It is interesting to mention that just before the discovery of quantum mechanics and the theory of relativity, many physicists believed that the classical physics was the ultimate theory that could explain all physical phenomena. In 1900 Lord Kelvin said: "There is nothing left to be discovered in physics. All that remains is more and more precise measurement", and he could not be more wrong.

A particle of particular interest in this thesis, the neutrino, was postulated in 1930 by W. Pauli in order to explain the continuous spectra of beta decay. However, at that time introducing an "invisible" particle was a manner of bad taste, and the theory was not accepted very well, Bohr being its most prominent opponent. The neutrino was experimentally confirmed 26 years later, in the experiment of Cowan and Reines.

Today, all the particles observed are well accommodated in the Standard Model (SM), together with the basic forces. However, there are both experimental and theoretical hints that the SM can not be a complete theory and that New Physics is needed. Some of the theoretical problems are:

- The flavor-puzzle, i.e., why are there three copies of particles differing only by their mass. Most of the free parameters [1] in the SM are linked to this puzzle. They have been measured, but their values do not follow any clear pattern and their origin remains elusive.

- The strong CP problem, that is, why the CP symmetry is conserved in the strong interactions in the SM, which is not ensured by any gauge symmetry.

- How to combine quantum mechanics with general relativity, since the attempts to do this lead to non-renormalizable theories. Furthermore, gravity necessarily introduces a new scale, the Planck scale, which leads to the hierarchy problem.

- The hierarchy problem: why is the electroweak scale so much smaller than the Planck mass. If there were new particles heavier than the electroweak scale, their coupling with the Higgs boson would induce quantum corrections to the Higgs mass naturally of the order of those higher masses.

On the other hand, there are also experimental hints for physics beyond the SM:

- Neutrinos were assumed massless in the SM but the well established phenomena of neutrino oscillations implies that they are massive, and the SM has to be modified.

- The dominance of baryons over antibaryons in the Universe can not be explained within the SM.

- The origin of Dark Matter that accounts for $\sim$ 25 % of the gravitating matter in the Universe. A solution to this problem might lie in the existence of a new weakly-interating particle that is not yet discovered.

- The dark energy, a force responsible for the Universe's accelerating expansion, contributes to $\sim 70\%$ of the total energy in the Universe. The nature of this energy is unknown.

Two of the mentioned hints, non-zero neutrino masses and the baryon asymmetry, will be addressed in the thesis in the context of the low-scale Seesaw Models.

[1] There are at least 25 free parameters in the SM with massive neutrinos, 20 of them corresponding to masses and mixings.

Chapter 2

Standard Model in a nutshell

The Standard Model (SM) is a quantum field theory (QFT) that describes the interactions of all the known particles [5–15]. In this chapter we will briefly review main features of the SM.

2.1 Gauge symmetries of SM

The gauge group of the SM is based on the symmetry group

$$SU(3)_c \times SU(2)_L \times U(1), \tag{2.1}$$

which describes strong, weak and electromagnetic interactions respectively via the exchange of 8 massless gluons, 1 massless photon and 3 massive bosons ($W^{\pm}$ and Z). The matter content of one family of the SM and their charges under the gauge group is summarized in Table 2.1. Leptons and quarks come in three families that have the same properties under gauge transformations and only differ in their couplings to the Higgs boson.

	$l_L = \begin{pmatrix}\nu_L \\ e_L\end{pmatrix}$	e_R	$Q_L = \begin{pmatrix}u_L \\ d_L\end{pmatrix}$	u_R	d_R	Φ
$SU(3)_c$	1	1	3	3	3	1
$SU(2)_L$	2	1	2	1	1	2
$U(1)_Y$	$-\frac{1}{2}$	-1	$\frac{1}{6}$	$\frac{2}{3}$	$-\frac{1}{3}$	$\frac{1}{2}$

Table 2.1: Gauge charges of the particles in one SM family

.

The transformation properties under the gauge symmetries are implemented by replacing derivatives in the Lagrangian with covariant derivatives:

$$D_\mu = \partial_\mu - ig_s\frac{\lambda_a}{2}G^a_\mu - ig\tau_a W^a_\mu - ig'B_\mu, \tag{2.2}$$

where τ_a are the generators of the three dimensional $SU(2)$ group, represented with the Pauli matrices, while λ_a are the generators of the eight-dimensional $SU(3)$ group, represented with the Gell-Mann matrices. The allowed terms in the Lagrangian that are invariant under this symmetry are

- kinetic term for all fermions:

$$L = \sum_f i\overline{\psi}^f\gamma^\mu D_\mu\psi^f, \tag{2.3}$$

- kinetic terms for the gauge bosons:

$$L = -\frac{1}{4}G^a_{\mu\nu}G^{\mu\nu}_a - \frac{1}{4}W^a_{\mu\nu}W^{\mu\nu}_a - \frac{1}{4}B_{\mu\nu}B^{\mu\nu}, \tag{2.4}$$

where the field strength tensors are:

$$G^a_{\mu\nu} \equiv \partial_\mu G^a_\nu - \partial_\nu G^a_\mu + g_s f^{abc}G^b_\mu G^c_\nu, \tag{2.5}$$
$$W^a_{\mu\nu} \equiv \partial_\mu W^a_\nu - \partial_\nu W^a_\mu + g\epsilon^{abc}W^b_\mu W^c_\nu, \tag{2.6}$$
$$B_{\mu\nu} \equiv \partial_\mu B_\nu - \partial_\nu B_\mu, \tag{2.7}$$

and $f^{abc}(\epsilon^{abc})$ are the structure constants for $SU(3)(SU(2))$ groups. The conserved charges for $SU(3)$, $SU(2)$ and $U(1)$ are called color, isospin and hypercharge.

2.2 Higgs mechanism

The electroweak group is spontaneously broken to the electromagnetic group:

$$SU(2)_L \times U(1)_Y \to U(1)_Q. \tag{2.8}$$

The mechanism of this spontaneous symmetry breaking (SSB), called Brout–Englert– Higgs mechanism, is achieved by adding complex scalar field

$$\Phi = \begin{pmatrix} \Phi^+ \\ \Phi^0 \end{pmatrix}, \tag{2.9}$$

which is a doublet under $SU(2)$ transformations, as shown in Table 2.1. The Lagrangian of this scalar field consists of kinetic term and a potential:

$$L_{Higgs} = (D_\mu \Phi)^\dagger D^\mu \Phi + \mu^2 \Phi^\dagger \Phi - \lambda (\Phi^\dagger \Phi)^2. \tag{2.10}$$

The ground state is given by the minimum of the potential, which, in the case of positive μ^2 is

$$|\Phi| = \sqrt{\frac{\mu^2}{2\lambda}} \equiv \frac{v}{\sqrt{2}}. \tag{2.11}$$

v is called the Higgs vacuum expectation value (VEV) and is measured to be $v \simeq 246$ GeV [16].

There is a degeneracy of the vacua since eq. 2.11 is invariant under a $U(1)$ field redefinition $\Phi \to e^{i\alpha}\Phi$, i.e. there is infinitive number of vacua that are the minima of the potential. The Higgs field, H, is introduced as the perturbation around this ground state:

$$\Phi = \exp\left(i\theta^a \frac{\sigma^a}{2v}\right) \begin{pmatrix} 0 \\ \frac{v+H}{\sqrt{2}} \end{pmatrix}, \tag{2.12}$$

with $a = 1, 2, 3$. Using the so called "unitary gauge", the θ^a fields are gauged away, and the kinetic piece of the scalar Lagrangian leads, after diagonalization, to the mass term of the gauge bosons:

$$(D_\mu \Phi)^\dagger D^\mu \Phi \to \frac{1}{2}\partial_\mu H \partial^\mu H + (v+H)^2 \left(\frac{g^2}{4} W_\mu^+ W^{\mu^-} + \frac{g^2}{\cos\theta_W} Z_\mu Z^\mu\right). \tag{2.13}$$

The physical $W^\pm$, Z and A fields are linear combination of the original W and B fields:

$$W^\pm \equiv \frac{1}{\sqrt{2}}(W_1 \mp i W_2), \tag{2.14}$$

$$Z_\mu \equiv -\sin\theta_W B_\mu + \cos\theta_W W_\mu^3, \tag{2.15}$$

$$A_\mu \equiv \cos\theta_W B_\mu + \sin\theta_W W_\mu^3, \tag{2.16}$$

where θ_W is the Weinberg angle

$$\tan\theta_W = \frac{g'}{g}. \tag{2.17}$$

The three Goldston bosons, θ^a fields, reappear as the longitudinal components of $W^\pm$ and Z that became massive:

$$m_W = \frac{gv}{2}, \quad m_Z = \frac{v\sqrt{g^2+g'^2}}{2}. \tag{2.18}$$

The photon remains massless as dictated by the unbroken $U(1)_Q$ symmetry.

2.3 Fermion masses and mixings

The mass term for a Dirac fermion is of the form:

$$L_{mass} = -m\overline{\psi}_L\psi_R + h.c., \tag{2.19}$$

which in the SM is forbidden by the $SU(2)$ symmetry, since left and right components n Table 2.1 have different $SU(2)$ charges. However, mass terms can be obtained via SSB from the so called Yukawa terms:

$$L_{Yuk} = -\sum_{i,j}\left\{\bar{l}_{Li}Y^{(l)}_{ij}\Phi l_{Rj} + \overline{Q}_{Li}\left(Y^{(d)}_{ij}\Phi d_{Rj} + Y^{(u)}_{ij}\tilde{\Phi}u_{Rj}\right)\right\}, \tag{2.20}$$

where the Y matrices are general complex matrices and the field $\tilde{\Phi} \equiv i\sigma_2\Phi^*$ carries hypercharge $-1/2$.

After SSB, the Higgs field gets a VEV and the Lagrangian becomes:

$$L_{Yuk} = -\left(1+\frac{H}{v}\right)\left(\overline{u}_L M_u u_R + \overline{d}_L M_d d_R + \bar{l}_L M_l l_R + h.c.\right), \tag{2.21}$$

where u, d and l are the quarks and charged leptons fields in the so-called flavour basis. Neutrinos remain massless because no Yukawa term can be writen for them in the absence of right-handed components.

The matrices M are not diagonal, but can be taken to a diagonal form with two unitary matrices U and W

$$M_u = U_u^\dagger D_u W_u, \quad M_d = U_d^\dagger D_d W_d, \quad M_l = U_l^\dagger D_l W_l, \tag{2.22}$$

so that matrices D are diagonal. By redefining the fields we get the mass eigenstates of the quarks and lepton fields

$$\begin{aligned} d'_L &= U_d d_L, \quad u'_L = U_u u_L, \quad l'_L = U_l l_L, \\ d'_R &= W_d d_R, \quad u'_R = W_u u_R, \quad l'_R = W_l l_R. \end{aligned} \tag{2.23}$$

This transformation on the fields introduces flavour mixing in the charged current (CC) interactions

$$L_{CC} = -\frac{g}{2\sqrt{2}} \left\{ W^+_\mu \left[\sum_{ij} \bar{u}'_i \gamma^\mu (1-\gamma^5) V_{ij} d'_j + \sum_l \bar{\nu}'_l \gamma^\mu (1-\gamma^5) l' \right] + h.c \right\}, \tag{2.24}$$

where matrix $V \equiv U_u U_d^\dagger$ is the Cabibbo-Kobayashi-Maskawa (CKM) matrix [17, 18].

In the SM there is no leptonic mixing matrix, since the neutrino field can be redefined as $\nu'_L = U_l \nu_L$ so that $\bar{\nu}_L l_L = \bar{\nu}_L U_l^\dagger l'_L = \bar{\nu}'_L l'_L$. Note that this is only due to the vanishing neutrino mass, and will not be the case in the models that accommodate massive neutrinos, that will be discussed in the next chapters.

Chapter 3

Neutrino masses

Even though the SM was constructed with massless neutrinos, oscillation experiments have shown that neutrinos are massive. In this section a simple introduction to basic models that give rise to neutrino mass terms is presented. For further details the reader is referred to the reviews [16,19–24] or the book [25].

3.1 Neutrino mass models

There are two simple ways to extend the SM in order to accommodate neutrino masses. As we have seen that a mass term couples states of different chiralities (see eq. (2.3)), one needs therefore to identify the right-handed component of the neutrino field.

3.1.1 Dirac mass

The most straightforward way to give neutrinos a mass in the SM is by adding 3 right-handed singlets ν_R with charges (1,1,0) under $SU(3) \times SU(2) \times U(1)_Y$. With these extra states, the neutrino mass can be generated in the same way as the charged leptons, via the Yukawa term:

$$L_{Yuk} = -\bar{l}_{Li}\tilde{\Phi}Y_{\nu ij}\nu_{Rj} + h.c. \ . \tag{3.1}$$

This solution implies that neutrinos are Dirac particles, i.e., they are 4-component spinors. In this way all the symmetries of the SM are preserved, but the drawback is that it does not seem natural that neutrinos are so lighter that the other charged fermions. The Yukawa matrix should satisfy $m_\nu = Y_\nu v/\sqrt{2}$ which leads to the

coupling at least 11 orders of magnitude smaller than the top quark coupling, for neutrino masses in the eV range.

3.1.2 Majorana mass

A more economical way of introducing the neutrino mass matrix is by using only the two component Weyl neutrino that already exists in the SM, and adding a Majorana mass term:

$$L_{Maj} = -\frac{m}{2}(\bar{\psi}_L \psi_L^c + h.c), \tag{3.2}$$

where

$$\psi_L^c = C\bar{\psi_L}^T. \tag{3.3}$$

C is the charge conjugation matrix which in the Dirac representation of the γ matrices is given by

$$C = i\gamma_0\gamma_2. \tag{3.4}$$

When dealing with interacting particles one has to take care of the conserved charges. Obviously the Majorana mass term is allowed only for electrically neutral particles since otherwise it would violate charge conservation. Therefore, the only candidates to have a Majorana mass in the SM are neutrinos. Furthermore, the eq. (3.2) for the neutrino field as it stands would break also $U_Y(1)$ hypercharge symmetry, however, this mass term can be obtained via the so called Weinberg operator [26]:

$$L_{Weinberg} = -\frac{1}{\Lambda}(\bar{l}_{L_i}\tilde{\Phi})Y_{ij}(\tilde{\Phi}^T {l_L}^c) + h.c.. \tag{3.5}$$

Here Y is a complex symmetric matrix and Λ is unknown energy scale of new physics.

After the Higgs field gets a VEV this term becomes a Majorana mass term for the neutrinos:

$$L_{Majorana} = -\frac{1}{2}\bar{\nu}_L M_\nu \nu_L^c + h.c., \tag{3.6}$$

where

$$M_\nu = Y\frac{v^2}{\Lambda}. \tag{3.7}$$

The Weinberg operator obeys all the symmetries of the SM, but leads to a non-renormalizable theory, hence, the theory with the Weinberg operator must be seen as a low-energy effective field theory, and needs an ultraviolet (UV) completion.

One of the popular ways for the UV completion is the Seesaw mechanism.

3.2 Seesaw mechanism

The three most popular extensions of the SM that are UV complete involve the addition of extra singlet fermions, a scalar triplet or fermionic triplets and are called seesaw of Types I,II and III respectively. Another popular model, the so called "inverse seesaw" is a subset of the Type I seesaw, when an approximate global $U(1)$ symmetry is imposed.

3.2.1 Type I seesaw

This model assumes no new physics except a number of right-handed singlet fermions (N_R). The only additional terms in the Lagrangian allowed by the gauge symmetries are the Majorana mass terms for the new right-handed fermions, and their Yukawa interaction:

$$-L_{\text{TypeI}} = \bar{l}_L \tilde{\Phi} Y_\nu N_R + \frac{1}{2}\bar{N}_R^c M_R N_R + h.c. \ . \tag{3.8}$$

For energies much smaller than the Majorana mass, M_R, the exchange of the right-handed neutrinos resembles a contact interaction like that in the Weinberg operator, see Fig. 3.1.

After SSB this term can be written as

$$-L_{\text{Type I}} = \frac{1}{2}\bar{N}_R^c M_R N_R + \bar{\nu}_L m_D N_R + h.c. + ... \ . \tag{3.9}$$

Defining $\nu = (\nu_L, N_R^c)$ this can be represented in a matrix notation:

$$-L_{\text{Type I}} = \frac{1}{2}\bar{\nu}\mathcal{M}\nu^c + h.c. \ , \tag{3.10}$$

where

$$\mathcal{M} = \begin{pmatrix} 0 & m_D \\ m_D^T & M_R \end{pmatrix} . \tag{3.11}$$

In the case $M_R \ll m_D$ the neutrinos would be predominately Dirac particles. In the opposite case where $M_R \gg m_D$ the mass eigenstates are approximately:

$$\begin{aligned} M_N &\simeq M_R, \\ m_\nu &\simeq -m_D \frac{1}{M_R} m_D^T \ . \end{aligned} \tag{3.12}$$

This is the original seesaw formula proposed in Refs. [25, 27–29]. More details about allowed parameter space and its phenomenology will be explained in Chapter 5.

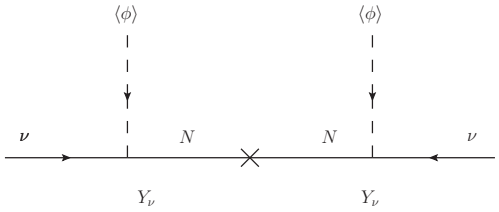

Figure 3.1: Seesaw Type I

3.2.2 Type II seesaw

As proposed in Refs. [30–32] the neutrino masses in the SM can be explained with additional scalar triplet, that carries hypercharge 1 and lepton number -2:

$$\chi = \frac{1}{\sqrt{2}}\vec{\chi}\cdot\vec{\sigma} \ , \tag{3.13}$$

where σ are the Pauli matrices. The allowed Lagrangian is :

$$-L_{\text{Type II}} = \overline{l_L^c} Y_\chi \chi l_L + h.c. + V(\phi,\chi) \ , \tag{3.14}$$

with Y being a generic symmetric complex matrix. In order for neutrinos to obtain mass, the scalar triplet must get a VEV. The potential is

$$V(\phi,\chi) = m_\chi^2 Tr[\chi^\dagger\chi] - \mu\tilde{\Phi}^\dagger\chi\Phi + h.c. + ... \ , \tag{3.15}$$

where μ coupling term explicitly violates lepton number and induces VEV of χ field, via the VEV of the Higgs field (v):

$$\langle\chi\rangle \equiv v_\chi \simeq \frac{\mu v^2}{2m_\chi^2} \ . \tag{3.16}$$

This procedure leads to light majorana neutrino masses:

$$m_\nu = 2Y_\chi v_\chi = Y_\chi \frac{\mu v^2}{m_\chi^2} \ . \tag{3.17}$$

If $\mu \ll m_\chi$ the light neutrino masses come out naturally, since in the limit $\mu \to 0$ lepton number is recovered. The current constraints demand $v_\chi \leq 6$ GeV [33]. The diagram giving the Weinberg interaction is presented in Fig. 3.2.

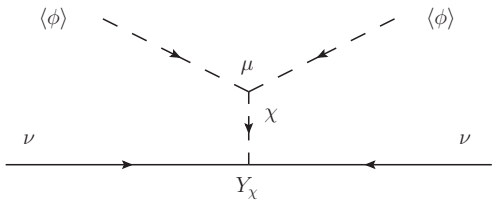

Figure 3.2: Seesaw Type II

3.2.3 Type III seesaw

Instead of adding right handed fermion singlets, neutrino masses can be obtained with right-handed $SU(2)_L$ fermionc triplets, $\vec{T}_F$, with zero hypercharge [34–36] :

$$-L_{\text{Type III}} = \bar{l_L^c} Y_T \vec{\sigma} \cdot \vec{T}_F \Phi + \frac{1}{2} \overline{\vec{T}_F^c} M_T \vec{T}_F + h.c. \ , \tag{3.18}$$

where Y_T is the Yukawa coupling of the triplet to the SM leptons and the Higgs, and M_T the Majorana mass for the triplet. As in the Type I seesaw, after SSB the light neutrino mass matrix is

$$m_\nu = -m_D^T \frac{1}{M_T} m_D, \tag{3.19}$$

where $m_D = Y_T v$.

The triplet has a charged component and has been strongly constrained in collider experiments, thus this model is more constrained than the Type I seesaw, and the Majorana mass has to be higher than several hundreds of GeV [37, 38]. The Weinberg operator arises as in Type I from the exchange of the heavy triplet instead of the singlet.

3.2.4 Inverse seesaw

In the inverse seesaw (IS) models, for each right-handed neutrino, N_R, another singlet fermion, S, with opposite lepton number is added to the SM [39, 40]. In the original proposal the Majorana mass of the N_R fields was omitted and the

relevant part of the Lagrangian is

$$-L_{IS} = \bar{l_L}\tilde{\Phi}Y_\nu N_R + \frac{1}{2}\bar{S^c}M_S S + \bar{S^c}M_R N_R + h.c. \ . \tag{3.20}$$

The full mass matrix is then

$$\mathcal{M} = \begin{pmatrix} 0 & m_D & 0 \\ m_D^T & 0 & M_R \\ 0 & M_R^T & M_S \end{pmatrix}, \tag{3.21}$$

which after the diagonalization leads to the light neutrino masses

$$m_\nu = -m_D \frac{1}{M_R^T} M_S \frac{1}{M_R} m_D^T \ . \tag{3.22}$$

Small neutrino masses can be explained in this case even if the scale M_R is at the electroweak scale and Yukawa couplings of $\mathcal{O}(1)$ if M_S is sufficiently small. This can be understood because in the limit $M_S \to 0$, there is an exact global lepton number symmetry, the light neutrinos remain massless while the heavy spectrum consists of Dirac neutrinos. The inverse seesaw model is equivalent of a Type I model with an even number of right-handed neutrinos and specific textures of the Yukawa matrix.

3.3 Neutrino mixing matrix

Independently of the specific mechanism that gives neutrinos a mass, neutrinos mix. The neutrino mass matrix in general will not be diagonal in the flavor basis.

In the case of Dirac neutrinos, the diagonalization is performed as in the case of the charged leptons, by two unitary matrices:

$$D_\nu = U_\nu M_\nu W_\nu^\dagger. \tag{3.23}$$

The W and U matrices can be absorbed in the field redefinition:

$$\begin{aligned} N'_R &= W_\nu N_R, \ \ l'_R = W_l l_R, \\ \nu'_L &= U_\nu \nu_L, \quad l'_L = \ U_l l_L, \end{aligned} \tag{3.24}$$

so that the CC interactions in the mass basis is non-diagonal :

$$L_{CC} = -\frac{g}{\sqrt{2}}\bar{\nu}'_L U_{PMNS}\gamma_\mu l'_L W^+_\mu + h.c. \tag{3.25}$$

The matrix U_{PMNS}, the so called Pontecorvo–Maki–Nakagawa–Sakata (PMNS) matrix [41, 42],

$$U_{PMNS} = U_\nu U_l^\dagger, \tag{3.26}$$

is the analogue of the CKM matrix in the quark sector.

U_{PMNS} depends on a number of physical parameters. A generic unitary matrix of dimension n can be parametrized in terms of $\frac{n(n-1)}{2}$ angles and $\frac{n(n+1)}{2}$ phases. However, rephasing left-handed fields can remove $(2n-1)$ phases[1] which can be absorbed in the right handed field in order to leave the Lagrangian invariant. This means that the total number of physical parameters for $n = 3$ are 3 angles and 1 phase. The usual parametrization is

$$U_{PMNS} = \begin{pmatrix} 1 & 0 & 0 \\ 0 & c_{23} & s_{23} \\ 0 & -s_{23} & c_{23} \end{pmatrix} \begin{pmatrix} c_{13} & 0 & s_{13}e^{-i\delta} \\ 0 & 1 & 0 \\ -s_{13}e^{i\delta} & 0 & c_{13} \end{pmatrix} \begin{pmatrix} c_{12} & s_{12} & 0 \\ -s_{12} & c_{12} & 0 \\ 0 & 0 & 1 \end{pmatrix}, \tag{3.27}$$

where $s_{ij}(c_{ij}) = \sin(\theta_{ij})(\cos(\theta_{ij}))$.

If the neutrinos are Majorana particles, the mass term is symmetric and can be diagonalized with only one unitary matrix:

$$D_\nu = U_\nu^\dagger M_\nu U_\nu^*, \tag{3.28}$$

so that the fields in the mass basis are

$$\begin{aligned} N'_R &= U_\nu^* N_R, \;\; l'_R = W_l l_R, \\ \nu'_L &= U_\nu \nu_L, \quad l'_L = \; U_l l_L. \end{aligned} \tag{3.29}$$

Again, the mixing matrix is

$$U_{PMNS} = U_\nu U_l^\dagger, \tag{3.30}$$

[1] The rephasing of the fields would naively remove $2n$ phases, but the global phase redefinition of the mass eigenstate would leave U_{PMNS} invariant, hence the number of phases that can be removed is $2n - 1$.

but the number of physical phases is different. In this case only n phases can be removed since the Lagrangian is no longer invariant under neutrino field rephasing. Therefore, the mixing matrix can be parametrized as

$$\begin{aligned} U_{PMNS} &= \begin{pmatrix} 1 & 0 & 0 \\ 0 & c_{23} & s_{23} \\ 0 & -s_{23} & c_{23} \end{pmatrix} \begin{pmatrix} c_{13} & 0 & s_{13}e^{-i\delta} \\ 0 & 1 & 0 \\ -s_{13}e^{i\delta} & 0 & c_{13} \end{pmatrix} \begin{pmatrix} c_{12} & s_{12} & 0 \\ -s_{12} & c_{12} & 0 \\ 0 & 0 & 1 \end{pmatrix} \\ &\times \begin{pmatrix} 1 & 0 & 0 \\ 0 & e^{i\phi_1} & 0 \\ 0 & 0 & e^{i\phi_2}, \end{pmatrix} \end{aligned} \tag{3.31}$$

where the two phases ϕ_1 and ϕ_2 are the CP violating Majorana phases. Hence, 3ν models with Majorana neutrinos would have 2 additional phases compared to Dirac neutrinos.

3.4 Neutrino oscillations in vacuum

A consequence of non-zero neutrino masses and CC mixing matrix brings in the phenomenon of neutrino oscillations.

In neutrino oscillation experiments, neutrinos are produced and detected via CC interaction processes, i.e. in the flavor eigenstates. After production, the states propagate undisturbed, and, since the mass eigenstate have slightly different phase velocities, the detected state might have different flavor than the produced one.

There are many ways to calculate the oscillation probability, here the simple one using plane waves approximation will be briefly described.

A neutrino flavor α produced at t_0 will be a superposition of mass eigenstates:

$$|\nu_\alpha(t_0)\rangle = \sum_i U^*_{\alpha i} |\nu_i(\mathbf{p})\rangle , \tag{3.32}$$

where the mass eigenstates are the eigenstates of the free Hamiltonian

$$\hat{H} |\nu_i(\mathbf{p})\rangle = E_i(\mathbf{p}) |\nu_i(\mathbf{p})\rangle , \quad E_i(\mathbf{p}) = \mathbf{p}^2 + m_i^2. \tag{3.33}$$

After time t the state α will evolve to

$$|\nu_\alpha(t)\rangle = e^{-i\hat{H}(t-t_0)} |\nu_\alpha(t_0)\rangle = \sum_i U^*_{\alpha i} e^{-iE_i(\mathbf{p})(t-t_0)} |\nu_i(\mathbf{p})\rangle . \tag{3.34}$$

The probability that the state changed to $|\nu_\beta\rangle = \sum_i U_{\beta k} |\nu_k(\mathbf{p})\rangle$ is

$$P(\nu_\alpha \to \nu_\beta)(t) = |\langle \nu_\beta | \nu_\alpha \rangle|^2 = \sum_{i,j} U_{\beta i} U^*_{\alpha i} U^*_{\beta j} U_{\alpha j} e^{-i(E_i(\mathbf{p_i}) - E_j(\mathbf{p_j}))(t-t_0)}, \quad (3.35)$$

where we used the orthogonality relation for the states $\langle \nu_k | \nu_i \rangle = \delta_{ik}$. Assuming equal-momentum $\mathbf{p}_i = \mathbf{p}_j = \mathbf{p}$, for ultrarelativistic neutrinos the energy difference is

$$E_i(\mathbf{p_i}) - E_j(\mathbf{p_j}) \simeq \frac{1}{2} \frac{m_i^2 - m_j^2}{|\mathbf{p}|} + \mathcal{O}(m^4), \quad (3.36)$$

which leads to the famous oscillation probability formula:

$$P(\nu_\alpha \to \nu_\beta) = \sum_{i,j} U^*_{\beta j} U_{\alpha j} U_{\beta i} U^*_{\alpha i} e^{-i \frac{\Delta m^2_{ij} L}{2|E_\nu|}}, \quad (3.37)$$

with $\Delta m^2_{ij} \equiv m^2_i - m^2_j$.

It is important to note that plane-wave derivation does not take into account two mandatory ingredients for this phenomenon:

- quantum coherence in propagation over macroscopically large distances, and
- sufficient uncertainty in momentum at production and detection, so that a coherent state can be produced,

which show up explicitly in the more precise wave packet derivation [43, 44].

The probability can be divided in the CP conserving and CP violating part (it has opposite sign for neutrinos and antineutrinos):

$$P_{\alpha\beta} = \delta_{\alpha\beta} - 4 \sum_{i<j} \mathrm{Re}[U^\star_{\beta j} U_{\alpha j} U_{\beta i} U^\star_{\alpha i}] \sin^2 \left(\frac{\Delta m^2_{ij} L}{2E_\nu} \right) \quad (3.38)$$

$$\pm \; 2 \sum_{i<j} \mathrm{Im}[U^\star_{\beta j} U_{\alpha j} U_{\beta i} U^\star_{\alpha i}] \sin \left(\frac{\Delta m^2_{ij} L}{2E_\nu} \right). \quad (3.39)$$

It is common to express the macroscopic length L in meters (m) so that the phase factor becomes $1.27 \frac{\Delta m^2{}_{ij}}{eV^2} \frac{L/E}{\mathrm{m/MeV}}$. Eq. (3.39) shows that the probability is oscillatory function of the distance L with the period

$$L^{osc} = \frac{4\pi E_\nu}{\Delta m^2_{ij}}. \quad (3.40)$$

The oscillation probability is not sensitive to Majorana phases, which is expected, since the neutrino oscillations is a lepton number conserving process.

In the case of just 2 neutrino families the mixing matrix simplifies to :

$$V = \begin{pmatrix} \cos\theta & \sin\theta \\ -\sin\theta & \cos\theta \end{pmatrix}, \tag{3.41}$$

and the oscillation probability becomes

$$P_{\alpha\beta} = \sin^2 2\theta \sin^2\left(\frac{\Delta m^2_{ij} L}{2E_\nu}\right), \quad \alpha \neq \beta. \tag{3.42}$$

If the length L is too large the wave packet can become decoherent. When this happens the neutrinos do not oscillate any more and the transition probability becomes independent of L:

$$P_{\alpha\beta} = \frac{1}{2}\sin^2 2\theta. \tag{3.43}$$

It is interesting to note that the smearing in L and E_ν produces the same effect when $L \gg L^{osc}$, i.e. any real experiment would measure the average $\langle P_{\alpha\beta}\rangle = \frac{1}{2}\sin^2 2\theta$.

3.5 Neutrino oscillations in matter

When neutrinos propagate in a dense medium the oscillations will be modified due to (i) incoherent interaction and (ii) forward scattering. The incoherent interactions are very suppressed due to the low cross section, but are important in the really dense medium, such as Early Universe plasma. Here, only the effect of the forward scattering will be described.

Recall that the plane wave solutions satisfy Schrödinger equation:

$$i\frac{d}{dt}\nu = H\nu. \tag{3.44}$$

The coherent scattering of the neutrinos on the particles in the plasma will induce corrections to the Hamiltonian, $H = H_0 + V_{mat}$, where $H_0 = \frac{1}{2E} Diag(m_1^2, m_2^2, m_3^2)$.

For neutrinos propagating through a matter such as the Earth, Sun, etc only electron neutrinos interact via the charged current, while any flavour can interact via the neutral current, as presented in Fig. 3.3. Note that this is not the case in the Early Universe plasma, where the muons and taus are as abundant as

electrons. The effective charged current interaction in matter is

$$V_{CC} = \left\langle H_{CC}^{(e)} \right\rangle = \left\langle 2\sqrt{2}G_F \left[\bar{e}\gamma_\mu P_L \nu_e\right]\left[\bar{\nu}_e\gamma^\mu P_L e\right]\right\rangle = 2\sqrt{2}G_F \left\langle\left[\bar{e}\gamma_\mu P_L e\right]\left[\bar{\nu}_e\gamma^\mu P_L \nu_e\right]\right\rangle$$
$$= \sqrt{2}G_F n_e \bar{\nu}_e\gamma^0(1-\gamma_5)\nu_e \equiv \bar{\nu}V_{CC}^{(e)}\gamma^0(1-\gamma_5)\nu, \quad (3.45)$$

where n_e is a number density of electrons.

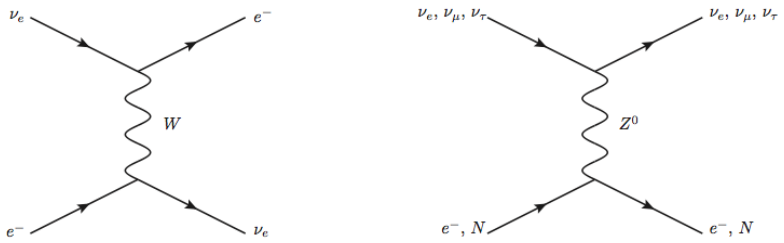

Figure 3.3: Charged and neutral current interactions of neutrinos in the matter.

Similarly, the neutral interactions effective potential can be derived

$$V_{NC} = \frac{\sqrt{2}}{2}G_F\left[-n_e(1-4\sin^2\theta_W) + n_p(1-4sin^2\theta_W) - n_n\right], \quad (3.46)$$

with n_n and n_p being neutron and proton densities. For neutrally charged matter proton and neutron contributions in the neutral current potential cancel, and the sum of two potential, including all families, is

$$V_{mat} = V_{NC} + V_{CC} = \begin{pmatrix} \frac{G_F}{\sqrt{2}}(n_e - \frac{n_n}{2}) & 0 & 0 \\ 0 & \frac{G_F}{\sqrt{2}}(-\frac{n_n}{2}) & 0 \\ 0 & 0 & \frac{G_F}{\sqrt{2}}(-\frac{n_n}{2}) \end{pmatrix}. \quad (3.47)$$

The effect of matter results in an effective mass matrix:

$$\tilde{M}_\nu^2 = M_\nu^2 \pm 4EV_{mat}, \quad (3.48)$$

where

$$\tilde{M}_\nu^2 = \tilde{U}^* Diag(\tilde{m}_1^2, \tilde{m}_2^2, \tilde{m}_3^2)\tilde{U}^T, \quad (3.49)$$

and

$$\tilde{M}_\nu^2 = \tilde{U}^* Diag(m_1^2, m_2^2, m_3^2)\tilde{U}^T \pm 2EV_{mat}. \quad (3.50)$$

In the case of 2 families, the effective mass and angle are

$$\Delta\tilde{m}^2 = \sqrt{(\Delta m \cos 2\theta \mp 2EV_{mat})^2 + (\delta m^2 \sin 2\theta)^2} \quad (3.51)$$

$$\sin^2 2\tilde{\theta} = \frac{(\Delta m^2 \sin 2\theta)^2}{(\Delta\tilde{m}^2)}, \quad (3.52)$$

where $\pm$ sign stands for neutrinos and antineutrinos. The corresponding oscillation amplitude has a resonance when neutrino energy satisfies:

$$\Delta m \cos 2\theta \mp 2EV_{mat} = 0 \rightarrow \sin^2 2\tilde{\theta} = 1, \quad (3.53)$$

i.e. the mixing becomes maximal independently of the value of the vacuum mixing angle. This is the Mikheyev-Smirnov-Wolfenstein (MSW) resonance [45, 46], relevant to explain the solar neutrino flavour transition.

In the next chapter we will review experimental evidence for neutrino oscillations, as well as other experiments that put constraints on the neutrino parameters.

Chapter 4

Standard 3-neutrino picture

In this chapter we will review the experimental results that have determined neutrino masses and mixings in the standard 3 neutrino paradigm.

4.1 Oscillation experiments

Based on the origin of neutrinos, neutrino oscillation experiments can be divided into four groups: atmospheric, solar, reactor and accelerator. From the eq. (3.39) we see that the oscillation probability depends on the ratio L/E, i.e., the mass difference that experiments are sensitive to depends on the experimental setup. The experiments based on the mass difference that they are most sensitive to are summarized in Fig 4.1.

4.1.1 Atmospheric neutrinos

Atmospheric neutrinos are produced in the atmosphere through collisions of cosmic rays with nuclei leading to a hadron shower containing mainly pions. Pions further decay via the processes :

$$\begin{aligned} \pi^+ &\rightarrow \mu^+ + \nu_\mu, \\ &\quad \mu^+ \rightarrow \bar{\nu}_\mu + \mathrm{e}^+ + \nu_e, \qquad (4.1) \\ \pi^- &\rightarrow \mu^- + \bar{\nu}_\mu, \\ &\quad \mu^- \rightarrow \nu_\mu + \mathrm{e}^- + \bar{\nu}_e. \qquad (4.2) \end{aligned}$$

The fluxes of produced neutrinos can be predicted within 10-20% accuracy, but many of the uncertainties cancel when considering the ratio of muon over electron

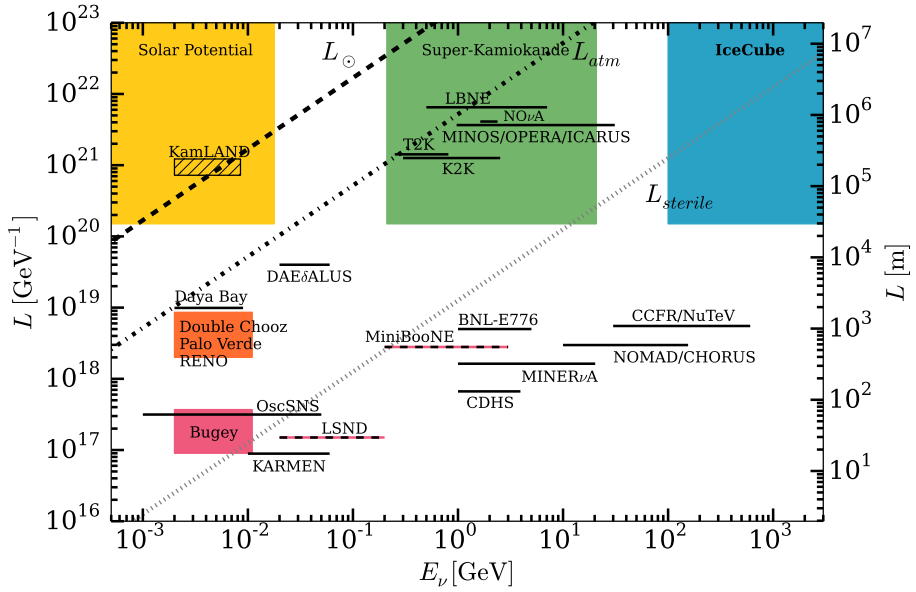

Figure 4.1: Summary of neutrino oscillation experiments based on the mass splitting they are sensitive on (L) versus the energy of the neutrino E_ν plane, from Refs. [47, 48].

neutrinos. This ratio was first measured by Kamiokande [49], IMB [50], Soudan2 [51] and Macro [52], and a discrepancy with he expectation for massless neutrinos was found.

It was SuperKamiokande in 1998 that finally clarified the puzzle [53][1]. Beside being able to distinguish between electron and muon events, they were also able to predict the incoming neutrino angle through measurements of the outgoing lepton angle. By doing so, they could measure how the neutrino flux depends on a distance they travelled.

The events for the electron neutrino were in the rough agreement with prediction, while muon events showed strong dependence on the zenith angle: there is almost twice more neutrinos coming from above ($\theta = 0$) than the ones coming from below ($\theta = \pi$). Fitting the data with the two neutrino oscillations hypothesis a value of $\Delta m^2 \simeq 3 \times 10^{-3}\text{eV}^2$ and maximal mixing, gives a good description of the data. The schematic view of detector position, as well as the best fit for electron and muon like events is given in Fig. 4.2.

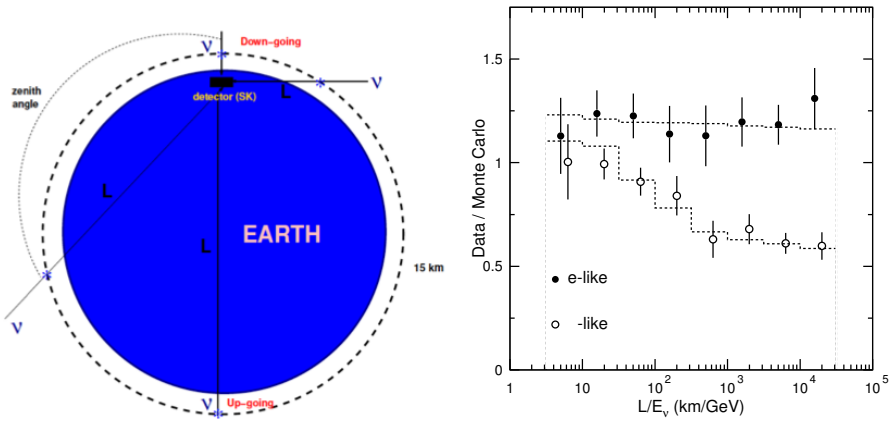

Figure 4.2: Left: Distance travelled by atmospheric neutrino as a function of zenith angle. Right: Ratio of the data to the predicted MC events in the case of no oscillations versus L/E_ν for electron like and muon like events. The dashed curves are the best-fit expectation for $\nu_\mu \leftrightarrow \nu_\tau$ oscillations (from Ref. [53]).

More recent data of Super Kamiokande can be found in [54, 55].

[1]The 2015 Nobel Prize was awarded to Takaaki Kajita on behalf of SK group, and to Arthur B. McDonald, the founder of SNO group.

4.1.2 Solar neutrinos

Solar neutrinos are produced in the chain of nuclear reactions, resulting in the overall fusion of protons into ^4He:

$$4p \rightarrow^4 He + 2e^+ + 2\nu_e + \gamma. \tag{4.3}$$

The spectrum of the solar neutrino flux is given in Fig. 4.3, that is the result of simulations of the Sun interior, the so-called standard solar model (SSM) [56].

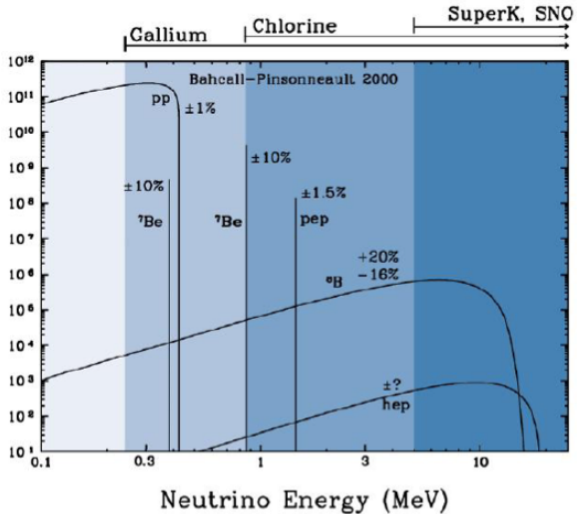

Figure 4.3: Solar neutrino fluxes as a function of their energy for different reactions, as well as the threshold of several experiments, from Ref. [57].

The first result on the detection of solar neutrinos was announced by Ray Davis Jr. and his collaborators from Brookhaven in 1968 [58] where they measured less neutrinos than theoretically predicted [59]. This became the "solar neutrino problem", that was later-on confirmed in Gallex/GNO [60], SAGE [61] and already mentioned Super Kamiokande [62–64] experiments. These experiments were sensitive to the total number of electron neutrinos, and their interpretation depends on the solar neutrino flux normalization that was extracted from the standard model of the sun interior [59].

Sudbury Neutrino Observatory (SNO) Cherenkov water detector [65, 66] was designed to give a model independent explanation of the solar neutrino problem. They could distinguish between CC (involves only electron neutrino) , and NC

(involves all neutrino flavors) interactions, hence could measure the rate of electron neutrinos over the total number of neutrinos coming from the Sun, which is independent of the flux normalization. They found a deficit in the CC interaction, but no deficit in the NC interactions, which was a definite proof of solar neutrinos flavor transitions. Note that this is not the effect of neutrino oscillation, but flavour mixing. The measurements demonstrate that there are approximately twice more ν_μ and ν_τ coming from the Sun than ν_e, and that the total neutrino flux is consistent with the SSM. The flux of muon and tau neutrinos, versus the one of the electron neutrino is given in the left panel of Fig. 4.4, which demonstrated also that the standard solar model predicts the correct total solar neutrino flux.

Solar neutrino data can be interpreted in terms of mass and mixing, with $\Delta m_\odot \simeq 7 - 8 \times 10^{-5}$ eV and $\theta_\odot \approx 0.56$, as shown on the right panel of Fig. 4.4. It should be stressed that the sensitivity of solar neutrinos to the mass difference is a result of the MSW effect which can explain the energy dependence of the effect as seen in the different electron neutrino fluxes measured in radiochemical experiments, that are sensitive to the lowest energy spectrum, and SuperKamiokande or SNO that are sensitive to the higher end. The experiment that has got closer to the resonant energy which determines the transition between the high and low energy regimes is the recent Borexino experiment [67–69]. Their recent results are in a good agreement with oscillation interpretation of other solar data, as presented in Fig. 4.5.

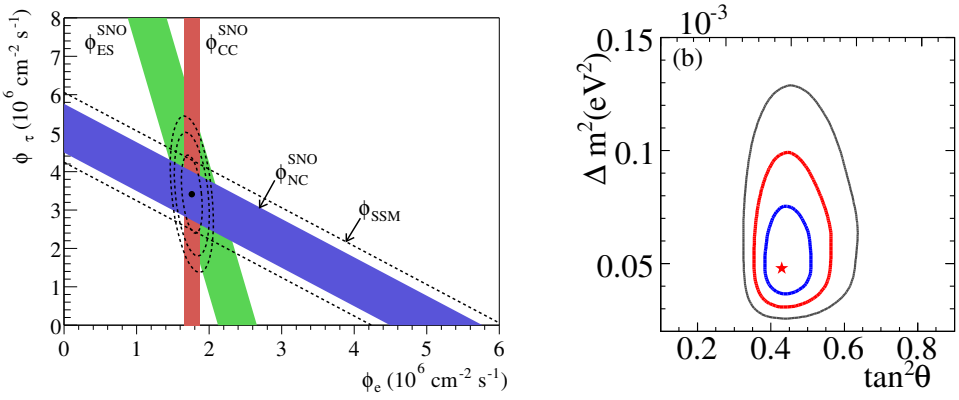

Figure 4.4: Left: Flux of tau and muon neutrinos versus electron one, as measured from three reactions in the SNO experiments. The dashed line is the prediction of the SSM (from Ref. [65]). Right: Fit of SNO measurements in terms of oscillation parameters (from Ref. [70]).

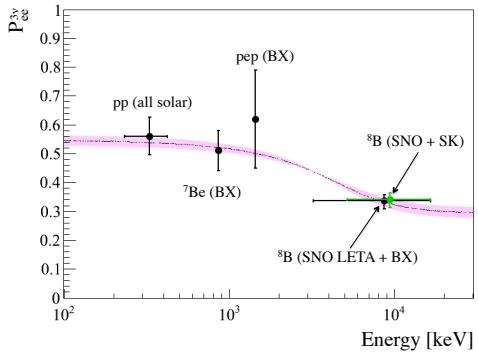

Figure 4.5: Electron neutrino survival probability as a function of neutrino energy according to MSW model calculated for ^8B solar neutrinos (purple band) with the data from Borexino and other solar and reactor experiments (from Ref. [69]).

4.1.3 Reactor neutrinos

Nuclear reactors produce electron antineutrino beam with energies $\sim$ MeV. Since this energy is under muon and tau mass, these experiments can measure only electron (anti)neutrino and are necessarily disappearance experiments.

In the KamLAND experiment [71] electron antineutrinos are coming from nuclear plants around Kamiokande mine in Japan, and are detected in 1 kton liquid scintillator detector via inverse beta decay after travelling $\langle L \rangle = 175$ km. The L/E_ν ratio in KamLAND experiment is in the regime of solar neutrino oscillations. In Fig. 4.6 the KamLAND fit of oscillation parameters is presented, together with the results of solar experiments.

Another set of reactor experiments with L/E_ν in the atmospheric neutrino oscillations regime, where the baseline is $\mathcal{O}$(1km): CHOOZ [73], DoubleCHOOZ [74], Palo Verde [75], DayaBay [76], RENO [77] had been extremely important in establishing that the atmospheric oscillation also affects electron neutrinos and not only muons as seen in atmospheric neutrino experiments.

4.1.4 Accelerator neutrinos

Using well controlled ν_μ beams from pion decays produced in fixed-target experiments in proton accelerators, and choosing the right baseline, accelerator neutrino experiments are able to measure the atmospheric oscillation parameters with high precision. The experiments MINOS [78–81] ($L = 730$ km) and K2K

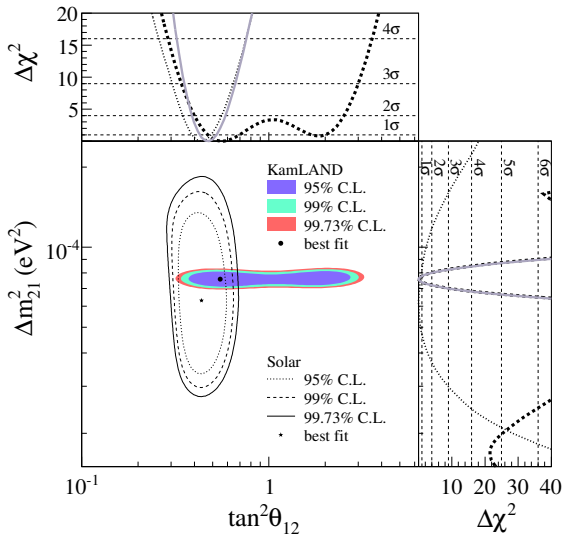

Figure 4.6: KamLAND fit of the oscillation parameters together with the solar neutrino oscillation experiments result (from Ref. [72]).

($L = 250$ km) [82, 83] measured the disappearance of muon neutrinos were the first to confirm the atmospheric oscillation in an accelerator neutrino beam. The experiment OPERA [84] ($L = 730$ km) confirmed that the leading channel in atmospheric oscillations is $\nu_\mu \to \nu_\tau$, by explicitly measuring the appearance of ν_τ. The T2K experiment has been able to measure for the first time the ν_e appearance in a ν_μ beam [85]. Finally the NOvA experiment has measured the appearance of ν_e at $\mathcal{O}(1000)$ km distance [86].

4.1.5 Neutrino Observatories

Currently running IceCube experiment [87], ANTARES [88] and planned KM3Net [89] have measured the high energy tail of atmospheric neutrinos and are optimized to search for astrophysical neutrinos at very high energies $E_\nu \sim \mathcal{O}$(PeV). IceCube has recently presented evidence for a PeV neutrino component in the astrophysical neutrino flux [90], whose origin is still not understood.

4.1.6 Global fit

Two mass differences in the neutrino mass matrix are conventionally assigned to solar and atmospheric mass splitting as:

$$\Delta m^2_{13} = m^2_3 - m^2_1 = \Delta m^2_{\rm atm}, \quad \Delta m^2_{12} = m^2_2 - m^2_1 = \Delta m^2_{\odot}. \tag{4.4}$$

The strong hierarchy between them $|\Delta m^2_{\odot}| \ll |\Delta m^2_{\rm atm}|$ and the smallness of $\sin\theta_{13}$ allow us to write 3 neutrino probabilities as 2-by-2 mixing phenomena, depending on which term is dominating in the oscillation probability formula.

For $E_\nu/L \sim |\Delta m^2_{\rm atm}|$, the solar mass splitting can be neglected and the oscillation probabilities n vacuum are:

$$P(\nu_e \to \nu_\mu) \simeq s^2_{23} \sin^2 2\theta_{13} \sin^2\left(\frac{\Delta m^2_{13} L}{4E_\nu}\right) \tag{4.5}$$

$$P(\nu_e \to \nu_\tau) \simeq c^2_{23} \sin^2 2\theta_{13} \left(\frac{\Delta m^2_{13} L}{4E_\nu}\right) \tag{4.6}$$

$$P(\nu_\mu \to \nu_\tau) \simeq c^4_{13} \sin^2\theta_{23} \sin^2\left(\frac{\Delta m^2_{13} L}{4E_\nu}\right) \tag{4.7}$$

$$P(\nu_e \to \nu_e) = P(\bar\nu_e \to \bar\nu_e) \simeq \sin^2 2\theta_{13} \sin^2\left(\frac{\Delta m^2_{13} L}{4E_\nu}\right). \tag{4.8}$$

If we further take $\theta_{13} \to 0$ only $P(\nu_\mu \to \nu_\tau)$ survives, hence the atmospheric and accelerator experiments are mostly sensitive to θ_{23} angle and can be identified $(\Delta m^2_{\rm atm}, \theta_{\rm atm}) \to (\Delta m^2_{23}, \theta_{23})$. The reactor neutrino experiments measure ν_e disappearance and are sensitive to the θ_{13} angle, that was the last one to be measured [91].

In the solar regime $E_\nu/L \sim |\Delta m^2_{\odot}|$, the atmospheric oscillations are too fast and get averaged out:

$$P(\nu_e \to \nu_e) = P(\bar\nu_e \to \bar\nu_e) \simeq c^4_{13}\left(1 - \sin^2 2\theta_{12} \sin^2\left(\frac{\Delta m^2_{12} L}{4E_\nu}\right)\right) + s^4_{13}. \tag{4.9}$$

Again, in the limit $\theta_{13} \to 0$ we can therefore identify $(\Delta m^2_{\odot}, \theta_{\odot}) \to (\Delta m^2_{12}, \theta_{12})$.

Since the sign of the mass difference is not measured there are two possibility for neutrino mass patterns, as shown in Fig. 4.7:

- Normal hierarchy where the difference between the lightest neutrino (m_1) and the second one is the solar mass splitting, while the third one is much heavier (i.e. the atmospheric mass splitting)

- Inverted hierarchy with one light state (m_3) and two heavier quasi-degenerate ones separated by the solar splitting.

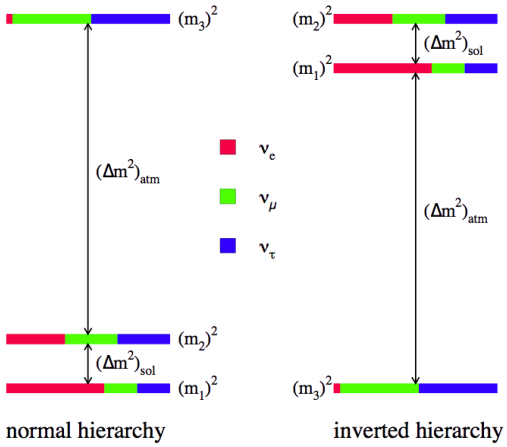

Figure 4.7: Schematic view of normal and inverted hierarchy (from Ref. [92]).

However, the fact that $\theta_{13} \neq 0$ implies that a proper analysis of 3-by-3 mixing is needed [93–96]. Results of the global fit preformed by NuFit group [96] are given in Table 4.1.

4.1.7 Neutrino Anomalies

Not all the oscillation experiments data can be explained in terms of only two mass differences. First to observe hints for physics beyond the standard 3ν picture was LSND experiment [97] which measured excess in the appearance channel $\bar{\nu}_\mu \to \bar{\nu}_e$ at $E/L \sim 1\text{eV}^2$. This anomaly was further explored by the MiniBooNe [98–100], where no significant excess in the higher energy was observed, but the yet to be explained excess in the lower energy appeared. Radioactive source experiments SAGE [101] and GALLEX [102] have observed somehow smaller event rate than expected which can be explained by disappearance of ν_e due to the oscillations to a new state that provides a new mass splitting $\Delta m^2 \geq 1$ eV [103] (Gallium anomaly). Re-analysis of the neutrino flux emitted by nuclear reactors [104, 105] gave further hints on new 1eV mass splitting [106]. It is important to notice that these results are in tension with ν_μ disappearance results [107–109]. Recent analysis of IceCube experiment [110] shows no hint of sterile neutrinos. For recent reviews about eV neutrinos look at [111, 112].

Table 4.1: Best fit of 3ν oscillation parameters, for normal and inverted hierarchy (from Ref. [94, 96]).

NuFIT 3.0 (2016)

	Normal Ordering (best fit)		Inverted Ordering ($\Delta\chi^2 = 0.83$)		Any Ordering
	bfp $\pm 1\sigma$	3σ range	bfp $\pm 1\sigma$	3σ range	3σ range
$\sin^2\theta_{12}$	$0.306^{+0.012}_{-0.012}$	$0.271 \to 0.345$	$0.306^{+0.012}_{-0.012}$	$0.271 \to 0.345$	$0.271 \to 0.345$
$\theta_{12}/^\circ$	$33.56^{+0.77}_{-0.75}$	$31.38 \to 35.99$	$33.56^{+0.77}_{-0.75}$	$31.38 \to 35.99$	$31.38 \to 35.99$
$\sin^2\theta_{23}$	$0.441^{+0.027}_{-0.021}$	$0.385 \to 0.635$	$0.587^{+0.020}_{-0.024}$	$0.393 \to 0.640$	$0.385 \to 0.638$
$\theta_{23}/^\circ$	$41.6^{+1.5}_{-1.2}$	$38.4 \to 52.8$	$50.0^{+1.1}_{-1.4}$	$38.8 \to 53.1$	$38.4 \to 53.0$
$\sin^2\theta_{13}$	$0.02166^{+0.00075}_{-0.00075}$	$0.01934 \to 0.02392$	$0.02179^{+0.00076}_{-0.00076}$	$0.01953 \to 0.02408$	$0.01934 \to 0.02397$
$\theta_{13}/^\circ$	$8.46^{+0.15}_{-0.15}$	$7.99 \to 8.90$	$8.49^{+0.15}_{-0.15}$	$8.03 \to 8.93$	$7.99 \to 8.91$
$\delta_{\rm CP}/^\circ$	261^{+51}_{-59}	$0 \to 360$	277^{+40}_{-46}	$145 \to 391$	$0 \to 360$
$\frac{\Delta m^2_{21}}{10^{-5}\ \text{eV}^2}$	$7.50^{+0.19}_{-0.17}$	$7.03 \to 8.09$	$7.50^{+0.19}_{-0.17}$	$7.03 \to 8.09$	$7.03 \to 8.09$
$\frac{\Delta m^2_{3\ell}}{10^{-3}\ \text{eV}^2}$	$+2.524^{+0.039}_{-0.040}$	$+2.407 \to +2.643$	$-2.514^{+0.038}_{-0.041}$	$-2.635 \to -2.399$	$\begin{bmatrix} +2.407 \to +2.643 \\ -2.629 \to -2.405 \end{bmatrix}$

It is important to mention that an eV sterile neutrino with mixings that can explain these anomalies ($|U_\alpha 4|^2 \sim \mathcal{O}(10^{-2})$) is incompatible with the Standard Cosmology [113, 114].

4.2 Kinematic Constraints from Weak Decays

The standard method of measuring the electron neutrino mass is looking at the end-point of the electron energy spectrum in beta decays:

$$n \to p + e^- + \bar{\nu}_e. \tag{4.10}$$

The energy spectrum of emitted electron is given by

$$\frac{dN}{dE_e} = Cp(E+m_e)(E_0-E_e)\sqrt{(E_0-E_e)^2 - m_\nu^2}F(E_e) = R(E)\sqrt{(E_0-E_e)^2-m_\nu^2}, \tag{4.11}$$

where p, E_e, m_e is electron energy and mass, m_ν is neutrino mass and E_0 is the maximum energy electron can get, the so-called "end-point" energy. F is the Fermi function that takes into account electromagnetic interactions of emitted electron with daughter nucleus. C is a normalization constant and $R(E)$ is conveniently defined so it does not depend on neutrino mass. A non-zero neutrino mass has the effect of changing the slope of electron energy spectra, and the end-point energy. The effect of 1 eV mass in the tritium beta decay spectrum is shown in Fig. 4.8.

The preferred elements are the ones that have low end-point energy, the most used being tritium with $E_0 = 18.4$ keV.

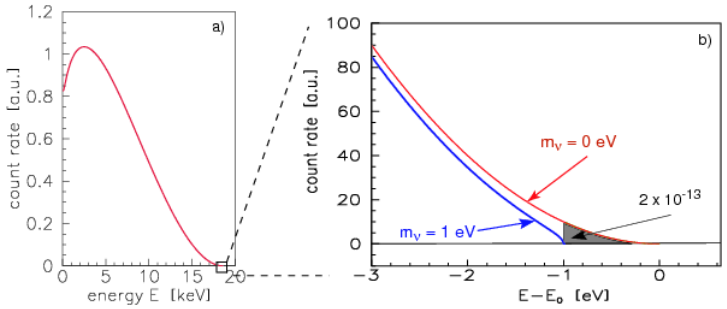

Figure 4.8: Neutrino mass effect on the tritium beta decay spectrum (from Ref. [115]).

Lepton mixing would modify eq. (4.2) as:

$$\frac{dN}{dE_e} = R(E) \sum_i |U_{ei}|^2 \sqrt{(E_0 - E_e)^2 - m_i^2}\,, \tag{4.12}$$

which in the realistic limit of $E_0 - E_e \gg m_i$ simplifies to

$$\frac{dN}{dE_e} = R(E) \sum_i |U_{ei}|^2 (E_0 - E_e) \left(1 - \frac{m_i^2}{2(E_0 - E_e)}\right), \tag{4.13}$$

and can be parametrized with a single parameter

$$m_\beta^2 = \sum_i |U_{ei}|^2 m_i^2, \tag{4.14}$$

as

$$\frac{dN}{dE_e} = R(E) \sqrt{(E_0 - E_e)^2 - m_\beta^2}. \tag{4.15}$$

The best limits on m_β are obtained in Mainz and Troisk experiments with $m_\beta <$ 2.3eV [116–118]. KATRIN should reach sensitivity of 0.2eV [115], and there are other proposals Project 8 [119], MARE [120], ECHo [121]. A recent review on the experimental status of direct neutrino mass measurement is Ref. [122].

The only way of directly measuring muon and tau neutrino masses are through decays of pions and taus. Muon neutrino mass is bounded from pion decay at rest $\pi^+ \to \mu^+ + \nu_\mu$ to be $m_{\nu_\mu} < 190$ keV, while the tau neutrino was searched for in tau decays at the LEP e^+e^-collider

$$\begin{aligned} &e^- + e^+ \to \tau^- + \tau^+; \\ &\tau \to \nu_\tau + 5\pi^\pm(\pi(0)), \end{aligned} \tag{4.16}$$

which gives m_{ν_τ} <18.2 MeV.

4.3 Neutrinoless double beta decay

Certain isotopes cannot decay through the standard beta decay because the mass of such isotope is smaller than the mass of the daughter isotope, but they are allowed to decay through simultaneous double beta decay:

$$(A, Z) \to (A, Z + 2) + 2e^- + 2\bar{\nu}_e. \tag{4.17}$$

In the case of neutrinos being Majorana particles, the emitted right handed antineutrino from one nucleus can be absorbed as left handed neutrino in the second nucleus, and the whole process will have no neutrinos in the final state. Such a process obviously violates lepton number by 2 units, and is sensitive both to Majorana phases of neutrinos and their absolute mass scale. In Fig. 4.9 the schematic process of neutrinoless double beta decay ($0\nu\beta\beta$) is shown.

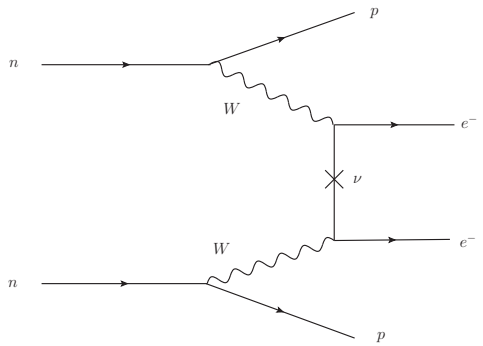

Figure 4.9: Neutrinoless double beta decay process.

The half-life of the decay is expressed as

$$T_{0\nu}^{-1} = G^{0\nu} \left| M^{0\nu}(m_i) \frac{\sum_i U_{ei}^2 m_i}{m_e} \right|^2 , \tag{4.18}$$

where $G^{0\nu}$ is a known phase-space integral, m_e is electron mass and $M^{0\nu}$ is a nuclear matrix element. The largest theoretical uncertainty comes from calculating the nuclear matrix element, for reviews on the different methods to estimate these matrix elements see Refs. [123–126]. For neutrino masses $\ll 100MeV$ the dependence of the amplitude on the neutrino masses and mixings factorizes into the effective $0\nu\beta\beta$ neutrino mass:

$$m_{\beta\beta} = \sum_i U_{ei}^2 m_i. \tag{4.19}$$

Beside determining the nature of neutrinos, another interesting consequence of this measurement is that it could distinguish between inverted and normal hierarchy if the lightest neutrino mass is below 0.1 eV. In Fig. 4.10 , the dark bands are the prediction of the effective mass from the best fit oscillation data, and in the lighter bands the known oscillation parameters are varied within the 3σ

allowed regions. The strongest upper bound have been obtained recently by the KamLand-ZEN experiment [127] using the ^{136}Xe isotope, while previous bounds are represented with grey shadings. Also, the bound depending on the nucleus is given on the side-panel of the plot.

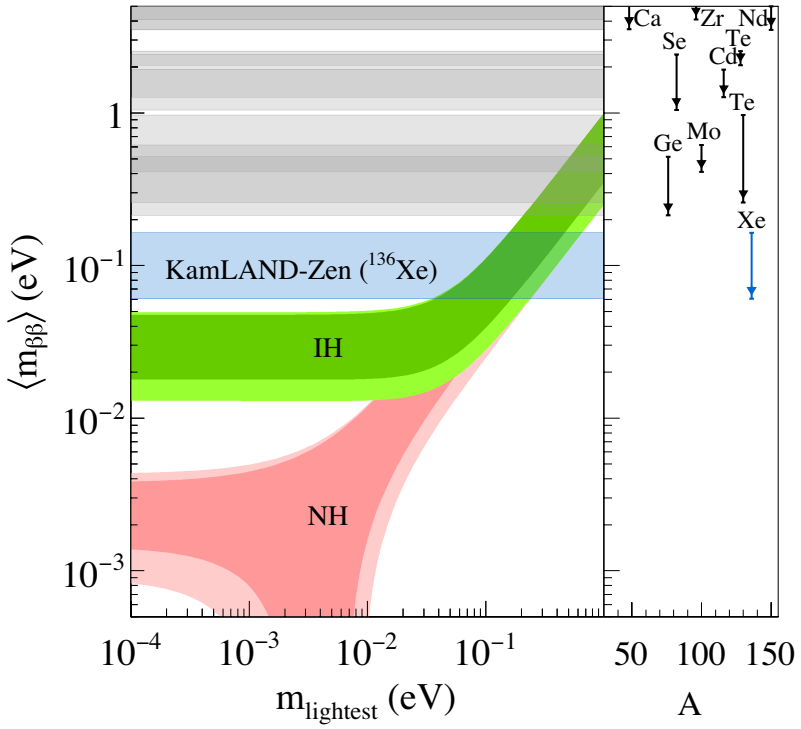

Figure 4.10: Effective neutrino mass as a function of the lightest neutrino mass. The shaded regions are the predictions for NH and IH based on best fit oscillation data. The grey regions are exclusions from experiments, and blue band is KamLand-Zen result. The side-panel shows corresponding nucleus for each band (from Ref. [127]).

4.4 Neutrino masses from cosmology

The strongest bound on the absolute neutrino mass is at present given by cosmological measurements. The current bound for the sum of neutrino masses

obtained by the Planck collaboration is $\sum m_\nu < 0.23$ eV [128], though some stronger bounds have been derived using different data sets [129–131].

4.5 Open questions

Even though three neutrino paradigm seems to fit the data well, there are still some unresolved issues:

- The neutrino mass hierarchy, whether it is inverted or normal. Due to MSW effect in the propagation of GeV neutrinos through the Earth, the accelerator experiment NOvA [132] and the future DUNE (former LBNE) project [133,134] are sensitive to the mass ordering. The detector upgrades of IceCube and KM3Net, PINGU [135] and ORCA [136] could also pin down the hierarchy from the measurement of the atmospheric neutrino flux. Finally, measuring very precisely the reactor neutrinos spectrum at a baseline around 50 km, the atmospheric oscillation can be seen on top of the solar one, with a different pattern for the different mass orderings. This is the strategy of the proposed JUNE experiment [137].

- Leptonic CP violation requires a value of the CP phase δ different from $0, \pi$. At present there is only a slight preference for it to be above $180°$, but in the future it can be measured much more precisely in DUNE [133, 134] and Hyper-Kamiokande [138] experiments, by comparing fluxes of neutrinos and antineutrinos.

- Neutrinoless double beta decay experiments are most likely to establish whether neutrinos are Majorana particles.

- The absolute mass scale is not known and for now there are only upper limits. Important progress is expected from β decay experiments and more precise cosmological measurements.

There are also many open theoretical questions: what is the origin of neutrino masses, are there sterile neutrinos, as predicted by some seesaw models, and, if so, what is their mass scale ? Could these extra states explain the observed dark matter ? Can CP violation in the leptonic sector be the cause of the matter-antimatter asymmetry observed in the Universe ? Why are the PMNS matrix angles much larger than the CKM ones ? Some of these questions will be addressed in this thesis.

Chapter 5

Low-scale seesaw Models

One of the ways to implement neutrino masses in the SM is Type I Seesaw mechanism. As mentioned in Chapter 3 this mechanism predicts heavy Majorana neutrinos. In this section we will review the phenomenology of the Type I Seesaw for the masses of right handed neutrinos below the EW scale.

5.1 The scale of New Physics

Originally, Type I Seesaw [27] assumed that masses of heavy sterile neutrinos are $M_R = 10^{12-15}$ GeV, what corresponds to light neutrino masses of order of the atmospheric mass splitting, and coefficients in the Yukawa matrix of order 1. This is very appealing since it hints at a scale near the Grand Unification Scale [139], but the drawback is that this model requires a fine tuning in stabilizing the Higgs mass since quantum corrections to the Higgs mass in this model gives quadratic corrections in M_R. Furthermore, those scales would be impossible to test experimentally.

In the other extreme, $M_R = 0$, neutrinos are Dirac particles, which would recover lepton number symmetry but would imply Yukawa couplings of $y_\nu \sim \mathcal{O}(10^{-12})$ which is 6 orders of magnitude smaller than the electron one. Attempts to naturally obtain these couplings using extra dimension can be found in Refs. [140, 141]. In the case of small but nonzero Majorana masses (pseudo Dirac), solar neutrino oscillation data constrain these masses to be smaller than $M_R < 10^{-9}$ eV [142].

Anywhere between the two scales, (10^{-9} eV-10^{15} GeV), the right handed neutrino masses are possible by adjusting Yukawa couplings in the range 10^{-12} - 1.

Masses of 1 eV might explain short baseline anomalies. If the mass is at keV scale, the right-handed neutrinos could be a good warm dark matter candidate. Leptogenesis could be explained via the decay of sterile neutrinos at a mass scale above 10^7 GeV, or via oscillations if they are at $O(\text{GeV})$.

5.2 The Model

The model is an extension of the SM with N right handed neutrinos:

$$\mathcal{L} = \mathcal{L}_{SM} - \sum_{\alpha,i} \bar{L}^{\alpha} Y^{\alpha i} \tilde{\Phi} N_R^i - \sum_{i,j=1}^{N} \frac{1}{2} \bar{N}_R^{ic} M_R^{ij} N_R^j + h.c.,$$

where Y is $N \times N$ complex matrix. We will examine the number of parameters of this model following Ref. [143]. The general rule for a number of physical parameters is

$$N_{Phys} = N_{general} - N_{broken}. \tag{5.1}$$

$N_{general}$ are all the parameters in a generic Yukawa representation. N_{broken} is the difference of the numbers of parameters that define the symmetry groups for vanishing, and non-zero Yukawa couplings. We will also separate parameters on real (R), that will become angles and masses, and imaginary (I), that will describe phases. The matrices in the neutrino sector are 3×3 charged leptons Yukawa matrix, $3 \times N$ neutral leptons Yukawa matrix and $N \times N$ symmetric mass matrix of right-handed states. The number of free parameters is [1]:

$$I_{general} = R_{general} = 9 + 3N + N\frac{N+1}{2}. \tag{5.2}$$

In the case of vanishing Yukawa matrices the symmetry group is $U(3)$ for the left doublets, $U(N)$ for the right handed neutrinos, and $U(3)$ for the right handed charged leptons. After introducing non-zero masses there is no symmetry remaining so the total number of N_{broken} is :

$$R_{broken} = 3 + 3 + N\frac{N-1}{2}, \quad I_{broken} = 6 + 6 + N\frac{N+1}{2}, \tag{5.3}$$

[1] A general complex matrix of dimension $n \times m$ has has $I = R = n \times m$ parameters, a symmetric complex one of dimension n has $I = R = n\frac{n+1}{2}$, while a unitary matrix of dimension n has $R = n\frac{n-1}{2}$ and $I = n\frac{n+1}{2}$

that gives the total number of physical parameters:

$$R_{phys} = 3 + 4N, \quad I_{phys} = 3(N-1). \tag{5.4}$$

The number of zero modes in neutrino mass matrix is $3 - N$ (for $N \leq 3$) so the total number of mass parameters is:

$$R_{mass} = 3 + N + 3 - (3 - N) = 3 + 2N, \tag{5.5}$$

and the angles are the remaining real parameters:

$$R_{angles} = 2N. \tag{5.6}$$

All imaginary parameters are represented with phases:

$$N_{phases} = 3(N-1). \tag{5.7}$$

The model with only one extra right handed state can not describe observed neutrino oscillations data [143], hence $N = 2, 3$ or higher. The number of parameters for this two models are summarized in Table 5.1, where the mass parameters of the charged leptons have been taken out.

Table 5.1: Number of parameters for Type I Seesaw Models

Model	# zero modes	# m	# Angles	# Phases
$3+2$	1	4	4	3
$3+3$	0	6	6	6

5.3 Parametrization

One of the popular parametrization of this model is the Casas-Ibarra parametrization [144], that uses as input parameters the masses and mixings of the light neutrino sector, the masses of the heavy sector and a generic complex orthogonal matrix of dimensions N. The drawback of this parametrization is that it is valid only in the regime $M_R \gg m_Y$, or up to a non-unitarity effects. Here the more general parametrization from Ref. [145] will be described, which also accounts for non-unitarity effects.

The complete mass matrix of the neutrino sector after the electroweak symmetry breaking is, according to eq. (3.11):

$$M_\nu = \begin{pmatrix} 0 & m_Y \\ m_Y^T & M_R \end{pmatrix}, \tag{5.8}$$

with $m_Y \equiv Yv$.

It can be diagonalized with one unitary matrix

$$M_\nu = U^* Diag(m_l, M_h) U^\dagger, \tag{5.9}$$

where m_l and M_h are mass eigenstates of the light mostly active and the heavy mostly sterile neutrinos. If we write matrix U in terms of block matrices

$$U = \begin{pmatrix} U_{aa} & U_{as} \\ U_{sa} & U_{ss} \end{pmatrix}, \tag{5.10}$$

it can be shown, in all generality, that they can be parametrized as

$$\begin{aligned} U_{aa} &= U_{PMNS} H && (5.11)\\ U_{as} &= i U_{PMNS} H m_l^{1/2} R^\dagger M_h^{-1/2} && (5.12)\\ U_{as} &= i U_{PMNS} H m_l^{1/2} R^\dagger M_h^{-1/2} && (5.13)\\ U_{ss} &= \bar{H}. && (5.14) \end{aligned}$$

The matrix R is a generic orthogonal complex matrix that has one complex angle in the case of $N = 2$, or three complex angles in the case $N = 3$.

Matrices H and $\bar{H}$ are given in terms of mass eigenstates and R matrix

$$\begin{aligned} H^{-2} &= I + m_l^{1/2} R^\dagger M_h^{-1} R m_l^{-1/2} \\ \overline{H}^{-2} &= I + M_h^{1/2} R m_l R^\dagger M_h^{-1/2}. \end{aligned} \tag{5.15}$$

U_{PMNS} is a generic unitary matrix, which in the case of sufficiently heavy sterile neutrinos so that non-unitarity effects can be neglected ($H \to I + \mathcal{O}\left(\frac{m_l}{M_h}\right)$), can be identified with the standard PMNS matrix from eq. (3.31). This limit gives the Casas-Ibarra original parametrization.

5.4 Experimental constraints

If the heavy neutrinos are at electroweak scale they can be accessible in present experiments. Generally we can consider two types of experiments: the ones with the heavy neutrino as a final state particle, i.e. direct searches, and the ones where the heavy neutrino is a virtual off-shell particle, i.e. indirect searches. For now there is no experimental evidence for heavy neutrino states and the current experimental data can be translated in bounds on the active-sterile neutrino mixing angles, $U_{\alpha 4}$ depending on the heavy neutrino mass M_1 [2]. The most constraining bounds are presented in Figs. 5.2, 5.3, 5.4 and 5.5. For recent reviews on experimental constraints look at Refs. [146–149].

5.4.1 Kink searches

For masses roughly between 10 eV and 1 MeV, the most sensitive probe is the search for kinks in the β decay spectra. The electron energy is sensitive to the admixture of sterile neutrinos with the SM neutrinos, what induces a kink at the energy

$$E_k = E_e - M_1, \tag{5.16}$$

where E_e is the end point energy [3]. An example for unrealistically large mixing $\sin^2\theta = 0.2$ is presented in Fig. 5.1.

The bounds from different nuclei (^{187}Re [151], ^{3}Ht [152] , ^{63}Ni [153] , ^{35}S [154], ^{20}F [155]) are presented in Fig. 5.2. The limits are at 95% C.L, except the one from Ref. [155] which are at 90% C.L.

5.4.2 Peak searches

If the mass of the heavy neutrino M_1 is smaller than the mass of the pion and kaons, it can be produced in their leptonic decays. In that case the lepton spectrum would show the monochromatic line :

$$E_l = \frac{m_H^2 + m_l^2 - M_1^2}{2m_H}, \tag{5.17}$$

where m_H and m_l are the meson and lepton masses. The branching ratio of this decay compared to the branching ratio of the decay to the light SM neutrino is

[2] Even though we always discuss the bounds in the $U_{\alpha 4}$ vs M_1 plane, they apply to all the extra states

[3] See section 4.2 for more details.

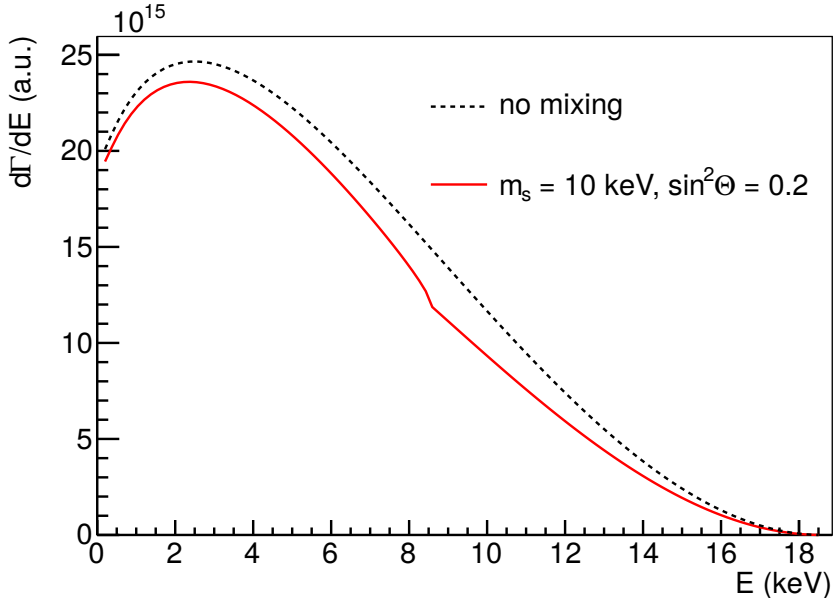

Figure 5.1: The kink in electron spectra induced by sterile neutrino compared to the spectra with no additional neutrinos (from Ref. [150])

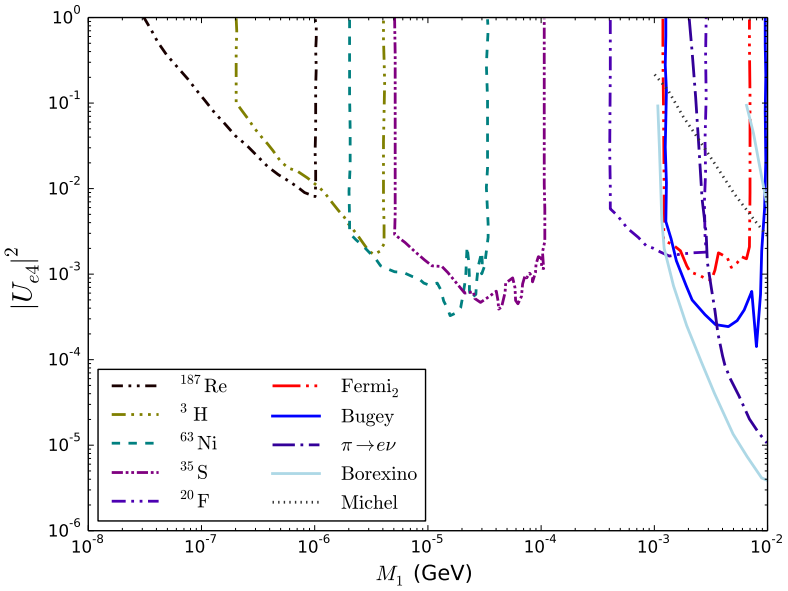

Figure 5.2: Bounds on $|U_{e4}|^2$ versus M_1 in the mass range 10 eV–10 MeV. The lines labeled as ^{187}Re, ^{3}H, ^{63}Ni, ^{35}S, ^{20}F and Fermi$_2$ [155] are bounds from kink searches, while $\pi \to e\nu$ bound is coming from peak searches [156]. The lines labeled as Borexino and Bugey are excluded at 90% C.L. by searches of heavy neutrinos decays from the Borexino Counting Test facility [157] and Ref. [158] respectively. The bound from Michel spectrum is at 99% C.L.

proportional to the mixing angle. Bounds coming from pion and kaons decays [156, 159, 160] are presented in Figs. 5.3, 5.4.

5.4.3 Beam dump experiments

Beam dump experiments are performed as follows : the proton beam is "dumped" in a fixed target, where a heavy neutrino, sufficiently light, might be produced in a decay of mesons. If no other interactions of the heavy neutrinos are assumed, its decay length is long enough that it does not decay inside the target, and placing the detector on a macroscopic distance from the target the decay of the heavy neutrino to the charged particles could be detected. Since no such decay has been observed, various experiments have placed a bound on the mixing angles PS191 [161], NuTeV [162], CHARM [163], CHARM II [164], NA3 [165], BEBC [166], FMMF [167] and NOMAD [168][4].

5.4.4 Production in the gauge boson decays

If the heavy neutrino is lighter than the Z boson, it can be produced in LEP experiments:

$$e^+e^- \to Z \to N_1\nu. \tag{5.18}$$

Those particles would decay as in the beam dump experiments, and the absence of their decay product can put a bound on the mixings with the active neutrinos. The bounds from DELPHI [170] and L3 [171] are presented in Figs. 5.3 and 5.4. If M_1 is heavier than the Z boson, it will be kinetically forbidden, but the total Z boson decay width to invisibles particles will be sensitive to extra neutrinos presence through nonunitarity of the U matrix [172].

5.4.5 Lepton number violating decays

Existence of Majorana neutrinos necessarily means that the lepton number is violated and that they can mediate lepton number violating decays [173–175]. In Ref. [146] the bounds from lepton number violating (LNV) decays are discussed, but in the case of more than one heavy neutrino the application of these bounds is not straightforward. Namely, in the case of the inverse seesaw, which corresponds to a special pattern of R matrix, such that an approximate lepton number symmetry exists, these bounds can always be avoided. One example of this is the popular νMSM [176, 177] with two neutrinos in GeV and one in keV mass range.

[4] In Ref. [169] it was pointed that using neutral current constraints from CHARM and PS191 stronger bounds on combination of mixings can be obtained.

In Ref. [178] LNV processes were shown to be sub-leading, further confirmed in Ref. [179]. For this reason, in all the work done for this thesis, the LNV bounds are not applied.

5.4.6 Lepton universality test

In the SM the coupling of the charge current interaction to the three lepton families is universal, i.e. $g_e = g_\mu = g_\tau$. Heavy neutrinos would change these couplings and the effect can be measured via the decays of mesons, bosons and leptons [180–183]. Even though these decays depend on hadronic effects, the uncertainties cancel to a high degree when ratios of decays are considered: $\frac{\Gamma(M\to l_\alpha\nu_\alpha)}{\Gamma(M\to l_\beta\nu_\beta)}$. The conservative bounds when $M_1 > M_W$, calculated in Ref. [149], are $|U_{e4}|^2 < 5.9\times10^{-3}$, $|U_{\mu4}|^2 < 2.5\times10^{-3}$ and $|U_{\tau4}|^2 < 5.9\times10^{-3}$.

5.4.7 Dipole moment

In Ref. [184] the impact of sterile neutrinos on charged lepton electric dipole moments was studied and they concluded that a significant contribution could be found if the sterile neutrino masses are above the electroweak scale. This measurement however does not provide model independent bounds at present.

5.4.8 Michel Spectrum

A heavy neutrino produced in a muon decay could change the electron energy spectra [185, 186]:

$$\frac{d\Gamma(\mu\to e\bar{\nu}\nu)}{dx} = \frac{G_F^2 m_\mu^5}{192\pi^3}\left(1-|U_{e4}|^2-|U_{\mu4}|^2\right)f(x,0,\rho)+\left(|U_{e4}|^2+|U_{\mu4}|^2\right)f(x,\delta,\rho)+\text{rad.cor.}, \tag{5.19}$$

where $x \equiv 2E_e/m_\mu$, $\delta \equiv M_1/m_\mu$, ρ is the Michel parameter predicted to be 3/4 in the SM and f is a function that describes the kinematics of the process and does not depend on the heavy neutrino mixing.

In Ref. [149], the TWIST data [187] is used to put a bound on the sum of two mixing matrix elements. Their bounds for the choice $|U_{e4}|^2 = |U_{\mu4}|^2$ are presented in Figs. 5.3 and 5.4 at 99% C.L.

5.4.9 Neutrino oscillation experiments

The strongest bounds for very light sterile neutrinos ($\sim \mathcal{O}(1)$ eV) are coming from the neutrino oscillation experiments. The experiments that have observed a hint for an eV sterile neutrino are explained in Chapter 4.

5.4.10 Electroweak precision tests

Heavy sterile neutrino can effect processes below their mass due to the mixings with the active ones [188, 189]. The effective muon decay is modified if the heavy neutrino mass is below muon mass

$$G_\mu = G_F \sqrt{(1 - |U_{\mu I}|^2)(1 - |U_{\mu I}|^2)}. \tag{5.20}$$

Furthermore, the bounds can be taken from the unitarity of the PMNS matrix and flavour changing neutral currents such as $\mu \to e\gamma$, $\mu \to ee^+e^-$ or $\mu - e$ conversions. However, those bounds are not competitive with direct searches in the mass regime we are interested in [146, 148].

5.4.11 Colider searches

Both ATLAS [190] and CMS [191] have performed a search for heavy neutrinos above 50 GeV looking for a same sign leptons pair and high p_T jet final state products, in the run $\sqrt{s} = 8$TeV . The ATLAS analysis is performed for both electrons and muons, while CMS has put the bound on $U_{\mu 4}$ only.

5.4.12 Future experiments

By increasing the flux of initial hadrons, the beam dump experiments can provide stronger bounds in the mass scale below the meson mass. One of proposed experiment is SHiP [192], that would use high intensity proton beam at CERN to search for sterile neutrinos in charmed meson decays. Another opportunity to improve present bounds is provided by the DUNE project (former LBNE) [133] where heavy neutrinos would be produced in the charmed mesons decays. For higher masses ($10 - 80$ GeV) the proposed FCC [193–195] a high luminosity Z-factory can provide bounds up to $|U|^2 \sim 10^{-12}$. These future bounds are summarized and compared in Fig. 5.6.

5.4.13 Neutrinoless double beta decay

A new particle would change the half-life of the neutrinoless double beta decay process by adding additional states in the sum

$$T_{0\nu}^{-1} = G^{0\nu} \left| \sum_i M^{0\nu}(m_i) \frac{U_{ei}^2 m_i}{m_e} + \sum_I M^{0\nu}(M_I) \frac{U_{eI}^2 M_I}{m_e}^2 \right|, \tag{5.21}$$

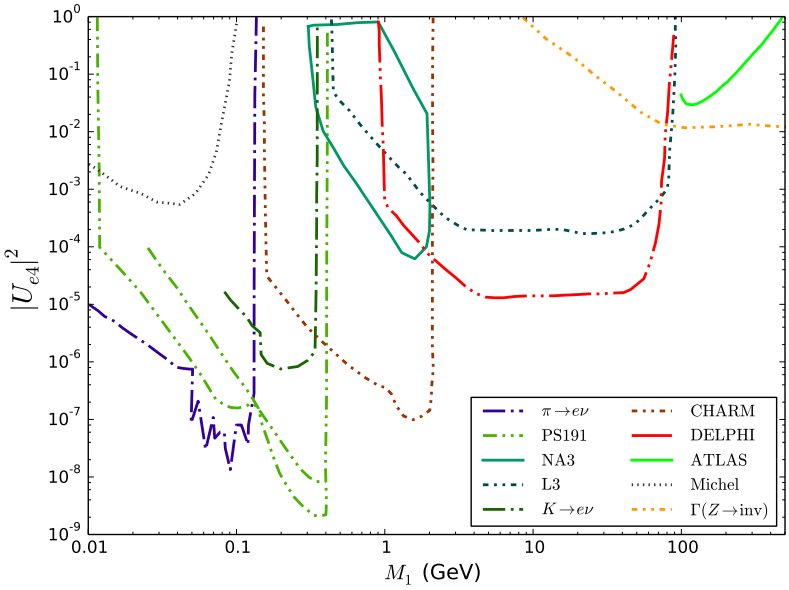

Figure 5.3: Bounds on $|U_{e4}|^2$ versus M_1 in the mass range 10 MeV–100 GeV. The contours labelled $\pi \to e\nu$ and $K \to e\nu$ are the bounds from peak searches [156, 159]. Limits for contours PS191, N13 and CHARM are at 90 % C.L , limits from DELPHI and L3 are at 95% C.L., and the limits from Michel spectrum and invisible Z decay are at 99% C.L.

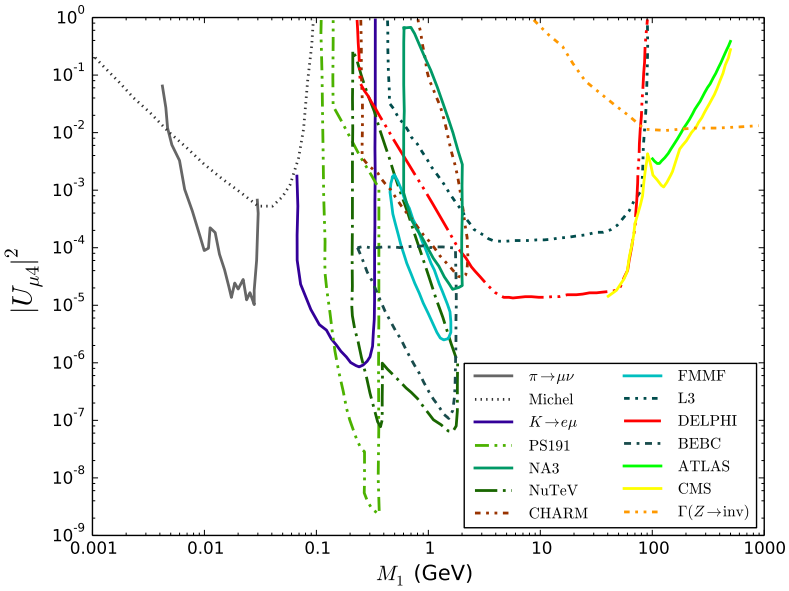

Figure 5.4: Limits on $|U_{\mu 4}|^2$ versus M_1 in the mass range 1 MeV–100 GeV come from peak searches and from ν_h decays. The area with the contour labelled $K \to \mu\nu$ [160] is excluded by peak searches. The bounds indicated by contours labelled by PS191, NA3, BEBC , FMMF, NuTeV and CHARMII are at 90% C.L., DELPHI and L3 are at 95% C.L., and the limits from Michel spectrum and invisible Z decay are at 99% C.L.

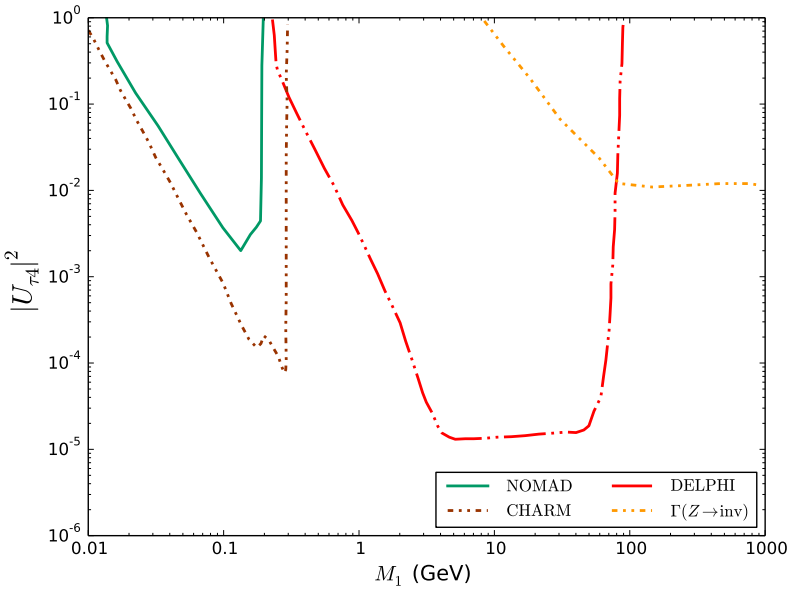

Figure 5.5: Bounds on $|U_{\tau 4}|^2$ versus M_1 from searches of decays of heavy neutrinos from CHARM, NOMAD (90% C.L.) and DELPHI (95 % C.L.) and invisible Z decay limit is at 99% C.L taken from Ref. [149]

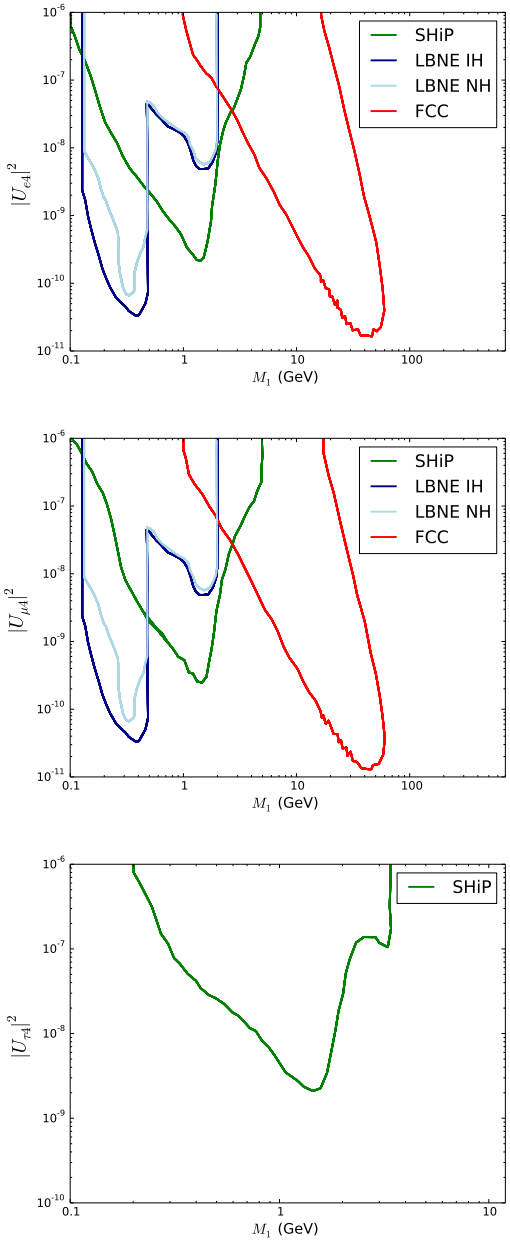

Figure 5.6: Predicted bounds for $|U_{e4}|^2$ (up), $|U_{\mu 4}|^2$ (middle) and $|U_{\tau 4}|^2$ (down) versus M_1 for SHiP [192], DUNE [133] and FCC [193–195] experiments, where DUNE curve depends on the light neutrino ordering.

where capital I denotes additional mass states, while i stands for standard light neutrinos. The dependence of nuclear matrix element on the mass of the sterile neutrinos has been calculated in the Ref. [196] and is presented in Fig. 5.7 for different nuclei. After factorizing a factor of the neutrino mass, the amplitude for this process contains a residual dependence on the neutrino mass through the neutrino propagator, i.e. $\sim \frac{1}{p^2+m_\nu^2}$, where p is the momentum of the propagating neutrino. Since the preferred momentum for the virtual neutrino in this process is 100 MeV [123,197], the behaviour of the curves is easy to understand. For masses below this value, the dominant term in the propagator is the momentum, hence the nuclear matrix element is almost independent on the neutrino mass. As the mass grows, it becomes dominant in the propagator, and the $M(m_\nu)$ decreases as $\sim m_\nu^{-2}$. The amplitude can be expressed as in eq. (4.3) with modified $m_{\beta\beta}$:

$$m_{\beta\beta} = \sum_i U_{ei}^2 m_i + \sum_I U_{eI}^2 M_I \frac{M^{0\nu}(M_I)}{M^{0\nu}(0)}; \tag{5.22}$$

where we assumed $M^{0\nu}(m_i) \sim M^{0\nu}(0)$ since $m_i \ll 100$ MeV. The parameter space where heavy neutrinos can dominate this process has been studied in [198–201].

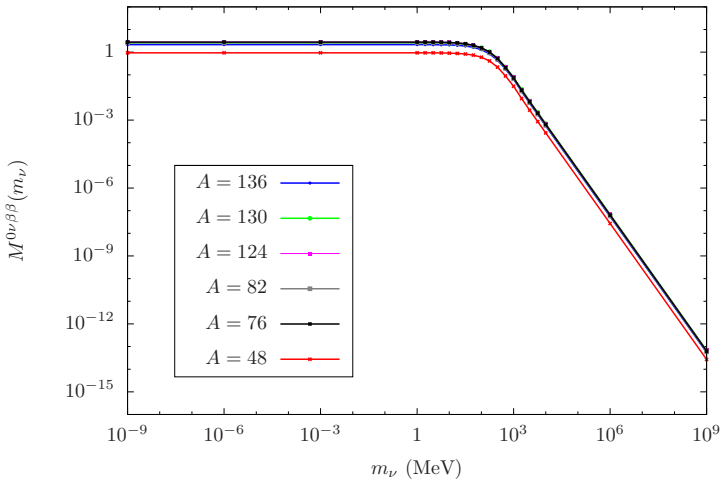

Figure 5.7: Nuclear matrix element versus neutrino mass for different nuclei (from Ref [196]).

As already mentioned, cosmology can be sensitive to the both the light and the extra heavy neutrinos. In the next chapters we will review the standard cosmological model, and, in particular, the neutrinos role in it.

Chapter 6

Overview of the Standard Cosmological model

In this chapter we will briefly review the Standard Cosmological Model. For more detailed discussion interested reader is referred to the standard books [202, 203].

6.1 The homogeneous and isotropic Universe

Originally the assumption of an isotropic (rotational invariant) and homogeneous (translational invariant) Universe was made to simplify the mathematical analysis. However, observations have confirmed the validity of this assumption: the difference of the cosmic microwave background temperature between any two points in the sky normalized by the averaged temperature is approximate 10^{-5}, so an homogeneous and isotropic Universe is indeed a good first order approximation.

With this simplification, the metric $g_{\mu\nu}$ can be written as

$$ds^2 \equiv g_{\mu\nu}dx^\mu dx^\nu = -dt^2 + a^2(t)\left[\frac{dr^2}{1-kr^2} + r^2(d\theta^2 + \sin^2\theta d\phi^2)\right], \qquad (6.1)$$

which is the so-called Friedman-Robertson-Walker (FRW) metric. Here, t is a physical time, and r, θ and ϕ are spatial comoving coordinates[1]. The scale factor $a(t)$ parametrizes the evolution of space-time and is defined up to an arbitrary

[1]Comoving coordinates do not "feel" the expansion of the Universe, the real physical distance is obtained multiplying comoving distances by the scale factor a.

constant rescaling. The parameter k represents the spatial curvature, and can take values $k = 0, +1, -1$ by suitable redefinition of the coordinate r. These three values corespond to a flat 3-dimensional plane, a positive curvature (i.e. a sphere) and a negative curvature space (i.e. hyperbolic), respectively. The value of the curvature today is very close to 0.

It is also convenient to define a conformal time τ as

$$d\tau \equiv \frac{dt}{a(t)}, \tag{6.2}$$

since the metric simplifies to a static Minkowski metric multiplied by a time dependent conformal factor:

$$ds^2 = a^2(\tau)\left[-d\tau^2 + \frac{dr^2}{1-kr^2} + r^2(d\theta^2 + \sin^2\theta d\phi^2)\right]. \tag{6.3}$$

Expressed in terms of the conformal time, the light cone ($ds^2 = 0$) corresponds to straight lines, as in a static space-time.

Free falling particles in the gravitatory field obeys the geodesic equation

$$\frac{d^2x^\mu}{d^2\lambda} + \Gamma^\mu_{\nu\rho}\frac{dx^\nu}{d\lambda}\frac{dx^\rho}{d\lambda} = 0, \tag{6.4}$$

where $\Gamma^\mu_{\nu\rho}$ is the affine connection (or Christoffel symbols) which are related to first derivatives of the metric:

$$\Gamma^\mu_{\nu\rho} = \frac{g^{\mu\sigma}}{2}\left(\frac{\partial g_{\sigma\rho}}{\partial x^\nu} + \frac{\partial g_{\nu\sigma}}{\partial x^\rho} - \frac{\partial g_{\nu\rho}}{\partial x^\sigma}\right). \tag{6.5}$$

For a massive particle, a 4-vector momentum can be defined as $P^\mu = m\frac{dx^\mu}{d\lambda}$, that satisfies the mass shell condition :

$$g_{\mu\nu}P^\mu P^\nu = -m^2. \tag{6.6}$$

where λ is a function of the proper time $d\lambda = d\tau/m \equiv \sqrt{-g_{\mu\nu}dx^\mu dx^\nu}/m$. From $P^0 \equiv dt/d\lambda$ follows

$$P^0\frac{dP^\mu}{dt} + \Gamma^\nu_{\nu\rho}P^\nu P^\rho = 0, \tag{6.7}$$

which in case of a flat Universe becomes:

$$E\left(\frac{dP^i}{dt} + 2\frac{\dot{a}}{a}P^i\right) = 0. \tag{6.8}$$

The ratio $\dot{a}/a \equiv H$ will often appear in the calculations and is called Hubble parameter. Its value today, the Hubble constant, H_0, is usually expressed in terms of a dimensionless parameter h as

$$H_0 = 100\ h\ \text{km s}^{-1}\text{Mpc}^{-1}, \tag{6.9}$$

where $h \sim 0.7$, depending on the different experimental datasets used to determine it.

One can also define physical momentum (such that $-E^2 + p^2 = -m^2$):

$$p^i = a(t)P^i. \tag{6.10}$$

Then eq. (6.8) gives:

$$\dot{p^i} + \frac{\dot{a}}{a}p^i = 0, \tag{6.11}$$

and the scaling of the two momenta are therefore

$$P^i \sim a^{-2}, p^i \sim a^{-1}. \tag{6.12}$$

In the case of massless particles[2] eq. (6.7) still holds provided $g_{\mu\nu}P^\mu P^\nu = 0$, and leads to the relation between the observed and emitted photon wavelengths:

$$\frac{\lambda_{obs}}{\lambda_{em}} = \frac{E_{obs}}{E_{em}} = \frac{a(t_{obs})}{a(t_{em})} \equiv 1 + z. \tag{6.13}$$

The parameter z is called redshift. When representing a redshift of a given object, $a(t_{obs})$ is the scale factor today:

$$z = \frac{a_0}{a_{em}} - 1. \tag{6.14}$$

The change in the metric in the presence of matter is described by Einstein's field equations of General Relativity:

$$R_{\mu\nu} - \frac{1}{2}g_{\mu\nu}R + \Lambda g_{\mu\nu} = 8\pi G T_{\mu\nu}. \tag{6.15}$$

The Ricci tensor ($R_{\mu\nu}$) and scalar ($R = g_{\mu\nu}R^{\mu\nu}$) are expressed through the affine connections:

$$R_{\mu\nu} = \frac{\partial\Gamma^\sigma_{\mu\nu}}{\partial_{x^\sigma}} - \frac{\partial\Gamma^\sigma_{\mu\sigma}}{\partial_{x^\nu}} + \Gamma^\sigma_{\rho\sigma}\Gamma^\rho_{\mu\nu} - \Gamma^\sigma_{\rho\nu}\Gamma^\rho_{\mu\sigma}. \tag{6.16}$$

[2]Note that in the case of massless particles λ can not be chosen as proper time.

G is the Newton constant and defines a mass scale (the Planck mass) in natural units:

$$M_{Pl} = G^{-1/2} = 1.22 \times 10^{19}\text{GeV}. \tag{6.17}$$

The cosmological constant Λ causes the observed accelerated expansion of the Universe[3]. Finally the energy-momentum tensor ($T_{\mu\nu}$) gets a contribution from all the matter species that fill the Universe. It is symmetric and is covariantly conserved:

$$\nabla_\mu T^{\nu\mu} = \frac{\partial T^{\mu\nu}}{\partial x^\mu} + \Gamma^\nu_{\mu\rho} T^{\rho\mu} + \Gamma^\mu_{\mu\rho} T^{\nu\rho} = 0. \tag{6.18}$$

Eq. (6.15) can be derived via the principle of least action ($\delta S = 0$) from the Hilbert-Einstein action:

$$S = \int d^4x \sqrt{-detg_{\mu\nu}} \left(\frac{1}{16\pi G} (R - 2\Lambda) + L_m \right), \tag{6.19}$$

where L_m is the matter Lagrangian whose variation with respect to the metric gives rise to the energy-momentum tensor $T_{\mu\nu}$.

In many applications it is a good approximation to describe the primordial plasma as a perfect fluid with no viscosity:

$$T_{\mu\nu} = (\rho + p) u^\nu u^\mu + p g^{\mu\nu}, \tag{6.20}$$

where ρ and p are the fluid energy density and pressure, and u^μ is a 4-component velocity vector of the fluid. If the fluid has zero velocity in the comoving frame ($u^\mu = (1, 0, 0, 0)$), the energy tensor is of the form

$$T^\mu_\nu = Diag(-\rho, p, p, p). \tag{6.21}$$

The energy conservation law (setting $\mu = 0$ in eq. (6.18)) gives:

$$0 = \frac{d\rho}{dt} + \frac{3\dot{a}}{a} (\rho + p), \tag{6.22}$$

which can be easily solved for an equation of the state in the form $p = \omega\rho$,

$$\rho \propto a^{-3(1+\omega)}, \tag{6.23}$$

where ω is time independent.

For example, cold matter (e.g. dust) has $\omega_{matter} = 0$ and the energy density is $\rho_{matter} \propto a^{-3}$, while hot matter (e.g. radiation) has $\omega_{rad} = \frac{1}{3}$ which gives

[3]Historically the cosmological constant term was introduced to explain a "static" Universe.

$\rho_{rad} \propto a^{-4}$. Note that cosmological constant term can also be redefined as a term in the stress-energy tensor:

$$T_{\mu\nu,\Lambda} = -\frac{\Lambda}{8\pi G} g_{\mu\nu}, \tag{6.24}$$

so that $\rho_\Lambda = -p_\Lambda$ ($\omega_\Lambda = -1$) and eq. (6.23) gives $\rho_\Lambda =$ constant.

Eqs. (6.1),(6.20), (6.15) determine the dynamics of the evolution. The 0-0 and spatial components of the eq. (6.15) give[4]:

$$\begin{aligned} -\frac{2k}{a^2} - \frac{2\dot{a}^2}{a^2} - \frac{\ddot{a}}{a} &= -4\pi G(\rho - p); \\ \frac{3\ddot{a}}{a} &= -4\pi G(3p + \rho). \end{aligned} \tag{6.25}$$

Adding three times the first equation to the second leads to the familiar Friedmann equation:

$$\frac{\dot{a}^2}{a^2} + \frac{k}{a^2} = \frac{8\pi G}{3}\rho. \tag{6.26}$$

Note that the cosmological constant term is embedded in the $T_{\mu\nu}$ term as in eq. (6.24), i.e. ρ appearing here is $\rho = \rho_{matter} + \rho_{rad} + \rho_\Lambda$.

If there is a single dominant contribution to ρ and in the case of a flat Universe ($k = 0$) the solution of eq. (6.26) is simple:

$$a(t) = \begin{cases} t^{\frac{2}{3(1+\omega)}} & \omega \neq -1, \\ e^{\bar{H}t} & \omega = -1, \end{cases} \tag{6.27}$$

where $\bar{H}$ is a constant. Hence, for the radiation dominated Universe $a \propto \sqrt{t}$ and for matter dominated Universe $a \propto t^{2/3}$.

The Friedman equation can also be written in terms of a critical density

$$\rho_c \equiv \frac{3H^2}{8\pi G}, \tag{6.28}$$

as

$$\Omega(a) - 1 = \frac{k}{H^2 a^2}, \tag{6.29}$$

where $\Omega(a) \equiv \rho/\rho_c$. We can also define $\Omega_K \equiv -\frac{k}{H^2 a^2}$.

[4] R_{i0} is a three-vector and must vanish due to the isotropy of the metric so those equations are not relevant.

An important concept in cosmology are horizons. An event horizon defines a set of points from which a signal sent at time τ will never be observed in the future.

A particle horizon is the maximum comoving distance that a given particle can propagate in the time interval $t - t_i$:

$$\chi_p(t) = \int_{t_i}^{t} \frac{dt'}{a(t')}. \tag{6.30}$$

The physical size of a particle horizon is

$$d_p(t) = a(t)\chi_p. \tag{6.31}$$

It is usual to choose $t_i = 0$, which determines the beginning of the Universe ("The Big Bang"):

$$\chi_p(t) = \int_0^t \frac{dt'}{a(t')} = \int_0^{a(t)} \frac{da}{Ha^2} = \int_z^\infty \frac{dz'}{H(z')}, \tag{6.32}$$

where z is the redshift.

The relation between conformal time (comoving distance) with the observables luminosity distance (for point like sources) and angular distance (for extended objects) is

$$d_L = a_0\chi_p^2(1+z), \tag{6.33}$$

$$d_A = \frac{a_0\chi_p^2}{(1+z)^2}, \tag{6.34}$$

$$\tag{6.35}$$

where a flat Universe is assumed[5].

6.2 Expansion stages

In this section we will review expansion stages of the Universe, from popular inflation theories until the present time.

6.2.1 Inflation

The conventional Big Bang Theory confronts two main problems, the so-called flatness and horizon problems. The flatness problem is related to the curvature

[5]In the case of $k \neq 0$ instead of χ^2 will be $\sinh^2\chi$ for $k = -1$ and $\sin^2\chi$ for $k = +1$.

contribution to the total energy (6.29) which increases in time if $\ddot{a} < 0$. At sufficiently early times, the curvature contribution to the total energy in front of the one from the radiation and matter in eq. (6.26) can be neglected since the radiation and matter contribution grows as $a \to 0$:

$$\Omega_K = -\frac{|k|}{a^2 H^2} \sim |k| a^{1+3\omega}. \tag{6.36}$$

Observations show that the density today is close to the critical one, which implies Ω_K is close to 0. If $1+3\omega > 0$, which is the case of matter and radiation dominated evolution, one should fine tune the curvature radius in the early Universe to extremely small-scale. To put some numbers, if $\Omega_K < 1$ today then at the temperatures $\sim 10^{10}$ K, Ω_K has to be smaller than 10^{-16}.

The second problem refers to the homogeneity of the Universe. As will be discussed later at a redshift of $z \sim 10^3$ the Universe became transparent to photons, and formed the Cosmic Microwave Background (CMB), which is homogeneous up to very small fluctuations $\delta T/T \sim 10^{-5}$ over all 4π solid angle. Since the comoving particle horizon is a growing function of time:

$$\chi_p \sim a^{(1+3\omega)/2}, \tag{6.37}$$

the horizon distance of the photons at the last scattering surface assuming the Universe was radiation and matter dominated would be seen today at around 1.6°. This means that the photons coming from larger angles were never casually connected, and the smoothness of the CMB cannot be explained.

In the pioneering work of Starobinsky [204] and Guth [205], it was proposed to solve these problems by assuming a period of accelerated expansion prior to the radiation dominated Universe. In this case the comoving Hubble radius ($(aH)^{-1}$) is decreasing, Ω_K from eq. (6.36) will be driven to small values, i.e. to a flat Universe. Eq. (6.32) can be rewritten in terms of comoving Hubble radios as $\chi_p(t) = \int_0^a d \ln a \left(\frac{1}{aH}\right)$, which mean that if at some point Ha was decreasing, the particle horizon today could be much larger than Ha today, ie that the particles can not communicate now, but were causally connected in the past. The sketch of how accelerated expansion solves horizon problem is given in Fig. 6.1. The three equivalent conditions for inflation are decreasing Hubble radios, accelerated expansion and negative pressure:

$$\frac{d}{dt}\left(\frac{1}{aH}\right) < 0 \Rightarrow \frac{-\ddot{a}}{(Ha)^2} < 0 \Rightarrow \ddot{a} > 0 \Rightarrow (3p + \rho) < 0. \tag{6.38}$$

The negative pressure is usually modeled with a scalar field with potential energy much greater than the kinetic energy ("slow roll inflaton"). The scalar field is usually coupled with ordinary mater, and when the inflation finishes (when the kinetic energy becomes comparable to the potential one), the decay products are ordinary radiation. This period is called reheating. A review on inflation theories can be found at [206].

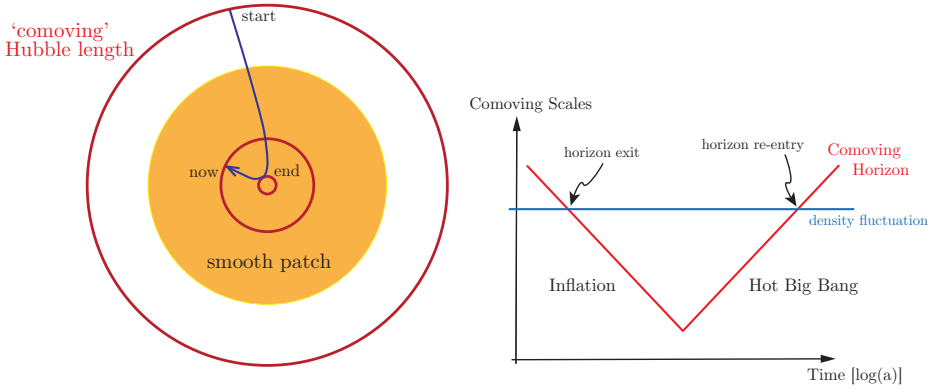

Figure 6.1: Left: The comoving Hubble radios before and after inflation. Right: At sufficiently early times all scales relevant for cosmology were inside the Hubble radios, ie casually connected. Similarly, at relatively recent times the scales come back within the Hubble radius(from Ref. [206]).

6.2.2 Radiation and matter dominated

After inflation is over, the energy density of the Universe becomes dominated by radiation $\rho_R \sim a^{-4}$, and later on, by matter $\rho_M \sim a^{-3}$. The thermodynamics of this period will be explained in the next chapter. Here we will just list the phenomena that are relevant for this period:

- Baryon asymmetry generation. The present dominance of matter over antimatter can be understood if some baryon number violating process took place in the early Universe. The temperature of this process is not known but is likely to exceed electroweak phase transition $T \sim 100$GeV, at least in the popular models of baryogenesis through leptogenesis.

- Electroweak phase transition. At around $T \sim 100$ GeV the SM gauge group was spontaneously broken and particles became massive. Before this period

lepton and baryon number were broken through non-perturbative sphaleron processes.

- Quark-gluon transition. At around $\Lambda_{QCD} \sim 200$ MeV quarks hadronize and become confined in baryons and mesons. This process is still not fully understood theoretically.

- Primordial nucleosynthesis. At around $T \sim$ MeV weak interactions are no longer efficient and neutrinos decouple from the plasma, which leads to an almost constant value of proton-to-neutron ratio.

- As temperature drops below the electron mass all antibaryons have disappeared and the parameter

$$\eta_B = \frac{n_B - \overline{n}_B}{n_\gamma} \sim \frac{n_B}{n_\gamma}, \tag{6.39}$$

  remains constant as long as the photon density scale as $1/a^3$. The baryon fractional density can be expressed as :

$$\Omega_B = \frac{m_N n_B}{\rho_{c,0}} = \eta_B \frac{m_N n_{\gamma,0}}{\rho_{c,0}} \sim 0.365 \times 10^8 \eta_B h^{-2}. \tag{6.40}$$

- Matter-radiation equality. Since the temperature is decreasing with time, eventually most of the particles will become non relativistic and the energy density will be dominated by matter, which happens at $T \sim 0.7$ eV.

- At around $T \sim 0.1$ eV the matter becomes transparent to radiation, and photons move almost unperturbed along null geodesics. This moment is called last scattering, and gives the image of the CMB that is seen today. The CMB image is not completely homogeneous, and anisotropies can be explained adding primordial perturbations to the metric.

- Once the Universe is matter-dominated the large scale structures (LSS) start forming. The primordial perturbations, amplified by gravitational instabilities, lead to the formation of clusters and galaxies.

6.2.3 Dark Energy dominated

Two independent experimental groups found that the expansion of the Universe today (at small redshifts $z \leq 1$) is accelerated [207, 208]. The evidence

came from observing the luminosity distance of Type I supernovae (the "standard candles" since the wavelength of emitted photons is known), which showed that they appear fainter than expected in typical matter dominated expansion. This observation can be explained by the acceleration of the expansion at late times. From eq. (6.26) this condition leads to $p \leq -\rho/3$, and a cosmological constant with $p = -\rho$ is a very good fit. The combined analysis of CMB spectra and supernova data fit the current energy content of the Universe to be a large fraction of Dark Energy $\Omega_\Lambda = 0.694$, smaller fraction of cold matter $\Omega_C = 0.258$, and even smaller baryon content $\Omega_B = 0.048$, while $\Omega_K \simeq 0$ [128]. The origin of Dark Energy and cold non-baryonic matter (conventionally named Dark Matter) are yet to be explained. The most popular models for Dark Matter are the ones including a weakly interacting massive particle (WIMP) that would be produced and decoupled early in the history of the Universe, giving the right abundance today, but such a particle has not yet been detected.

The evolution of the Universe is summarized in Fig. 6.2.

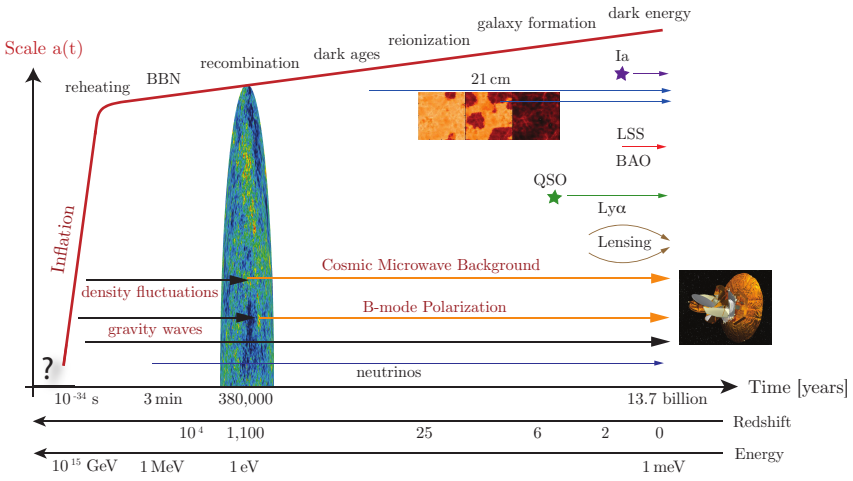

Figure 6.2: Graphical representation of the evolution of the Universe (from Ref. [206]).

Chapter 7

Thermodynamics of the Early Universe

After inflation the Universe contained a very hot plasma made of all the particles known. Before reviewing useful thermodynamical quantities we will briefly discuss the meaning of the thermal equilibrium condition in an expanding Universe.

7.1 Equilibrium Thermodynamics

Equilibrium is reached by interactions that are either scatterings processes (that redistribute particle momenta and are essential for kinetic equilibrium) and interactions that do not conserve the number of a given species and are responsible for chemical equilibrium. A more precise way of evolving particles in the expanding Universe is by using kinetic theory, but a useful rule of thumb to ensure that a given species is in thermal equilibrium is to compare its interaction rate ($\Gamma(T)$) with the rate of expansion of the Universe, given by the Hubble parameter ($H(T)$). As long as

$$\Gamma(T) > H(T), \tag{7.1}$$

holds, the particle is in thermal equilibrium. If at some temperature, the interaction rate falls below the Hubble rate the species decouples from the plasma. This happens at the so called decoupling temperature (T_d) that satisfies

$$\Gamma(T_d) = H(T_d). \tag{7.2}$$

Note that even when decoupling will always extend over some range of temperatures, the approximation of instantaneous decoupling already gives good results, as will be demonstrated in the example of neutrino decoupling.

The number density n, energy density ρ and pressure p of a diluted weakly-interacting gas are:

$$n = \frac{g}{(2\pi)^3}\int f(p)d^3p \tag{7.3}$$

$$\rho = \frac{g}{(2\pi)^3}\int E(p)f(p)d^3p \tag{7.4}$$

$$p = \frac{g}{(2\pi)^3}\int \frac{p^2}{3E}f(p)d^3p. \tag{7.5}$$

Here, g is the number of internal degrees of freedom, $f(p)$ is a phase space distribution function and $E^2 = p^2 + m^2$.

The momentum distribution of fermions/bosons in kinetic equilibrium is the Fermi-Dirac/Bose-Einstein distribution:

$$f(p) = \frac{1}{e^{E-\mu} \pm 1}, \tag{7.6}$$

where +1 stands for Fermi-Dirac and -1 for Bose-Einstein. μ is the chemical potential of the species. Chemical equilibrium implies that the sum of chemical potentials of species that interact is the same as the sum of chemical potentials of the products of the interaction. For example, in the interaction of species i, j, k and l

$$i + j \leftrightarrow k + l, \tag{7.7}$$

the relation between chemical potentials is

$$\mu_i + \mu_j = \mu_l + \mu_k. \tag{7.8}$$

Note that whenever reaction of type particle + antiparticle $\leftrightarrow \gamma + \gamma$ occurs, the chemical potential of particles and antiparticles will have equal magnitude and opposite sign[1].

[1] Chemical potential of photon gas in equilibrium is always 0.

Replacing eq. (7.6) in (7.5) gives:

$$n = \frac{g}{2\pi^2}\int_m^\infty \frac{(E^2-m^2)^{1/2}}{e^{(E-\mu)/T}\pm 1}EdE, \tag{7.9}$$

$$\rho = \frac{g}{2\pi^2}\int_m^\infty \frac{(E^2-m^2)^{1/2}}{e^{(E-\mu)/T}\pm 1}E^2dE, \tag{7.10}$$

$$p = \frac{g}{6\pi^2}\int_m^\infty \frac{(E^2-m^2)^{3/2}}{e^{(E-\mu)/T}\pm 1}dE, \tag{7.11}$$

and the integral for $\mu = 0$ and $m \ll T$ leads to

$$\rho = 3p = \begin{cases} \frac{\pi^2}{30}gT^4 & \text{(BOSE)}, \\ \frac{7}{8}\frac{\pi^2}{30}gT^4 & \text{(FERMI)}, \end{cases} \tag{7.12}$$

$$n = \begin{cases} \frac{\zeta(3)}{\pi^2}gT^3 & \text{(BOSE)}, \\ \frac{3}{4}\frac{\zeta(3)}{\pi^2}gT^3 & \text{(FERMI)}. \end{cases} \tag{7.13}$$

The average energy per particle in this case is

$$\langle E\rangle \equiv \frac{\rho}{n} = \frac{\pi^4}{30\zeta(3)}T \simeq 2.701\text{(BOSE)}, \tag{7.14}$$

$$\langle E\rangle \equiv \frac{\rho}{n} = \frac{7\pi^4}{180\zeta(3)}T \simeq 3.151\text{(FERMI)}. \tag{7.15}$$

For relativistic fermions and for $|\mu| \ll T$ the approximate formulas are

$$n = \frac{3}{4}\frac{\zeta(3)}{\pi^2}gT^3\left(1+\frac{\pi^2}{9\zeta(3)}\frac{\mu}{T}+\frac{ln(4)}{3\zeta(3)}\frac{\mu^2}{T^2}+...\right), \tag{7.16}$$

$$\rho = 3p = \frac{7}{8}\frac{\pi^2}{30}gT^4\left(1+\frac{540\zeta(3)}{7\pi^4}\frac{\mu}{T}+\frac{30}{7\pi^2}\frac{\mu^2}{T^2}+...\right). \tag{7.17}$$

For relativistic bosons and $m < |\mu| \ll T$ [2]:

$$n = \frac{\zeta(3)}{\pi^2}gT^3\left(1+\frac{\pi^2}{6\zeta(3)}\frac{\mu}{T}+...\right) \tag{7.18}$$

$$\rho = 3p = \frac{\pi^2}{30}gT^4\left(1+\frac{90\zeta(3)}{\pi^4}\frac{\mu}{T}+...\right). \tag{7.19}$$

[2] If the chemical potential of boson gas is smaller than its mass it means that the Bose-Einstein condensate forms, a case that has to be studied separately.

The difference between particles and antiparticles is an often used quantity

$$n - \bar{n} = \begin{cases} \frac{g}{3} T^2 \mu & \text{(BOSE)}, \\ \frac{g}{6} T^2 \mu & \text{(FERMI)}. \end{cases} \tag{7.20}$$

In the non-relativistic limit ($m \gg T$) the distribution of fermions and bosons are the same and reduce to the Maxwell-Boltzmann one:

$$n = g \left(\frac{mT}{2\pi} \right)^{3/2} e^{-\frac{m-\mu}{T}}, \tag{7.21}$$

$$\rho = mn, \tag{7.22}$$

$$p = nT \ll \rho, \tag{7.23}$$

and the average energy is

$$\langle E \rangle = m + \frac{3}{2} T. \tag{7.24}$$

Note that the number and energy density of non-relativistic particle in thermal equilibrium in the case of vanishing chemical potential is Boltzmann suppressed $\sim e^{-m/T}$. However, this is not the case for species that carry conserved charge, such as lepton and baryon number at low temperatures, that have a chemical potential associated to a conserved charge.

It is convenient to express total energy density and pressure of all species in equilibrium in terms of photon temperature T:

$$\rho_T = T^4 \sum_i \left(\frac{T_i}{T} \right)^4 \frac{g_i}{2\pi^2} \int_{x_i}^{\infty} \frac{(u^2 - x_i)^{1/2} u^2 du}{e^{u - \xi_i} \pm 1}, \tag{7.25}$$

$$p_T = T^4 \sum_i \left(\frac{T_i}{T} \right)^4 \frac{g_i}{6\pi^2} \int_{x_i}^{\infty} \frac{(u^2 - x_i)^{3/2} du}{e^{u - \xi_i} \pm 1}, \tag{7.26}$$

where x_i and ξ_i are mass and chemical potential normalized to the photon temperature: $x_i \equiv \frac{m_i}{T}$ and $\xi_i \equiv \frac{\mu}{T}$. The summation includes all species that obey Fermi-Bose distribution, taking into account that their temperature (T_i) might be different to the photon one if they are decoupled, as for example, the neutrino temperature that will be discussed later.

For further discussion we will neglect chemical potential of all species.

Since for non-relativistic particles the energy density and pressure are exponentially suppressed ($\sim e^{-m_i/T_i}$) it is a good approximation to assume that the main contribution to the total energy density and pressure will be the one of the

relativistic particles, i.e. radiation. In that case eq. (7.25) simplifies to:

$$\rho_R = 3p_R = \frac{\pi^2}{30} g_* T^4, \tag{7.27}$$

where g_* counts all effectively massless degrees of freedom:

$$g_* = \sum_{i=bosons} g_i \left(\frac{T_i}{T}\right)^4 + \frac{7}{8} \sum_{i=fermions} g_i \left(\frac{T_i}{T}\right)^4. \tag{7.28}$$

Another important thermodynamic quantity is entropy. In equilibrium conditions entropy in a comoving volume is constant:

$$s(T)a^3 = constant. \tag{7.29}$$

From the second law of thermodynamics the entropy density is[3]:

$$s = \frac{\rho + p}{T}. \tag{7.30}$$

Again, the entropy density will be dominated by the relativistic particles

$$s = \frac{2\pi^2}{45} g_{*S} T^3, \tag{7.31}$$

where

$$g_{*S} = \sum_{i=bosons} g_i \left(\frac{T_i}{T}\right)^3 + \frac{7}{8} \sum_{i=fermions} g_i \left(\frac{T_i}{T}\right)^3. \tag{7.32}$$

Eqs. (7.29) and (7.31) imply that whenever g_{*S} is kept unchanged, the temperature scales as $T \sim 1/a$. When a particle becomes non-relativistic and disappears (when $m \gg T$), the number and energy density are exponentially suppressed, eq. (7.21) and g_{*S} will change. When g_{*S} changes the temperature evolves as:

$$T \propto g_{*S}^{1/3} a^{-1}. \tag{7.33}$$

If a massless particle that was initially in thermal equilibrium decouples from the plasma it will not "share" its energy with the plasma any more, the phase-space distribution will remain as the equilibrium one and the expansion of the Universe will just redshift momenta with the scale factor. In practice this is

[3]It is straightforward to include chemical potential, in that case $TdS = d(\rho V) + pdV - \mu d(nV)$ and $s = (\rho + p - \mu n)/T$).

equivalent to saying that the temperature of the species after decoupling scales as $T \propto a^{-1}$, independently of how the temperature of the plasma evolves from that point.

During the evolution of the Universe, almost all the particles have stayed in the equilibrium until they became non-relativistic, leading to $g_{*S} = g_*$. The only exception were neutrinos, that decoupled at the temperature $T_D \sim 1$ MeV, i.e. while still being relativistic. The process of decoupling of neutrinos triggers light elements production, the so called Big Bang Nucleosynthesis (BBN). As previously discussed, the momentum distribution of neutrinos will remain as the equilibrium one, and the temperature T_ν will scale as $1/a$. After neutrino decoupling the only relativistic particles in equilibrium are photons and electrons, at the same temperature as decoupled neutrinos, with

$$g_{*S} = 2 + \frac{7}{8} \times 4 = \frac{11}{2}. \tag{7.34}$$

When temperature drops below electron mass, only photons remain, hence $g_{*S} = 2$. From the entropy conservation in the plasma before and after electrons become non-relativistic, it follows:

$$\frac{T}{T_\nu} = \left(\frac{11}{4}\right)^{1/3}, \tag{7.35}$$

where T is the temperature of the photons. Today the temperature of the photons is 2.725 K, leading to $T_\nu \simeq 1.95$ K. The evolution of g_* and g_{*S} as a function of temperature is given in Fig. 7.1.

During the radiation dominated expansion, the Hubble expansion is

$$H(T) = \sqrt{\frac{8\pi G}{3} g_* \frac{\pi^2}{30} T^4} \sim \sqrt{g_*} \frac{T^2}{M_{pl}}. \tag{7.36}$$

7.2 Boltzmann equation

A way to describe non-equilibrium production or decoupling of particles is to use the Boltzmann kinetic equation that describes the evolution of the phase space distribution $f[p, x]$:

$$\hat{L}[f] = C[f], \tag{7.37}$$

where $\hat{L}$ is the Liouville operator and C is the collision integral.

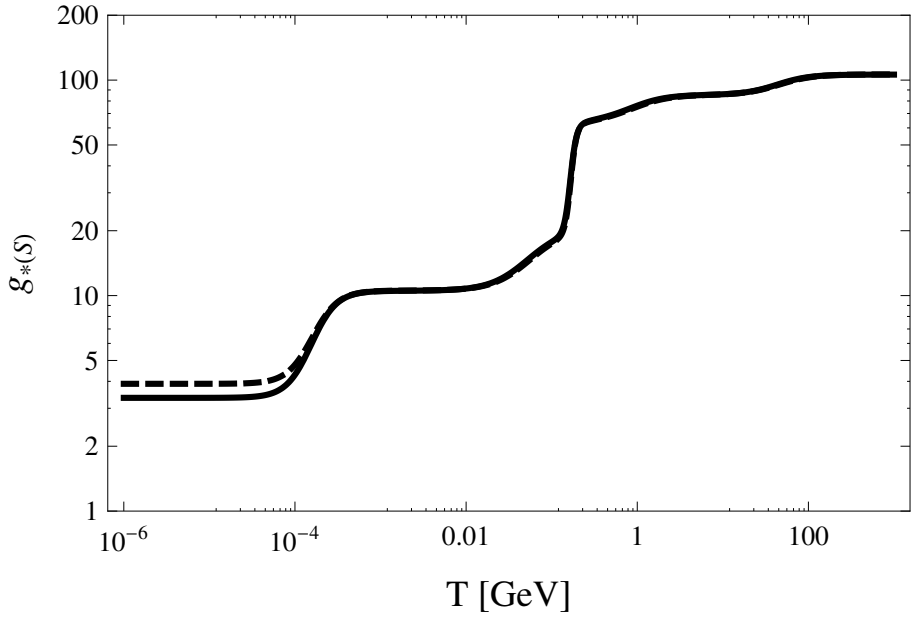

Figure 7.1: Evolution of $g_\star$ (solid line) and $g_{\star S}$ (dashed line) as a function of temperature.

The relativistic form of Liouville operator is

$$\hat{L} = p^\alpha \frac{\partial}{\partial x^\alpha} - \Gamma^\alpha_{\beta\gamma} p^\beta p^\gamma \frac{\partial}{\partial p^\alpha}. \tag{7.38}$$

For the FRW metric and spatially homogeneous and isotropic phase space the Boltzmann equation is

$$\hat{L}[f(E,t)] = E\frac{\partial f}{\partial t} - H|p|^2 \frac{\partial f}{\partial E}. \tag{7.39}$$

The collisional integral accounts for all the processes where a given particle is produced or annihilated. For example, in the case of $a + b \to c + d$ scattering, the collision integral for production/ annihilation of particle a would be:

$$C[f_a] = \frac{1}{E_a}\int d\pi(p_b) d\pi(p_c) d\pi(p_d) (2\pi)^4 \delta^{(4)}(p_a + p_b - p_c - p_d) \times \tag{7.40}$$

$$\Big[|M_{cd,ab}|^2 f_c(p_c,t) f_d(p_d,t)(1 \pm f_a(p_a,t))(1 \pm f_b(p_b,t)) \tag{7.41}$$

$$- |M_{ab,cd}|^2 f_a(p_a,t) f_b(p_b,t)(1 \pm f_c(p_c,t))(1 \pm f_d(p_d,t)) \Big]. \tag{7.42}$$

The relativistic measure is $d\pi(p) \equiv \frac{d^3p}{(2\pi)^3 2E(p)}$, and the Dirac delta ensures conservation of energy and momentum. $|M_{cd,ab}|$ and $|M_{ab,cd}|$ are amplitudes for the processes $c+d \to a+b$ and $a+b \to c+d$, and if the processes are invariant under the time reversal the amplitudes are the same and the expression has simpler form. Finally $\pm$ sign is the consequence of different statistics of fermions (minus sign, consequence of Pauli blocking) and bosons (plus sign). In the case of a diluted system and negligible chemical potential the gas obeys classical statistics and those factors become unities.

Note that this form of collisional integral is a consequence of molecular chaos, that the particle momenta is uncorrelated to their position. In that case the total number of particles of type a and type b is given simply by the product of two one-particle phase space distributions, i.e. there are no two-particle correlation functions (f_{ab}).

Written in terms of number density the Boltzmann equation is:

$$\frac{dn}{dt} + 3Hn = \frac{g}{(2\pi)^3}\int C[f]\frac{d^3p}{E}. \tag{7.43}$$

This equation is a good tool for describing particle freeze-out. As mentioned in the previous section a massive particle that remained in thermal equilibrium

would have negligible abundance ($\propto \exp(-m/T)$), but if the particle freezes-out at the temperature $T \geq m$ it can have a significant relic abundance. Looking again at the $a + b \leftrightarrow c + d$ process, under the simplification that the amplitudes for the direct and inverse processes are the same, and that the particles b,c and d are in thermal equilibrium with small chemical potential, the Boltzmann equation for the density of particle a becomes

$$Ha\frac{dn_a}{da} + 3Hn_a = \int d\pi(p_b)d\pi(p_c)d\pi(p_d)(2\pi)^4\delta^{(4)}(p_a + p_b - p_c - p_d) \times \quad (7.44)$$

$$|M_{ab,cd}|^2[e^{-(E_c+E_d)/T}e^{\mu_c/T}e^{\mu_d/T} - e^{-(E_a+E_b)/T}e^{\mu_a/T}e^{\mu_b/T}]. \quad (7.45)$$

Using

$$\begin{aligned}\int |M_{ab,cd}|^2(2\pi)^4\delta^{(4)}(p_a + p_b - p_c - p_d)d\pi(p_a)d\pi(p_b) &= \sigma\sqrt{(p_a \cdot p_b)^2 - (m_a m_b)^2} \\ &= \sigma v E_a E_b \end{aligned} \quad (7.46)$$

the equation becomes

$$a^{-2}\frac{d}{da}(n_a a)^3 = \frac{< \sigma|v| > n_b}{H} n_a \left(\exp\left(\frac{\mu_c + \mu_d - \mu_a - \mu_b}{T}\right) - 1\right). \quad (7.47)$$

The interaction rate $\Gamma \equiv< \sigma|v|n_b >$ is the thermal averaged product of the cross section and relative velocity and the number density of the particles b, therefore the scale dependence of the number density is controlled with the familiar ratio Γ/H factor. If this factor is small, the densities do not evolve, while they evolve quickly

7.3 Density matrix formalism

Since this thesis will focused on the non-equilibrium evolution of neutrino distribution functions, here we will describe a proper formalism to include both the quantum effect of neutrino oscillations, and non-equilibrium processes, following the Raffelt-Sigl [209] derivation. Assuming that neutrinos are only in left (or right) helicity state their wave function can be written as

$$\psi(x) = \int dp \left(a_p(t)u_p + b^\dagger_{-p}(t)v_{-p}\right) e^{ipx}. \quad (7.48)$$

This assumption is fine as long as $M/T \ll 1$. In the same manner we refer to antiparticles as particles with opposite helicity.

The starting point is the definition of the so-called density matrices, ρ_p and $\bar{\rho}_p$:

$$\left\langle a_j^\dagger(p) a_i(p') \right\rangle = (2\pi)^3 \delta^{(3)}(p-p')(\rho_p)_{ij} \tag{7.49}$$

$$\left\langle b_i^\dagger(p) b_j(p') \right\rangle = (2\pi)^3 \delta^{(3)}(p-p')(\overline{\rho}_p)_{ij}, \tag{7.50}$$

where the indices refer to different flavours. The diagonal terms are therefore one particle number densities. Note the reverse order of indices in the definition of (anti)neutrino matrices which ensures that both matrices transform in the same way under unitary transformations.

In the absence of interactions, annihilation and creation operators satisfy

$$a_p(t) = a_p(0)\exp(-i\Omega_p^0 t), \quad b_p(t) = b_p(0)\exp(-\Omega_p^0 t), \tag{7.51}$$

where $\Omega_p^0 \equiv (p^2+M^2)^{1/2}$, and evolution of $\rho(\bar{\rho})$ is found to be

$$\dot{\rho}_p = -i\left[\Omega_p^0, \rho_p\right], \quad \dot{\bar{\rho}}_p = i\left[\Omega_p^0, \overline{\rho}_p\right]. \tag{7.52}$$

The solution describes the usual vacuum oscillations in the density formalism.

Including an interaction Hamiltonian $H_{int}(B,\psi)$ that describes the interaction of the neutrinos with some background field B and taking the expectation value the equation for the density matrix becomes:

$$\dot{\rho}_p = -i\left[\Omega_p^0, \rho_p\right] + i\left\langle [H_{int}(B,\psi), a_p^+ a_p] \right\rangle. \tag{7.53}$$

Assuming that interaction is weak enough, the equation can be solved perturbatively. In the first order of perturbation (the fields on the right hand side obey vacuum evolution eq. (7.51)), and factorizing medium and neutrino part in the expectation value, the result is just a forward scattering.

As explained in Sec. 3.5, forward scattering can always be represented in terms of a matter potential, and added to the free oscillating Hamiltonian.

The second order in perturbation will lead to the collision term. Under the assumption that the medium is not changed by the neutrino interactions, and that the duration of one collision is much smaller than the time over which the density matrix varies substantially, the evolution can be written as

$$\dot{\rho}_p = -i\left[\Omega_p^0, \rho_p\right] - i\left[\Omega_p^0, \rho_p\right] + (\dot{\rho}_p)_{CC} + (\dot{\rho}_p)_{NC} + (\dot{\rho}_p)_S, \tag{7.54}$$

where CC, NC and S stands for collisions produced in charged and neutral current, and self interactions.

If the charged current Hamiltonian is given by

$$H_{CC} = \frac{G_F}{\sqrt{(2)}} \int d^3x \bar{\xi}(x)\psi(x) + h.c \tag{7.55}$$

then the $(\dot{\rho})_{CC}$ can be written as

$$(\dot{\rho})_{CC} = \{P_p, (1-\rho_p)\} - \{A_p, \rho_p\}. \tag{7.56}$$

P_p and A_p are matrices describing production and annihilation processes for each neutrino flavour and have simple form in the case of diluted media. In the previous example the production and annihilation of particle a in the $a + b \to c + d$ scattering are

$$\begin{aligned} P_p &= \int d\pi(p_b)d\pi(p_c)d\pi(p_d)(2\pi)^4\delta^{(4)}(p_a + p_b - p_c - p_d) \\ &\times |M_{cd,ab}|^2 f_c(p_c,t)f_d(p_d,t)(1 \pm f_b(p_b,t)) \end{aligned} \tag{7.57}$$

$$\begin{aligned} A_p &= \int d\pi(p_b)d\pi(p_c)d\pi(p_d)(2\pi)^4\delta^{(4)}(p_a + p_b - p_c - p_d) \\ &\times |M_{ab,cd}|^2 f_b(p_b,t)(1 \pm f_c(p_c,t))(1 \pm f_d(p_d,t)). \end{aligned} \tag{7.58}$$

Note that right hand side of eq. (7.56) is for one flavour the same as the collision term in the Boltzmann equation.

When solving eq.(7.56) it is convenient to do a change of variables

$$(t,p) \to (x \equiv ma(t), y \equiv \frac{p}{T}), \tag{7.59}$$

where m is an arbitrary mass scale constant, so that the total time derivative becomes

$$\frac{d}{dt} \to xH_u(x)\frac{\partial}{\partial x}\rho(x,y)\Big|_{\text{fixed y}} \tag{7.60}$$

In the next chapters we will provide explicit examples of sterile neutrino evolution in the primordial plasma, in the context of low-scale Seesaw Models. We will focus on the period before electroweak symmetry breaking, where the sterile neutrinos can explain observed baryon asymmetry, and on their evolution after the electroweak phase transition, where bounds from cosmological observables can constraint significantly the parameter space of the models.

Chapter 8

Neutrinos before the electroweak phase transition - Baryogenesis

In this chapter we will briefly review baryogenesis and focus on baryogenesis via leptogenesis. For further details good references are the book [203], or reviews such as [210, 211]. The papers III and IV focus on the mechanism of leptogenesis via neutrino oscillations.

8.1 Sakharov conditions

Observations show that matter is far more abundant than the antimatter in the Universe. The baryon to photon ratio (η_B) is an important quantity that affects both BBN and CMB, and it has been measured to be the same at the corresponding epochs.

The firstly proposed solution to explain this difference was to assume an initial asymmetry at the Big Bang, but in the context of inflatory models, the period of inflation would erase all pre-existing asymmetries, hence, the asymmetry has to be dynamically produced after inflation. The three necessary conditions to produce an asymmetry were firstly pointed out in 1967 by Sakharov [212]:

- B-violating interactions,
- C and CP symmetry violating interactions and
- non-equilibrium processes.

The necessity of the first condition is quite obvious, if all the interaction were baryon number preserving the total baryon number would always keep its initial vanishing value. A process of type $X \to Y + B$, where Y and X do not have baryon number, and $B \neq 0$, must exist.

Looking at the decay of the X state, if the charge conjugation symmetry, C, is conserved, the decay of its antiparticle $\bar{X}$ will be the same

$$\Gamma(X \to Y + B) = \Gamma(\bar{X} \to \bar{Y} + \bar{B}). \tag{8.1}$$

This means that even if baryon number was produced it would be erased in the C conjugated process and no net baryon asymmetry would be created.

To explain the need for CP violation we can consider a hypothetical process of an X boson where the C conjugated channels have different decay rates. For example, the decay in a pair of left or right handed quarks $X \to q_L q_L$, $X \to q_R q_R$. If the CP is a symmetry then

$$\Gamma(\bar{X} \to \bar{q}_R \bar{q}_R) = \Gamma(X \to q_L q_L) \text{ and } \Gamma(\bar{\mathrm{X}} \to \bar{\mathrm{q}}_\mathrm{L} \bar{\mathrm{q}}_\mathrm{L}) = \Gamma(\mathrm{X} \to \mathrm{q}_\mathrm{R} \mathrm{q}_\mathrm{R}). \tag{8.2}$$

Thus, even though the rates of C conjugated processes are not the same, the total rate of production of baryons and antibaryons is the same

$$\Gamma(X \to q_L q_L) + \Gamma(X \to q_R q_R) = \Gamma(\bar{X} \to \bar{q}_L \bar{q}_L) + \Gamma(\bar{X} \to \bar{q}_R \bar{q}_R). \tag{8.3}$$

Note that in the standard model both C and CP are violated, C is maximally violated by $SU(2)_L$ gauge symmetry, and the source of CP asymmetry are complex angles in CKM and PMNS matrices [1].

If the third condition is not satisfied, the particles will obey standard Fermi-Dirac or Bose-Einstein distribution. With the baryon number violating processes in equilibrium, the chemical potential vanishes and the phase-space distribution of baryons and antibaryons must be the same, because the mass of particles and antiparticles is the same by CPT.

8.2 B number violation in the Standard Model

Baryon number in the SM is conserved classically, while quantum corrections violate this symmetry [213, 214]. Today baryon number violating processes are negligible, since they happen only due to quantum tunneling, but at high enough temperatures they were fast enough to lead to substantial baryon number vio-

[1] The PMNS complex angles are still not measured, see Chapter 4 for details.

lation. These processes are called sphalerons and play a essential role in two mechanisms for generating the baryon asymmetry:

- In electroweak baryogenesis all three Sakharov conditions are fulfilled in the process of sphaleron freeze out [215]. However, this would require an electroweak phase transition to be of first order, which in the SM cannot happen, since it would require the Higgs mass to be below 80 GeV [216]. This mechanism needs therefore beyond standard model physics, as provided in sypersymmetry theories, or to assume composite Higgs, or an extended Higgs sector, etc...

- In baryogenesis through leptogenesis, the asymmetry originates in the lepton sector and then gets transfered to the baryons through efficient sphaleron processes [217].

Sphalerons are a consequence of anomalies in gauge theories, the currents associated to certain global symmetries are broken at the quantum level. In the SM theory, both lepton and baryon number symmetries are anomalous:

$$\partial_\mu J^{(B)_\mu} = \partial_\mu J^{(L)_\mu} = \frac{N_f}{32\pi^2}\left(g^2 W_{a\rho\sigma}\tilde{W}_a^{\rho\sigma} + g'^2 B_{\rho\sigma}\tilde{B}^{\rho\sigma}\right), \tag{8.4}$$

where N_f is the number of generations. $W_a^{\rho\sigma}$ and $B^{\rho\sigma}$ are the field strength of the $SU(2)$ and $U_Y(1)$ gauge groups and $\tilde{W}_a^{\rho\sigma}$, $\tilde{B}^{\rho\sigma}$ their corresponding dual tensors ($\tilde{W}^{\rho\sigma} \equiv 1/2\epsilon^{\mu\nu\rho\sigma}W_{\rho\sigma}$, $\tilde{B}^{\rho\sigma} \equiv 1/2\epsilon^{\mu\nu\rho\sigma}B_{\rho\sigma}$ where ϵ is antisymmetric Levi-Civita tensor). It is important to notice that even though $B+L$ is violated, $B-L$ is still a conserved charge. Integration of eq. (8.2) relates baryon number with the so-called Chern-Simons number

$$B(t_f) - B(t_i) = N_f(N_{cs}(t_f) - N_{cs}(t_i)), \tag{8.5}$$

where the Chern-Simons number take value $0, \pm 1, \pm 2$..etc, and are related to the probabilities of transition from one non abelium vacuum to another. At small energies this probability occurs via tunneling, the so called instantons, and is very tiny since it is suppressed by a factor $\exp(-16\pi^2/g^2) \sim 10^{-160}$.

However in the early Universe, with temperatures high enough, kinetic energies can overcome the potential barrier and the transition is no longer suppressed. This solution is known as a sphaleron [218].

The schematic difference between instantons and sphalerons is shown in Fig. 8.1.

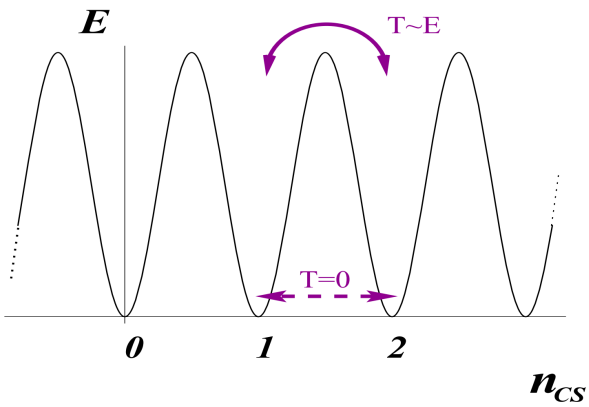

Figure 8.1: Schematic Yang-Mills vacuum structure. At zero temperatures the tunneling between vacua happens via instantons that are suppressed, while at finite temperatures these transitions can proceed via sphalerons.

A rough estimate of sphalerons transition rate [219] is

$$\Gamma \sim \left(\frac{g^2}{4\pi}T\right)^4 . \tag{8.6}$$

A more precise calculation was performed in Ref. [220], where they find that sphalerons are in equilibrium up to very high temperatures $\sim 10^{12}$ GeV. The precise temperature of sphalerons freeze-out is studied in [221], where they obtain that the freeze-out occurs at ~ 130 GeV.

To relate baryon and lepton number we have to look at all the processes that are fast in the early Universe:

- At high temperatures all gauge $SU(3)_C \times SU(2)_L \times U(1)_Y$ interactions are in equilibrium, which means that all the particles in the same group representation have the same chemical potential, and the chemical potential of bosons are zero.

- Sphaleron processes involving 12 particles leads to

$$\Sigma_\alpha \left(3\mu_{Q_{\alpha L}} + \mu_{L_{\alpha L}}\right) = 0, \tag{8.7}$$

- Left and right handed quarks interact via $SU(3)_C$ instanton effects

$$\sum_{\alpha} 2\mu_{Q_{\alpha L}} - \mu_{q^U_{\alpha R}} - \mu_{q^D_{\alpha R}} = 0. \tag{8.8}$$

- The Yukawa interactions give the relation among left and right handed fermions, and Higgs chemical potential

$$\begin{aligned} \mu_{Q_{\alpha L}} - \mu_{\Phi} - \mu_{q^D_{\alpha R}} &= 0, \\ \mu_{Q_{\alpha L}} + \mu_{\Phi} - \mu_{q^U_{\alpha R}} &= 0, \\ \mu_{L_{\alpha L}} - \mu_{\Phi} - \mu_{l_{\alpha R}} &= 0. \end{aligned} \tag{8.9}$$

- Finally, the conservation of hypercharge implies

$$\sum_{\alpha} \mu_{Q_{\alpha L}} + 2\mu_{q^U_{\alpha R}} - \mu_{q^D_{\alpha R}} - \mu_{L_{\alpha L}} - \mu_{l_{\alpha R}} = 2\mu_{\Phi}. \tag{8.10}$$

Using eq. (7.20) the total baryon and lepton numbers are related

$$\begin{aligned} B &= \frac{8N_f + 4}{22N_f + 13}(B - L) \\ L &= -\frac{14N_f + 9}{8N_f + 4}B, \end{aligned} \tag{8.11}$$

which for $N_f = 3$ gives $B = 28/79(B - L)$. Even though these result is valid only for $T \gg v$ at lower temperature they differ only by a small correction [222].

Note that after the electroweak phase transition, sphaleron processes decouple and baryon and lepton numbers are conserved.

8.3 Standard leptogenesis (Majorana neutrinos)

The first mechanism proposed to produce a net lepton asymmetry in seesaw models is through the out-of-equilibrium heavy Majorana neutrino decay [217]. The Yukawa couplings provide the necessary source of CP violation, and can naturally lead to ensure a non-equilibrium decay.

The Type I seesaw Lagrangian (eq. 3.8) is:

$$-L_{TypeI} = \sum_{i,j} \left(\bar{l}_{Li} \tilde{\Phi} Y_{\nu ij} N_{Rj} + \frac{1}{2} \bar{N}^c_{Ri} M_{Rij} N_{Rj} + h.c. \right). \tag{8.12}$$

If $M_1 \ll M_2, M_3$ the asymmetry possibly produced in the out of equilibrium decay of the two heavier states would be washed-out by the still fast Yukawa interactions of N_1, hence it is enough to consider only the decay of the lightest state.

At tree level, N_1 can decay via $N_1 \to l_a \Phi$, and, being a Majorana spinor, to the CP conjugate process. The total decay width is then

$$\Gamma_{D_3} = \frac{M_1}{8\pi}(Y_\nu^\dagger Y_\nu)_{11}. \tag{8.13}$$

The CP asymmetry arise from interference of the three level diagram, and loop corrections presented in Fig. 8.2:

$$\begin{aligned} \epsilon &= \frac{\sum_\alpha[\Gamma(N_1 \to l_\alpha \Phi) - \Gamma(N_1 \to \bar{l}_\alpha \bar{\Phi})]}{\sum_\alpha[\Gamma(N_1 \to l_\alpha \Phi) + \Gamma(N_1 \to \bar{l}_\alpha \bar{\Phi})]} \\ &\simeq \frac{1}{8\pi}\frac{1}{(Y_\nu^\dagger Y_\nu)_{11}} \sum_{i=2,3} \mathrm{Im}\left\{(Y_\nu^\dagger Y_\nu)_{1i}\left[f\left(\frac{M_i^2}{M_1^2}\right) + g\left(\frac{M_i^2}{M_1^2}\right)\right]\right\}, \end{aligned} \tag{8.14}$$

where $f(x)$ and $g(x)$ are function coming from the vertex loop correction and self energy correction:

$$\begin{aligned} f(x) &= \sqrt{x}\left[1 - (1+x)\ln\left(\frac{1+x}{x}\right)\right] \\ g(x) &= 6\sqrt{1-x}. \end{aligned} \tag{8.15}$$

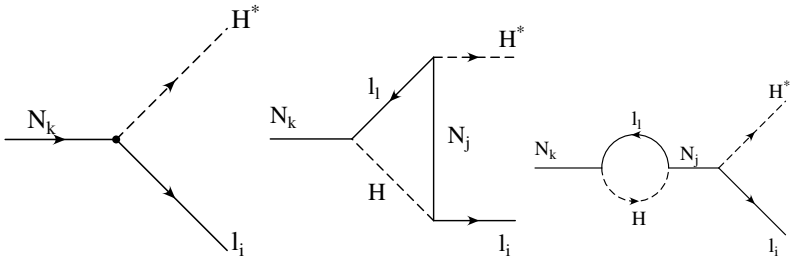

Figure 8.2: Decays of Majorana neutrino relevant for the CP asymmetry.

The washout effects can be parametrized with a dimensionless parameter k and the total produced asymmetry ϵ as

$$Y_L \equiv \frac{n_L - \bar{n}_L}{s} = k\frac{\epsilon}{g_*}. \tag{8.16}$$

If $k \ll 1$ all lepton number violating reactions are in equilibrium so no asymmetry can be produced. The case $k = 1$ corresponds to $T_D \ll M_1$. A more precise prediction requires solving the Boltzmann equation including the relevant lepton-generating and washout processes

- the already mention decay and inverse decay of N_1
- 2-2 scattering

$$\begin{aligned} \Delta L = 1 \ \ \mathrm{s-channel}: &\qquad N_1 l_\alpha \to t\bar{q}, \ \ N_1\bar{l}_\alpha \to t\bar{q} \\ \Delta L = 1 \ \ \mathrm{t-channel}: &\qquad N_1 t \to q\bar{l}_\alpha, \ \ N_1\bar{t} \to l_\alpha\bar{q} \\ \Delta L = 2 \ : &\qquad l\Phi \to \bar{l}\bar{\Phi}, \ \ ll \to \bar{\Phi}\bar{\Phi}, \ \ \overline{ll} \to \Phi\Phi. \end{aligned} \tag{8.17}$$

The Boltzmann equations for the RH neutrino number density and $B-L$ number density [223] are

$$\frac{dN_{N_1}}{dz} = -(D+S)(N_{N_1} - N_{N_1}^{eq}) \tag{8.18}$$

$$\frac{dN_{B-L}}{dz} = -\epsilon_1 D(N_{N_1} - N_{N_1}^{eq}) - W N_{B-L}\ , \tag{8.19}$$

where

$$(D, S, W) \equiv \frac{(\Gamma_D, \Gamma_S, \Gamma_W)}{Hz}, \quad z = \frac{M_1}{T}\ . \tag{8.20}$$

Γ_D accounts for decay and inverse decay, Γ_S for $\Delta L = 1$ scattering processes, while Γ_W represents a washout term and includes inverse decay and $\Delta L = 1, 2$ process. The Boltzmann equation should be solved numerically, and an example solution is given in Fig. 8.3

For strongly hierarchical right handed neutrinos, there is so called "Davidson-Ibarra" bound [224]:

$$|\epsilon_1| \leq \frac{3}{16\pi}\frac{M_1\sqrt{\Delta m_{atm}}}{v^2}, \tag{8.21}$$

which leads to $M_1 \geq 2 \times 10^9$ GeV.

Including flavor effects [225–228] the bound can also be reduced by 2-3 orders of magnitude [229, 230].

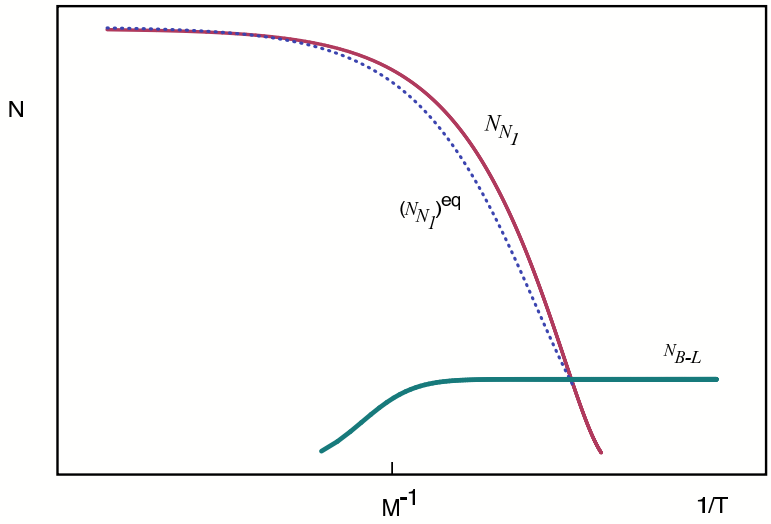

Figure 8.3: The evolution of the number density of the N_1 neutrino (purple), the equilibrium distribution (blue dotted) and the $B-L$ number density as function of time (inverse temperature)(from Ref. [210])

.

If the neutrinos are almost degenerate a very small difference between two Majorana neutrinos may enhance the contribution of the self energy diagram from Fig. 8.2 and lead to the resonant decay [231]. The mass scale of such neutrinos should be in TeV range.

8.3.1 Leptogenesis via neutrino oscillations

Another leptogenesis mechanism that works in the the Type I seesaw model, but for much smaller masses of the right-handed neutrinos, is the so-called leptogenesis via neutrino oscillations, first proposed in [232] and pursued in references [176, 177, 233–237].

Since this mechanism will be the main topic of the paper III and IV, here we will just sketch the basic idea. At least 2 heavy neutrinos must be in the GeV scale, while the third one can be lighter. For such light neutrinos, Majorana effects are negligible before electroweak phase transition, and $B - L$ is approximately conserved. Since sphalerons couple only to the left handed fermions, a lepton asymmetry can be created during the out of equilibrium production of the right handed neutrinos. As long as the right handed neutrinos do not reach thermal equilibrium before the electroweak phase transition temperature, T_{EW}, the asymmetry created in the lepton and baryon sector will not be washed out. The required CP phases are coming, as in standard leptogenesis, from the complex Yukawa matrices. A sketch of the evolution of the energy density of one of the neutrinos, and the produced baryon asymmetry is given in Fig. 8.3.1.

In type I seesaw models with majorana masses below the GeV, the thermalization of the sterile states takes place after the EWPT. The evolution equations of the sterile states change in this regime, as explained in the next chapter.

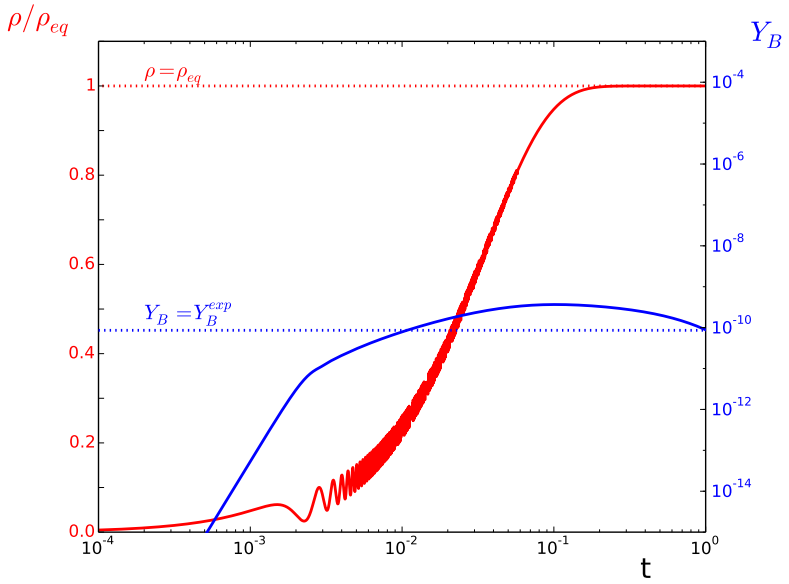

Figure 8.4: The evolution of the energy density normalized to the equilibrium one of one neutrino (red curve), and the produced baryon asymmetry (blue curve). Notice that once the equilibrium is reached the asymmetry starts to wash out.

Chapter 9

Neutrinos after electroweak phase transition

In this chapter we will focus on the evolution of sterile neutrinos after the Higgs field obtain its vacuum expectation value. Since the $SU(2)_L \times U(1)_Y$ breaks to $U(1)_Q$ the dominant channel of sterile neutrino interactions is via the mixings with the active ones.

We will briefly revisit the evolution of the neutrinos in this period and discuss constraints coming from BBN, CMB and LSS measurements, as well as from X-ray searches if one assumes that sterile neutrino is a warm dark matter candidate. Sterile neutrino evolution in this epoch and how the mentioned constraints reflect in the constraints on the sterile neutrino parameter space is the topic of the papers I and II.

9.1 Kinetic equations of sterile neutrinos below EW phase transition

As mentioned, after the EWPT the production/annihilation of sterile states happens mainly via the mixing with the active ones. A naive estimate suggests that the interaction rate of the sterile neutrinos should be proportional to that of the active ones times the probability of the active neutrino to oscillate into a sterile, which is true up to a factor of $1/2$, appearing after the proper consideration

of kinetic equations for neutrino density 6×6 matrix [238][1]

$$\Gamma_{s_j} \simeq \frac{1}{2} \sum_a \langle P(\nu_a \to \nu_{s_j}) \rangle \times \Gamma_{\nu_\alpha}. \tag{9.1}$$

$\langle P(\nu_\alpha \to \nu_{s_j}) \rangle$ is the time-averaged probability $\nu_\alpha \to \nu_{s_j}$

$$\langle P(\nu_\alpha \to \nu_{s_j}) \rangle = \left(\frac{M_j^2}{2pV_\alpha(T) - M_j^2} \right)^2 | \, (U_{as})_{\alpha j} \, |^2, \tag{9.2}$$

where U_{as} describes the mixing between active state a and sterile state s. p and M_j are the momentum and mass of the neutrino and V_α is the matter potential induced by coherent scattering in the plasma. These potentials depend strongly on whether there is or not a large lepton asymmetry[2]. Note that only active neutrinos have non-zero matter potential since sterile ones do not interact with other particles in the plasma. In papers I and II the sterile neutrinos evolution was studied neglecting primordial lepton asymmetries, and the bound on neutrino phase space was put based on two cosmological parameters : $N_{\rm eff}$ and Ω_C.

Recall that the total density of radiation can be written in terms of g_* (eqs. (7.27),(7.28)), where it is useful to separate the neutrino contribution together with any other possible extra radiation as parameter $N_{\rm eff}$

$$g_* = \sum_{i=bosons} g_i \left(\frac{T_i}{T} \right)^4 + \frac{7}{8} \sum_i g_i \left(\frac{T_i}{T} \right)^4 + \frac{7}{8} N_{\rm eff}, \tag{9.3}$$

or defining

$$\Delta N_{\rm eff} \equiv N_{\rm eff} - N_\nu, \tag{9.4}$$

where N_ν is just the contribution of the SM neutrinos[3] $\Delta N_{\rm eff}$ can also be seen as a ratio of energy density of extra radiation normalized to the radiation of one massless neutrino:

$$\Delta N_{\rm eff} \equiv \frac{\epsilon_\nu}{\epsilon_\nu^0}. \tag{9.5}$$

[1] The calculation is explained in more details in the appendix of Paper II.

[2] Lepton asymmetries of the same order of magnitude as the baryon one give a negligible contribution to the matter potential.

[3] $N_{\rm eff}$ of the SM neutrinos is 3.046 (instead of naively expected 3 in the instantaneous decoupling approximation used in Sec. 7.1) due to neutrino interactions when electron/positron annihilation began.

$\Delta N_{\rm eff}$ is bounded both in BBN and CMB measurements. To calculate the contribution of a decoupled state to the $\Delta N_{\rm eff}$, we have to take into account a dilution factor, i.e., if the decoupling temperature of the state (T_{d_i}) is much higher than the BBN temperature the temperatures of those decoupled state and the active neutrino ones will be different due to the change in g_*. From entropy conservation we estimate that each sterile states that reached thermal equilibrium and decoupled while being relativistic contributes with $\Delta N_{{\rm eff}s_i}(T_{\rm BBN}) = (g_*(T_{\rm BBN})/g_*(T_{d_i}))^{4/3}$.

Also, if the sterile neutrino stays in thermal equilibrium with plasma after the temperature drops below its mass, its density would be exponentially suppressed[4], so the contribution of such a state to both matter or energy density would be negligible.

A massive particle would contribute to the matter density:

$$\Omega_{s_i} = \frac{M_i n_i}{\rho_{cr}} \leq \Omega_C, \tag{9.6}$$

where s_i is the i-th specie of sterile neutrino, M_i its mass, n_i the number density, and Ω_C is the density of cold matter. Expressed with the number density normalized to the Fermi-Dirac number density (n_0) the bound becomes

$$\frac{M_i}{\rm eV}\frac{n_i/n_0}{94.1} \leq \Omega_C. \tag{9.7}$$

Another important factor to take into account is whether he sterile neutrino decays and, if it does, at which period in the history of the Universe this happens. A neutrino that decays before BBN could have no impact on the observables. In the other extreme, a very long-lived sterile neutrino could be a candidate for warm dark matter, however the strong constraints on the sterile neutrino mixing from astrophysical X-ray measurements implies that a large enough contribution to dark matter can only be achieved if the sterile neutrino is produced in the presence of large leptonic asymmetries [239, 240]. The decay of neutrinos after BBN would effect the CMB radiation properties, since they would predominantly decay to the SM relativistic neutrinos and contribute as extra radiation in the last scattering epoch. For revisited bounds on sterile neutrino see [241].

[4]See Chapter 7 for details.

9.2 Bounds from BBN

Big Bang nucleosynthesis is the epoch in the early Universe where primordial light elements (^{2}H, ^{3}He,^{4}He and ^{7}Li) were synthesized [5].

The process starts with the decoupling of neutrinos. The interactions that keep neutrino in equilibrium are mainly scatterings over electrons/positrons and pair conversion $e^+e^- \leftrightarrow \nu_\alpha \bar{\nu}_\alpha$, with the interaction rate of the order

$$\Gamma_\nu \sim G_F^2 T^2 n_e \sim G_F^2 T^5, \tag{9.8}$$

where n_e is relativistic electron/positron number density.

The decoupling temperature is defined as

$$\Gamma_\nu = H(T_D) \implies T_D = \left(\frac{\sqrt{g_\star}}{G_F^2 m_{Pl}}\right)^{1/3} \sim g_\star^{1/6}\text{MeV} \sim 1\text{MeV}. \tag{9.9}$$

Shortly after, at around $T_F \sim 0.7$ MeV, the neutron to proton conversion rate becomes ineffective, and the neutron to proton number density freeze-out at its equilibrium value

$$\frac{X_n}{X_p} = e^{-Q/T_F} \sim \frac{1}{6}, \tag{9.10}$$

where $Q = 1.293$ MeV is the neutron-proton mass difference and X_i is the ratio of the number density of a given species over the total number density of all baryons[6]

$$X_i \equiv \frac{n_i}{n_B}, \quad n_B = n_p + n_n + \sum_i n_i. \tag{9.11}$$

However, the neutron to proton ratio does not stay constant due to neutron decay, that suppresses neutron abundance as $\exp(-t/\tau_n)$, where τ_n is the neutron lifetime. The ratio eventually becomes stable when neutrons get trapped inside nuclei.

The first link in the nucleosynthetic chain is the deuterium production $p+n \to d+\gamma$, that is efficient enough to lead deuterium to its equilibrium abundance

$$X_d \sim \eta_B \left(\frac{T}{m_N}\right) e^{B_d/T}, \tag{9.12}$$

[5] Heavier nuclei are only synthesized in stars.

[6] Note that at this epoch there are only protons and neutrons in the plasma

where m_N is a common nucleon mass[7], and, as defined before, $\eta_B = \frac{n_B}{n_\gamma}$. The binding energy of deuterium is $B_d \sim 2.2$ MeV, but even after the photon temperature drops below this value, the deuterium abundance is small due to a small baryon to photon ratio. This is the so-called deuterium bottleneck, which is overcame at around $T_d \sim 0.07$ MeV.

As soon as deuterium forms, it is transformed into ^{4}He that has the highest binding energy among light nuclei. By that time neutron to proton ratio dropped to $n/p \sim 1/7$. Assuming that all neutrons end up bound in ^{4}He, its mass fraction is

$$Y_p \equiv \frac{4n_{^4He}}{n_B} \sim \frac{4(n_n/2)}{n_n + n_p} \sim 0.25. \tag{9.13}$$

The prediction is in a good agreement with the measured value, $Y_p^{exp} = 0.245 \pm 0.004$ [242].

A more precise way of calculating light element abundance is to solve he set of coupled Boltzmann equations for all light nuclei, kinetic equations involving the oscillations for neutrinos, and taking into account baryon number conservation, charge neutrality, covariant conservation of the total energy density and Hubble dependence on the energy density during the radiation dominated period. The final abundance of light nuclei will depend on the η_B, the neutron lifetime τ_n and the $N_{\rm eff}$ encoded in the Hubble parameter. The publicly available numerical codes are given in [243–245], and the most used one being [246, 247].

Measured abundances are in a good agreement with the predicted ones, except for the still unexplained disagreement of lithium abundance, as shown in Fig. 9.1 from [16].

In the standard BBN model, the only free parameter is $\eta_{10} \equiv 10^{10}\eta_B$, while $N_{\rm eff} = 3.046$.

The dependence of light element abundance on both $N_{\rm eff}$ and η is shown in Fig. 9.2 for some particular values of $N_{\rm eff}$, from [248]. Note that the element most sensitive on $N_{\rm eff}$ is ^{4}He, while the best prediction for η_B is coming from the deuterium abundance.

The best fit of $N_{\rm eff}$ coming only from BBN predictions is $N_{\rm eff} = 3.01^{+0.95}_{-0.76}$ at 95% C.L. [249]. Combining η_B prediction from CMB with BBN measurements gives stronger bounds on $N_{\rm eff}$.

[7] In the pre-exponential factors the difference between m_p and m_n is not important, and we can mark it as common nucleon mass m_N.

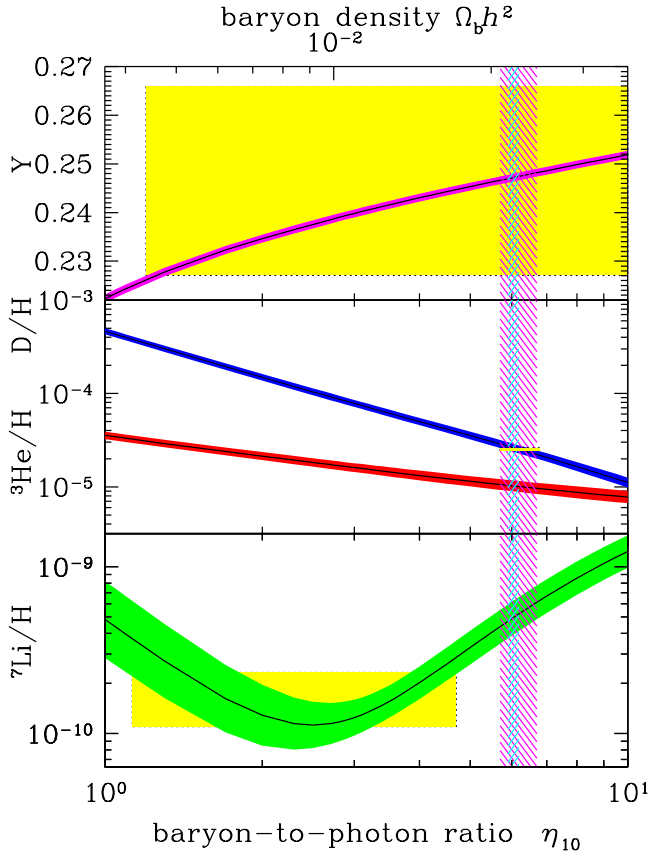

Figure 9.1: The primordial abundances of ^{4}He, D,^{3}He, and ^{7}Li as a function of η_B. Boxes indicate the observed light element abundances. Vertical bands indicate the CMB and the BBN measures of the cosmic baryon density (from Ref. [16])

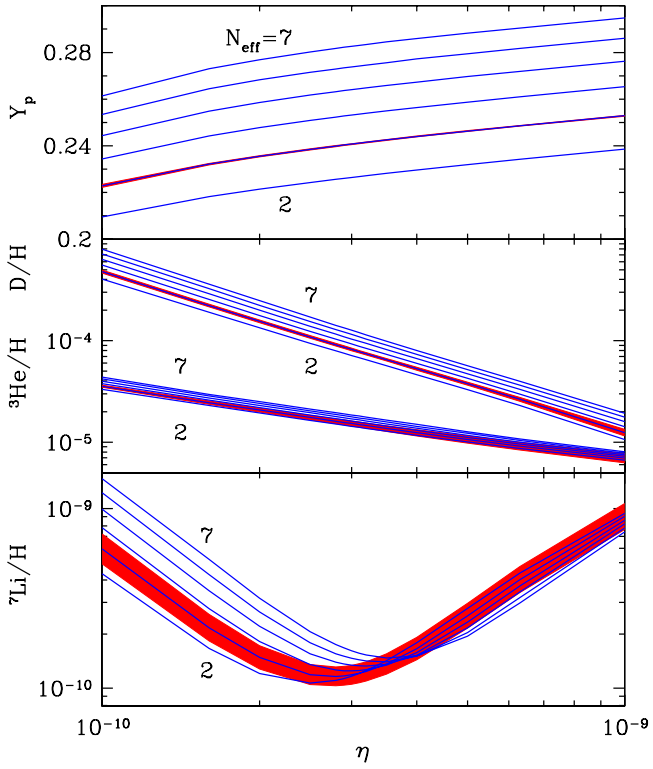

Figure 9.2: BBN abundance predictions as a function on η_B varying $N_{\rm eff}$ from 2 to 7. The bands are 1σ errors (from Ref. [248]).

9.3 Other cosmological bounds

After electrons decoupled and stable nuclei formed, the Universe became almost transparent to free streaming photons. The energy density, together with the polarization modes of the photons last scattering remained imprinted in CMB.

CMB temperature anisotropy is given in terms of the two point correlation function of the temperature fluctuations in the sky,

$$\left\langle \frac{\delta T}{\bar{T}}(\hat{n}) \frac{\delta T}{\bar{T}}(\hat{n}') \right\rangle = \sum_{l=0}^{\infty} \frac{(2l+1)}{4\pi} C_l P_l(\hat{n}\dot{\hat{n}}'), \tag{9.14}$$

where $P_l(x)$ are Legendre polynomials, $\hat{n}$ is the direction in the sky and $\bar{T}$ is the average temperature. A similar expressions can be found for the correlations between the different polarization modes called TE,EE,BB and EB power spectrum, where T stands for the temperature, and E and B for two modes of polarization.

The most precise measurement of CMB anisotropies is given by Planck collaboration [128] presented on Fig. 9.3, where $\Delta D_l \equiv l(l+1)C_l/2\pi$.

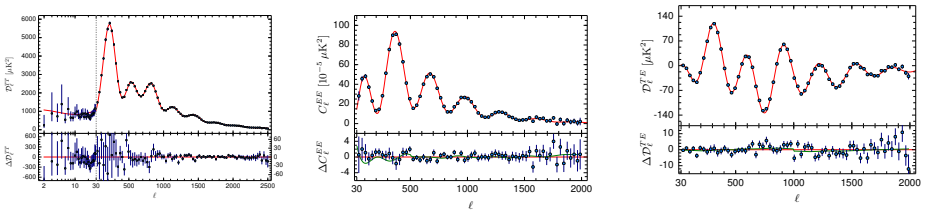

Figure 9.3: CMB power spectrum, for TT, EE and TE correlation functions. The theoretical prediction curve in the upper panels are computed from the best-fit ΛCDM model, while the lower ones are residuals with respect to this model (from Ref. [128])

The primordial power spectrum can be parametrized as many inflatory models suggest:

$$P_R = A_s (k/k_0)^{n_s - 1}, \tag{9.15}$$

where A_s is the amplitude and n_s spectral index.

Evolution of primordial perturbations involves a complicated set of coupled Einstein and Boltzmann equations, and is well beyond the scope of this thesis,

The other important observable related to the deviations from homogeneity and isotropy is large scale structure (LSS), a measure of the matter power spectrum at redshifts much closer to us. The total matter power spectrum is de-

Table 9.1: Best fit for the standard ΛCDM model extended with massive neutrinos and extra radiation. All the constraints except for the m_ν and $N_{\rm eff}$ (that are at 95% C.L) are at 68% C.L.

Parameter	Value	Description
H_0	67.64 ± 0.48	Hubble constant
$\Omega_b h^2$	0.0222 ± 0.0002	Baryon density
$\Omega_c h^2$	0.119 ± 0.001	Dark matter density
τ	0.065 ± 0.012	Optical reionization depth
$\ln(10^{10} A_s)$	3.062 ± 0.023	Amplitude of the primordial scalar perturbations
n_s	0.9667 ± 0.0053	Spectral index of the primordial scalar perturbations
$N_{\rm eff}$	3.2 ± 0.5	Effective relativistic degrees of freedom
$\sum m_\nu$ (eV)	< 0.32	Sum of the neutrino masses

fined as the Fourier transform of the two point correlation function of the matter density fluctuations after averaging over all directions

$$P_{matter}(k,z) = \left\langle |\delta_{matter}(k_i,z)|^2 \right\rangle = \left\langle \left| \frac{1}{(2\pi)^3} \int \frac{\rho(x)-\bar{\rho}}{\bar{\rho}} \exp(-ik_i x) \right| \right\rangle , \quad (9.16)$$

where $\rho(x)$ and $\bar{\rho}$ are local and averaged matter density. The measurement of the matter power spectrum can be done by studying distributions of galaxies [250–252], or through the absorption or inverse scattering of the light coming from known galaxy sources, such as Lyman-alpha-forest [253–255] or the Sunyaev Zeldovich spectrum [256].

The CMB temperature and polarization is also sensitive to the LSS due to gravitational lensing [128].

Part of the LSS data already enters in the region where the non linear effects may become relevant and a more conservative approach is to use only the data related to the imprint of the baryonic acoustic oscillations (BAO) in the total matter power spectrum [257, 258].

Other significant data are from type Ia supernovae [259, 260], that can constrain significantly the equation of the state of dark energy, and the direct measurement of the Hubble constant [261].

The parameters of the standard ΛCDM model extended with massive neutrinos and extra radiation are given in the Table 9.1. The data are combination of Planck TT,TE,EE +lowP +BAO, from Ref. [128].

Focusing again on $N_{\rm eff}$ parameter, there is a a good agreement between BBN and CMB measurements as shown in Fig. 9.4.

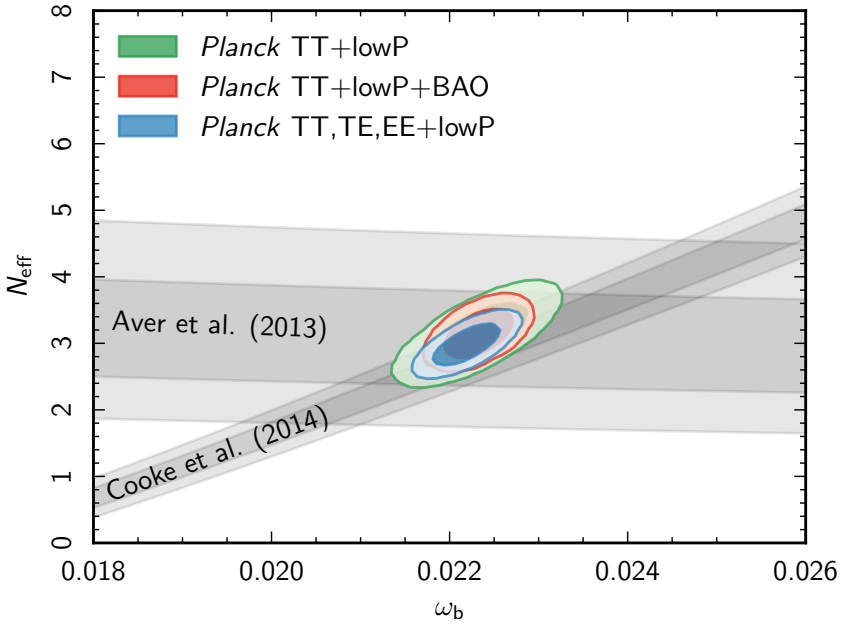

Figure 9.4: Comparison of BBN and CMB measurements. The BBN bounds are taken for ^4He from ref [262],mostly sensitive to $N_{\rm eff}$, and deuterium from ref [263], mostly sensitive to baryon density (from Ref. [128]).

When combining Planck+BAO data with Helium or Deuterium abundance measurements the bound on extra radiations is even more constraining [128]:

$$N_{\rm eff} = 2.99 \pm 0.39 \quad \text{He} + \textit{Planck}\text{TT, TE, EE} + \text{lowP} \tag{9.17}$$

$$N_{\rm eff} = 2.91 \pm 0.37 \quad \text{D} + \textit{Planck}\text{TT, TE, EE} + \text{lowP}. \tag{9.18}$$

$$\tag{9.19}$$

9.4 Bounds from X-ray searches

If a sterile neutrino was abundant in the Universe, its decay product would be potentially testable. A sub-dominant radiative decay $N_s \to \nu\gamma$ would produce an

active neutrino, and a photon of energy $E = M_s/2$ with the decay width [239,264]:

$$\Gamma_{N\to\gamma\nu_a} = \frac{9\alpha G_F^2}{256\times 4\pi^4}\ \sin^2 2\theta\ M_s^5 = 5.5\times 10^{-22}\theta^2\left[\frac{M_s}{\text{keV}}\right]^5 s^{-1}, \tag{9.20}$$

where θ is the mixing angle with the active neutrino. Assuming that the sterile neutrino abundance is the one required for the DM, the lack of a such X-ray signal can put the bounds in θ vs M_s plane[8]. The summarized constrain are given in Fig. 9.5.

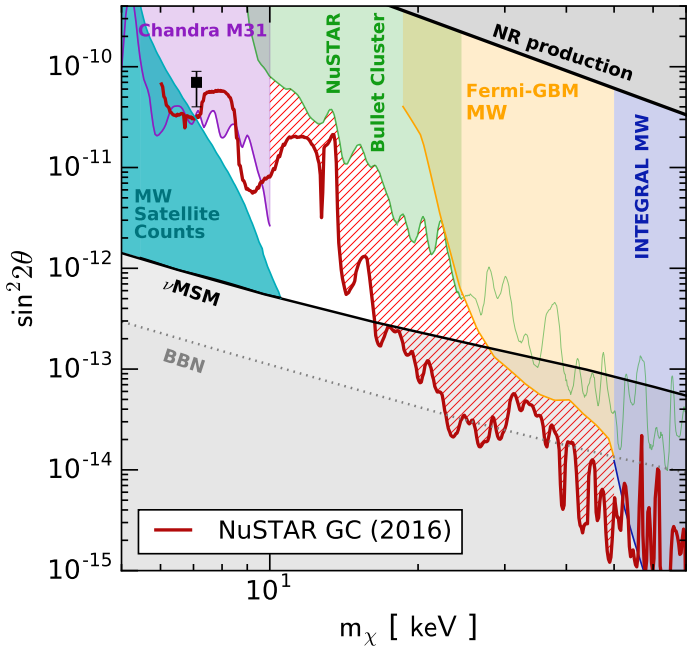

Figure 9.5: The constrains on the sterile neutrino mass and mixing based on structure formation (blue region) and X-ray astrophysical non-observation (purple, green and orange region), and NuStar bound (red hatched region). The region between solid black line can explain DM abundance, where the upper one assumes non-resonant production, and the lower one assumes large lepton asymmetry (from Ref. [265]).

[8]It is important to stress out that this bounds applies only if a sterile neutrino accounts for all the DM in the Universe.

How these cosmological measurements set bounds in low-scale seesaw models is the main topic of papers I and II.

Chapter 10

Summary of the scientific research and conclusions

In this chapter we will summarize the main results and conclusions of the scientific research we have carried out, referring for details to the previous chapters or the full articles collected in the second part of the thesis. The research focus on the type I seesaw models with two or three right handed neutrinos (3+2 MM and 3+3 MM) with masses below the electroweak scale and, particularly, on their impact on cosmology.

The first two papers studied the constrains on the parameter space of the models from cosmological measurements using the methods described in Chapter 9. The topic of the third and the fourth paper is the generation of baryon asymmetry in the Universe via neutrino oscillations, introduced in Chapter 8

10.1 Paper I

As mentioned in Chapter 9, a new particle abundant enough in the Early Universe could change the radiation and/or matter densities and modify therefore the properties of BBN, CMB and LSS. In this work we evaluated the contribution of the two extra neutrino states of the minimal low scale seesaw model to the radiation and matter densities in all generality, that is for any value of the unconstrained parameters of the model: the complex angle of the R matrix, two heavy masses and two CP phases. For details about the motivation, parametrization and current direct searches constraints of the model we refer the reader to Chapter 5.

After the electroweak phase transition sterile neutrinos can only be produced via their mixing with the active ones, hence, the interaction rate of the sterile neutrino can be estimated as the product of the interaction rate of the active neutrinos times the probability of the active neutrino oscillating into a sterile

$$\Gamma_{s_i} \simeq \frac{1}{2}\sum_a \langle P(\nu_a \to \nu_{s_i})\rangle \times \Gamma_a, \tag{10.1}$$

where the factor 1/2 will be explained later. The time-averaged probabilities in the primeval plasma is approximately

$$\langle P(\nu_a \to \nu_{s_i})\rangle \;=\; 2\left(\frac{M_i^2}{2pV_a - M_i^2}\right)^2 |U_{as_i}|^2 + \mathcal{O}\left(U_{as}^4\right), \tag{10.2}$$

where p is the neutrino momentum and $V_a \equiv A_a T^4 p$, is the matter potential, where we assumed no significant lepton asymmetries. The interaction rate of the active neutrinos is given by

$$\Gamma = \mathrm{Diag}(\Gamma_e, \Gamma_\mu, \Gamma_\tau, 0, 0) = y_a \frac{180\zeta(3)}{7\pi^4} G_F^2 T^4 p \mathrm{Diag}(y_e, y_\mu, y_\tau). \tag{10.3}$$

The coefficients y_a and A_a depend on the temperature. This is due to the fact that the charged leptons decouple from plasma at different temperatures, which makes the charged current interaction of the corresponding neutrino flavor less efficient. So we have $A_e = A$, while $A_{\mu/\tau} = B$ for T below the μ/τ threshold ($T \lesssim 20/180$ MeV) or $A_{\mu/\tau} = A$ for higher $T \gtrsim 20/180$ MeV, with

$$\begin{aligned} B &\equiv -2\sqrt{2}\left(\frac{7\zeta(4)}{\pi^2}\right)\frac{G_F}{M_Z^2}, \\ A &\equiv B - 4\sqrt{2}\left(\frac{7\zeta(4)}{\pi^2}\right)\frac{G_F}{M_W^2}. \end{aligned} \tag{10.4}$$

Similarly the coefficients y_a are $y_e = 3.6$, and $y_\mu = y_\tau = 2.5$ below the corresponding μ and τ thresholds, or $y_\mu = y_\tau = y_e = 3.6$ above the thresholds [266].

A more detailed description is provided by the density matrix formalism, described in Sec. 7.3. Separating the equations for the density matrix into the active A and sterile S blocks, assuming that the collisions of the active ones are fast enough to equilibrate ρ_{AA} and ρ_{AS}, and hierarchical heavy masses, it is

possible to show that the equations for each species approximately decouple as

$$\begin{aligned}\dot{\rho}_{ss} &= -\left(H^{\dagger}_{AS}\left\{\frac{\Gamma_{AA}}{(H_{AA}-H_{ss})^2+\Gamma^2_{AA}/4}\right\}H_{AS}\right)_{ss}\tilde{\rho}_{ss} \\ &\simeq -\frac{1}{2}\sum_a \langle P(\nu_s\to\nu_a)\rangle\Gamma_a\tilde{\rho}_{ss}, \end{aligned} \tag{10.5}$$

which proves eq. (10.1) and explains the factor 1/2.

To estimate whether a state thermalize or not we define a thermalization function

$$f_s(T)\equiv\Gamma_s(T)/H(T). \tag{10.6}$$

The function has a maximum at some temperature $T_{\max}$, so if $f(T_{\max})\geq 1$ the state reaches thermal equilibrium. Using averaged momentum $p=3.15T$, the $T_{\max}$ can be shown to be bounded as

$$\left(\frac{M_i^2}{59.5|A_e|}\right)^{1/6}\leq T_{\max}\leq\left(\frac{M_i^2}{59.5|A_\tau|}\right)^{1/6}. \tag{10.7}$$

Since $f_{s_i}(T_{\max})\propto|U_{as_i}|^2T^3_{\max}$, the naive seesaw scaling r $|U_{as_i}|^2\sim\mathcal{O}(m_l/M_i)$ then implies that $f_{s_i}(T_{\max})$ is roughly independent of M_i.

We confirmed the analytical approximation by numerical minimization of the $f(T_{\max})$ over the free parameters. We concluded that the two sterile neutrinos reach thermalization, for both inverted and normal light neutrino ordering, and is almost independent of the heavy neutrino mass in the range (1 eV- 1 GeV). The numerical minimization of $f(T_{\max})$ is presented in Fig. 10.1. It is important to stress that the result is a consequence of the constraint imposed by the light neutrino masses i.e. individual mixings with electron, muon or tau neutrino can get unlimitedly small, but not simultaneously if the light neutrino masses are to be accounted for.

The effect of these states in cosmology depends furthermore on whether:

- The state decouples while being relativistic.
- The state decouples late enough not to be completely diluted [1].
- The state does not decay before the BBN.

[1] The energy density is proportional to the temperature of the decoupled specie, that can be very different than the photon temperature if the state decouples much before the BBN (see Sec. 9.1 for details).

The decoupling temperature T_d can be calculated as the minimum temperature for which thermalization function has value 1, and, using constraints on the mixing elements discussed in details in Chapter 5, we obtain that the decoupling temperature is always higher than the mass of the neutrinos for neutrino masses below $\sim$ 100 MeV, as presented in Fig. 10.2. So for these range of masses, the neutrinos decouple while being relativistic.

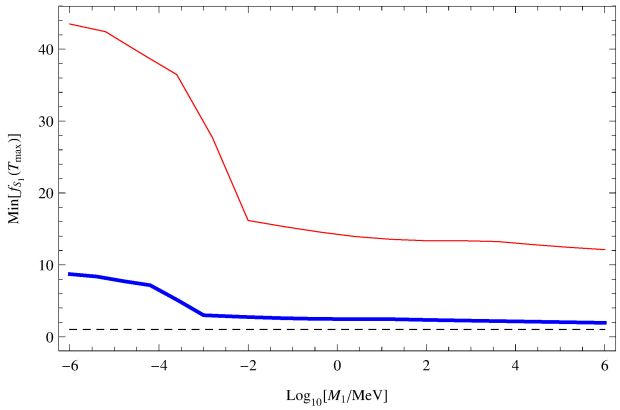

Figure 10.1: Min$[f_{s_i}(T_{\max})]$ for the lighter sterile state as function of M_i for a light neutrino spectrum with a NH (blue line) or IH (red line). The dashed line at 1 corresponds to the minimum value for thermalisation.

By evolving numerically eq. (10.5) we concluded the states with the masses below $\leq$ 10 keV would decouple late enough not to be significantly diluted, and the 2 σ constrains from BBN are sufficient to exclude these states.

More massive neutrinos would get diluted. Their impact however depends on when they decay. Neutrinos heavier than 10 MeV could decay before BBN for some range of parameters, which would make them invisible to the BBN/CMB data. The effect of the neutrinos in the range [10 MeV,140 MeV] has been studied in [267–269] and the bounds from BBN and accelerators exclude this possibility [169]. Below 10 MeV, the neutrinos could decay after BBN but above CMB and contribute too much extra radiation at the CMB time, since they would predominately decay to the already decoupled active neutrinos. If neutrino decay after CMB, the dilution is not enough to suppress their contribution to the matter density and are excluded by Planck measurements. For more details on the cosmological measurements look at Chapter 9.

The main conclusion of the paper is summarized in the Fig. 10.3 where the shaded region is the allowed mass scale of sterile neutrinos in the minimal seesaw

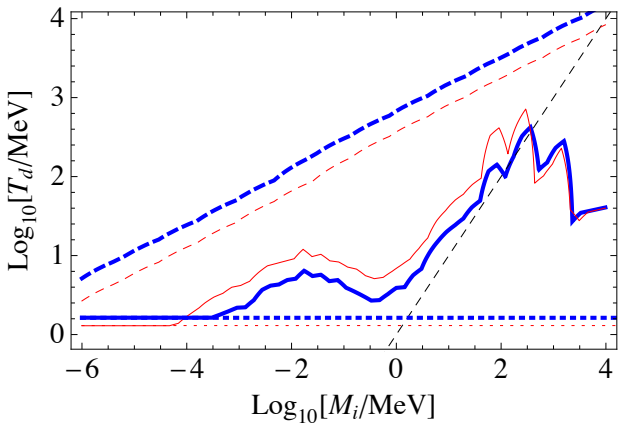

Figure 10.2: T_d as function of the the sterile mass for the NH (blue line), IH (red line) for parameters that minimize $f_s(T_{\max})$ (dashed), those that minimize T_d (dotted) and those that minimize T_d while being compatible with bounds from direct searches (solid). The single dashed line satisfies $T = M_i$.

model. Note that the sub-eV region, barely acceptable when our publication appeared, is now excluded at 2σ by the latest Planck 2015 analysis [128].

10.2 Paper II

The next to minimal model of light neutrino masses is a Type I seesaw with three additional states. The unconstrained parameters of the model are three complex angle of the R matrix, three heavy masses, three CP phases and the lightest neutrino mass. Even if the parameter space is larger, a similar analysis can also be done in this case.

Comparing to the previous work we also updated the interaction rate for the active neutrinos, $\Gamma_{\nu_\alpha}(T)$ which can be accurately parametrized in terms of $C_\alpha(T)$ as

$$\Gamma_{\nu_\alpha} \simeq C_\alpha(T) G_F^2 T^4 p, \tag{10.8}$$

where $C_\alpha(T)$ are calculated in Ref. [270].

As in the previous work, we defined the thermalization function that has a maximum at temperature $T_{\max}$, which, in the same approximations as before, is

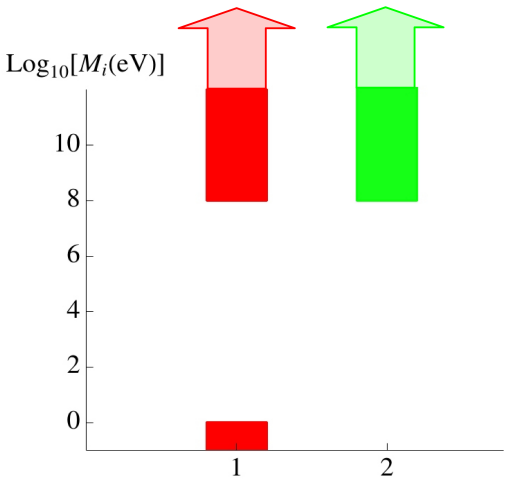

Figure 10.3: The allowed region for sterile neutrino masses in the 3+2 MM.

bounded by

$$T^{\tau}_{\rm max} \equiv \left(\frac{M_j^2}{59.5\ |A|}\right)^{1/6} \leq T_{\rm max} \leq \left(\frac{M_j^2}{59.5\ |B|}\right)^{1/6}, \tag{10.9}$$

where A and B are defined in the previous section.

Working out analytical approximation a lower bound on the maximum of thermalization function we find

$$f_{s_j}\left(T_{\rm max}\right) \geq \frac{\sum_\alpha |\left(U_{as}\right)_{\alpha j}|^2 M_j}{3.25\cdot 10^{-3}{\rm eV}}, \tag{10.10}$$

and using the Casas-Ibarra parametrization where

$$\sum_\alpha |\left(U_{as}\right)_{\alpha j}|^2 M_j \geq m_1. \tag{10.11}$$

we obtain that the maximum of thermalization only depends on one parameter, the lightest neutrino mass:

$$f_{s_j}\left(T_{\rm max}\right) \geq 1 \quad \text{for} \quad {\rm m}_1 \geq {\rm m}_{\rm th} \equiv 3.25\cdot 10^{-3}\ {\rm eV}. \tag{10.12}$$

In Fig. 10.4 we show the contour plots of the minimum of $f_{s_1}(T_{\rm max})$ (varying the unconstrained parameters in R and the CP phases in the full range), as a func-

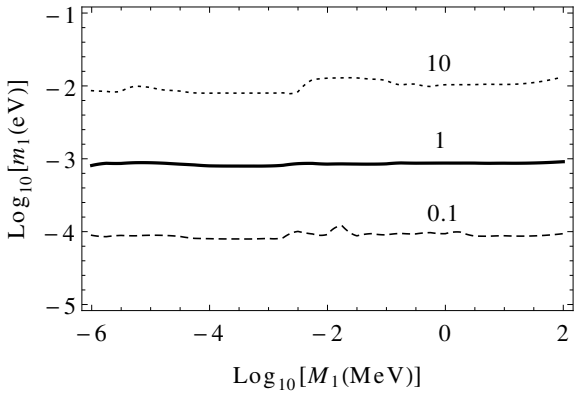

Figure 10.4: Contours of Min$[f_{s_1}(T_{\rm max})]$=0.1, 1, 10 on the plane (M_1, m_1).

tion of m_1 and M_1. The three lines correspond to Min$[f_{s_1}(T_{\rm max})] = 10^{-1}, 1, 10$. As expected the minimum is strongly correlated with m_1 and is roughly independent of M_1. Values of m_1 below the contour line at 1 correspond to non-thermalization giving the threshold $m_1^{th} \leq \mathcal{O}(10^{-3}\text{eV})$ for $M_1 \in$ [1eV-100MeV].

Note that the condition

$$\sum_{\alpha} |\,(U_{as})_{\alpha j}\,|^2 M_j \geq m_1^{th} \tag{10.13}$$

is always satisfied for at least two states to account for the atmospheric and solar mass splittings. This means that the two neutrinos will always thermalize, while the thermalization of one state depends on the lightest neutrino mass.

We can then distinguish two different scenarios

- $m_1 \geq m_{\rm th}$, and
- $m_1 \leq m_{\rm th}$.

In the first case, all three neutrinos reach thermal equilibrium and the conclusion from the first paper applies. The allowed mass spectra of the sterile states is summarized on the bottom plot in Fig. 10.5.

In the second case, the evolution of the non-thermalized sterile neutrino has to be studied more carefully. On the other hand, we checked that the evolution of the other two neutrinos is the same as in the 3+2 case, i.e. it is approximately independent on m_1 and M_1, so that the bounds on the two thermalized states apply as in the previous paper. The allowed mass range is then the one in the

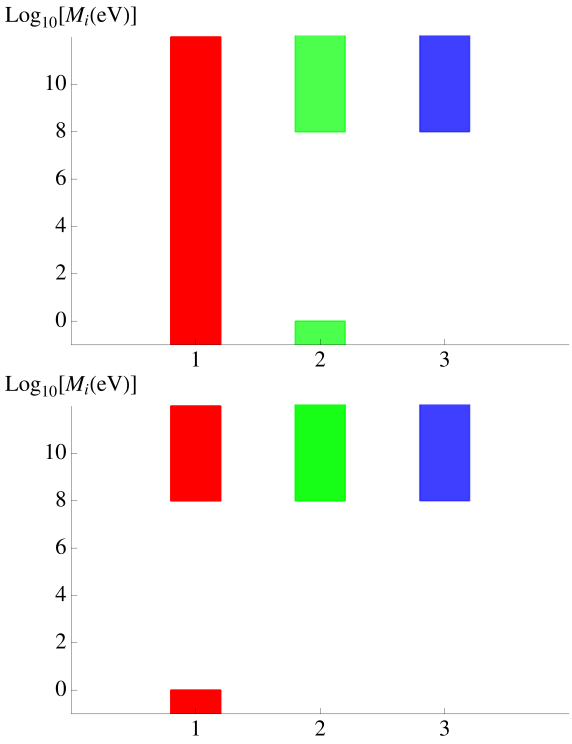

Figure 10.5: Allowed spectra of the heavy states M_i for $m_1 \geq m_1^{th}$ (up) and $m_1 \leq m_1^{th}$ (down).

upper plot of Fig. 10.5, where we have completely neglected the contribution of the nonthermal state to the energy density.

We examined the case of one non-thermal neutrino and two heavier than 100 MeV more thoughtfully. Assuming that two other neutrinos are above 100 MeV and do not have influence on BBN physics we calculated the distribution function of the non-thermal state as a function of M_1 and m_1 fixing other parameters to minimize f_{s_1}. In Fig. 10.6 we plotted the allowed parameter space, compatible with the cosmological bounds. Also, the recent X-ray constrained[2] exclude the possibility that the non-thermal neutrino can be a warm dark matter candidate in this model. Only in more complex models where a large leptonic asymmetry could be generated this is still possible.

Finally, we looked for a possible signal at neutrinoless double beta decay experiments, since the nonthermal neutrino below 100 MeV could contribute to $m_{\beta\beta}$. However, for the parameters compatible with cosmology, this contribution is always negligible.

10.3 Paper III

Neutrinos heavier than $\sim$ 100 MeV may have no impact on BBN, CMB or LSS, but they might seed the baryon asymmetry. In this work we studied the right handed neutrinos evolution before the electroweak phase transition, and analyzed the lepton asymmetry that might be generated. The main idea, firstly proposed in Ref. [232] is that the lepton asymmetry is created by the right handed neutrino oscillations, and transmitted to the baryons via sphaleron processes. Since the asymmetry is created during the production of the sterile neutrinos, their Yukawa couplings must be small enough to ensure that the created asymmetry is not washed out before the electroweak phase transition temperature T_{ew}. This condition, together with the constraints coming from the active neutrino mass measurements, forces the sterile neutrino mass to be below the electroweak scale, unlike in the standard leptogenesis scenario via the decay of very heavy sterile neutrinos. Furthermore, since the created asymmetry is stored in the sterile sector, at least one of the states must not reach thermal equilibrium before T_{ew}. What happens afterwards would not modify the baryon asymmetry since sphalerons are not active.

The baryon asymmetry, being a CP odd observable, should necessarily be proportional to the CP odd rephasing invariants [271]. The spectrum of this theory has six massive Majorana neutrinos, and the mixing is described in terms

[2]For recent constraints see Chapter 9.

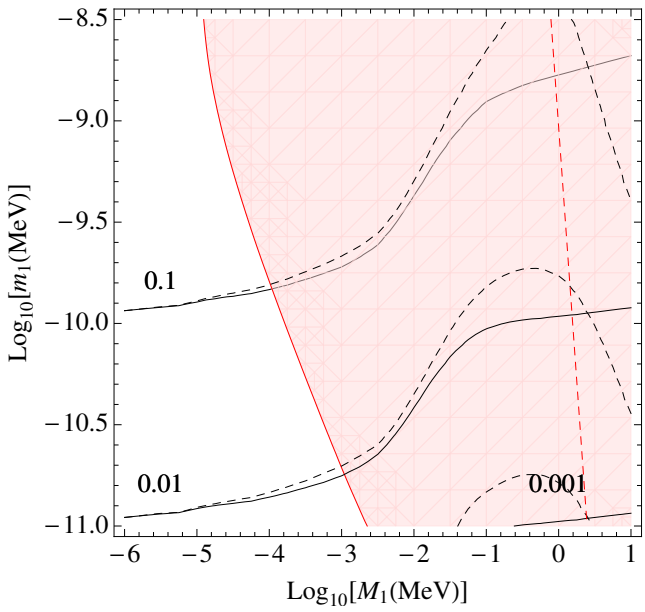

Figure 10.6: Contour plots for $\Delta N_{eff}^{(1)BBN} = 10^{-1}, 10^{-2}, 10^{-3}$ defined by the ratio of the energy density of the $j = 1$ sterile state and one standard neutrino as a function of m_1 and M_1. The solid (dashed) lines correspond to the contours of the ratio of sterile to active number (energy) densities. The shaded region corresponds to $\Omega_{s_1} h^2 \geq 0.1199$ and the dashed straight line is roughly the one corresponding to decay at recombination. The area left from this curve is excluded from $N_{eff}^{\rm CMB}$ constraints. The heavier neutrino masses have been fixed to $M_{2,3}$=1GeV, 10GeV and the unconstrained parameters have been chosen to minimize $f_1(T_{\rm max})$ and $f_2(T_{\rm max})$. The light neutrino spectrum has been assumed to be normal (NH).

of six angles and six CP phases generically, which accounts for six independent invariants [272], However, since the Majorana nature of the neutrinos is irrelevant at such high temperatures, we neglect those that correspond to Majorana phases, hence, there are only four independent invariants. At lowest order in the yukawas, they can be expressed via the two unitary matrices that diagonalize the Yukawa matrix $Y \equiv V^{\dagger}\mathrm{Diag}(y_1, y_2, y_3)W$ as:

$$\begin{aligned} I_1^{(2)} &= -\mathrm{Im}[W_{12}^* V_{11} V_{21}^* W_{22}] \\ I_1^{(3)} &= \mathrm{Im}[W_{12}^* V_{13} V_{23}^* W_{22}] \qquad (10.14) \\ I_2^{(3)} &= \mathrm{Im}[W_{13}^* V_{12} V_{22}^* W_{23}] \\ J_W &= -\mathrm{Im}[W_{23}^* W_{22} W_{32}^* W_{33}] \qquad (10.15) \end{aligned}$$

A generic expectation for the CP-asymmetry relevant for leptogenesis (that does not involve lepton number violation) is

$$\Delta_{CP} = \sum_{\alpha,k} |Y_{\alpha k}|^2 \, \Delta_\alpha, \qquad (10.16)$$

with

$$\Delta_\alpha = \sum_i \epsilon_{i\alpha}^L = \sum_{i,j} \mathrm{Im}[Y_{\alpha i} Y_{\alpha j}^* (Y^\dagger Y)_{ij}] f(M_i, M_j). \qquad (10.17)$$

and f an arbitrary function.

In the limit of vanishing y_3 (a generic restriction to ensure one non-thermal sterile neutrino), the asymmetry simplifies to

$$\begin{aligned} \Delta_{CP} &= y_1^2 y_2^2 (y_2^2 - y_1^2) \sum_{i,j} \mathrm{Im}[W_{1i}^* W_{1j} W_{2j}^* W_{2i}] f(M_i, M_j) \\ &+ y_1 y_2 (y_2^2 - y_1^2) \left\{ \left[(y_2^2 - y_1^2) I_1^{(2)} - y_2^2 I_1^{(3)} \right] [f(M_1, M_2) - f(M_2, M_1)] \right. \\ &+ \left. I_2^{(3)} [g(M_1) - g(M_3)] \right\} . \qquad (10.18) \end{aligned}$$

The original proposal [232] contained only the Jarlskog invariant J_W, while the famous νMSM model [176, 177] with two neutrinos in GeV and one in keV regime contains only $I_1^{(2)}$ and $I_1^{(3)}$ invariants since the third state is completely decoupled in that case.

A precise calculation of the produced asymmetry involves solving a set of kinetic equations for sterile neutrino sector. Following the formalism of [209] we derived the evolution equations of the CP-even and CP-odd parts of the neutrino

densities: $\rho_\pm \equiv \frac{\rho_N \pm \bar{\rho}_N}{2}$ and the lepton chemical potentials, μ_α, to linear order in μ_α, ρ_-:

$$\begin{aligned}
\dot{\rho}_+ &= -i[H_{\rm re}, \rho_+] + [H_{\rm im}, \rho_-] - \frac{\gamma_N^a + \gamma_N^b}{2}\{Y^\dagger Y, \rho_+ - \rho_{\rm eq}\} \\
&\quad + i\gamma_N^b {\rm Im}[Y^\dagger \mu Y]\rho_{\rm eq} + i\frac{\gamma_N^a}{2}\{{\rm Im}[Y^\dagger \mu Y], \rho_+\}, \\
\dot{\rho}_- &= -i[H_{\rm re}, \rho_-] + [H_{\rm im}, \rho_+] - \frac{\gamma_N^a + \gamma_N^b}{2}\{Y^\dagger Y, \rho_-\} \\
&\quad + \gamma_N^b {\rm Re}[Y^\dagger \mu Y]\rho_{\rm eq} + \frac{\gamma_N^a}{2}\{{\rm Re}[Y^\dagger \mu Y], \rho_+\}, \\
\dot{\mu}_\alpha &= -\mu_\alpha \left(\gamma_\nu^b {\rm Tr}[YY^\dagger I_\alpha] + \gamma_\nu^a {\rm Tr}[{\rm Re}[Y^\dagger I_\alpha Y] r_+]\right) \\
&\quad + (\gamma_\nu^a + \gamma_\nu^b){\rm Tr}[{\rm Re}[Y^\dagger I_\alpha Y] r_-]
\end{aligned} \tag{10.19}$$

where $H_{\rm re} \equiv {\rm Re}[H]$, $H_{\rm im} \equiv {\rm Im}[H]$, I_α is the projector on flavor α. $\gamma_N^{a,b}, \gamma_\nu^{a,b}$ are the rates of production/annihilation of a sterile neutrino or a lepton doublet, after factorizing the flavor structure in the Yukawas,

$$\gamma_{N(\nu)}^{a(b)} \equiv \frac{1}{2k_0}\sum_i \int_{\mathbf{p_1},\mathbf{p_2},\mathbf{p_3}} \rho_{\rm eq}(p_1)|\mathcal{M}_{N(\nu),i}^{(a(b))}|^2 (2\pi)^4 \delta(k + p_1 - p_2 - p_3), \tag{10.20}$$

where k is the momentum of the N or ν and

$$\gamma_{N,Q}^b = 2\gamma_{N,Q}^a = 2\gamma_{\nu,Q}^b = 4\gamma_{\nu,Q}^a = \frac{3}{16\pi^3}\frac{y_t^2 T^2}{k_0}. \tag{10.21}$$

In this work we only included top quark scattering in the calculation of the interaction rates.

In order to achieve some analytical understanding of the solutions of these complex equations, we proposed an analytical approach based on perturbation theory in the mixing angles of the V and W matrices. This analytical approximation allowed us to derive analytical solution also in the strong washout regime. For $y_3 =$, the asymmetry in the lepton sector can be written in the form:

$${\rm Tr}[\mu](t) = \sum_{I_{\rm CP}} I_{\rm CP} A_{I_{\rm CP}}(t). \tag{10.22}$$

Note that all the four CP invariants appear, $I_{\rm CP} = \left\{J_W, I_1^{(2)}, I_1^{(3)}, I_2^{(3)}\right\}$.

The functions $A_{I_{\rm CP}}(t)$ depend only on the Yukawa matrix eigenvalues and the mass differences of the sterile states. For explicit expression a reader is referred to the paper. Here we present the general behavior of those functions, each one for three cases: no degenerate sterile neutrino masses, two almost degenerate states, and the case where all three states are almost degenerate. The functions are given in Figs. 10.7,10.8.

The comparison of the analytic curves with the numerical ones in the case where only non-zero invariants are $I_1^{(2)}$ or $I_1^{(3)}$ is given if Fig. 10.9 where we chose highly degenerate case and the mixing angles of $(O)(10^-2)$.

The generated asymmetry in the lepton sector is transfered to the baryons so that the baryon asymmetry is given by [3]

$$Y_B = \frac{28}{79} Y_{B-L}, \tag{10.23}$$

which, neglecting spectator processes, is related to the chemical potentials as

$$Y_B \simeq 3 \times 10^{-3}\ \mathrm{Tr}[\mu(t)]|_{t_{EW}}\,. \tag{10.24}$$

As an example, we can estimate the asymmetry generated if the naive seesaw scaling with only two sterile neutrinos in the GeV range, and assume the lightest neutrino mass is in the eV range. If we choose $y_1^2 = y_2^2/2 = 10^{-14}$, we get

$$\mathrm{Tr}[\mu](t_{EW}) \;\simeq\; 7 \times 10^{-10} \frac{I_1^{(2)} - 2I_1^{(3)}}{|\Delta M_{12}^2(\mathrm{GeV}^2)|^{2/3}}. \tag{10.25}$$

This means that even if the CP invariants are $\mathcal{O}(1)$, the generation of the asymmetry would demand a large degree of degeneracy of the heavy neutrinos.

The analytic formulas allowed us to scan the parameter space for both 3+2 MM and 3+3 MM models. We obtained that in the case of the 3+2 models a mild degeneracy $\Delta M/M \sim 10^{-1}$ is needed for an inverted ordering of the light neutrinos, while it needs to be stronger for the normal ordering. In the case of 3 additional neutrinos no degeneracy is needed. However the approach based on the analytical approximation required that we restrict somewhat the allowed parameter space. The analytical approach should fail at sufficiently large times $t^{-1} \sim \mathcal{O}(\theta_{i3}^2 y_i^2 \gamma_N^{a,b})$ for $i = 1, 2$, where θ_{i3} are the mixing angles of he V, W matrices, so we impose constraints to avoid that this happened before or at the EW transition.

[3] For more details of the process look Chapter 9.

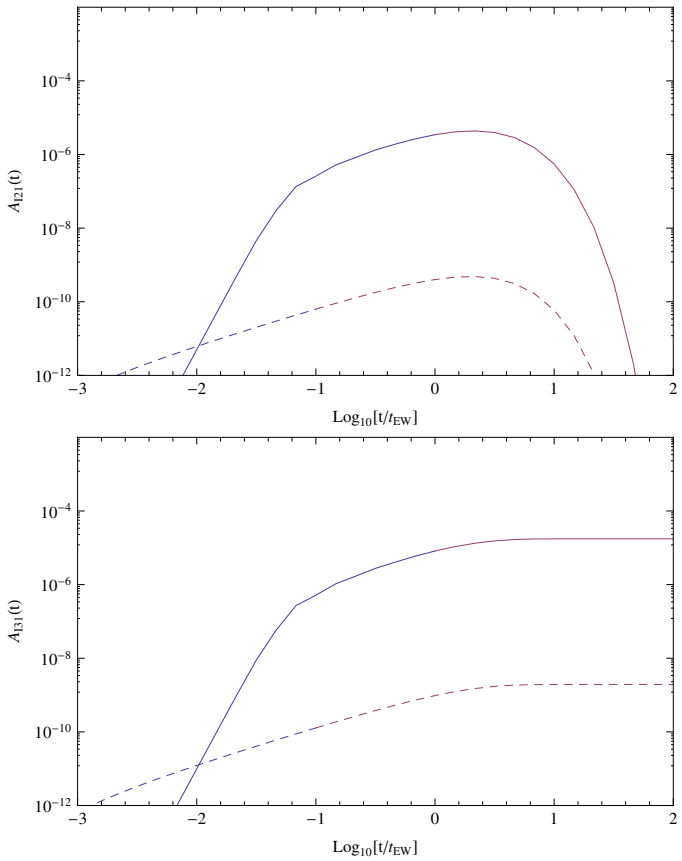

Figure 10.7: Functions $A_{I_1^{(2)}}(t)$ (top) and $A_{I_1^{(3)}}(t)$ (bottom) assuming the rates are dominated by top quark scattering, and taking $y_2/\sqrt{2} = y_1 = 10^{-7}$, for two choices of $\Delta M_{12} = 1\mathrm{GeV}^2$ (dashed) and $\Delta M_{12}^2 = 10^{-6}$ GeV^2 (solid). t_{EW} is the electroweak phase transition time, corresponding to $T_{EW} \simeq 140\mathrm{GeV}$.

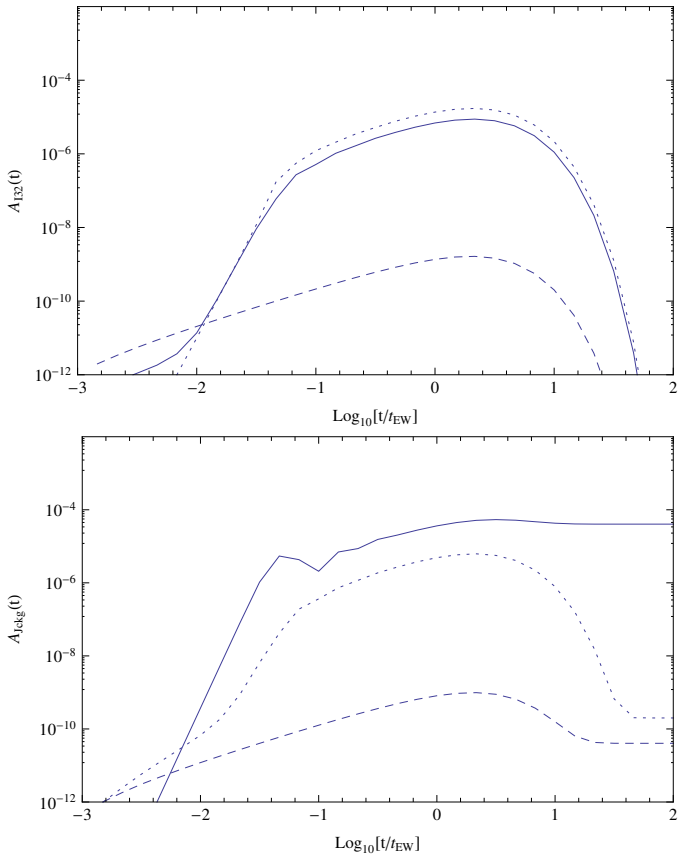

Figure 10.8: Functions $A_{I_2^{(3)}}(t)$ (top) and $A_{J_W}(t)$ (bottom) assuming the rates are dominated by top quark scattering, and taking $y_2/\sqrt{2} = y_1 = 10^{-7}$, for three choices of $[\Delta M_{12}^2, \Delta M_{13}^2] = [1, 2], [10^{-6}, 2]$ and $[10^{-6}, 2 \times 10^{-6}]$ in GeV^2 (dashed, dotted and solid). t_{EW} is the electroweak phase transition time, corresponding to $T_{EW} \simeq 140\mathrm{GeV}$.

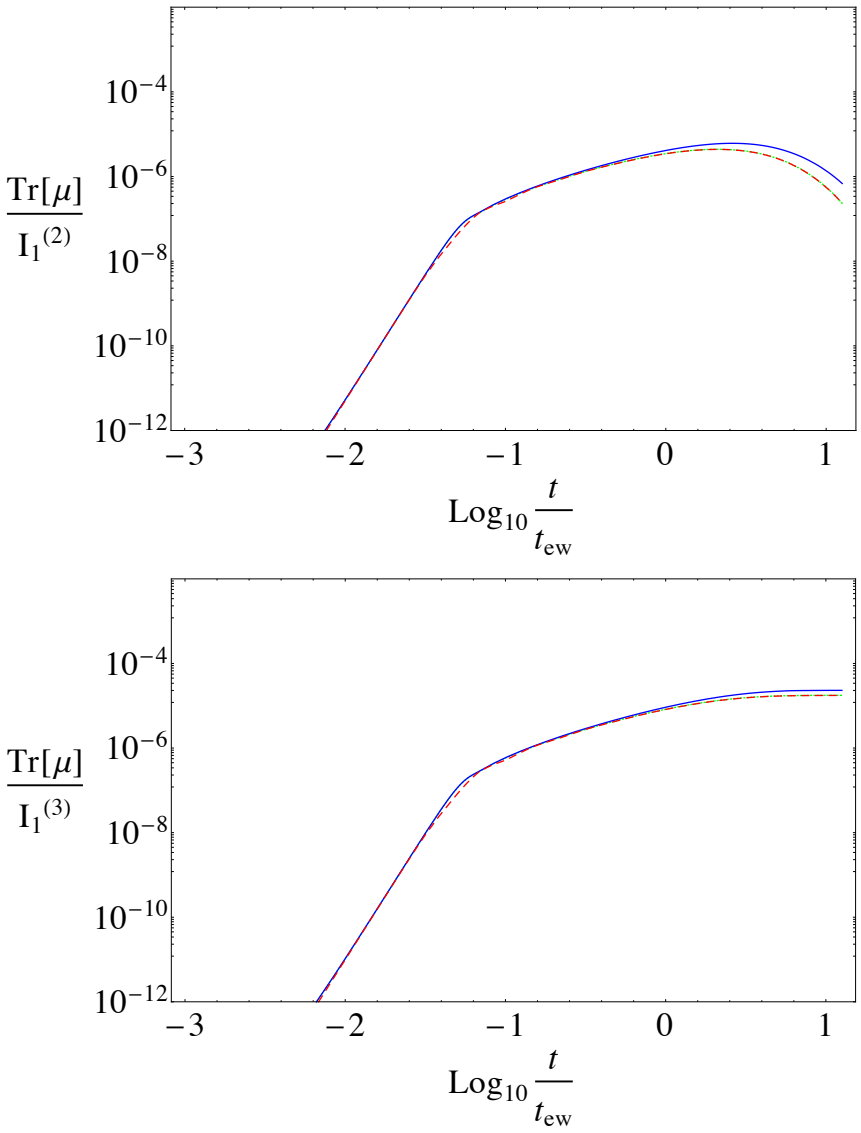

Figure 10.9: Full numerical solution (blue curve) and numerical solution neglecting non-linear effects (dotted green curve) compared to the analytic prediction (dashed red) for two choices of V, W such that the only non zero invariant is: $I_1^{(2)}$ (up) and $I_1^{(3)}$ (down). The other parameters are the same as in the degenerate case of Fig. 10.7

It is interesting to examine if the CP phases, or the neutrinoless double beta decay amplitude, could be affected by constraining the model to explain the baryon asymmetry. A precise numerical study of this question will be one of the topics of the next project.

10.4 Paper IV

In this work we pursued the possibility of explaining the baryon asymmetry in the context of the low scale seesaw models, with significant refinements

- We have included the contribution to the interaction rates of the gauge boson as well as the resumed $1 \to 2$ processes [273, 274]. These rates have been calculated in the previous literature assuming that the chemical potentials vanish. In our work, we have added the effect of the leptonic chemical potentials to linear order.

- We used consistently Fermi-Dirac or Bose-Einstein distributions throughout, as well as the spectator effects.

- We have optimized the numerical solution of the kinetic equations using the public software Squids [275] and Multinest [276–278]. This allowed us to explore the full parameter space of the 3+2MM model without any restrictions and analyze the Bayesian posterior probabilities assuming the model explains the baryon asymmetry within the experimental precision.

The processes in equilibrium involving the spectators, that do not appear explicitly in the kinetic equations, have the effect of redistributing the asymmetry generated in the lepton sector to the other particles in the plasma, without modifying the total $B/3 - L_\alpha$ number. Is therefore consistent to exclude these interactions if instead of the leptonic chemical potential, one includes the evolution of the densities, $n_B/3 - n_{L_\alpha}$ or the corresponding chemical potential. The new equations for the density matrices normalized to the equilibrium density, $r_N \equiv \rho_N/\rho_F$ and $r_{\bar{N}} \equiv \rho_{\bar{N}}/\rho_F$, describing the evolution with respect to the scale

factor $x = aT$ are:

$$\begin{aligned}
xH_u\frac{dr_N}{dx} &= -i[\langle H\rangle, r_N] - \frac{\langle\gamma_N^{(0)}\rangle}{2}\{Y^\dagger Y, r_N - 1\} \\
&\quad +\langle\gamma_N^{(1)}\rangle Y^\dagger\mu Y - \frac{\langle\gamma_N^{(2)}\rangle}{2}\big\{Y^\dagger\mu Y, r_N\big\}, \\
xH_u\frac{dr_{\bar N}}{dx} &= -i[\langle H^*\rangle, r_{\bar N}] - \frac{\langle\gamma_N^{(0)}\rangle}{2}\{Y^T Y^*, r_{\bar N} - 1\} \\
&\quad -\langle\gamma_N^{(1)}\rangle Y^T\mu Y^* + \frac{\langle\gamma_N^{(2)}\rangle}{2}\big\{Y^T\mu Y^*, r_{\bar N}\big\}, \\
xH_u\frac{d\mu_{B/3-L_\alpha}}{dx} &= \frac{\int_k\rho_F}{\int_k\rho_F'}\left\{\frac{\langle\gamma_N^{(0)}\rangle}{2}(Yr_NY^\dagger - Y^*r_{\bar N}Y^T)_{\alpha\alpha}\right. \\
&+ \left.\mu_\alpha\left(\frac{\langle\gamma_N^{(2)}\rangle}{2}(Yr_NY^\dagger + Y^*r_{\bar N}Y^T)_{\alpha\alpha} - \langle\gamma_N^{(1)}\rangle\mathrm{Tr}[YY^\dagger I_\alpha]\right)\right\}, \\
\mu_\alpha &= -\sum_\beta C_{\alpha\beta}\mu_{B/3-L_\beta},
\end{aligned} \tag{10.26}$$

where $\mu_{B/3-L_\alpha}$is defined to be

$$n_{B/3-L_\alpha} \equiv -2\mu_{B/3-L_\alpha}\int_k\rho_F' = \frac{1}{6}\mu_{B/3-L_\alpha}T^3. \tag{10.27}$$

and the matrix C is dictated by the fast interactions in the plasma [4]:

$$C_{\alpha\beta} = \frac{1}{711}\begin{pmatrix} 221 & -16 & -16 \\ -16 & 221 & -16 \\ -16 & -16 & 221 \end{pmatrix}, \tag{10.28}$$

The interaction rates are averaged in the momentum space and their values can be found in the published article reproduced in part II.

We have performed a Bayesian analysis of the posterior probability distributions in the model parameters assuming that the model explains the baryon asymmetry. For this we have used the public software codes Squids [279] and MultiNest [278]. An important consideration are the priors in the parameters. We have considered flat priors in all the Casas-Ibarra parameters except the masses where we have assumed two hypothesis: 1) flat prior in $\log_{10}\left(\frac{M_{1,2}}{\mathrm{GeV}}\right)$, within the range $M_{1,2} \in [0.1\mathrm{GeV}, 10^2\mathrm{GeV}]$, and 2) a flat prior in $\log_{10}\left(\frac{M_1}{GeV}\right)$ and

[4]For details look at Chapter 8

in $\log_{10}\left(\frac{|M_2-M_1|}{\text{GeV}}\right)$ in the range $M_2 - M_1 \in [10^{-8}\text{GeV}, 10^2\text{GeV}]$, that does not penalize the highly degenerate solutions. The results on the planes $(|U_{\alpha s}|^2, M_1)$ for $\alpha = e, \mu, \tau$ are shown in Figs.10.10, where we also include he present and future constraints. The blue regions corresponds to the first prior hypothesis, while the red corresponds to the second. The conclusion from this study is that the less degenerate solutions (achieved with the first hypothesis on the priors) are possible only for masses smaller than 1 GeV. This is precisely the region where he experiment SHiP reaches its maximum sensitivity.

Interestingly, the mild level of degeneracy in the masses of the blue contours is also correlated with a relatively large mixing, and a sizable contribution to the amplitude of neutrinoless double beta decay. These correlations are shown in Figs. 10.11.

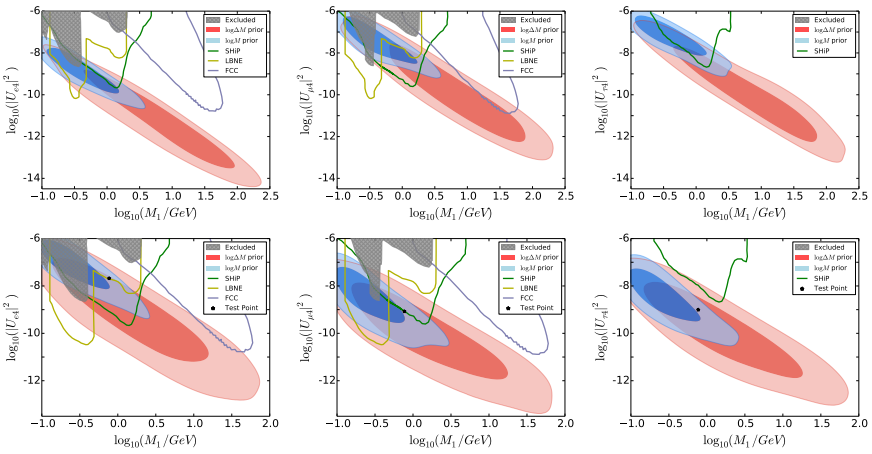

Figure 10.10: Comparison of the posterior probability contours at 68% and 90% on the planes mixings with e, μ, τ versus masses, with the present [146], [147] (shaded region) and future constraints from DUNE [133], SHiP [192] and FCC [193] for NH (up) and IH (down).

A very interesting question is whether the baryon asymmetry can be predicted if the sterile neutrinos were discovered in a putative measurement in ShiP, the CP phase in neutrino oscillations, δ, measured or neutrinoless double beta decay observed.

To answer this question, as a proof of principle we have studied the posterior probabilities for a hypothetical measurement of SHiP, corresponding to the point marked by a star in the plot 10.10 for IH. Assuming very optimistic errors for

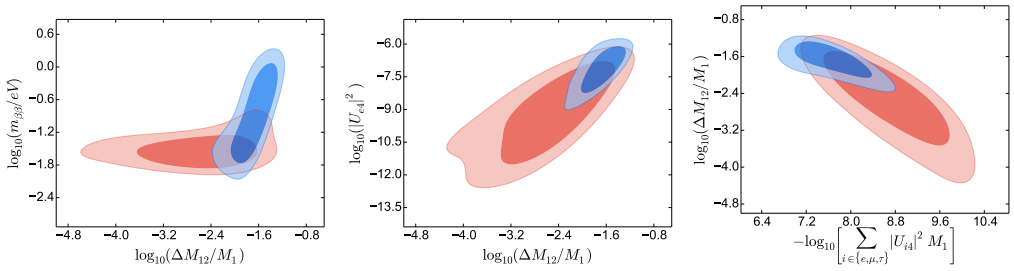

Figure 10.11: Posterior probabilities for the amplitude of neutrinoless double beta decay (left), electron mixing (middle) and the mass degeneracy versus $\sum_{\alpha=e,\mu,\tau}|U_{\alpha 4}|^2 M_1$ (right).

this experiment in determining the mixings and masses at the 0.1% and 1% level respectively (red region), as well as a putative δ measurement, with the error of 0.17 rad (blue region), we found a strong correlation between $m_{\beta\beta}$ and Y_B, which is presented in Fig 10.12. If a precise measurement of $m_{\beta\beta}$ was possible (which is challenging due to the uncertainty in the nuclear matrix elements), this plot shows that it might be possible to predict the baryon asymmetry up to a sign. For NH, the expectations would be dimmer since $m_{\beta\beta}$ is much smaller in this case.

Another interesting observation that resulted from this work is that, independently of whether the baryon asymmetry can be explained or not, the discovery in SHiP of the extra neutrinos in the 3+2 MM model and the measurement of the ratio of the mixing to electron and muon could allow the determination with high precision a combination of the two CP violating phases in the PMNS matrix. The posterior probability of such a measurement on the plane of these two phases is shown in Fig. 10.13. At leading order of small parameter $\mathcal{O}(\epsilon) : r \equiv \sqrt{\frac{\Delta m^2_{sol}}{\Delta m^2_{atm}}} \sim \theta_{13} \sim e^{-\frac{\gamma}{2}}$,, the ratio of the electron and muon mixing is expected to be well approximated by:

$$\text{IH}: \quad \frac{|U_{e4}|^2}{|U_{\mu 4}|^2} \simeq \frac{1}{c_{23}^2}\frac{1+\sin\phi_1 \sin 2\theta_{12}}{1-\sin\phi_1 \sin 2\theta_{12}} + \mathcal{O}(\epsilon). \tag{10.29}$$

This analytical expectation is the line on the same plot.

This measurement provides a new method to discover leptonic CP violation, using CP even observables.

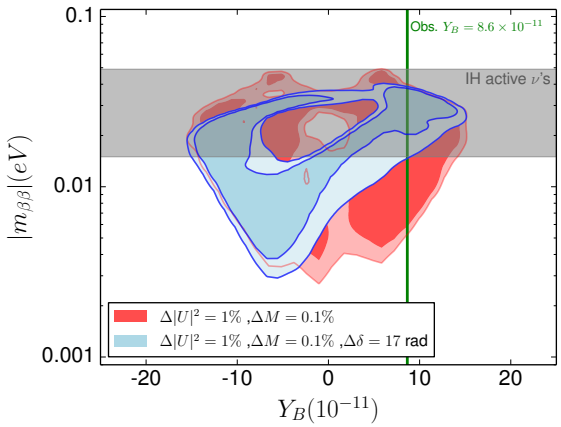

Figure 10.12: Posterior probabilities in the $|m_{\beta\beta}|$ vs Y_B plane from a putative measurement at SHiP, assuming $0.1\%, 1\%$ uncertainty (red) and an additional measurement of δ (blue), where the vertical green line denotes the observed baryon asymmetry.

The case of three additional neutrinos has more free parameters and is more difficult to analyse, both analytically and numerically and is left for future work.

10.5 Final remarks

This thesis was devoted to the study of low scale seesaw models with additional 2 and 3 right handed neutrinos, and their impact on cosmological observables. The main original results have been to demonstrate that BBN and CMB physics severely constrain the allowed value of the Majorana neutrino masses in the range below 100 MeV, and to show that in the range of 1-10 GeV, the sterile neutrinos might naturally explain the baryon asymmetry of the Universe and do so in a testable way, giving a strong theoretical motivation for future accelerator experiments that can significantly improve the searches of sterile neutrinos in this range of masses.

My personal opinion is that the more precise measurements that will come from cosmology and the possibility to discover sterile neutrinos in the GeV range makes this a very interesting period to work on the phenomenology of these models.

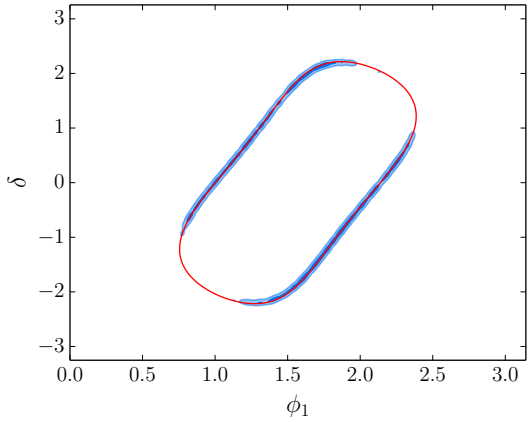

Figure 10.13: Posterior probabilities from a SHiP measurement of the masses and mixings with e, μ on the plane (ϕ_1, δ) compared with the result of the analytical ratio (red line) for parameters in the test point.

Chapter 11

Resumen de la Tesis

11.1 Objetivos

El modelo estándar (SM) es la teoría que explica las tres interacciones fundamentales: electromagnetismo y las fuerzas fuerte y débil. El contenido del SM se compone de tres familias de quarks y leptones, que se difieren sólo por sus masas, mientras que las interacciones se describen con tres bosones masivos $W^{\pm}$, Z y uno boson sin masa, el fotón, para el caso electrodébil, y ocho gluones sin masa para la interacción fuerte. Las masas de los bosones y fermiones se obtienen a través de su interacción con el campo escalar del Higgs, donde los términos de interacción se denominan términos de interacción de Yukawa, y el acoplamiento correspondiente se llama acoplamiento de Yukawa.

Los neutrinos son los únicos leptones sin masa en el modelo estándar, simplemente porque cuando se construyó la teoría se creía que los neutrinos no tenían masa. Sin embargo, los experimentos de oscilaciones han demostrado que esta hipótesis no es correcta. El premio Nobel de 2015 fue concedido conjuntamente a Takaaki Kajita a la cabeza de la colaboración SuperKamiokande (SK) y a Arthur B. McDonald, el fundador del Sudbury Neutrinos Observatory (SNO), por "el descubrimiento de las oscilaciones de neutrinos, lo que demuestra que los neutrinos tienen masa". Las oscilaciones son un fenómeno cuántico que implica que un neutrino producido en un sabor puede ser detectado como uno de otro sabor diferente después de viajar una distancia macroscópica. Esto es debido que los autoestados del Hamiltoniano libre (autoestados de masa) y los del Hamiltoniano de interacciones (autoestados de sabor) no son los mismos. La probabilidad de

oscilación viene dada por:

$$P(\nu_\alpha \to \nu_\beta) = \sum_{i,j} U^*_{\beta j} U_{\alpha j} U_{\beta i} U^*_{\alpha i} e^{-i \frac{\Delta {m^2}_{ij} L}{2|E_\nu|}}, \tag{11.1}$$

y depende del matriz de mezcla (U), las diferencias de masas de los neutrinos ($\Delta {m^2}_{ij} \equiv m^2_j - m^2_i$) , la distancia ($L$) y la energía de neutrinos E_ν. Por lo tanto, las experimentos de oscilaciones de neutrinos no son sensibles a las masas absolutas de los neutrinos sino sólo a sus diferencias. Los resultados de varios experimentos con neutrinos solares, atmosféricos o bien neutrinos producidos en reactores o aceleradores puedes explicarse en términos de la oscilación de tres familias de neutrinos, que dependen de dos diferencias de masas, $\Delta m_\odot \simeq 10^{-5}$ eV, $\Delta m_{atm} \simeq 10^{-3}$ eV y una matriz de mezcla determinada por tres ángulos, que ya han sido medidos, y una fase de CP, que permanece indeterminada. Los datos actuales no permiten distinguir entre la dos posibles jerarquías, normal (NH) e invertida (IH), representadas en la Fig.11.1.

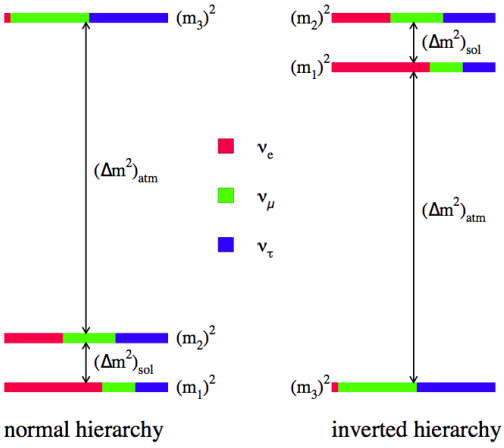

Figure 11.1: Representacion schematica de las jerarquías normal (NH) e invertida (IH).

La determinación de todos estos parámetros requiere un análisis global de todos los experimentos como el que es regularmente actualizado en [96].

La masa absoluta se puede medir en los experimentos de búsqueda directa, como la desintegración beta. Por ahora existe solo límite superior de la masa absoluta ≤ 2.3 eV [118]. Los límites más fuertes provienen de análisis cosmológicos

que han permitido constreñir la suma de masas de los neutrinos en el rango ≤ 0.23 eV [128].

El mecanismo más directo para dar masas a los neutrinos en el modelo estándar es de añadir neutrinos dextrógiros y sus correspondientes interacciones de Yukawa a los dobletes leptónicos y al Higgs. Sin embargo, como la masa de los neutrinos es al menos 10^{6-7} veces más pequeña que la masa del electrón, esto implicaría que el acoplamiento de Yukawa de los neutrinos ha de ser 6-7 órdenes de magnitud más pequeño que el de electrón, lo cual no es natural. Otra opción, más económica es utilizar sólo los neutrinos que ya existen en el modelo estándar y generar un término de masa de Majorana. Una partícula de Majorana es igual a su antipartícula y su existencia supone la violación del número leptónico, una de las simetrías globales accidentales del modelo estándar. La manera de generar una masa de Majorana para los neutrinos en el modelo estándar es a través del operador de Weinberg

$$L_{Weinberg} = \frac{1}{\Lambda}(\bar{l}_{L_i}\Phi)Y_{ij}(\Phi^T {l_L}^c), \tag{11.2}$$

donde Y es matriz de Yukawa y Λ tiene unidades de masa. En el vacío este término es una masa de Majorana para los neutrinos. Es, sin embargo, un operador no es renormalizable, y esa teoría necesita ser completada a altas energías. Para completar la teoría, la extensión más popular es el seesaw tipo I, donde se añaden singletes, un número, $n_R \leq 3$, de fermiones diestros de Majorana, $N_R = (N_R^1, ..N_R^{n_R})$, también llamados neutrinos estériles, dado que no tienen ninguna carga gauge. Las interacciones permitidas por la simetría gauge para estos nuevos campos son, a parte de su término cinético:

$$-L_{M_\nu} = \bar{L}\tilde{\Phi}Y_\nu N_R + \frac{1}{2}\bar{N}_R^c M_R N_R + h.c. \ , \tag{11.3}$$

donde el primer termino es el termino de Yukawa, y el segundo es la masa Majorana de los neutrinos diestros. Después de la rotura de la simetría electrodébil, el campo de Higgs obtiene su valor esperado de vacío, v, y si asumimos que la masa de los neutrinos diestros es mucho mas grande que la masa Dirac ($m_D = v/\sqrt{2}Y_\nu$), el espectro de la teoría contiene n_R neutrinos ligeros de masa:

$$M_\nu \ \simeq - \ \ m_D \frac{1}{M_R} m_D^T \ . \tag{11.4}$$

y n_R pesados con masas:

$$M_N \simeq M_R, \tag{11.5}$$

Hay además $3 - n_R$ neutrinos sin masa. Para acomodar dos diferencias de masas diferentes, es necesario que $n_R \geq 2$, mientras que para que los tres neutrinos más ligeros sean masivos $n_R \geq 3$. Tanto los neutrinos ligeros como los pesados son combinaciones de los neutrinos activos y los estériles, aunque los ligeros son predominantemente activos y los pesados estériles.

Esto significa que si la masa de Majorana, M_R, es suficiente alta, 10^{12-15} GeV, los acoplamientos de Yukawa pueden ser de $\mathcal{O}(1)$ y aun así explicar las masas tan diminutas de los neutrinos. Sin embargo, esta escala podría también tener un valor menor que la escala electrodébil y ello sería técnicamente natural, dado que en el límite $M_R \to 0$ se recupera la simetría leptónica.

La señal mas prometedora para descubrir si los neutrinos son de Majorana es la desintegraciones beta doble sin neutrinos ($0\nu\beta\beta$), representado en la Fig. 11.2. La amplitud de este proceso es proporcional a la masa efectiva de la desintegra-

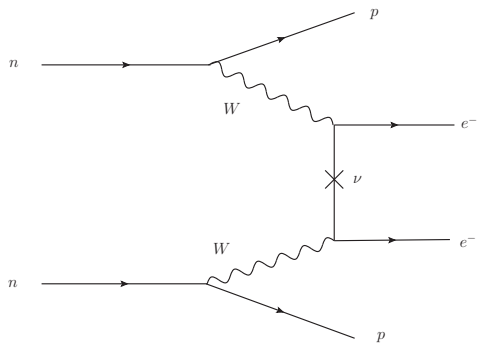

Figure 11.2: El proceso de la desintegracion beta doble sin neutrinos.

ciones beta doble sin neutrinos:

$$m_{\beta\beta} = \sum_i U_{ei}^2 m_i, \tag{11.6}$$

que depende de la matriz de mezcla y la masa de los neutrinos suficientemente ligeros ($m_i < 100$ MeV). En el caso de que haya sólo tres neutrinos ligeros, la matrix U depende de tres fases de CP, de las cuales sólo una, δ, se puede determinar en oscilaciones de neutrinos, las otras sin embargo modifican $m_{\beta\beta}$.

Los neutrinos pesados, dependiendo de su masa, pueden tener efectos no triviales en la cosmología estándar. A la escala GeV, podrían explicar la asimetría observada de materia-antimateria. Un neutrino en el rango de keV podría ser un buen candidato para la materia oscura (DM) . Neutrinos con masas por debajo del GeV afectan la producción de nucleos ligeros durante Big Bang Nucleosynthesis (BBN), las propiedades de la radiación de fondo de microondas (CMB) o la formación de la estructura a gran escala (LSS).

En esta tesis, hemos estudiado las implicaciones cosmológicas de que existan neutrinos pesados en el modelo seesaw con masas por debajo de la escala electrodébil.

11.2 Metodología

En esta sección vamos a revisar el modelo seesaw y su parametrización. Además introduciremos el formalismo de evolución cuántica de la función de distribución de los neutrinos en la universo temprano, lo cual nos permitirá determinarar sus efectos en el historia del Universo, antes y después de transición de fase electrodébil.

11.2.1 El Modelo

En esta tesis vamos a considerar el modelo seesaw tipo I mínimo con dos o tres neutrinos diestros añadidos, $n_R = 2, 3$ (3 + 2 MM y 3+3 MM) [1]

El Lagrangiano de esos modelos es

$$\mathcal{L} = \mathcal{L}_{SM} - \sum_{\alpha,i} \bar{L}^{\alpha} Y^{\alpha i} \tilde{\Phi} N_R^i - \sum_{i,j=1}^{n_R} \frac{1}{2} \bar{N}_R^{ic} M^{ij} N_R^j + h.c.,$$

donde Y es $3 \times n_R$ ($n_R = 2, 3$) matriz compleja y M es el matriz $n_R \times n_R$ real diagonal.

Una parametrización muy conveniente es el de Casas-Ibarra [144], donde la matriz de Yukawa se puede escribir en términos de los parámetros accesibles a bajas energías (las diferencias de masas y mezclas de los neutrinos ligeros):

$$Y = -iU^*_{\rm PMNS} \sqrt{m_{\rm light}} R(z_{ij})^T \sqrt{M} \frac{\sqrt{2}}{v}, \tag{11.7}$$

donde $m_{\rm light}$ es el matriz de masas de los neutrinos ligeros, $U_{\rm PMNS}(\theta_{12}, \theta_{13}, \theta_{23}, \delta, \phi_1, \phi_2)$ es la matriz de Pontecorvo–Maki–Nakagawa–Sakata (PMNS) [41,42] que describe la combinación de los neutrinos ligeros que se acoplan a los leptones cargados. M es la matriz de las masas de los neutrinos pesados, y R es una matriz ortogonal compleja, que depende de uno (tres) ángulo(s) complejo(s) z_{ij} para el caso de $n_R = 2$ ($n_R = 3$).

En el modelo 3+2 MM, hay un neutrino sin masa y depende por tanto de seis parámetros aun sin determinar: dos fases de CP en $U_{\rm PMNS}$, dos masas pesadas en M, y un ángulo complejo en R (cinco parámetros libres). En el modelo 3 + 3 MM, todos los neutrinos son masivos y el número de parámetros desconocidos es

[1] La extensión del SM con solo un neutrino diestro no puede puede explicar dos diferencias de masa observadas en los experimentos de oscilaciones [143].

significativamente mayor: 3 fases de CP en $U_{\rm PMNS}$, y la masa del neutrino más ligero, tres masas pesadas y tres ángulos complejos en R (13 parámetros libres).

Otra parametrizacion que vamos a usar es en término de dos matrices unitarias que diagonalizan el matriz de Yukawa (cada una de ellas con tres ángulos y tres fases de CP):

$$Y \equiv V^{\dagger}\mathrm{Diag}(y_1, y_2, y_3)W, \tag{11.8}$$

esta parametrizacion es muy útil para calcular los invariantes CP del modelo.

Los neutrinos pesados en modelos seesaw de baja escala pueden dar lugar a efectos observables en diversas búsquedas directas o indirectas. En el capítulo 5 hemos resumido los principales resultados de dichas búsquedas, que restringen fuertemente el espacio de parámetros. Las medidas más sensibles provienen acualmente de búsquedas directas en desintegraciones de mesones de piones y kaones, o en desintegraciones del Z en el colisionador e^+e^-, LEP, representados en las Figs. 5.2,5.3,5.4 y 5.5. Además la contribución de estos neutrinos, si $M_i \leq 100$ MeV, a la masa efectiva de $0\nu\beta\beta$:

$$m_{\beta\beta} = e^{i\alpha}m_1c_{12}^2c_{13}^2 + e^{i\beta}m_2c_{13}^2s_{12}^2 + m_3s_{13}^2 + \sum_i \left(U_{ei+3}\right)^2 M_i, \tag{11.9}$$

permite imponer cotas muy fuertes en las mezclas de estos neutrinos pesados.

11.2.2 Evolución de neutrinos estériles en el Universo Temprano

La termodinámica de los neutrinos en el universo temprano se describe mediante el formalismo de la matriz densidad, primero propuesto por Raffelt-Sigl [209]. Este formalismo permite determinar la evolución de las matrices densidad, ρ_p y $\bar{\rho}_p$, definidas como el valor esperado de los operadores número para partículas y antiparículas:

$$\left\langle a_j^{\dagger}(p)a_i(p')\right\rangle = (2\pi)^3\delta^{(3)}(p-p')(\rho_p)_{ij} \tag{11.10}$$

$$\left\langle b_i^{\dagger}(p)b_j(p')\right\rangle = (2\pi)^3\delta^{(3)}(p-p')(\overline{\rho}_p)_{ij}, \tag{11.11}$$

donde $a_i^{\dagger}(p)$ and $b_(^{\dagger}p)$ son los operadores de creación de un neutrino/antineutrino i con momento p. A pesar de que los neutrinos son de Majorana, estamos interesados en el régimen en que $M_i/T \ll 1$ y por tanto es posible considerar que el estado partícula es un estado de helicidad dado y el de antipartícula el de helicidad opuesta.

Asumiendo que el plasma de partículas es un medio diluido, que las interacciones son de suficiente corto alcance y que las interacciones de los neutrinos no cambian el estado del plasma, se puede derivar la evolución de la matriz de densidad:

$$\dot{\rho}_p = -i \left[\Omega_p^0, \rho_p\right] + (\dot{\rho_p})_{\text{colision}}, \tag{11.12}$$

donde el primer término incluye el efecto del Hamiltoniano libre, que da lugar a las oscilaciones, mientras que el segundo término representa las colisiones.

Si el Hamiltoniano de interacción es de la forma

$$H_{int} = \frac{G_F}{\sqrt{(2)}} \int d^3x \bar{\xi_i}(x) N_i(x) + h.c \tag{11.13}$$

entonces $(\dot{\rho})_{\text{colision}}$ se puede escribir como

$$(\dot{\rho})_{\text{colision}} = \{P_p, (1-\rho_p)\} - \{A_p, \rho_p\}. \tag{11.14}$$

P_p y A_p son matrices que describen los procesos de producción y la aniquilación de cada sabor de neutrinos y tienen forma sencilla en el caso de los medios diluidos. Por ejemplo, en el caso de colisiones de partículas $N_i + b \leftrightarrow c + d$, producción y aniquilación del neutrino N_i es

$$\begin{aligned} P_p &= \int d\pi(p_b) d\pi(p_c) d\pi(p_d) (2\pi)^4 \delta^{(4)}(p + p_b - p_c - p_d) \\ &\times |M_{cd,ib}|^2 f_c(p_c, t) f_d(p_d, t)(1 \pm f_b(p_b, t)) \qquad (11.15) \\ A_p &= \int d\pi(p_b) d\pi(p_c) d\pi(p_d) (2\pi)^4 \delta^{(4)}(p + p_b - p_c - p_d) \\ &\times |M_{ib,cd}|^2 f_b(p_b, t)(1 \pm f_c(p_c, t))(1 \pm f_d(p_d, t)). \qquad (11.16) \end{aligned}$$

Dependiendo de las interacciones que pueden producir/aniquilar neutrinos estériles, en el universo temprano hay dos épocas diferentes: antes y después de transición de fase electrodébil. En primer caso los neutrinos estériles son principalmente producidos/anihilados con los colisiones del boson de Higgs, mientras, cuando el Higgs obtiene su VEV los interacciones principales vienen de la mezcla con los neutrinos activos que ya existen en la plasma.

11.2.3 Neutrinos estériles antes de la transacción de fase electrodébil

La observación del universo muestra que la materia es más abundante que la antimateria. La fracción de bariónes a fotones, $\eta_B \sim 6 \times 10^{-10}$, es la misma en BBN y CMB . Una solución posibles es asumir que la asimetría existe desde el principio, pero si esto fuera así la inflacción borraría dicha asimetría, entonces, la asimetría tiene que ser producida de forma dinámica trás el periodo inflaccionario. Los tres condiciones necesarias para producir un asimetría a partir de una situación con simetría entre materia y antimateria fueron establecidas por Sakharov [212];

- las interacciones deben violar la conservación del numero de baryones (B),
- deben violar las simetría discretas C y CP
- dichas interacciones deben estar fuera del equilibrio

La asimetría podría producirse en primer lugar en el sector leptónico en un proceso denominado leptogénesis. Si esto ocurre por encima de la transición de fase electrodébil, la asimetría leptónica produciría una bariónica a través de los esfalerones. Los esfalerones son la consecuencia de la estructura no trivial del vacío electrodébil. La transición entre los distintos vacíos conlleva un cambio el número leptónico y bariónico que mantiene constante la diferencia. A bajas energías estas transiciones sólo pueden ocurrir debido al efecto túnel, descrito por los instantones, y están por lo tanto muy suprimidas. Sin embargo a energías suficientemente altas como en el universo temprano la energía cinética de las partículas es lo suficientemente alta para superar la barrera y el proceso puede ocurrir eficientemente hasta la transición de fase electrodébil $T > T_{EW}$.

La leptogńenesis estándar asume neutrinos muy pesados que alcazan el equilibrio térmico a muy altas temperaturas y se desintegran fuera del equilbrio de forma ligeramente asimétrica en leptones y antileptones [217] Este mecanismo requiere que la escala se Majorana del modelo seesaw sea mucho mayor que la escala electrodébil. Sin embargo en el caso de que esta escala sea mucho menor, del orden del GeV, otro mecanismo de leptogénesis es posible. En este caso, el valor de los yukawas es tan pequeño que alguno de los neutrinos estériles puede no llegar al equilibrio térmico antes de la transición de fase. En este caso una asimetría leptónica puede aparecer durante la producción de los neutrinos diestros, ser transmitida a los bariones por los esfalerones y sobrevivir hasta la transición de fase electrodébil [232].

11.2.4 Neutrinos estériles después de electroweak phase transition

Neutrinos suficiemente ligeros pueden contribuir a la densidad de radiación, o la densidad de materia, durante las épocas de BBN o CMB, medidas con los parámetros N_{eff} y Ω_C. La densidad total de radiación se parametriza en términos número de grados de libertad relativistas, g_*,

$$\rho_R = \frac{\pi^2}{30} g_\star T^4. \tag{11.17}$$

N_{eff} mide la contribución de los neutrinos a la densidad de radiación:

$$g_\star = \sum_{i=bosons} g_i \left(\frac{T_i}{T}\right)^4 + \frac{7}{8} \sum_{i=fermions-neutrinos} g_i \left(\frac{T_i}{T}\right)^4 + \frac{7}{8} N_{eff}, \tag{11.18}$$

donde

$$N_{eff} = N_\nu + \Delta N_{eff} \equiv N_{eff}, \tag{11.19}$$

y $N_\nu = 3.046$ es la contribución de los tres neutrinos estándar, mientras que ΔN_{eff} mide la contribución de los neutrinos extra [2].

Para calcular la contribución de un neutrino adicional a ΔN_{eff}, tenemos que tener en cuenta un factor de dilución, es decir, si la temperatura de desacoplo de dicho estado (T_{d_i}) es mucho mayor que la temperatura BBN las temperaturas de los estado desacoplado y los neutrinos activos serán diferentes debido a la variación de g_* entre esas dos temperaturas. De la conservación de la entropía se estima que cada uno de los estados estéril contribuye, por tanto, con $\Delta N_{\mathrm{eff}\,s_i}(T_{\mathrm{BBN}}) = (g_*(T_{\mathrm{BBN}})/g_*(T_{d_i}))^{4/3}$.

Si los neutrinos se descoplan siendo no relativistas su densidad está exponencialmente suprimida $n_i \propto \exp -M_i/T_{d_i}$, donde M_i es su masa y T_{d_i} la temperatura de plasma durante el desacoplo, y por lo tanto, su contribución a la expansión del universo es despreciable en este caso.

Una partícula masiva contribuye a la densidad de materia

$$\Omega_{s_i} = \frac{M_i n_i}{\rho_{cr}} \leq \Omega_c, \tag{11.20}$$

donde s_i es el i-ésima especie de neutrino estéril, M_i su masa, n_i la numero de partículas por unidad de volumen y $\Omega_c = 0.119 \pm 0.001$ es la densidad de la materia

[2] El N_ν no es exactamente 3 porque los distribuciones de spectra de momento de los neutrinos no son exactamente los de equilibrio.

oscura [128]. Expresado en términos de la densidad del número normalizada a la densidad del número de la distribución de Fermi-Dirac (n_0) la condición de que la contribución no supere el total de la materia oscura es

$$\frac{M_i}{\text{eV}}\frac{n_i/n_0}{94.1} \leq \Omega_c. \tag{11.21}$$

Neutrinos estériles estables podrían ser un candidato para la materia oscura templada sólo si una asimetría leptónica fundamentación está presente en el plasma [239, 240], que es la consecuencia de las curvas de exclusión de rayos X.

Otro factor importante a tener en cuenta es si el neutrino estéril decae y, si lo hace, en que momento de la evolución del universo esto sucede. Un neutrino que se desintegra antes de BBN no tiene ningún impacto en estos observables, porque $g_\star$ sería el mismo que en el modelo estándar. La desintegración después de BBN afectaría el contenido de la radiación durante el CMB. Los límites actuales para neutrinos estériles como función de su masa y mezcla se pueden encontrar en [241].

Las medidas de BBN dependen fuertemente de $g_\star$ en esta epoca, lo cual constriñe $N_{eff}^{BBN} = 3.01^{+0.95}_{-0.76}$ at 95% C.L. [249]. Por otra parte la medida de las perturbaciones en la radiación de fondo de microondas permite determinar con precisión $N_{eff}^{CMB} = 3.2 \pm 0.5$.

11.3 Resultados

En esta sección vamos a resumir los principales resultados de nuestra investigación, contenidos en los artículos de la parte II de esta tesis.

11.3.1 Articulo I

Una nueva partícula lo suficientemente abundante en el Universo temprano podría cambiar la densidad de la radiación / materia en el momento de BBN y CMB, así como la estructura a gran escala LSS. En este trabajo calculamos la contribución a la densidad de radiación / materia de los dos estados adicionales del modelo de seesaw tipo I mínimo con dos neutrinos estériles.

Si sus masas son menores que 1GeV o así, estos neutrinos se producen sólo después de la transición de fase electrodébil a través de la mezcla con los activos, por lo tanto, la frecuencia de interacción de los neutrino estériles es proporcional a la de interacción de los neutrinos de sabor a multiplicada por la probabilidad que un neutrino de sabor a oscile a un estéril

$$\Gamma_{s_i} \simeq \frac{1}{2}\sum_a \langle P(\nu_a \to \nu_{s_i})\rangle \times \Gamma_a. \tag{11.22}$$

La probabilidad promediada en el tiempo en el plasma es

$$\langle P(\nu_a \to \nu_{s_i})\rangle \;=\; 2\left(\frac{M_i^2}{2pV_a - M_i^2}\right)^2 |U_{as_i}|^2 + \mathcal{O}\left(U_{as}^4\right), \tag{11.23}$$

donde V_a es el potencial debido a la interacción coherente con las partículas del plasma, que depende de la temperatura [266].

La frencuencia de la interacción de los neutrinos de sabor es

$$\Gamma = \mathrm{Diag}(\Gamma_e, \Gamma_\mu, \Gamma_\tau, 0, 0) = \frac{180\zeta(3)}{7\pi^4} G_F^2 T^4 p \mathrm{Diag}(y_e, y_\mu, y_\tau), \tag{11.24}$$

donde los coeficientes y_a fueron calculados a temperaturas cercanas a BBN en [266], y también dependen de la temperatura.

La evolución de los neutrinos estériles se calcula con el formalismo de matrices de densidad, y después de separar el matriz en los sectores de neutrinos activos (A) y estériles (S), y asumir que las interacciones son suficientemente rápidas

para equilibrar ρ_{AA} y ρ_{AS}, podemos obtener la eq. (11.22)

$$\begin{aligned}\dot{\rho}_{ss} &= -\left(H_{AS}^{\dagger}\left\{\frac{\Gamma_{AA}}{(H_{AA}-H_{ss})^2+\Gamma_{AA}^2/4}\right\}H_{AS}\right)_{ss}\tilde{\rho}_{ss} \\ &\simeq -\frac{1}{2}\sum_a \langle P(\nu_s\to\nu_a)\rangle\Gamma_a\tilde{\rho}_{ss}, \end{aligned} \tag{11.25}$$

que justifica la estimación eq. 11.22, corregido por un factor 1/2.

Para calcular si un neutrino está termalizado o no, podemos definir la función de termalización

$$f_s(T) \equiv \Gamma_s(T)/H(T). \tag{11.26}$$

Esta función tiene un máximo a la temperatura $T_{\max}$. Sólo si $f(T_{\max}) \geq 1$ el estado puede alcanzar una distribución térmica. Usando el momento promediado $p = 3.15T$, se puede demostrar que $T_{\max}$ está acotado entre

$$\left(\frac{M_i^2}{59.5|A_e|}\right)^{1/6} \leq T_{max} \leq \left(\frac{M_i^2}{59.5|A_\tau|}\right)^{1/6}, \tag{11.27}$$

y para $|U_{as_i}|^2 \sim \mathcal{O}(m_l/M_i)$ significa que $f_{s_i}(T_{\max})$ es casi independiente de la masa del neutrino estériles M_i. Los funciones A y B són [266]

$$\begin{aligned} B &\equiv -2\sqrt{2}\left(\frac{7\zeta(4)}{\pi^2}\right)\frac{G_F}{M_Z^2}, \\ A &\equiv B - 4\sqrt{2}\left(\frac{7\zeta(4)}{\pi^2}\right)\frac{G_F}{M_W^2}. \end{aligned} \tag{11.28}$$

Además de la estimación analítica, la minimización numérica de los $f(T_{\max})$ sobre los parámetros libres del modelo demostró que los dos neutrinos pesados del modelo siempre alcanzan la termalización tanto en el caso de NH y IH, y es casi independiente en la masa de los neutrinos pesados en el rango (<1 GeV).

Es importante hacer hincapié en que el resultado es consecuencia de que debido a la necesidad de explicar las diferencias de masas de los neutrinos ligeros, y la relación inversa entre la masa y la mezcla de los neutrinos pesados con los tres sabores electrones, muones o tau neutrinos, estas mezclas no pueden ser simultaneamente lo suficientemente pequeñas para evadir la termalización.

Aunque los estados termalicen, el efecto del estado en los observables N_{eff} y/o Ω_c depende además de si

- el estado desacopla mientras que es relativista.

- el estado desacopla lo suficientemente tarde como para no sea completamente diluido.
- el estado no se desintegra antes de BBN.

La temperatura de desacoplo T_d se puede calcular como la temperatura mínima para la cual la función termalization tiene valor mayor 1, y, usando los límites experimentales sobre las mezcla que vienen de los experimentos de busqueda directa de los neutrinos pesados, se obtiene que la temperatura de desacoplo es siempre mayor que la masa de los neutrinos para la masas por debajo de ~ 100 MeV.

Al evolucionar numéricamente eq. (11.25) encontramos que para las masas por debajo de ~ 10 keV, la contribución de cada neutrino pesado es $\Delta N_{eff}^{BBN} \simeq 2$, por lo que las medidas de BBN son suficientes para excluir esta posibilidad

Los neutrinos más pesados de 10 MeV, podrían decaer antes de BBN para cierto rango del espacio de parámetros (por ejemplo en el caso del patrón de seesaw inverso de la matriz de Yukawa). El efecto de los neutrinos en el intervalo [10 MeV, 140 MeV] se ha estudiado en [267–269] y los límites de BBN y aceleradores a de excluir esta posibilidad [169].

Los neutrinos por debajo de 10MeV se desintegran después de BBN y contribuirían a la densidad de radiación adicional en el momento CMB, ya que añadirían una componente de radiación en forma de neutrinos activos, resultantes de la desintegración, ya desacoplados. Tanto si los neutrinos decaen como si son estables hasta CMB, la contribución extra a la densidad de energía está excluida por las medidas de N_{eff} y Ω_c de Planck.

La conclusión principal de este trabajo se resume en la figura. 11.3 donde la región sombreada es la escala de masas de los neutrinos estériles permitido trás imponer las restricciones que se derivan de nuestro estudio. Es importate recalcar que esto es independiente del valor de los parámetros desconocidos del modelo.

11.3.2 Articulo II

En este trabajo analizamos el modelo seesaw tipo I con tres estados adicionales, que como hemos dicho, tiene 13 parámetros libres aún sin determinar. En comparación con el trabajo previo también hemos actualizado la frecuencia de interacción de los neutrinos activos que ha sido calculada con mayor precisión [270]. $\Gamma_a(T)$ que se puede parametrizar con precisión en términos de lo $C_a(T)$ como

$$\Gamma_a \simeq C_a(T) G_F^2 T^4 p. \tag{11.29}$$

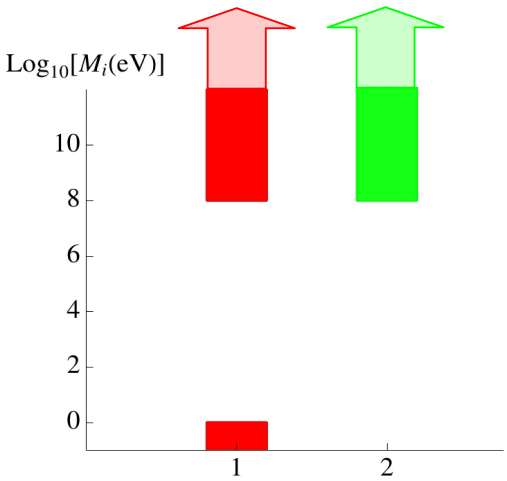

Figure 11.3: La región permitida para masas de los neutrinos estériles para 3+2 MM

Como en el trabajo previo definimos la función de la termalización que tiene el máximo en una temperatura $T_{\rm max}$, que se puede acotar por

$$T^{\tau}_{\rm max} \equiv \left(\frac{M_j^2}{59.5\ |A|}\right)^{1/6} \leq T_{\rm max} \leq \left(\frac{M_j^2}{59.5\ |B|}\right)^{1/6}. \tag{11.30}$$

.

El máximo de la función de termalización puede acotarse

$$f_{s_j}\left(T_{\rm max}\right) \geq \frac{\sum_\alpha |\left(U_{as}\right)_{\alpha j}|^2 M_j}{3.25\cdot 10^{-3}{\rm eV}}, \tag{11.31}$$

y usando la parametrización de Casas-Ibarra :

$$\sum_\alpha |\left(U_{as}\right)_{\alpha j}|^2 M_j \geq m_1, \tag{11.32}$$

se obtiene que la termalización de los neutrinos estériles depende de solo un parámetro: la masa de el neutrino activo mas ligero (m_1)

$$f_{s_j}\left(T_{\rm max}\right) \geq 1 \quad \text{for} \quad {\rm m}_1 \geq {\rm m}_{\rm th} \equiv 3.25\cdot 10^{-3}\ {\rm eV}. \tag{11.33}$$

Podemos distinguir entre dos escenarios diferentes

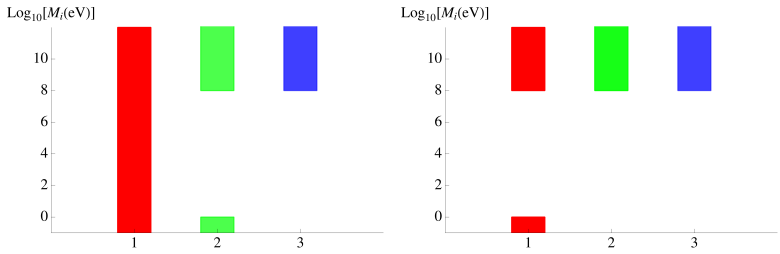

Figure 11.4: La región permitida para masas de los neutrinos estériles M_i para $m_1 \geq m_1^{th}$ (izquierda) y $m_1 \leq m_1^{th}$ (derecha).

- $m_1 \geq m_{\rm th}$, and
- $m_1 \leq m_{\rm th}$.

En el primer caso, los tres neutrinos alcanzan el equilibrio térmico y la conclusión del primer artículo aplica. Los espectros de masas permitido de los estados estériles se resume en el panel derecho de la figura. 11.4.

En el segundo caso, uno de los estados puede no alcanzar el equilibrio y por tanto su masa podría tomar cualquier valor para m_1 lo suficientemente pequeño, mientras que los otros dos se comportan con el modelo mínimo 3+2 MM y termalizan siempre, por lo que los límites sobre la masa de estos estados es igual que en el caso anterior. El intervalo de masa permitido es entonces la de la panel de la izquierda de la figura. 11.4, donde asumimos que el neutrino cuya masa no está constreñida tiene una contribución aceptable a la densidad de energía, lo cual siempre se pued garantizar en un rango del espacio de parámetros.

Por último, hemos estudiado el impacto de los neutrinos pesados en los experimentos de desintegración beta doble sin neutrinos. Dado que el neutrino que no termaliza puede tener una masa por debajo de los 100 MeV, podría contribuir a la amplitud de doble desintegración beta sin neutrinos. Hemos probado que para los parámetros compatibles con cosmología, esta contribución es siempre despreciable.

11.3.3 Articulo III

En este trabajo nos centramos en estudiar la evolución de los neutrinos pesados suponiendo que tienen una masa por encima de los 100 MeV para evadir las fuertes cotas cosmológicas. La producción de estos neutrinos antes de la transición de fase electrodébil puede dar lugar a la producción de asimetrías leptónicas. Esta

posibilidad fue propuesta por primera vez en Ref. [232]. La asimetría se produce en la oscilación de los neutrinos estériles, mientras estos no alcacen el equilibrio, y se transmite a los bariones a través de los esfalerones. Al menos un yukawa tiene que ser suficientemente pequeño para asegurar que uno de los estados no llegue a termalizarse antes de la transición de fase electrodébil. Si esto es así lo que pase después no modificará la asimetría bariónica porque los esfalerones se desacoplan y ya no es posible violar el número bariónico. El tamaño de los yukawas es natural en el contexto de los modelos seesaw para neutrinos de masa alrededor del GeV.

La asimetría bariónica es un observable impar bajo CP que debe ser invariante bajo reparametrizaciones de las fases. Es posible clasificar los invariantes de este tipo y establecer tantos invariantes independientes como número de fases de CP físicas haya. El espectro de esta teoría tiene seis neutrinos de Majorana masivos, y la mezcla se describe en términos de seis ángulos y seis fases CP. Sin embargo, dado que la naturaleza de los neutrinos de Majorana es irrelevante, en tanto en cuanto la generación de la asimetría ocurre a temperaturas tales que $M_i \ll T$, hay dos fases que se pueden despreciar, por lo que el resultado va a depender de cuatro invariantes independientes. Expresados en términos de las dos matrices unitarias que diagonalizan la matriz de Yukawa $Y \equiv V^\dagger \mathrm{Diag}(y_1, y_2, y_3) W$ se pueden elegir los siguientes invariantes:

$$\begin{aligned} I_1^{(2)} &= -\mathrm{Im}[W_{12}^* V_{11} V_{21}^* W_{22}] \\ I_1^{(3)} &= \mathrm{Im}[W_{12}^* V_{13} V_{23}^* W_{22}], \qquad (11.34) \\ I_2^{(3)} &= \mathrm{Im}[W_{13}^* V_{12} V_{22}^* W_{23}] \\ J_W &= -\mathrm{Im}[W_{23}^* W_{22} W_{32}^* W_{33}] \qquad (11.35) \end{aligned}$$

El cálculo de la asimetría requiere resolver el conjunto de ecuaciones cinéticas para las densidades de neutrinos/antineutrinos estériles y los potenciales químicos para los tres leptones cargados, μ_α, que se asumen en equilibrio cinético. En términos de partes CP-even y CP-odd, $\rho_\pm \equiv \frac{\rho_N \pm \bar{\rho}_N}{2}$ y a primer orden en μ_α, ρ_-,

las ecuaciones que se derivan del formalismo de Raffelt-Sigl tienen la forma:

$$\begin{aligned}
\dot{\rho}_+ &= -i[H_{\rm re},\rho_+] + [H_{\rm im},\rho_-] - \frac{\gamma_N^a+\gamma_N^b}{2}\{Y^\dagger Y,\rho_+ - \rho_{\rm eq}\} \\
&\quad + i\gamma_N^b {\rm Im}[Y^\dagger\mu Y]\rho_{\rm eq} + i\frac{\gamma_N^a}{2}\{{\rm Im}[Y^\dagger\mu Y],\rho_+\}, \\
\dot{\rho}_- &= -i[H_{\rm re},\rho_-] + [H_{\rm im},\rho_+] - \frac{\gamma_N^a+\gamma_N^b}{2}\{Y^\dagger Y,\rho_-\} \\
&\quad + \gamma_N^b {\rm Re}[Y^\dagger\mu Y]\rho_{\rm eq} + \frac{\gamma_N^a}{2}\{{\rm Re}[Y^\dagger\mu Y],\rho_+\}, \\
\dot{\mu}_\alpha &= -\mu_\alpha\left(\gamma_\nu^b {\rm Tr}[YY^\dagger I_\alpha] + \gamma_\nu^a {\rm Tr}\left[{\rm Re}[Y^\dagger I_\alpha Y] r_+\right]\right) \\
&\quad + (\gamma_\nu^a+\gamma_\nu^b){\rm Tr}\left[{\rm Re}[Y^\dagger I_\alpha Y] r_-\right],
\end{aligned} \tag{11.36}$$

donde H es el Hamiltoniano libre de los neutrinos estériles, que incluye el potencial inducido por el plasma, y $H_{\rm re}$, $H_{\rm im}$, sus partes real e imaginaria. I_α es el proyector en sabor α y $\gamma_N^{a,b}, \gamma_\nu^{a,b}$ son la tasas de producción/aniquiilación de neutrinos estériles, N, o los dobletes leptónicos, ν, y después de factorizar los Yukawas:

$$\gamma_{N(\nu)}^{a(b)} \equiv \frac{1}{2k_0}\sum_i \int_{\mathbf{p_1},\mathbf{p_2},\mathbf{p_3}} \rho_{\rm eq}(p_1)|\mathcal{M}_{N(\nu),i}^{(a(b))}|^2 (2\pi)^4\delta(k+p_1-p_2-p_3), \tag{11.37}$$

donde k es el momento de N o ν y

$$\gamma_{N,Q}^b = 2\gamma_{N,Q}^a = 2\gamma_{\nu,Q}^b = 4\gamma_{\nu,Q}^a = \frac{3}{16\pi^3}\frac{y_t^2 T^2}{k_0}, \tag{11.38}$$

donde sólo se ha incluido la contribución de la interacción con el top quark a través del Higgs.

En este trabajo, propusimos un nuevo método para resolver estas complejas ecuaciones analíticamente mediante una expansión perturbativa en los ángulos de mezcla de las matrices V y W, que permite acceder al régimen donde algunos de los neutrinos han termalizado. Anterioremente las aproximaciones analíticas en una expansión en Yukawas no permitían acceder a este régimen. Con esta aproximación obtuvimos la solución para los potenciales leptónicos en términos de los invariantes CP esperados de la forma:

$${\rm Tr}[\mu](t) = \sum_{I_{\rm CP}} I_{\rm CP} A_{I_{\rm CP}}(t), \tag{11.39}$$

donde $I_{\rm CP} = \left\{J_W, I_1^{(2)}, I_1^{(3)}, I_2^{(3)}\right\}$ y las funciones $A_{I_{\rm CP}}(t)$ dependen solo de los autovalores de los Yukawas y las masas de los neutrinos estériles. El comportamiento general de estas funciónes se muestra en las figuras 10.7,10.8, y para la fórmula explícita remitimos al lector al artículo completo, reproducido en la parte II.

A partir de los potenciales químicos, la asimetría bariónica se puede estimar como

$$Y_B \simeq 3 \times 10^{-3}\ {\rm Tr}[\mu(t)]|_{t_{EW}}\ . \tag{11.40}$$

Las fórmulas analíticas nos permitieron escanear el espacio de parámetros para los modelos de 3 + 2 y 3 + 3, a pesar del gran número de parámetros libres involucrados, aunque ello nos obligó a restringir ciertos rangos para asegurar que la aproximación analítica era lo suficientemente buena. Concluimos que en el caso de los modelos de 3 + 2 una degeneración leve de los dos neutrinos pesados, $\Delta M/M \sim 10^{-1}$, es necesaria para explicar la asimetría bariónica del universo en el caso de IH, mientras que para NH es necesaria una degeneración mayor. En el caso de 3 neutrinos adicionales no se necesita ninguna degeneración.

11.3.4 Articulo IV

En este trabajo estudiamos de nuevo la posibilidad de explicar la asimetría bariónica en el contexto de los modelos de seesaw tipo I de baja escala, con los siguientes refinamientos importantes.

- Hemos incluido en las tasas de interacción de los neutrinos las contribución debidas a la dispersión por bosones gauge, además de las desintegraciones y procesos inversos para los que es necesario hacer una resumación [273, 274]. Estos efectos han sido calculados en la literatura asumiendo que los potenciales químicos para los leptones se anulan. En nuestro cálculo, hemos añadido el efecto de estos potenciales químicos a primer orden.

- Hemos empleado las distribuciones de equilibrio cuánticas de Fermi-Dirac/Bose-Einstein en todos los pasos y hemos incluído los efectos de los espectadores.

- Hemos optimizado la solución numérica de las ecuaciones cinéticas implementadolas en el código público [275]. Hemos explorado el espacio de parámetros completo sin restricciones en el modelo 3+2 y hemos realizado la inferencia bayesiana de las distribuciones de probabilidad posteriores, asumiendo que el modelo explica la asimetría bariónica.

Las interacciones en equilibrio con los espectadores, que no aparecen explicitamente en las ecuaciones, tienen el efecto de redistribuir la asimetría generada en el sector de leptones a otras sectores en el plasma, pero no de modifican el número $B/3 - L_\alpha$. Es consistente por tanto no incluir estas interacciones si en lugar del número leptónico se considera la evolución de la densidad $n_{B/3} - n_{L_\alpha}$ o el potencial químico correspondiente. Las nuevas ecuaciones para las matrices densidad normalizadas a la densidad de equilibrio, $r_N = \rho_N/\rho_F$ y $r_{\bar{N}} = \rho_{\bar{N}}/\rho_F$, en términos del factor de escala x son:

$$\begin{aligned}
xH_u\frac{dr_N}{dx} &= -i[\langle H\rangle, r_N] - \frac{\langle\gamma_N^{(0)}\rangle}{2}\{Y^\dagger Y, r_N - 1\} \\
&\quad + \langle\gamma_N^{(1)}\rangle Y^\dagger\mu Y - \frac{\langle\gamma_N^{(2)}\rangle}{2}\{Y^\dagger\mu Y, r_N\}, \\
xH_u\frac{dr_{\bar{N}}}{dx} &= -i[\langle H^*\rangle, r_{\bar{N}}] - \frac{\langle\gamma_N^{(0)}\rangle}{2}\{Y^T Y^*, r_{\bar{N}} - 1\} \\
&\quad - \langle\gamma_N^{(1)}\rangle Y^T\mu Y^* + \frac{\langle\gamma_N^{(2)}\rangle}{2}\{Y^T\mu Y^*, r_{\bar{N}}\}, \\
xH_u\frac{d\mu_{B/3-L_\alpha}}{dx} &= \frac{\int_k \rho_F}{\int_k \rho_F'}\left\{\frac{\langle\gamma_N^{(0)}\rangle}{2}(Y r_N Y^\dagger - Y^* r_{\bar{N}} Y^T)_{\alpha\alpha}\right. \\
&+ \left.\mu_\alpha\left(\frac{\langle\gamma_N^{(2)}\rangle}{2}(Y r_N Y^\dagger + Y^* r_{\bar{N}} Y^T)_{\alpha\alpha} - \langle\gamma_N^{(1)}\rangle \mathrm{Tr}[YY^\dagger I_\alpha]\right)\right\}, \\
\mu_\alpha &= -\sum_\beta C_{\alpha\beta}\mu_{B/3-L_\beta},
\end{aligned} \tag{11.41}$$

donde $\mu_{B/3-L_\alpha}$ es

$$n_{B/3-L_\alpha} \equiv -2\mu_{B/3-L_\alpha}\int_k \rho_F' = \frac{1}{6}\mu_{B/3-L_\alpha}T^3. \tag{11.42}$$

y C viene dado por:

$$C_{\alpha\beta} = \frac{1}{711}\begin{pmatrix} 221 & -16 & -16 \\ -16 & 221 & -16 \\ -16 & -16 & 221 \end{pmatrix}, \tag{11.43}$$

Las tasas de interacción son promediadas en momentos y se pueden encontrar en el artículo reproducido en la parte II.

Hemos realizado un ánalisis bayesiando de las distribuciones de probabilidad posteriores asumiendo que el modelo explica la asimetría bariónica. Una consideración importante son los *priors* en los paámetros. Hemos considerado priors planos en todos los parámetros de Casas-Ibarra, excepto las masas, donde hemos considerado dos hipótesis: 1) prior planos en $\log_{10}\left(\frac{M_{1,2}}{\text{GeV}}\right)$, dentro del rango de $M_{1,2} \in [0.1\text{GeV}, 10^2\text{GeV}]$, 2) prior plano en $\log_{10}\left(\frac{M_1}{GeV}\right)$ y en $\log_{10}\left(\frac{|M_2-M_1|}{\text{GeV}}\right)$ en el rango de $M_2 - M_1 \in [10^{-8}\text{GeV}, 10^2\text{GeV}]$, que no penaliza las soluciones más degeneradas en las masas. Los resultados en el plano $|U_{\alpha s}|^2$ vs $M_{1,2}$ para $\alpha = e, \mu, \tau$ se muestran en las figuras Figs. 11.5. Las regiones azules corresponden a la primera hipótesis para los priors, mientras que las regiones rojas corresponden a la segunda. La conclusión de este estudio es que las soluciones menos degeneradas son posibles sólo para masas menores que 1 GeV. Esta es justamente la región donde el experimento SHiP [192] tiene su máxima sensitividad.

Las Figs. 11.5muestran la región de la mezcla versus la masa en comparación con las restricciones presentes y futuras de neutrinos. Hasta la fecha, este es el

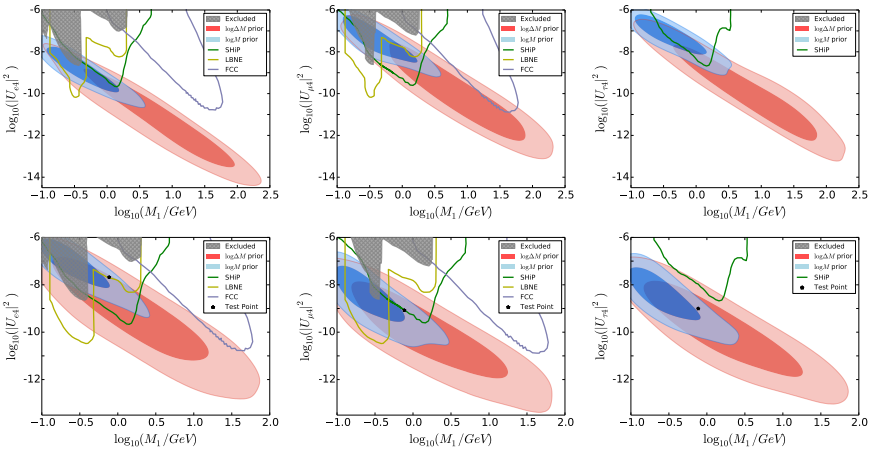

Figure 11.5: La comparación de las curvas de nivel de probabilidad posterior a 68 % y 90 % en los planos mezclas con e, μ, τ frente a las masas, con el presente (región sombreada) y las limitaciones futuras de DUNE, FCC y SHiP para el NH (arriba) e IH (abajo).

único escaneo de parámetros completo realizado sin ningún tipo de aproximaciones.

Una cuestión muy interesante es si la asimetría bariónica se podría predecir si los neutrinos estériles se descubrieran en las mediciones futuros en experimentos como SHiP o si se midieran la fase de CP δ en oscilaciones de neutrinos o si se detectara la señal de la desintegracón doble-beta sin neutrinos.

Para responder a esta pregunta y como una prueba de principio, hemos estudiado las probabilidades posteriores para una hipotética medición de la SHiP, que corresponde al punto marcado en las figuras 11.5 por una estrella, es decir para el caso de IH. Asumiendo errores muy optimistas para este experimento en su determinación de las mezclas y masas de 0.1 % y un 1 % de los dos estados pesados, así como una medida futura de δ con un error de 0.17 rad, notamos una fuerte correlación entre $m_{\beta\beta}$ y Y_B, que se presenta en el panel izquierdo de la figura 11.6. Si fuera posible una medida precisa de $m_{\beta\beta}$ (lo cual es dificil debido a la incertidumbre en los elementos de matriz nucleares para este proceso), sería posible predecir en este modelo la asimetría bariónica salvo por un signo.

Para NH, las expectativas son más pesimistas, ya que la medida de $m_{\beta\beta}$ sería mucho más dificil al ser la contribución mucho menor.

Otra observación interesante, que ha resultado de este trabajo, es que independientemente de si se explica o no la asimetría bariónica, el descubrimiento en SHiP de los neutrinos estériles en el modelo 3+2 y la medida de la razón entre su mezcla con el electrón y el muón, permitiría determinar con mucha precisión una combinación de las dos fases de CP de la matriz PMNS. La probabilidad posterior en el plano de estas dos fases se muestra en la figura 11.6. Esta sería un método alternativo de descubrir la violación de CP leptónica mediante la medida de observables pares bajo CP como son los valores absolutos de los elementos de la matriz de mezcla.

Todos estos resultados se pueden entender muy bien con aproximaciones analíticas. Este análisis se puede encontrar en el artículo completo de la parte II.

El caso de los tres neutrinos adicionales tiene mucho mas parámetros libre y es más difícil de analizar, tanto analítica y numéricamente y se deja para el trabajo futuro.

11.3.5 Observaciones finales

Esta tesis se ha centrado en las implicaciones cosmológicas de los modelos mínimos de seesaw tipo I con 2 y 3 neutrinos estériles adicionales de masas menores que la escala electrodébil. Un resultado importante de este trabajo ha sido el de excluir la posibilidad de que dos de los neutrinos tengan masas en el rango < 100 MeV, donde la física de BBN y las medidas del CMB y de la estructura a gran escala se verían (LSS) fuertemente modificadas con respecto al modelo

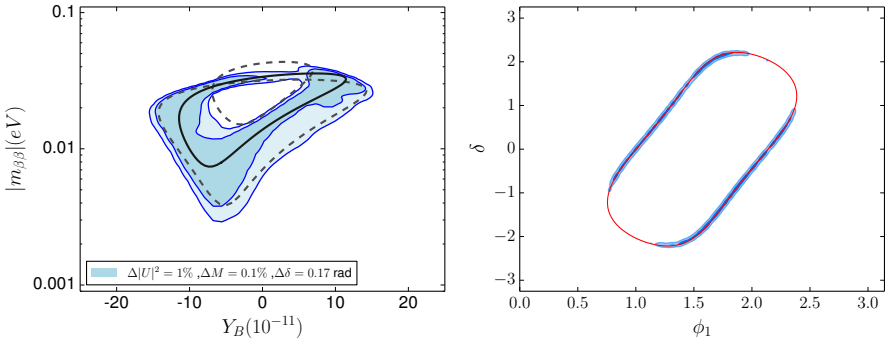

Figure 11.6: Izquierda: Probabilidades posteriores en el plano $|_{m\beta\beta}|$ vs Y_B de una medición futura en SHiP, suponiendo la incertidubre $0,1\%, 1\%$ y una medición adicional de δ, junto con las líneas de predicciones analíticas. Derecha: Probabilidades posteriores de una medición en ShIP de la masas y mezclas con e, mu en el plano (phi_1, $delta$) en comparación con el resultado de la relación analítica (línea roja) para los parámetros en el punto de prueba.

estándar cosmológico. El segundo resultado importante de este trabajo es que los neutrinos estériles en estos modelos con masas alrededor del GeV pueden explicar la asimetría bariónica observada en el universo, y que esta hipótesis podría ser testeable con futuros experimentos. El número elevado de parámetros libres de esos modelos obliga a que sea necesaria la combinación de varios test experimentales. En particular, hemos demonstrado, en el contexto del modelo mínimo 3+2, que la sinergía entre las medidas de busqueda directa de los neutrinos estériles en experimentos como SHiP, junto con la medida de la fase CP de la matriz PMNS en futuros experimentos de oscilaciones de neutrinos y la determinación precisa de la amplitud del proceso de desintegración doble-beta sin neutrinos, podría permitir la predicción cuantitativa de la asimetría bariónica sin hipótesis teóricas adicionales, algo que no se pensaba posible hasta la fecha.

Mi opinión personal es que la cosmología de precisión, así como las potenciales medidas futuras de las masas y mezclas de neutrinos adicionales en el rango del GeV hace que este periodo sea muy interesante para trabajar en la fenomenología de estos modelos.

Abbreviations

SM Standard Model
NP new physics
ΛCDM Standard cosmological model
EW electroweak
EWSB electroweak symmetry breaking
EWPT electroweak phase transition
C/P/CP charge / parity / charge parity
QFT Quantum Field Theory
VEV vacuum expectation scale
QED Quantum Electrodynamics
SSB spontaneous symmetry breaking
CKM Cabibbo-Kobayashi-Maskawa matrix
UV ultraviolet
PMNS Pontecorvo-Maki-Nagakawa-Sakata matrix
IS inverse seesaw
NH Normal Hierarchy
IH Inverted Hierarchy
SSM Standard Solar Model
CC /NC charge/neutral current
0$\nu\beta\beta$ neutrinoless double beta decay
LNV lepton number violation
MSM Minimal Standard Model
FLRW Friedmann-Lemaitre-Robertson-Walker metric
CMB Cosmic Microwave Background
LSS Large Scale Structures
BBN Big Bang Nucleosynthesis
HEP high energy physics
CL confidence level

List of Figures

List of Tables

Bibliography

[1] P. Hernandez, M. Kekic, and J. Lopez-Pavon. Low-scale seesaw models versus N_{eff}. *Phys. Rev.*, D89(7):073009, 2014.

[2] P. Hernandez, M. Kekic, and J. Lopez-Pavon. $N_{\rm eff}$ in low-scale seesaw models versus the lightest neutrino mass. *Phys. Rev.*, D90(6):065033, 2014.

[3] P. Hernández, M. Kekic, J. López-Pavón, J. Racker, and N. Rius. Leptogenesis in GeV scale seesaw models. *JHEP*, 10:067, 2015.

[4] P. Hernández, M. Kekic, J. López-Pavón, J. Racker, and J. Salvado. Testable Baryogenesis in Seesaw Models. *JHEP*, 08:157, 2016.

[5] S. L. Glashow. Partial Symmetries of Weak Interactions. *Nucl. Phys.*, 22:579–588, 1961.

[6] Steven Weinberg. A Model of Leptons. *Phys. Rev. Lett.*, 19:1264–1266, 1967.

[7] Abdus Salam. Weak and Electromagnetic Interactions. *Conf. Proc.*, C680519:367–377, 1968.

[8] Peter W. Higgs. Broken Symmetries and the Masses of Gauge Bosons. *Phys. Rev. Lett.*, 13:508–509, 1964.

[9] Peter W. Higgs. Broken symmetries, massless particles and gauge fields. *Phys. Lett.*, 12:132–133, 1964.

[10] Peter W. Higgs. Spontaneous Symmetry Breakdown without Massless Bosons. *Phys. Rev.*, 145:1156–1163, 1966.

[11] G. S. Guralnik, C. R. Hagen, and T. W. B. Kibble. Global Conservation Laws and Massless Particles. *Phys. Rev. Lett.*, 13:585–587, 1964.

[12] T. W. B. Kibble. Symmetry breaking in nonAbelian gauge theories. *Phys. Rev.*, 155:1554–1561, 1967.

[13] M. Y. Han and Yoichiro Nambu. Three Triplet Model with Double SU(3) Symmetry. *Phys. Rev.*, 139:B1006–B1010, 1965.

[14] F. Englert and R. Brout. Broken Symmetry and the Mass of Gauge Vector Mesons. *Phys. Rev. Lett.*, 13:321–323, 1964.

[15] H. Fritzsch, Murray Gell-Mann, and H. Leutwyler. Advantages of the Color Octet Gluon Picture. *Phys. Lett.*, B47:365–368, 1973.

[16] K. A. Olive et al. Review of Particle Physics. *Chin. Phys.*, C38:090001, 2014.

[17] Makoto Kobayashi and Toshihide Maskawa. CP Violation in the Renormalizable Theory of Weak Interaction. *Prog. Theor. Phys.*, 49:652–657, 1973.

[18] Nicola Cabibbo. Unitary Symmetry and Leptonic Decays. *Phys. Rev. Lett.*, 10:531–533, 1963. [,648(1963)].

[19] S. T. Petcov. The Nature of Massive Neutrinos. *Adv. High Energy Phys.*, 2013:852987, 2013.

[20] R. N. Mohapatra et al. Theory of neutrinos: A White paper. *Rept. Prog. Phys.*, 70:1757–1867, 2007.

[21] P. Hernandez. Neutrino physics. In *High-energy physics. Proceedings, 5th CERN-Latin-American School, Recinto Quirama, Colombia, March 15-28, 2009*, page False, 2010.

[22] Renata Zukanovich Funchal, Benoit Schmauch, and Gaëlle Giesen. The Physics of Neutrinos. 2013.

[23] G. Senjanovic. Neutrino mass: From LHC to grand unification. *Riv. Nuovo Cim.*, 34:1–68, 2011.

[24] M. C. Gonzalez-Garcia and Michele Maltoni. Phenomenology with Massive Neutrinos. *Phys. Rept.*, 460:1–129, 2008.

[25] R. N. Mohapatra and P. B. Pal. Massive neutrinos in physics and astrophysics. *World Sci. Lect. Notes Phys.*, 41:1–318, 1991.

[26] Steven Weinberg. Baryon and Lepton Nonconserving Processes. *Phys. Rev. Lett.*, 43:1566–1570, 1979.

[27] Peter Minkowski. $\mu \to e\gamma$ at a Rate of One Out of 10^9 Muon Decays? *Phys. Lett.*, B67:421–428, 1977.

[28] Pierre Ramond. The Family Group in Grand Unified Theories. In *International Symposium on Fundamentals of Quantum Theory and Quantum Field Theory Palm Coast, Florida, February 25-March 2, 1979*, pages 265–280, 1979.

[29] Murray Gell-Mann, Pierre Ramond, and Richard Slansky. Complex Spinors and Unified Theories. *Conf. Proc.*, C790927:315–321, 1979.

[30] M. Magg and C. Wetterich. Neutrino Mass Problem and Gauge Hierarchy. *Phys. Lett.*, B94:61–64, 1980.

[31] George Lazarides, Q. Shafi, and C. Wetterich. Proton Lifetime and Fermion Masses in an SO(10) Model. *Nucl. Phys.*, B181:287–300, 1981.

[32] Rabindra N. Mohapatra and Goran Senjanovic. Neutrino Masses and Mixings in Gauge Models with Spontaneous Parity Violation. *Phys. Rev.*, D23:165, 1981.

[33] Shinya Kanemura and Kei Yagyu. Radiative corrections to electroweak parameters in the Higgs triplet model and implication with the recent Higgs boson searches. *Phys. Rev.*, D85:115009, 2012.

[34] Robert Foot, H. Lew, X. G. He, and Girish C. Joshi. Seesaw Neutrino Masses Induced by a Triplet of Leptons. *Z. Phys.*, C44:441, 1989.

[35] R. N. Mohapatra and J. W. F. Valle. Neutrino Mass and Baryon Number Nonconservation in Superstring Models. *Phys. Rev.*, D34:1642, 1986.

[36] Ernest Ma and D. P. Roy. Heavy triplet leptons and new gauge boson. *Nucl. Phys.*, B644:290–302, 2002.

[37] Serguei Chatrchyan et al. Search for heavy lepton partners of neutrinos in proton-proton collisions in the context of the type III seesaw mechanism. *Phys. Lett.*, B718:348–368, 2012.

[38] Andrea Gozzelino. *Search for heavy lepton partners of neutrinos in the context of type III seesaw mechanism in 2012 LHC CMS data.* PhD thesis, INFN, Padua, 2014.

[39] R. N. Mohapatra. Mechanism for Understanding Small Neutrino Mass in Superstring Theories. *Phys. Rev. Lett.*, 56:561–563, 1986.

[40] M. C. Gonzalez-Garcia and J. W. F. Valle. Fast Decaying Neutrinos and Observable Flavor Violation in a New Class of Majoron Models. *Phys. Lett.*, B216:360–366, 1989.

[41] B. Pontecorvo. Neutrino Experiments and the Problem of Conservation of Leptonic Charge. *Sov. Phys. JETP*, 26:984–988, 1968. [Zh. Eksp. Teor. Fiz.53,1717(1967)].

[42] Ziro Maki, Masami Nakagawa, and Shoichi Sakata. Remarks on the unified model of elementary particles. *Prog. Theor. Phys.*, 28:870–880, 1962.

[43] Evgeny Kh. Akhmedov and Alexei Yu. Smirnov. Paradoxes of neutrino oscillations. *Phys. Atom. Nucl.*, 72:1363–1381, 2009.

[44] Evgeny Kh. Akhmedov and Joachim Kopp. Neutrino oscillations: Quantum mechanics vs. quantum field theory. *JHEP*, 04:008, 2010. [Erratum: JHEP10,052(2013)].

[45] L. Wolfenstein. Neutrino Oscillations in Matter. *Phys. Rev.*, D17:2369–2374, 1978.

[46] S. P. Mikheev and A. Yu. Smirnov. Resonance Amplification of Oscillations in Matter and Spectroscopy of Solar Neutrinos. *Sov. J. Nucl. Phys.*, 42:913–917, 1985. [Yad. Fiz.42,1441(1985)].

[47] Jorge S. Diaz and V. Alan Kostelecky. Three-parameter Lorentz-violating texture for neutrino mixing. *Phys. Lett.*, B700:25–28, 2011.

[48] `https://wwww.taup-conference.to.infn.it/2015/day4/parallel/nua/2_salvado.pdf`.

[49] Y. Fukuda et al. Atmospheric muon-neutrino / electron-neutrino ratio in the multiGeV energy range. *Phys. Lett.*, B335:237–245, 1994.

[50] W. Gajewski. A search for oscillation of atmospheric neutrinos with the IMB detector. *Nucl. Phys. Proc. Suppl.*, 28A:161–164, 1992. [,161(1992)].

[51] W. W. M. Allison et al. The Atmospheric neutrino flavor ratio from a 3.9 fiducial kiloton year exposure of Soudan-2. *Phys. Lett.*, B449:137–144, 1999.

[52] M. Ambrosio et al. Measurement of the atmospheric neutrino induced upgoing muon flux using MACRO. *Phys. Lett.*, B434:451–457, 1998.

[53] Y. Fukuda et al. Evidence for oscillation of atmospheric neutrinos. *Phys. Rev. Lett.*, 81:1562–1567, 1998.

[54] R. Wendell et al. Atmospheric neutrino oscillation analysis with sub-leading effects in Super-Kamiokande I, II, and III. *Phys. Rev.*, D81:092004, 2010.

[55] E. Richard et al. Measurements of the atmospheric neutrino flux by Super-Kamiokande: energy spectra, geomagnetic effects, and solar modulation. 2015.

[56] John N. Bahcall. *NEUTRINO ASTROPHYSICS*. 1989.

[57] John N. Bahcall, Aldo M. Serenelli, and Sarbani Basu. New solar opacities, abundances, helioseismology, and neutrino fluxes. *Astrophys. J.*, 621:L85–L88, 2005.

[58] Raymond Davis, Jr., Don S. Harmer, and Kenneth C. Hoffman. Search for neutrinos from the sun. *Phys. Rev. Lett.*, 20:1205–1209, 1968.

[59] John N. Bahcall, Neta A. Bahcall, and G. Shaviv. Present status of the theoretical predictions for the Cl-36 solar neutrino experiment. *Phys. Rev. Lett.*, 20:1209–1212, 1968.

[60] F. Kaether, W. Hampel, G. Heusser, J. Kiko, and T. Kirsten. Reanalysis of the GALLEX solar neutrino flux and source experiments. *Phys. Lett.*, B685:47–54, 2010.

[61] J. N. Abdurashitov et al. Measurement of the solar neutrino capture rate with gallium metal. III: Results for the 2002–2007 data-taking period. *Phys. Rev.*, C80:015807, 2009.

[62] J. Hosaka et al. Solar neutrino measurements in super-Kamiokande-I. *Phys. Rev.*, D73:112001, 2006.

[63] J. P. Cravens et al. Solar neutrino measurements in Super-Kamiokande-II. *Phys. Rev.*, D78:032002, 2008.

[64] K. Abe et al. Solar neutrino results in Super-Kamiokande-III. *Phys. Rev.*, D83:052010, 2011.

[65] Q. R. Ahmad et al. Measurement of the rate of $\nu_e + d \rightarrow p + p + e^-$ interactions produced by ^8B solar neutrinos at the Sudbury Neutrino Observatory. *Phys. Rev. Lett.*, 87:071301, 2001.

[66] B. Aharmim et al. Combined Analysis of all Three Phases of Solar Neutrino Data from the Sudbury Neutrino Observatory. *Phys. Rev.*, C88:025501, 2013.

[67] G. Bellini et al. Precision measurement of the 7Be solar neutrino interaction rate in Borexino. *Phys. Rev. Lett.*, 107:141302, 2011.

[68] G. Bellini et al. Measurement of the solar 8B neutrino rate with a liquid scintillator target and 3 MeV energy threshold in the Borexino detector. *Phys. Rev.*, D82:033006, 2010.

[69] G. Bellini et al. Final results of Borexino Phase-I on low energy solar neutrino spectroscopy. *Phys. Rev.*, D89(11):112007, 2014.

[70] Q. R. Ahmad et al. Direct evidence for neutrino flavor transformation from neutral current interactions in the Sudbury Neutrino Observatory. *Phys. Rev. Lett.*, 89:011301, 2002.

[71] A. Gando et al. Constraints on θ_{13} from A Three-Flavor Oscillation Analysis of Reactor Antineutrinos at KamLAND. *Phys. Rev.*, D83:052002, 2011.

[72] S. Abe et al. Precision Measurement of Neutrino Oscillation Parameters with KamLAND. *Phys. Rev. Lett.*, 100:221803, 2008.

[73] M. Apollonio et al. Limits on neutrino oscillations from the CHOOZ experiment. *Phys. Lett.*, B466:415–430, 1999.

[74] Y. Abe et al. Reactor electron antineutrino disappearance in the Double Chooz experiment. *Phys. Rev.*, D86:052008, 2012.

[75] F. Boehm et al. Final results from the Palo Verde neutrino oscillation experiment. *Phys. Rev.*, D64:112001, 2001.

[76] Wei Tang. Recent Results from the Daya Bay Neutrino Experiment. In *Proceedings, Workshop on Neutrino Physics : Session of CETUP* 2015 and 9th International Conference on Interconnections between Particle Physics and Cosmology (PPC2015): Lead/Deadwood, South Dakota, USA, July 6-17, 2015*, 2015.

[77] Soo-Bong Kim. Measurement of neutrino mixing angle θ_{13} and mass difference Δm^2_{ee} from reactor antineutrino disappearance in the RENO experiment. *Nucl. Phys.*, B908:94–115, 2016.

[78] D. G. Michael et al. Observation of muon neutrino disappearance with the MINOS detectors and the NuMI neutrino beam. *Phys. Rev. Lett.*, 97:191801, 2006.

[79] P. Adamson et al. Measurement of the Neutrino Mass Splitting and Flavor Mixing by MINOS. *Phys. Rev. Lett.*, 106:181801, 2011.

[80] P. Adamson et al. Measurement of Neutrino and Antineutrino Oscillations Using Beam and Atmospheric Data in MINOS. *Phys. Rev. Lett.*, 110(25):251801, 2013.

[81] P. Adamson et al. Electron neutrino and antineutrino appearance in the full MINOS data sample. *Phys. Rev. Lett.*, 110(17):171801, 2013.

[82] M. H. Ahn et al. Indications of neutrino oscillation in a 250 km long baseline experiment. *Phys. Rev. Lett.*, 90:041801, 2003.

[83] M. H. Ahn et al. Measurement of Neutrino Oscillation by the K2K Experiment. *Phys. Rev.*, D74:072003, 2006.

[84] N. Agafonova et al. Observation of a first ν_τ candidate in the OPERA experiment in the CNGS beam. *Phys. Lett.*, B691:138–145, 2010.

[85] K. Abe et al. Indication of Electron Neutrino Appearance from an Accelerator-produced Off-axis Muon Neutrino Beam. *Phys. Rev. Lett.*, 107:041801, 2011.

[86] P. Adamson et al. First measurement of electron neutrino appearance in NOvA. *Phys. Rev. Lett.*, 116(15):151806, 2016.

[87] J. Ahrens et al. Sensitivity of the IceCube detector to astrophysical sources of high energy muon neutrinos. *Astropart. Phys.*, 20:507–532, 2004.

[88] M. Ageron et al. ANTARES: the first undersea neutrino telescope. *Nucl. Instrum. Meth.*, A656:11–38, 2011.

[89] A. Kappes. KM3NeT: A Next Generation Neutrino Telescope in the Mediterranean Sea. 2007.

[90] M. G. Aartsen et al. Observation of High-Energy Astrophysical Neutrinos in Three Years of IceCube Data. *Phys. Rev. Lett.*, 113:101101, 2014.

[91] F. P. An et al. Observation of electron-antineutrino disappearance at Daya Bay. *Phys. Rev. Lett.*, 108:171803, 2012.

[92] R. N. Cahn, D. A. Dwyer, S. J. Freedman, W. C. Haxton, R. W. Kadel, Yu. G. Kolomensky, K. B. Luk, P. McDonald, G. D. Orebi Gann, and A. W. P. Poon. White Paper: Measuring the Neutrino Mass Hierarchy. In *Proceedings, Community Summer Study 2013: Snowmass on the Mississippi (CSS2013): Minneapolis, MN, USA, July 29-August 6, 2013*, 2013.

[93] M. C. Gonzalez-Garcia, Michele Maltoni, and Thomas Schwetz. Global Analyses of Neutrino Oscillation Experiments. *Nucl. Phys.*, B908:199–217, 2016.

[94] Ivan Esteban, M. C. Gonzalez-Garcia, Michele Maltoni, Ivan Martinez-Soler, and Thomas Schwetz. Updated fit to three neutrino mixing: exploring the accelerator-reactor complementarity. 2016.

[95] M. C. Gonzalez-Garcia, Michele Maltoni, and Thomas Schwetz. Updated fit to three neutrino mixing: status of leptonic CP violation. *JHEP*, 11:052, 2014.

[96] nu-fit. `http://http://www.nu-fit.org/`.

[97] A. Aguilar-Arevalo et al. Evidence for neutrino oscillations from the observation of anti-neutrino(electron) appearance in a anti-neutrino(muon) beam. *Phys. Rev.*, D64:112007, 2001.

[98] A. A. Aguilar-Arevalo et al. A Search for electron neutrino appearance at the $\Delta m^2 \sim 1\mathrm{eV}^2$ scale. *Phys. Rev. Lett.*, 98:231801, 2007.

[99] A. A. Aguilar-Arevalo et al. Event Excess in the MiniBooNE Search for $\bar{\nu}_\mu \to \bar{\nu}_e$ Oscillations. *Phys. Rev. Lett.*, 105:181801, 2010.

[100] A. A. Aguilar-Arevalo et al. Improved Search for $\bar{\nu}_\mu \to \bar{\nu}_e$ Oscillations in the MiniBooNE Experiment. *Phys. Rev. Lett.*, 110:161801, 2013.

[101] J. N. Abdurashitov et al. Measurement of the response of the Russian-American gallium experiment to neutrinos from a Cr-51 source. *Phys. Rev.*, C59:2246–2263, 1999.

[102] W. Hampel et al. Final results of the Cr-51 neutrino source experiments in GALLEX. *Phys. Lett.*, B420:114–126, 1998.

[103] Mario A. Acero, Carlo Giunti, and Marco Laveder. Limits on nu(e) and anti-nu(e) disappearance from Gallium and reactor experiments. *Phys. Rev.*, D78:073009, 2008.

[104] Patrick Huber. On the determination of anti-neutrino spectra from nuclear reactors. *Phys. Rev.*, C84:024617, 2011. [Erratum: Phys. Rev.C85,029901(2012)].

[105] Th. A. Mueller et al. Improved Predictions of Reactor Antineutrino Spectra. *Phys. Rev.*, C83:054615, 2011.

[106] G. Mention, M. Fechner, Th. Lasserre, Th. A. Mueller, D. Lhuillier, M. Cribier, and A. Letourneau. The Reactor Antineutrino Anomaly. *Phys. Rev.*, D83:073006, 2011.

[107] M. Maltoni, T. Schwetz, M. A. Tortola, and J. W. F. Valle. Ruling out four neutrino oscillation interpretations of the LSND anomaly? *Nucl. Phys.*, B643:321–338, 2002.

[108] Alessandro Strumia. Interpreting the LSND anomaly: Sterile neutrinos or CPT violation or...? *Phys. Lett.*, B539:91–101, 2002.

[109] Marco Cirelli, Guido Marandella, Alessandro Strumia, and Francesco Vissani. Probing oscillations into sterile neutrinos with cosmology, astrophysics and experiments. *Nucl. Phys.*, B708:215–267, 2005.

[110] M. G. Aartsen et al. Searches for Sterile Neutrinos with the IceCube Detector. 2016.

[111] Joachim Kopp, Pedro A. N. Machado, Michele Maltoni, and Thomas Schwetz. Sterile Neutrino Oscillations: The Global Picture. *JHEP*, 05:050, 2013.

[112] G. H. Collin, C. A. Argüelles, J. M. Conrad, and M. H. Shaevitz. First Constraints on the Complete Neutrino Mixing Matrix with a Sterile Neutrino. 2016.

[113] Johannes Bergström, M. C. Gonzalez-Garcia, V. Niro, and J. Salvado. Statistical tests of sterile neutrinos using cosmology and short-baseline data. *JHEP*, 10:104, 2014.

[114] Alessandro Mirizzi, Gianpiero Mangano, Ninetta Saviano, Enrico Borriello, Carlo Giunti, Gennaro Miele, and Ofelia Pisanti. The strongest bounds on active-sterile neutrino mixing after Planck data. *Phys. Lett.*, B726:8–14, 2013.

[115] A. Osipowicz et al. KATRIN: A Next generation tritium beta decay experiment with sub-eV sensitivity for the electron neutrino mass. Letter of intent. 2001.

[116] V. N. Aseev et al. An upper limit on electron antineutrino mass from Troitsk experiment. *Phys. Rev.*, D84:112003, 2011.

[117] V. M. Lobashev et al. Direct search for neutrino mass and anomaly in the tritium beta-spectrum: Status of 'Troitsk neutrino mass' experiment. *Nucl. Phys. Proc. Suppl.*, 91:280–286, 2001.

[118] Ch. Kraus et al. Final results from phase II of the Mainz neutrino mass search in tritium beta decay. *Eur. Phys. J.*, C40:447–468, 2005.

[119] P. J. Doe et al. Project 8: Determining neutrino mass from tritium beta decay using a frequency-based method. In *Proceedings, Community Summer Study 2013: Snowmass on the Mississippi (CSS2013): Minneapolis, MN, USA, July 29-August 6, 2013*, 2013.

[120] A. Nucciotti. Neutrino mass calorimetric searches in the MARE experiment. *Nucl. Phys. Proc. Suppl.*, 229-232:155–159, 2012.

[121] S. Eliseev et al. Direct Measurement of the Mass Difference of ^{163}Ho and ^{163}Dy Solves the Q-Value Puzzle for the Neutrino Mass Determination. *Phys. Rev. Lett.*, 115(6):062501, 2015.

[122] G. Drexlin, V. Hannen, S. Mertens, and C. Weinheimer. Current direct neutrino mass experiments. *Adv. High Energy Phys.*, 2013:293986, 2013.

[123] Fedor Simkovic, Amand Faessler, Vadim Rodin, Petr Vogel, and Jonathan Engel. Anatomy of nuclear matrix elements for neutrinoless double-beta decay. *Phys. Rev.*, C77:045503, 2008.

[124] Amand Faessler, Vadim Rodin, and Fedor Simkovic. Nuclear matrix elements for neutrinoless double-beta decay and double-electron capture. *J. Phys.*, G39:124006, 2012.

[125] Fedor Šimkovic, Vadim Rodin, Amand Faessler, and Petr Vogel. $0\nu\beta\beta$ and $2\nu\beta\beta$ nuclear matrix elements, quasiparticle random-phase approximation, and isospin symmetry restoration. *Phys. Rev.*, C87(4):045501, 2013.

[126] Stefano Dell'Oro, Simone Marcocci, Matteo Viel, and Francesco Vissani. Neutrinoless double beta decay: 2015 review. *Adv. High Energy Phys.*, 2016:2162659, 2016.

[127] A. Gando et al. Search for Majorana Neutrinos near the Inverted Mass Hierarchy Region with KamLAND-Zen. 2016.

[128] P. A. R. Ade et al. Planck 2015 results. XIII. Cosmological parameters. 2015.

[129] Elena Giusarma, Martina Gerbino, Olga Mena, Sunny Vagnozzi, Shirley Ho, and Katherine Freese. On the improvement of cosmological neutrino mass bounds. 2016.

[130] Nathalie Palanque-Delabrouille et al. Neutrino masses and cosmology with Lyman-alpha forest power spectrum. *JCAP*, 1511(11):011, 2015.

[131] Antonio J. Cuesta, Viviana Niro, and Licia Verde. Neutrino mass limits: robust information from the power spectrum of galaxy surveys. *Phys. Dark Univ.*, 13:77–86, 2016.

[132] D. S. Ayres et al. NOvA: Proposal to build a 30 kiloton off-axis detector to study nu(mu) —> nu(e) oscillations in the NuMI beamline. 2004.

[133] C. Adams et al. The Long-Baseline Neutrino Experiment: Exploring Fundamental Symmetries of the Universe. 2013.

[134] R. Acciarri et al. Long-Baseline Neutrino Facility (LBNF) and Deep Underground Neutrino Experiment (DUNE). 2015.

[135] M. G. Aartsen et al. Letter of Intent: The Precision IceCube Next Generation Upgrade (PINGU). 2014.

[136] Ulrich F. Katz. The ORCA Option for KM3NeT. In *Proceedings of the 15th International Workshop on Neutrino Telescopes (Neutel 2013): Venice, March 11-15, 2013*, 2014.

[137] Fengpeng An et al. Neutrino Physics with JUNO. *J. Phys.*, G43(3):030401, 2016.

[138] K. Abe et al. Physics potential of a long-baseline neutrino oscillation experiment using a J-PARC neutrino beam and Hyper-Kamiokande. *PTEP*, 2015:053C02, 2015.

[139] H. Georgi and S. L. Glashow. Unity of All Elementary Particle Forces. *Phys. Rev. Lett.*, 32:438–441, 1974.

[140] Keith R. Dienes, Emilian Dudas, and Tony Gherghetta. Neutrino oscillations without neutrino masses or heavy mass scales: A Higher dimensional seesaw mechanism. *Nucl. Phys.*, B557:25, 1999.

[141] Nima Arkani-Hamed, Savas Dimopoulos, G. R. Dvali, and John March-Russell. Neutrino masses from large extra dimensions. *Phys. Rev.*, D65:024032, 2002.

[142] Andre de Gouvea, Wei-Chih Huang, and James Jenkins. Pseudo-Dirac Neutrinos in the New Standard Model. *Phys. Rev.*, D80:073007, 2009.

[143] A. Donini, P. Hernandez, J. Lopez-Pavon, and M. Maltoni. Minimal models with light sterile neutrinos. *JHEP*, 07:105, 2011.

[144] J. A. Casas and A. Ibarra. Oscillating neutrinos and muon —> e, gamma. *Nucl. Phys.*, B618:171–204, 2001.

[145] A. Donini, P. Hernandez, J. Lopez-Pavon, M. Maltoni, and T. Schwetz. The minimal 3+2 neutrino model versus oscillation anomalies. *JHEP*, 07:161, 2012.

[146] Anupama Atre, Tao Han, Silvia Pascoli, and Bin Zhang. The Search for Heavy Majorana Neutrinos. *JHEP*, 05:030, 2009.

[147] Frank F. Deppisch, P. S. Bhupal Dev, and Apostolos Pilaftsis. Neutrinos and Collider Physics. *New J. Phys.*, 17(7):075019, 2015.

[148] Enrique Fernandez-Martinez, Josu Hernandez-Garcia, and Jacobo Lopez-Pavon. Global constraints on heavy neutrino mixing. *JHEP*, 08:033, 2016.

[149] André de Gouvêa and Andrew Kobach. Global Constraints on a Heavy Neutrino. *Phys. Rev.*, D93(3):033005, 2016.

[150] S. Mertens, T. Lasserre, S. Groh, G. Drexlin, F. Glueck, A. Huber, A. W. P. Poon, M. Steidl, N. Steinbrink, and C. Weinheimer. Sensitivity of Next-Generation Tritium Beta-Decay Experiments for keV-Scale Sterile Neutrinos. *JCAP*, 1502(02):020, 2015.

[151] M. Galeazzi, F. Fontanelli, F. Gatti, and S. Vitale. Limits on the existence of heavy neutrinos in the range 50-eV - 1000-eV from the study of the Re-187 beta decay. *Phys. Rev. Lett.*, 86:1978–1981, 2001.

[152] K. H. Hiddemann, H. Daniel, and O. Schwentker. Limits on neutrino masses from the tritium beta spectrum. *J. Phys.*, G21:639–650, 1995.

[153] E. Holzschuh, W. Kundig, L. Palermo, H. Stussi, and P. Wenk. Search for heavy neutrinos in the beta spectrum of Ni-63. *Phys. Lett.*, B451:247–255, 1999.

[154] E. Holzschuh, L. Palermo, H. Stussi, and P. Wenk. The beta-spectrum of S-35 and search for the admixture of heavy neutrinos. *Phys. Lett.*, B482:1–9, 2000.

[155] J. Deutsch, M. Lebrun, and R. Prieels. Searches for admixture of massive neutrinos into the electron flavor. *Nucl. Phys.*, A518:149–155, 1990.

[156] D. I. Britton et al. Measurement of the pi+ —> e+ neutrino branching ratio. *Phys. Rev. Lett.*, 68:3000–3003, 1992.

[157] G. Bellini et al. New limits on heavy sterile neutrino mixing in B8 decay obtained with the Borexino detector. *Phys. Rev.*, D88(7):072010, 2013.

[158] C. Hagner, M. Altmann, F. von Feilitzsch, L. Oberauer, Y. Declais, and E. Kajfasz. Experimental search for the neutrino decay neutrino (3) —> j-neutrino + e+ + e- and limits on neutrino mixing. *Phys. Rev.*, D52:1343–1352, 1995.

[159] D. A. Bryman, R. Dubois, T. Numao, B. Olaniyi, A. Olin, M. S. Dixit, D. Berghofer, J. M. Poutissou, J. A. Macdonald, and B. C. Robertson. New Measurement of the $\pi \to \nu_e$ Branching Ratio. *Phys. Rev. Lett.*, 50:7, 1983.

[160] Alexander Kusenko, Silvia Pascoli, and Dmitry Semikoz. New bounds on MeV sterile neutrinos based on the accelerator and Super-Kamiokande results. *JHEP*, 11:028, 2005.

[161] G. Bernardi et al. FURTHER LIMITS ON HEAVY NEUTRINO COUPLINGS. *Phys. Lett.*, B203:332–334, 1988.

[162] A. Vaitaitis et al. Search for neutral heavy leptons in a high-energy neutrino beam. *Phys. Rev. Lett.*, 83:4943–4946, 1999.

[163] F. Bergsma et al. A Search for Decays of Heavy Neutrinos in the Mass Range 0.5-GeV to 2.8-GeV. *Phys. Lett.*, B166:473–478, 1986.

[164] P. Vilain et al. Search for heavy isosinglet neutrinos. *Phys. Lett.*, B343:453–458, 1995. [Phys. Lett.B351,387(1995)].

[165] J. Badier et al. Mass and Lifetime Limits on New Longlived Particles in 300-GeV/$c\pi^-$ Interactions. *Z. Phys.*, C31:21, 1986.

[166] A. M. Cooper-Sarkar *et al. Phys. Lett.* **160** *B, 207 (1985).*

[167] E. Gallas et al. Search for neutral weakly interacting massive particles in the Fermilab Tevatron wide band neutrino beam. *Phys. Rev.*, D52:6–14, 1995.

[168] P. Astier et al. Search for heavy neutrinos mixing with tau neutrinos. *Phys. Lett.*, B506:27–38, 2001.

[169] Oleg Ruchayskiy and Artem Ivashko. Experimental bounds on sterile neutrino mixing angles. *JHEP*, 06:100, 2012.

[170] P. Abreu et al. Search for neutral heavy leptons produced in Z decays. *Z. Phys.*, C74:57–71, 1997. [Erratum: Z. Phys.C75,580(1997)].

[171] O. Adriani et al. Search for isosinglet neutral heavy leptons in Z0 decays. *Phys. Lett.*, B295:371–382, 1992.

[172] S. Schael et al. Precision electroweak measurements on the Z resonance. *Phys. Rept.*, 427:257–454, 2006.

[173] A. Ibarra, E. Molinaro, and S. T. Petcov. Low Energy Signatures of the TeV Scale See-Saw Mechanism. *Phys. Rev.*, D84:013005, 2011.

[174] A. Abada, V. De Romeri, and A. M. Teixeira. Effect of steriles states on lepton magnetic moments and neutrinoless double beta decay. *JHEP*, 09:074, 2014.

[175] A. Abada, Manuel E. Krauss, W. Porod, F. Staub, A. Vicente, and Cedric Weiland. Lepton flavor violation in low-scale seesaw models: SUSY and non-SUSY contributions. *JHEP*, 11:048, 2014.

[176] Takehiko Asaka and Mikhail Shaposhnikov. The nuMSM, dark matter and baryon asymmetry of the universe. *Phys. Lett.*, B620:17–26, 2005.

[177] Mikhail Shaposhnikov. The nuMSM, leptonic asymmetries, and properties of singlet fermions. *JHEP*, 08:008, 2008.

[178] Dmitry Gorbunov and Inar Timiryasov. Testing νMSM with indirect searches. *Phys. Lett.*, B745:29–34, 2015.

[179] Marco Drewes and Björn Garbrecht. Experimental and cosmological constraints on heavy neutrinos. 2015.

[180] Takehiko Asaka, Shintaro Eijima, and Kazuhiro Takeda. Lepton Universality in the νMSM. *Phys. Lett.*, B742:303–309, 2015.

[181] A. Abada, D. Das, A. M. Teixeira, A. Vicente, and C. Weiland. Tree-level lepton universality violation in the presence of sterile neutrinos: impact for R_K and R_π. *JHEP*, 02:048, 2013.

[182] Lorenzo Basso, Oliver Fischer, and Jochum J. van der Bij. Precision tests of unitarity in leptonic mixing. *Europhys. Lett.*, 105(1):11001, 2014.

[183] A. Abada, A. M. Teixeira, A. Vicente, and C. Weiland. Sterile neutrinos in leptonic and semileptonic decays. *JHEP*, 02:091, 2014.

[184] Asmaa Abada and Takashi Toma. Electric Dipole Moments of Charged Leptons with Sterile Fermions. *JHEP*, 02:174, 2016.

[185] P. Kalyniak and John N. Ng. Muon Decays Revisited: Effects of Massive Neutrinos, Their Mixings and Grand Unification. *Phys. Rev.*, D24:1874, 1981.

[186] M. S. Dixit, P. Kalyniak, and J. N. Ng. ON THE MIXINGS OF HEAVY NEUTRINOS AND MUON DECAYS. *Phys. Rev.*, D27:2216–2218, 1983.

[187] A. Grossheim et al. Decay of negative muons bound in Al-27. *Phys. Rev.*, D80:052012, 2009.

[188] Enrico Nardi, Esteban Roulet, and Daniele Tommasini. Limits on neutrino mixing with new heavy particles. *Phys. Lett.*, B327:319–326, 1994.

[189] F. del Aguila, J. de Blas, and M. Perez-Victoria. Effects of new leptons in Electroweak Precision Data. *Phys. Rev.*, D78:013010, 2008.

[190] Georges Aad et al. Search for heavy Majorana neutrinos with the ATLAS detector in pp collisions at $\sqrt{s} = 8$ TeV. *JHEP*, 07:162, 2015.

[191] Vardan Khachatryan et al. Search for heavy Majorana neutrinos in $\mu^{\pm}\mu^{\pm}$+ jets events in proton-proton collisions at $\sqrt{s} = 8$ TeV. *Phys. Lett.*, B748:144–166, 2015.

[192] Sergey Alekhin et al. A facility to Search for Hidden Particles at the CERN SPS: the SHiP physics case. 2015.

[193] Alain Blondel, E. Graverini, N. Serra, and M. Shaposhnikov. Search for Heavy Right Handed Neutrinos at the FCC-ee. In *Proceedings, 37th International Conference on High Energy Physics (ICHEP 2014): Valencia, Spain, July 2-9, 2014*, 2016.

[194] Stefan Antusch and Oliver Fischer. Testing sterile neutrino extensions of the Standard Model at future lepton colliders. *JHEP*, 05:053, 2015.

[195] A. Abada, V. De Romeri, S. Monteil, J. Orloff, and A. M. Teixeira. Indirect searches for sterile neutrinos at a high-luminosity Z-factory. *JHEP*, 04:051, 2015.

[196] Mattias Blennow, Enrique Fernandez-Martinez, Jacobo Lopez-Pavon, and Javier Menendez. Neutrinoless double beta decay in seesaw models. *JHEP*, 07:096, 2010.

[197] J. Menendez, A. Poves, E. Caurier, and F. Nowacki. Disassembling the Nuclear Matrix Elements of the Neutrinoless beta beta Decay. *Nucl. Phys.*, A818:139–151, 2009.

[198] A. Ibarra, E. Molinaro, and S. T. Petcov. TeV Scale See-Saw Mechanisms of Neutrino Mass Generation, the Majorana Nature of the Heavy Singlet Neutrinos and $(\beta\beta)_{0\nu}$-Decay. *JHEP*, 09:108, 2010.

[199] Manimala Mitra, Goran Senjanovic, and Francesco Vissani. Neutrinoless Double Beta Decay and Heavy Sterile Neutrinos. *Nucl. Phys.*, B856:26–73, 2012.

[200] J. Lopez-Pavon, S. Pascoli, and Chan-fai Wong. Can heavy neutrinos dominate neutrinoless double beta decay? *Phys. Rev.*, D87(9):093007, 2013.

[201] J. Lopez-Pavon, E. Molinaro, and S. T. Petcov. Radiative Corrections to Light Neutrino Masses in Low Scale Type I Seesaw Scenarios and Neutrinoless Double Beta Decay. *JHEP*, 11:030, 2015.

[202] Steven Weinberg. *Cosmology*. 2008.

[203] Edward W. Kolb and Michael S. Turner. The Early Universe. *Front. Phys.*, 69:1–547, 1990.

[204] Alexei A. Starobinsky. A New Type of Isotropic Cosmological Models Without Singularity. *Phys. Lett.*, B91:99–102, 1980.

[205] Alan H. Guth. The Inflationary Universe: A Possible Solution to the Horizon and Flatness Problems. *Phys. Rev.*, D23:347–356, 1981.

[206] Daniel Baumann. Inflation. In *Physics of the large and the small, TASI 09, proceedings of the Theoretical Advanced Study Institute in Elementary Particle Physics, Boulder, Colorado, USA, 1-26 June 2009*, pages 523–686, 2011.

[207] Adam G. Riess et al. Observational evidence from supernovae for an accelerating universe and a cosmological constant. *Astron. J.*, 116:1009–1038, 1998.

[208] S. Perlmutter et al. Measurements of Omega and Lambda from 42 high redshift supernovae. *Astrophys. J.*, 517:565–586, 1999.

[209] G. Sigl and G. Raffelt. General kinetic description of relativistic mixed neutrinos. *Nucl. Phys.*, B406:423–451, 1993.

[210] Mu-Chun Chen. TASI 2006 Lectures on Leptogenesis. In *Proceedings of Theoretical Advanced Study Institute in Elementary Particle Physics : Exploring New Frontiers Using Colliders and Neutrinos (TASI 2006): Boulder, Colorado, June 4-30, 2006*, pages 123–176, 2007.

[211] Antonio Riotto and Mark Trodden. Recent progress in baryogenesis. *Ann. Rev. Nucl. Part. Sci.*, 49:35–75, 1999.

[212] A. D. Sakharov. Violation of CP Invariance, c Asymmetry, and Baryon Asymmetry of the Universe. *Pisma Zh. Eksp. Teor. Fiz.*, 5:32–35, 1967. [Usp. Fiz. Nauk161,61(1991)].

[213] Stephen L. Adler. Axial vector vertex in spinor electrodynamics. *Phys. Rev.*, 177:2426–2438, 1969.

[214] J. S. Bell and R. Jackiw. A PCAC puzzle: pi0 –> gamma gamma in the sigma model. *Nuovo Cim.*, A60:47–61, 1969.

[215] V. A. Kuzmin, V. A. Rubakov, and M. E. Shaposhnikov. On the Anomalous Electroweak Baryon Number Nonconservation in the Early Universe. *Phys. Lett.*, B155:36, 1985.

[216] K. Kajantie, M. Laine, K. Rummukainen, and Mikhail E. Shaposhnikov. The Electroweak phase transition: A Nonperturbative analysis. *Nucl. Phys.*, B466:189–258, 1996.

[217] M. Fukugita and T. Yanagida. Baryogenesis Without Grand Unification. *Phys. Lett.*, B174:45–47, 1986.

[218] N. S. Manton. Topology in the Weinberg-Salam Theory. *Phys. Rev.*, D28:2019, 1983.

[219] S. Yu. Khlebnikov and M. E. Shaposhnikov. The Statistical Theory of Anomalous Fermion Number Nonconservation. *Nucl. Phys.*, B308:885–912, 1988.

[220] Dietrich Bodeker. On the effective dynamics of soft nonAbelian gauge fields at finite temperature. *Phys. Lett.*, B426:351–360, 1998.

[221] Michela D'Onofrio, Kari Rummukainen, and Anders Tranberg. Sphaleron Rate in the Minimal Standard Model. *Phys. Rev. Lett.*, 113(14):141602, 2014.

[222] S. Yu. Khlebnikov and M. E. Shaposhnikov. Melting of the Higgs vacuum: Conserved numbers at high temperature. *Phys. Lett.*, B387:817–822, 1996.

[223] W. Buchmuller, P. Di Bari, and M. Plumacher. Cosmic microwave background, matter - antimatter asymmetry and neutrino masses. *Nucl. Phys.*, B643:367–390, 2002. [Erratum: Nucl. Phys.B793,362(2008)].

[224] Sacha Davidson and Alejandro Ibarra. A Lower bound on the right-handed neutrino mass from leptogenesis. *Phys. Lett.*, B535:25–32, 2002.

[225] A. Abada, S. Davidson, A. Ibarra, F. X. Josse-Michaux, M. Losada, and A. Riotto. Flavour Matters in Leptogenesis. *JHEP*, 09:010, 2006.

[226] Asmaa Abada, Sacha Davidson, Francois-Xavier Josse-Michaux, Marta Losada, and Antonio Riotto. Flavor issues in leptogenesis. *JCAP*, 0604:004, 2006.

[227] Enrico Nardi, Yosef Nir, Esteban Roulet, and Juan Racker. The Importance of flavor in leptogenesis. *JHEP*, 01:164, 2006.

[228] F. X. Josse-Michaux and A. Abada. Study of flavour dependencies in leptogenesis. *JCAP*, 0710:009, 2007.

[229] J. Racker, Manuel Pena, and Nuria Rius. Leptogenesis with small violation of B-L. *JCAP*, 1207:030, 2012.

[230] Stefan Antusch, Steve Blanchet, Mattias Blennow, and Enrique Fernandez-Martinez. Non-unitary Leptonic Mixing and Leptogenesis. *JHEP*, 01:017, 2010.

[231] Apostolos Pilaftsis. CP violation and baryogenesis due to heavy Majorana neutrinos. *Phys. Rev.*, D56:5431–5451, 1997.

[232] Evgeny K. Akhmedov, V. A. Rubakov, and A. Yu. Smirnov. Baryogenesis via neutrino oscillations. *Phys. Rev. Lett.*, 81:1359–1362, 1998.

[233] Takehiko Asaka, Shintaro Eijima, and Hiroyuki Ishida. Kinetic Equations for Baryogenesis via Sterile Neutrino Oscillation. *JCAP*, 1202:021, 2012.

[234] Laurent Canetti, Marco Drewes, Tibor Frossard, and Mikhail Shaposhnikov. Dark Matter, Baryogenesis and Neutrino Oscillations from Right Handed Neutrinos. *Phys. Rev.*, D87:093006, 2013.

[235] Marco Drewes and Björn Garbrecht. Leptogenesis from a GeV Seesaw without Mass Degeneracy. *JHEP*, 03:096, 2013.

[236] Brian Shuve and Itay Yavin. Baryogenesis through Neutrino Oscillations: A Unified Perspective. *Phys. Rev.*, D89(7):075014, 2014.

[237] Asmaa Abada, Giorgio Arcadi, Valerie Domcke, and Michele Lucente. Lepton number violation as a key to low-scale leptogenesis. *JCAP*, 1511(11):041, 2015.

[238] A. D. Dolgov. Neutrinos in cosmology. *Phys. Rept.*, 370:333–535, 2002.

[239] R. Adhikari et al. A White Paper on keV Sterile Neutrino Dark Matter. *Submitted to: White paper*, 2016.

[240] Kevork Abazajian and Savvas M. Koushiappas. Constraints on Sterile Neutrino Dark Matter. *Phys. Rev.*, D74:023527, 2006.

[241] Aaron C. Vincent, Enrique Fernandez Martinez, Pilar Hernández, Massimiliano Lattanzi, and Olga Mena. Revisiting cosmological bounds on sterile neutrinos. *JCAP*, 1504(04):006, 2015.

[242] Erik Aver, Keith A. Olive, and Evan D. Skillman. The effects of He I λ10830 on helium abundance determinations. *JCAP*, 1507(07):011, 2015.

[243] Robert V. Wagoner, William A. Fowler, and Fred Hoyle. On the Synthesis of elements at very high temperatures. *Astrophys. J.*, 148:3–49, 1967.

[244] Robert V. Wagoner. Big bang nucleosynthesis revisited. *Astrophys. J.*, 179:343–360, 1973.

[245] Michael S. Smith, Lawrence H. Kawano, and Robert A. Malaney. Experimental, computational, and observational analysis of primordial nucleosynthesis. *Astrophys. J. Suppl.*, 85:219–247, 1993.

[246] O. Pisanti, A. Cirillo, S. Esposito, F. Iocco, G. Mangano, G. Miele, and P. D. Serpico. PArthENoPE: Public Algorithm Evaluating the Nucleosynthesis of Primordial Elements. *Comput. Phys. Commun.*, 178:956–971, 2008.

[247] `http://parthenope.na.infn.it/`.

[248] Richard H. Cyburt, Brian D. Fields, and Keith A. Olive. Primordial nucleosynthesis with CMB inputs: Probing the early universe and light element astrophysics. *Astropart. Phys.*, 17:87–100, 2002.

[249] Ryan J. Cooke. Big Bang Nucleosynthesis and the Helium Isotope Ratio. *Astrophys. J.*, 812(1):L12, 2015.

[250] Shaun Cole et al. The 2dF Galaxy Redshift Survey: Power-spectrum analysis of the final dataset and cosmological implications. *Mon. Not. Roy. Astron. Soc.*, 362:505–534, 2005.

[251] Max Tegmark et al. Cosmological parameters from SDSS and WMAP. *Phys. Rev.*, D69:103501, 2004.

[252] Kyle S. Dawson et al. The Baryon Oscillation Spectroscopic Survey of SDSS-III. *Astron. J.*, 145:10, 2013.

[253] Tirthankar Roy Choudhury, Ewald Puchwein, Martin G. Haehnelt, and James S. Bolton. Lyman α emitters gone missing: evidence for late reionization? *Mon. Not. Roy. Astron. Soc.*, 452(1):261–277, 2015.

[254] Andrei Mesinger, Aycin Aykutalp, Eros Vanzella, Laura Pentericci, Andrea Ferrara, and Mark Dijkstra. Can the intergalactic medium cause a rapid drop in Ly α emission at $z > 6$. *Mon. Not. Roy. Astron. Soc.*, 446:566–577, 2015.

[255] Sourav Mitra, T. Roy Choudhury, and Andrea Ferrara. Cosmic reionization after Planck. *Mon. Not. Roy. Astron. Soc.*, 454(1):L76–L80, 2015.

[256] P. A. R. Ade et al. Planck 2015 results. XXIV. Cosmology from Sunyaev-Zeldovich cluster counts. *Astron. Astrophys.*, 594:A24, 2016.

[257] Florian Beutler, Chris Blake, Matthew Colless, D. Heath Jones, Lister Staveley-Smith, Lachlan Campbell, Quentin Parker, Will Saunders, and Fred Watson. The 6dF Galaxy Survey: Baryon Acoustic Oscillations and the Local Hubble Constant. *Mon. Not. Roy. Astron. Soc.*, 416:3017–3032, 2011.

[258] Lauren Anderson et al. The clustering of galaxies in the SDSS-III Baryon Oscillation Spectroscopic Survey: Baryon Acoustic Oscillations in the Data Release 9 Spectroscopic Galaxy Sample. *Mon. Not. Roy. Astron. Soc.*, 427(4):3435–3467, 2013.

[259] A. Conley et al. Supernova Constraints and Systematic Uncertainties from the First 3 Years of the Supernova Legacy Survey. *Astrophys. J. Suppl.*, 192:1, 2011.

[260] N. Suzuki et al. The Hubble Space Telescope Cluster Supernova Survey: V. Improving the Dark Energy Constraints Above z>1 and Building an Early-Type-Hosted Supernova Sample. *Astrophys. J.*, 746:85, 2012.

[261] Adam G. Riess, Lucas Macri, Stefano Casertano, Hubert Lampeitl, Henry C. Ferguson, Alexei V. Filippenko, Saurabh W. Jha, Weidong Li, and Ryan Chornock. A 3% Solution: Determination of the Hubble Constant with the Hubble Space Telescope and Wide Field Camera 3. *Astrophys. J.*, 730:119, 2011. [Erratum: Astrophys. J.732,129(2011)].

[262] Erik Aver, Keith A. Olive, R. L. Porter, and Evan D. Skillman. The primordial helium abundance from updated emissivities. *JCAP*, 1311:017, 2013.

[263] Ryan Cooke, Max Pettini, Regina A. Jorgenson, Michael T. Murphy, and Charles C. Steidel. Precision measures of the primordial abundance of deuterium. *Astrophys. J.*, 781(1):31, 2014.

[264] Palash B. Pal and Lincoln Wolfenstein. Radiative Decays of Massive Neutrinos. *Phys. Rev.*, D25:766, 1982.

[265] Kerstin Perez, Kenny C. Y. Ng, John F. Beacom, Cora Hersh, Shunsaku Horiuchi, and Roman Krivonos. (Almost) Closing the Sterile Neutrino Dark Matter Window with NuSTAR. 2016.

[266] Dirk Notzold and Georg Raffelt. Neutrino Dispersion at Finite Temperature and Density. *Nucl. Phys.*, B307:924–936, 1988.

[267] A. D. Dolgov, S. H. Hansen, G. Raffelt, and D. V. Semikoz. Cosmological and astrophysical bounds on a heavy sterile neutrino and the KARMEN anomaly. *Nucl. Phys.*, B580:331–351, 2000.

[268] George M. Fuller, Chad T. Kishimoto, and Alexander Kusenko. Heavy sterile neutrinos, entropy and relativistic energy production, and the relic neutrino background. 2011.

[269] Oleg Ruchayskiy and Artem Ivashko. Restrictions on the lifetime of sterile neutrinos from primordial nucleosynthesis. *JCAP*, 1210:014, 2012.

[270] Takehiko Asaka, Mikko Laine, and Mikhail Shaposhnikov. Lightest sterile neutrino abundance within the nuMSM. *JHEP*, 01:091, 2007. [Erratum: JHEP02,028(2015)].

[271] Gustavo C. Branco, Takuya Morozumi, B. M. Nobre, and M. N. Rebelo. A Bridge between CP violation at low-energies and leptogenesis. *Nucl. Phys.*, B617:475–492, 2001.

[272] Elizabeth Ellen Jenkins and Aneesh V. Manohar. Rephasing Invariants of Quark and Lepton Mixing Matrices. *Nucl. Phys.*, B792:187–205, 2008.

[273] Denis Besak and Dietrich Bodeker. Thermal production of ultrarelativistic right-handed neutrinos: Complete leading-order results. *JCAP*, 1203:029, 2012.

[274] I. Ghisoiu and M. Laine. Right-handed neutrino production rate at T $>$ 160 GeV. *JCAP*, 1412(12):032, 2014.

[275] `https://github.com/jsalvado/SQuIDS`.

[276] Farhan Feroz and M. P. Hobson. Multimodal nested sampling: an efficient and robust alternative to MCMC methods for astronomical data analysis. *Mon. Not. Roy. Astron. Soc.*, 384:449, 2008.

[277] F. Feroz, M. P. Hobson, and M. Bridges. MultiNest: an efficient and robust Bayesian inference tool for cosmology and particle physics. *Mon. Not. Roy. Astron. Soc.*, 398:1601–1614, 2009.

[278] F. Feroz, M. P. Hobson, E. Cameron, and A. N. Pettitt. Importance Nested Sampling and the MultiNest Algorithm. 2013.

[279] Carlos A. Argüelles Delgado, Jordi Salvado, and Christopher N. Weaver. A Simple Quantum Integro-Differential Solver (SQuIDS). *Comput. Phys. Commun.*, 196:569–591, 2015.

Part II

Scientific Research

PHYSICAL REVIEW D **89,** 073009 (2014)

Low-scale seesaw models versus $N_{\rm eff}$

P. Hernández,[1] M. Kekic,[1] and J. López-Pavón[2,3]

[1]*IFIC (CSIC-UVEG), Edificio Institutos Investigación, Apartado de Correos 22085, E-46071 Valencia, Spain*
[2]*SISSA, via Bonomea 265, 34136 Trieste, Italy*
[3]*INFN, Sezione di Trieste, 34126 Trieste, Italy*

(Received 2 December 2013; published 9 April 2014)

We consider the contribution of the extra sterile states in generic low-scale seesaw models to extra radiation, parametrized by $N_{\rm eff}$. We find that the value of $N_{\rm eff}$ is roughly independent of the seesaw scale within a wide range. We explore the full parameter space in the case of two extra sterile states and find that these models are strongly constrained by cosmological data for any value of the seesaw scale below $\mathcal{O}(100\ \text{MeV})$.

DOI: 10.1103/PhysRevD.89.073009 PACS numbers: 14.60.St, 98.80.Cq

I. INTRODUCTION

The simplest extension of the standard model (SM) that can account for the observed neutrino masses is a type I seesaw model with $N \geq 2$ extra singlet Majorana fermions. The Majorana masses, that we globally denote as M, constitute a new scale of physics, that we will refer to as seesaw scale, and which is presently unknown. Since the light neutrino masses are a combination of the Yukawa couplings, the electroweak scale and the seesaw scale, the latter can be arbitrary if the Yukawas are adjusted accordingly. As a result, the seesaw scale is presently unconstrained to lie anywhere above $\mathcal{O}(\text{eV})$ up to $\mathcal{O}(10^{15}\ \text{GeV})$ [1]. The determination of this scale is one of the most important open questions in neutrino physics. Although it is often assumed that the seesaw scale is very high, above the electroweak scale, in the absence of any other hint of new physics beyond the SM, the possibility that the seesaw scale could be at the electroweak scale or lower should be seriously considered. As far as naturalness goes, the model with a low scale is technically natural, since in the limit $M \to 0$, a global lepton number symmetry is recovered: neutrinos becoming Dirac particles by the pairing up of the Majorana fermions.

The generic feature of type I seesaw models is that there exist sterile neutrinos with masses at the seesaw scale, and that their mixing with the active neutrinos is strongly correlated with that scale (the naive seesaw scaling being $|U_{as}|^2 \sim M^{-1}$). The possibility that such sterile states could be responsible for any of the anomalies found in various experiments is of course very interesting, since this could open a new window into establishing the origin of neutrino masses.

Models with extra light sterile neutrinos with masses in the range of $\mathcal{O}(1\ \text{eV})$ could provide an explanation to some of the neutrino anomalies [2], such as the appearance signal $\bar{\nu}_\mu \to \bar{\nu}_e$ of the LSND experiment [3], undisproved by the MiniBOONE [4] experiment, or the deficit of neutrinos ($\bar{\nu}_e \to \bar{\nu}_e$) in short-baseline reactor experiments, the so-called reactor neutrino anomaly [5]. Sterile species in the keV range could still be valid candidates for warm dark matter [6], while species in the GeV range could account for the baryon asymmetry in the Universe [7].

The explanation of the neutrino anomalies with N extra sterile neutrinos is usually considered in the context of phenomenological models with a generic neutrino mass matrix of size $3 + N$, without specifying whether neutrinos are Dirac or Majorana. In the former case, a renormalizable Lagrangian representing such a model would require the addition of $3 + 2N$ extra singlet Weyl fermions to the minimal SM so that they can be paired up into $3 + N$ Dirac neutrinos. In the case of $3 + N$ Majorana neutrinos, renormalizable Majorana couplings among the three doublet neutrinos are forbidden by gauge symmetry, and therefore the $3 + N$ mass matrix is not generic, i.e. it has a vanishing 3×3 block [8]. We have in this case precisely a standard $3 + N$ type I seesaw model with a low seesaw scale. These are the so-called mini-seesaw [9] or minimal models [10]. These models are much more constrained/predictive than the phenomenological models with the same neutrino spectrum because, as mentioned above, the active-sterile mixings are not independent of the ratio of neutrino masses.

The possibility to explain the neutrino anomalies in these minimal models if $N = 2$ has been studied in [11]. The order of magnitude for the active-sterile mixing for a seesaw scale of $\mathcal{O}(1\ \text{eV})$ is in the right ballpark to explain the neutrino anomalies, which is remarkable. As a result the minimal models provide similar fits to the data as the phenomenological ones. Minimal models with $N = 3$, and a much higher seesaw scale, have also been proposed as candidates to explain dark matter and the baryon asymmetry [12].

It is well known that light sterile neutrinos with significant active-sterile mixing can be strongly constrained by cosmological measurements. The energy density of the extra neutrino species, ϵ_s, is usually quantified in terms of $N_{\rm eff}$ (when they are relativistic) defined by

 © 2014 American Physical Society

$$N_{\rm eff} \equiv \frac{\epsilon_s + \epsilon_\nu}{\epsilon_\nu^0}, \tag{1}$$

where ϵ_ν^0 is the energy density of one SM massless neutrino with a thermal distribution [below $e^\pm$ annihilation it is $\epsilon_\nu^0 \equiv (7\pi^2/120)(4/11)^{4/3} T_\gamma^4$ at the photon temperature T_γ]. In the minimal SM with massless neutrinos $N_{\rm eff} = 3.046$ at CMB [13]. One fully thermal extra sterile state that decouples being relativistic contributes $\Delta N_{\rm eff} \simeq 1$ when it decouples.

$N_{\rm eff}$ at big bang nucleosynthesis (BBN) strongly influences the primordial helium production. A recent analysis of BBN bounds [14] gives $N_{\rm eff}^{\rm BBN} = 3.68(3.80)^{0.80}_{-0.70}$ at 2σ, where the central value depends on the choice for the neutron lifetime, and assumes no lepton asymmetry. $N_{\rm eff}$ also affects the anisotropies of the cosmic microwave background (CMB). Recent CMB measurements from Planck give $N_{\rm eff}^{\rm CMB} = 3.30 \pm 0.27(1\sigma)$ [15], which includes WMAP-9 polarization data [16] and high multipole measurements from the South Pole Telescope [17] and the Atacama Cosmology Telescope [18].

The contribution of extra sterile states to $N_{\rm eff}$ within phenomenological models has been extensively studied [19–22]. For recent analyses see [23–26]. In particular the models that could accommodate the neutrino anomalies seem to be in strong tension with cosmology, especially those with two extra species. We expect a similar conclusion for the minimal models with $M \sim \mathcal{O}(\text{eV})$, since the spectrum and active-sterile mixings that best fit these neutrino anomalies are very similar in both cases [11].

The purpose of this paper is to evaluate $N_{\rm eff}$ as a function of the seesaw scale in the minimal models. Interestingly in spite of the fact that the active-sterile mixings decrease with increasing seesaw scale, the rate of thermalization of the sterile neutrinos is roughly independent of that scale. Following the well-known results of [19], it can be shown that the rate of thermalization of a sterile neutrino of mass M, in the approximation of two active-sterile neutrino mixing, depends on the combination $|U_{as}|^2 M$. Therefore, the naive seesaw scaling would imply that the thermalization rate is roughly independent of the seesaw scale, M. We will show that this naive expectation does actually hold for the $3+2$ minimal model. Cosmological bounds on the seesaw scale are therefore very strong in a wide range of scales.

II. THERMALIZATION IN MINIMAL $3+N$ MODELS

The minimal models are described by the most general renormalizable Lagrangian including N extra singlet Weyl fermions, ν_R^i:

$$\mathcal{L} = \mathcal{L}_{\rm SM} - \sum_{\alpha,i} \bar{L}^\alpha Y^{\alpha i} \tilde{\Phi} \nu_R^i - \sum_{i,j=1}^{N} \frac{1}{2} \bar{\nu}_R^{ic} M_N^{ij} \nu_R^j + \text{H.c.},$$

where Y is a $3 \times N$ complex matrix and M_N a diagonal real matrix. The model with $N = 1$, that contains only two massive states, cannot explain the measured neutrino masses and mixings [10]. For $N = 2$, the spectrum contains four massive states and one massless mode, whose mixing is described by four angles and three physical CP phases. For $N = 3$, there are six massive states and the mixing is described in terms of six angles and six CP phases. We will concentrate on the simplest model that can explain neutrino data, i.e. $N = 2$. The case with $N = 3$ will be considered elsewhere.

We assume that the eigenvalues of M_N are significantly larger than the atmospheric and solar neutrino mass splittings, which implies a hierarchy $M_N \gg Yv$ and therefore the seesaw approximation is good. A convenient parametrization in this case is provided by that of Casas-Ibarra [27], or its extension to all orders in the seesaw expansion as described in [11] (for an alternative see [28]). The mass matrix can be written as

$$\mathcal{M}_\nu = U^* \text{Diag}(m_l, M_h) U^\dagger, \tag{2}$$

where m_l is a diagonal matrix with a zero and the two lighter masses, and M_h contains the N heaviest. Denoting by a the active/light neutrinos and s the sterile/heavy species, the unitary matrix can be written as

$$U = \begin{pmatrix} U_{aa} & U_{as} \\ U_{sa} & U_{ss} \end{pmatrix}, \tag{3}$$

with

$$\begin{aligned} U_{aa} &= U_{PMNS} \begin{pmatrix} 1 & 0 \\ 0 & H \end{pmatrix}, \qquad U_{ss} = \bar{H}, \\ U_{sa} &= i \begin{pmatrix} 0 & \bar{H} M_h^{-1/2} R m_l^{1/2} \end{pmatrix}, \\ U_{as} &= i U_{PMNS} \begin{pmatrix} 0 \\ H m_l^{1/2} R^\dagger M_h^{-1/2} \end{pmatrix}, \end{aligned} \tag{4}$$

where U_{PMNS} is a 3×3 unitary matrix, R is a generic 2×2 orthogonal complex matrix, while H and $\bar{H}$ are defined by

$$\begin{aligned} H^{-2} &= I + m_l^{1/2} R^\dagger M_h^{-1} R m_l^{1/2}, \\ \bar{H}^{-2} &= I + M_h^{-1/2} R m_l R^\dagger M_h^{-1/2}. \end{aligned} \tag{5}$$

At leading order in the seesaw expansion, i.e. up to $\mathcal{O}(\frac{m_l}{M_h})$, $H \simeq \bar{H} \simeq 1$, and we recover the Casas-Ibarra parametrization.

The measured neutrino masses and mixings fix most of the parameters in these models. The only free parameters are two CP phases of U_{PMNS} (the third one is unphysical because the lightest neutrino is massless), that are presently

unconstrained, the matrix R that depends on a complex angle and the two heavy masses in M_h.

The active neutrinos in the minimal SM are in thermal equilibrium in the early Universe at temperatures above $\mathcal{O}(1\ \text{MeV})$. The presence of extra singlets can modify the value of $N_{\rm eff}$ because the active-sterile mixing can also bring the singlets into thermal equilibrium. Obviously the thermalization process depends very strongly on the mixing parameters and the neutrino masses. We assume throughout that neutrinos are relativistic.

In [19] a simple estimate for the thermalization of one sterile neutrino was given as follows. Assuming that the active neutrinos are in thermal equilibrium with a collision rate given by Γ_a, the collision rate for the sterile neutrinos can be estimated to be

$$\Gamma_{s_i} \simeq \frac{1}{2}\sum_a \langle P(\nu_a \to \nu_{s_i})\rangle \times \Gamma_a, \tag{6}$$

where $\langle P(\nu_a \to \nu_s)\rangle$ is the time-averaged probability $\nu_a \to \nu_s$ (the factor $1/2$ results from a more detailed analysis, see below). This probability depends strongly on temperature because the neutrino index of refraction in the early Universe is modified by coherent scattering of neutrinos with the particles in the plasma [29]. Thermalization will be achieved if there is any temperature where this rate is higher than the Hubble expansion rate, i.e. $\Gamma_s(T) \geq H(T)$. One can therefore define the function $f_s(T)$, which measures the sterile production rate in units of the Hubble expansion rate,

$$f_s(T) \equiv \frac{\Gamma_s(T)}{H(T)}. \tag{7}$$

This function reaches a maximum at some temperature, $T_{\rm max}$, and if this maximum is larger than one, thermalization will be achieved. We can estimate the contribution to $N_{\rm eff}$ as

$$N_{\rm eff} \simeq N_{\rm eff}^{\rm SM} + \sum_i (1 - \exp(-\alpha f_{s_i}(T^i_{\rm max}))), \tag{8}$$

at decoupling, where α is an $\mathcal{O}(1)$ numerical constant. Provided $f_{s_i}(T^i_{\rm max})$ is sufficiently larger than one, $N_{\rm eff}$ saturates to the number of thermalized species, up to exponentially small corrections. The Hubble expansion rate is $H(T) = \sqrt{\frac{4\pi^3 g_*(T)}{45}}\frac{T^2}{M_{\rm Planck}}$, where $g_*(T)$ is a function of the temperature.

The calculation of the neutrino oscillation probabilities in the primeval plasma requires to consider the full $3+2$ mixing. This means that obtaining a manageable expression can be complicated. The method described in Ref. [30] simplifies enormously this task, reducing the hardcore computation to the calculation of the eigenvalues of the Hamiltonian which characterizes the neutrino propagation. Employing this method and expanding over m_l/M_h and the active-sterile mixing, we find the time-averaged probabilities to be approximately

$$\langle P(\nu_a \to \nu_{s_i})\rangle = 2\left(\frac{M_i^2}{2pV_a - M_i^2}\right)^2 |U_{as_i}|^2 + \mathcal{O}(U_{as}^4), \tag{9}$$

where p is the neutrino momentum and $V_a \equiv A_a T^4 p$, with $A_e = A$, while $A_{\mu/\tau} = B$ for T below the μ/τ threshold ($T \lesssim 20/180$ MeV) or $A_{\mu/\tau} = A$ for higher $T \gtrsim 20/180$ MeV, where

$$B \equiv -2\sqrt{2}\left(\frac{7\zeta(4)}{\pi^2}\right)\frac{G_F}{M_Z^2},$$
$$A \equiv B - 4\sqrt{2}\left(\frac{7\zeta(4)}{\pi^2}\right)\frac{G_F}{M_W^2}. \tag{10}$$

Note that there is no resonant mixing in this model, and that we have assumed no primordial lepton asymmetry.

A more detailed description is provided by the quantum density matrix formalism [31–34]:

$$\dot{\rho} = -i[\hat{H}, \rho] - \frac{1}{2}\{\Gamma, \rho - \rho_{eq} I_A\}, \tag{11}$$

where $\hat{H}$ is the Hamiltonian describing the propagation of relativistic neutrinos in the plasma, which in the flavor basis is given by

$$\hat{H} = U^* \text{Diag}\left(\frac{m_l^2}{2p}, \frac{M_h^2}{2p}\right) U^T + \text{Diag}(V_e, V_\mu, V_\tau, 0, 0), \tag{12}$$

and the collision term $\Gamma = \text{Diag}(\Gamma_e, \Gamma_\mu, \Gamma_\tau, 0, 0)$

$$\Gamma_a = y_a \frac{180\zeta(3)}{7\pi^4} G_F^2 T^4 p, \tag{13}$$

with $y_e = 3.6$, and $y_\mu = y_\tau = 2.5$ below the corresponding μ and τ thresholds, becoming equal to y_e above [35]. Finally ρ_{eq} is the Fermi-Dirac distribution and $I_A = \text{Diag}(1, 1, 1, 0, 0)$.

Separating the equations into the active A and sterile S blocks and assuming that $\Gamma_a(T) \gg H(T)$, collisions are then fast enough to equilibrate ρ_{AA} and ρ_{AS}, i.e. $\dot{\rho}_{AA} = \dot{\rho}_{AS} = 0$ (the so-called static approximation [20], see also [36,37]). If we assume hierarchical heavy masses, and take into account the seesaw expansion, it is possible to show that the thermalization of the different sterile states approximately decouples, and the equation for each species simplifies to

$$\dot{\rho}_{ss} = -\left(H^{\dagger}_{AS}\left\{\frac{\Gamma_{AA}}{(H_{AA}-H_{ss})^2+\Gamma^2_{AA}/4}\right\}H_{AS}\right)_{ss}\tilde{\rho}_{ss}$$
$$\simeq -\frac{1}{2}\sum_a \langle P(\nu_s\to\nu_a)\rangle\Gamma_a\tilde{\rho}_{ss}, \quad (14)$$

where $\tilde{\rho}_{ss}\equiv\rho_{ss}-\rho_{eq}$. This equation justifies the estimate of Eq. (6).

$T_{\max}$ is the value of the temperature at which $\Gamma_s(T)/H(T)$ is maximum. Taking $p\simeq 3.15T$, it is easy to see that for each sterile state of mass M_i, $T_{\max}$ can be bounded by

$$\left(\frac{M_i^2}{59.5|A_e|}\right)^{1/6} \le T_{\max} \le \left(\frac{M_i^2}{59.5|A_\tau|}\right)^{1/6}, \quad (15)$$

so it depends significantly on M_i but weakly on the mixings. Taking into account the seesaw scaling $|U_{as_i}|^2\sim\mathcal{O}(m_l/M_i)$, it follows that $f_{s_i}(T_{\max})$ is roughly independent of M_i.

III. $N_{\rm eff}$ IN MINIMAL 3 + 2 MODELS

In Fig. 1 we show the numerical results for the minimal value of $f_s(T_{\max})$ (almost identical for both species) scanning the whole parameter space for the two sterile states, assuming their masses differ a factor 10 or more. The light neutrino masses and mixings (i.e. the two nonzero eigenvalues of m_l and the three mixing angles in U_{PMNS}) have been fixed to their best fit values from oscillation experiments. We need to distinguish between the normal (NH) and inverted (IH) light neutrino hierarchies at this point. Varying $M_i\in[1\text{ eV}, 1\text{ GeV}]$, we find an almost constant value which is significantly larger than 1, which means that both species thermalize, contributing $\Delta N_{\rm eff}\simeq 2$ when they decouple. This is the case for both neutrino hierarchies normal and inverted (NH/IH), but

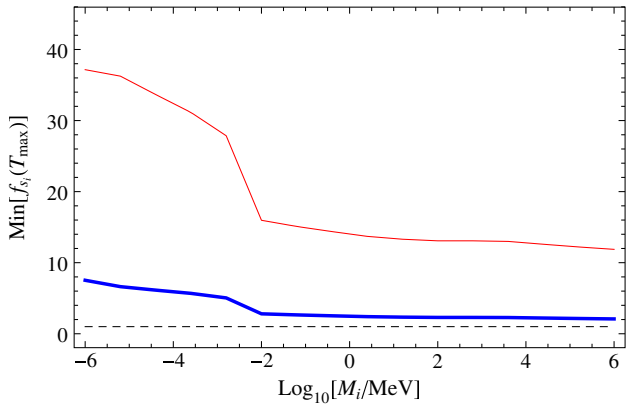

FIG. 1 (color online). Min$[f_{s_i}(T_{\max})]$ for the ith sterile state as a function of M_i for a light neutrino spectrum with a NH (thick line) or IH (thin line). The dashed line at 1 corresponds to the minimum value for thermalization.

Min$[f_s(T_{\max})]$ is significantly larger for IH. The dependence on M_i is mostly due to the change in $g_*(T_{\max})$.

We note that the thermalization is still possible for values of $M_i\gg 1$ MeV. At some point however, the decoupling temperature of the sterile species will be below their mass. In this case, the contribution to $N_{\rm eff}$ requires a different treatment and will be Boltzmann suppressed. We can estimate this decoupling temperature, T_d, from the requirement $f_s(T_d)=1$ for $T_d<T_{\max}$. In Fig. 2 we show the value of T_d as a function of M_i (again the same for both species) for three cases: the parameters that minimize $f_s(T_{\max})$ (dashed lines), the parameters that minimize T_d (dotted) and the ones that minimize T_d after taking into account direct search constraints on active-sterile mixings (solid). We see that there are regions of parameter space for all M_i where sterile neutrinos remain in equilibrium until $\mathcal{O}(1\text{ MeV})$. However, as M_i increases this is only possible for very special textures, inverse-seesaw–like, where neutrino masses are suppressed due to an approximate global symmetry. In any case, large mixings are strongly constrained by direct searches [38–40], when those bounds are included, we find that T_d is well above M_i for $M_i\le\mathcal{O}(1\text{ GeV})$. If neutrinos are below this mass they decouple when they are still relativistic, as we have assumed, and therefore contribute one unit to $\Delta N_{\rm eff}(T_d)$, but above this mass, they become nonrelativistic before decoupling and the contribution is suppressed by the Boltzmann factor.

After decoupling of the sterile species, however, two important effects could modify $\Delta N_{\rm eff}$ before the active neutrino decoupling at T_W [41]: dilution and decay.

First a dilution occurs if the sterile species decouple at $T_d\gg T_W$, due to the change in $g_*(T)$. The dilution can be estimated to be $\Delta N_{\rm eff}(T_{\rm W})=(g_*(T_{\rm W})/g_*(T_{d1}))^{4/3}+(g_*(T_{\rm W})/g_*(T_{d2}))^{4/3}$ provided they are still relativistic at $T_{\rm W}$ [41].

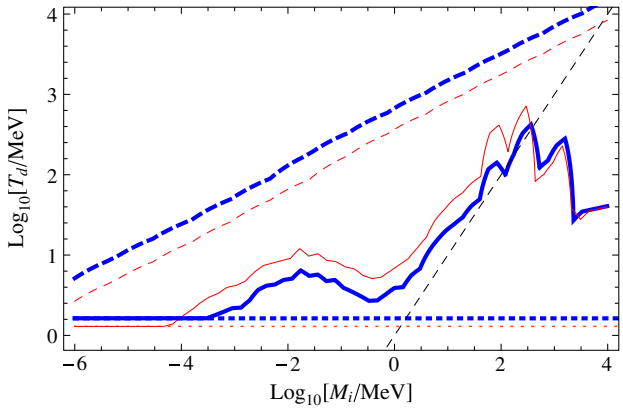

FIG. 2 (color online). Sterile neutrino decoupling temperature, T_d, as function of the sterile mass for the NH (solid thick line), IH (solid thin line) and for oscillation parameters that minimize $f_s(T_{\max})$ (dashed lines), those that minimize T_d (dotted) and those that minimize T_d while being compatible with bounds from direct searches (solid). The single dashed line satisfies $T=M_i$.

In order to numerically solve the kinetic equations, Eq. (11), we rewrite them, as is common practice, in terms of the new variables [34]

$$x = m_0 a(t), \qquad y = p a(t), \tag{16}$$

where m_0 is an arbitrary scale (fixed to be 1 MeV) and $a(t)$ is cosmic scale factor. Equation (11) becomes

$$H(x) x \frac{\partial}{\partial x}\rho(x,y)|_y = -i[\hat{H}(x,y), \rho(x,y)] - \frac{1}{2}\{\Gamma(x,y), \rho(x,y) - \rho(x,y)_{eq} I_A\}. \tag{17}$$

Since we consider a range of temperatures where $g_*(T)$ is varying, entropy conservation $g_*(T(x))T^3(x)x^3 = \text{constant}$ implies that temperature does not simply scale as $\frac{1}{a(t)}$ and we take this into account. In order to simplify the calculation we use the static approximation (i.e. impose the constraint $\dot{\rho}_{AA} = \dot{\rho}_{SA} = 0$). This has been shown to give a very good approximation when the production of sterile neutrinos occurs at a T where the collision term, Eq. (13), is large compared to the Hubble expansion [20], which is the case here.

We have checked that, for several choices of mass matrix parameters, the simple estimate above gives a reasonable approximation to the numerical solution of the Boltzmann equations. The difference comes from the continuous change in $g_*(T)$, that we can only take into account numerically. In Fig. 3 we show the evolution of the ratio of the sterile number density to that of one active neutrino as T varies, at fixed $y = 5$ and for two widely different values of M_i. We observe a double upward step reaching a value near 2 corresponding to the thermalization of the two species and a dilution at lower

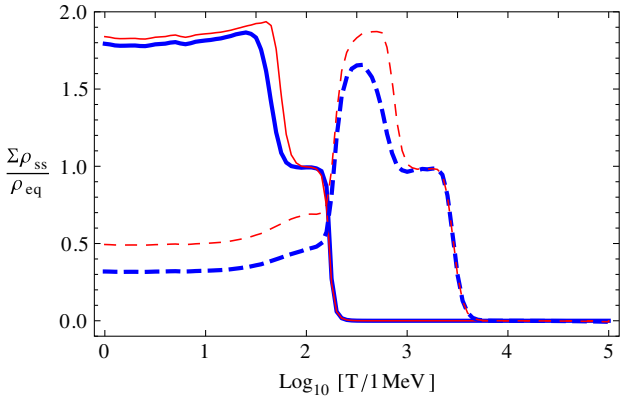

FIG. 3 (color online). Evolution of the ratio of the number density of sterile species over that of one active massless neutrino for $y = 5$ for $(M_1, M_2) \simeq (2 \times 10^{-5}, 10^{-3})$ (solid) and (0.1, 10) (dashed) in MeV and mixing parameters that minimize $f_{s_1}(T_{\rm max})$ for NH (thick) and IH (thin).

temperatures, significant only for masses above keV. The dependence on y of the ratio is significant due to the dilution effect and we take it into account in the definition of $\Delta N_{\rm eff}(T_W)$ which involves the integrated energy density. We have considered numerically the case with degenerate heavy masses $M_1 = M_2$. The only difference appears to be that the thermalization curve does not show a double step but a single one.

In Fig. 4, we show the constant $\Delta N_{\rm eff}(T_{\rm W})$ lines for the mixing parameters that minimize $f_{s_1}(T_{\rm max})$, as well as those corresponding to the relativistic component, $\Delta N_{\rm eff}^{\rm rel}(T_{\rm W}) \equiv (\epsilon_s - \epsilon_s^m)/\epsilon_\nu^0$, where ϵ_s^m is the contribution of the sterile species to the matter density. We only consider masses that remain relativistic at BBN, because more massive species would quickly dominate the energy density as cold dark matter, unless they decay before BBN. These results show that dilution allows one to relax the BBN bounds for masses in the range 10 keV–10 MeV, however these particles give a huge contribution to the energy density when they become nonrelativistic at later times, modifying in a drastic way CMB and structure formation. The only way BBN and CMB bounds could be evaded in this range is if the sterile states decay before BBN. We come back to this point later.

We note that the analysis might not be accurate for $T \gtrsim T_{\rm QCD}$ [42,43], however we do not expect the conclusions to change drastically even if hadronic uncertainties are included.

It is important to stress that the approximate independence of thermalization on the heavy masses M_i results from the approximate seesaw scaling of the mixings $|U_{as_i}|^2 M_i \sim m_l$, which is only approximate since there is dependence on several unknown parameters, see Eq. (4). Figure 5 shows the values of $|U_{es_i}|^2 M_i$ and $(|U_{\mu s_i}|^2 + |U_{\tau s_i}|^2)M_i$ within the full range of the unconstrained parameters for the normal hierarchy. We note that $|U_{es_i}|^2 M_i$ can get extremely small. Had we only considered the oscillations to electron neutrinos in this case, we would have found that for those parameters $f_s(T_{\rm max}) \ll 1$, but $(|U_{\mu s_i}|^2 + |U_{\tau s_i}|^2)M_i$ is in the expected ballpark and therefore the thermalization takes place through the oscillation to μ and τ. A similar pattern is observed for the IH, both combinations do not get very small simultaneously.

For sufficiently high mass the sterile neutrino could decay before BBN and our analysis is not valid for this situation. The lifetime is in the range $\tau \sim 6 \times 10^{11} [\frac{\rm MeV}{M_i}]^4 [\frac{0.05\ \rm eV}{|U_{as_i}|^2 M_i}] s$ (for a recent analysis see [38,39]), below the π_0 threshold, which means they decay after BBN below this threshold, for natural choices of mixings. However, the mixings might reach values significantly larger (see Fig. 5). For extreme mixings of $O(1)$, neutrinos as light as 10 MeV could decay before BBN. The bounds

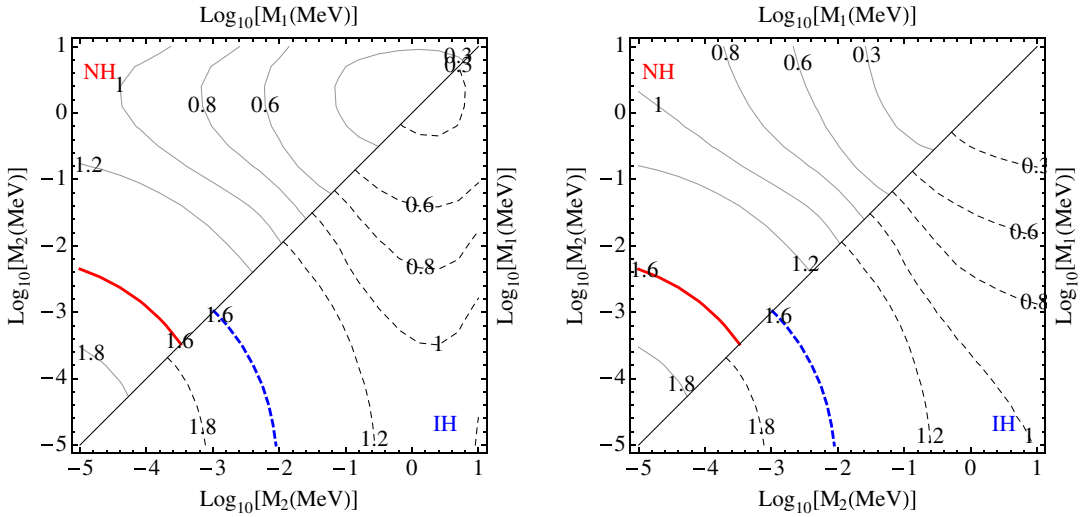

FIG. 4 (color online). $\Delta N_{\rm eff} = \epsilon_s/\epsilon_\nu^0$ (left) and $\Delta N_{\rm eff}^{\rm rel} = (\epsilon_s - \epsilon_s^m)/\epsilon_\nu^0$ (right) at $T_{\rm W}$ as a function of the sterile masses NH (upper octant) or IH (lower octant). The thick lines correspond to maximum allowed by BBN at 2σ.

on short-lived sterile neutrinos with masses in the range [10 MeV, 140 MeV] have been studied in [41,44,45]. Very strong bounds have been found combining BBN and direct accelerator searches, essentially excluding this possibility in the minimal model [40].

It should be stressed that in the generic seesaw models that we are considering, such short lifetimes result only from very specific textures in which an approximate global symmetry (and not small Yukawa couplings) suppresses light neutrino masses in front of the seesaw scale. The flavor structure of these models is even more constrained, but large active-sterile mixings can be reached. Note that in these corners of parameter space, thermalization will be more efficient and T_d will be closer to T_W, so dilution is less relevant.

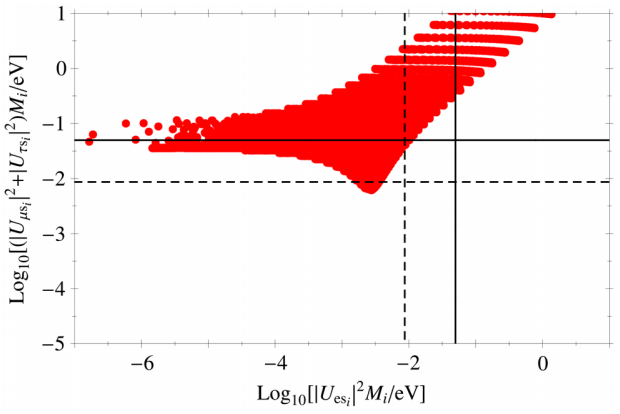

FIG. 5 (color online). Distribution of $(|U_{\mu s_i}|^2 + |U_{\tau s_i}|^2)M_i$ versus $|U_{e s_i}|^2 M_i$ varying all the unconstrained parameters for NH. The solid/dashed line corresponds to $m_3 \sim \sqrt{\Delta m^2_{\rm atm}}/m_2 \sim \sqrt{\Delta m^2_{\rm solar}}$.

IV. CONCLUSIONS

We have studied the contribution to $\Delta N_{\rm eff}$ of the extra sterile states in minimal type I seesaw models as a function of the seesaw scale. We have found that the extra states do thermalize independently of the scale of the Majorana masses up to $\mathcal{O}(100\ \text{MeV})$. This implies very strong constraints from cosmology on low-scale models. The following conclusions can be drawn.

(i) $M_{1,2} \lesssim \mathcal{O}(100\ \text{MeV})$: $\Delta N_{\rm eff}(T_d) \simeq 2$ and decay after BBN, which is incompatible with the present BBN or/and CMB constraints independently of the mass of the sterile states. These models are therefore strongly disfavored. The minimal $3+2$ model with eV Majorana masses that could alleviate the tension with the LSND and reactor anomalies is in this category.

(ii) $M_1 \lesssim \mathcal{O}(100\,\text{MeV})$, $M_2 \gtrsim \mathcal{O}(\text{GeV})$: $\Delta N_{\rm eff}(T_d) \simeq 1$, while the heavy state is Boltzmann suppressed at decoupling or decays before $T_{\rm W}$. BBN constraints can accommodate this case if M_1 is still relativistic at BBN. However CMB and LSS measurements close this window all the way down to $M_1 \leq 0.36$ eV or so at 95% C.L. [46]. Whether this very hierarchical option could also improve the agreement with LSND and reactor anomalies is under study.

(iii) $M_{1,2} \gtrsim \mathcal{O}(1\ \text{GeV})$ survive at present cosmological constraints on $N_{\rm eff}$, because they decouple while being nonrelativistic and therefore $\Delta N_{\rm eff}(T_d)$ is Boltzmann suppressed, or because they decay well before $T_{\rm W}$.

In the range 100 MeV–1 GeV we expect that BBN bounds will depend significantly on the other unknown mixing parameters, and exploring this regime requires a more detailed study.

ACKNOWLEDGMENTS

We thank A. Donini, J. Lesgourgues, O. Mena, C. Peña-Garay, J. Racker, N. Rius and J. Salvado for useful discussions. We warmly thank E. Fernández-Martinez for pointing out an error in an earlier version of the paper. This work was partially supported by Grants No. FPA2011-29678 (FEDER), No. PROMETEO/2009/116, No. CUP (CSD2008-00037) and No. ITN INVISIBLES (Marie Curie Actions, PITN-GA-2011-289442).

[1] The range 10^{-10} eV $-$ 1 eV can be excluded from oscillation data, while a scale above 10^{15} GeV would require nonperturbative Yukawas.
[2] A recent review see For J. Kopp, P. A. N. Machado, M. Maltoni, and T. Schwetz, J. High Energy Phys. 05 (2013) 050.
[3] A. Aguilar-Arevalo *et al.* (LSND Collaboration), Phys. Rev. D **64**, 112007 (2001).
[4] A. A. Aguilar-Arevalo *et al.* (MiniBooNE Collaboration), Phys. Rev. Lett. **110**, 161801 (2013).
[5] G. Mention, M. Fechner, Th. Lasserre, Th. A. Mueller, D. Lhuillier, M. Cribier, and A. Letourneau, Phys. Rev. D **83**, 073006 (2011); P. Huber, Phys. Rev. C **84**, 024617 (2011); **85**, 029901(E) (2012).
[6] S. Dodelson and L. M. Widrow, Phys. Rev. Lett. **72**, 17 (1994).
[7] E. K. Akhmedov, V. A. Rubakov, and A. Y. Smirnov, Phys. Rev. Lett. **81**, 1359 (1998).
[8] Obviously the zeros could be lifted by new physics beyond the N extra singlets, adding for example a scalar triplet to the field content of the model.
[9] A. de Gouvea, Phys. Rev. D **72**, 033005 (2005); A. de Gouvea, J. Jenkins, and N. Vasudevan, Phys. Rev. D **75**, 013003 (2007).
[10] A. Donini, P. Hernández, J. López-Pavón, and M. Maltoni, J. High Energy Phys. 07 (2011) 105.
[11] A. Donini, P. Hernández, J. López-Pavón, M. Maltoni, and T. Schwetz, J. High Energy Phys. 07 (2012) 161.
[12] L. Canetti, M. Drewes, T. Frossard, and M. Shaposhnikov, Phys. Rev. D **87**, 093006 (2013), and references therein.
[13] G. Mangano, G. Miele, S. Pastor, T. Pinto, O. Pisanti, and P. D. Serpico, Nucl. Phys. **B729**, 221 (2005).
[14] Y. I. Izotov and T. X. Thuan, Astrophys. J. **710**, L67 (2010).
[15] P. A. R. Ade *et al.* (Planck Collaboration), arXiv:1303.5076.
[16] G. Hinshaw *et al.* (WMAP Collaboration), Astrophys. J. Suppl. Ser. **208**, 19 (2013).
[17] Z. Hou *et al.*, Astrophys. J. **782**, 74 (2014).
[18] J. L. Sievers *et al.*, J. Cosmol. Astropart. Phys. 10 (2013) 060.
[19] R. Barbieri and A. Dolgov, Phys. Lett. B **237**, 440 (1990); Nucl. Phys. **B349**, 743 (1991); K. Kainulainen, Phys. Lett. B **244**, 191 (1990).
[20] A. D. Dolgov and F. L. Villante, Nucl. Phys. **B679**, 261 (2004).
[21] M. Cirelli, G. Marandella, A. Strumia, and F. Vissani, Nucl. Phys. **B708**, 215 (2005).
[22] A. Melchiorri, O. Mena, S. Palomares-Ruiz, S. Pascoli, A. Slosar, and M. Sorel, J. Cosmol. Astropart. Phys. 01 (2009) 036.
[23] S. Hannestad, I. Tamborra, and T. Tram, J. Cosmol. Astropart. Phys. 07 (2012) 025.
[24] E. Kuflik, S. D. McDermott, and K. M. Zurek, Phys. Rev. D **86**, 033015 (2012).
[25] T. D. Jacques, L. M. Krauss, and C. Lunardini, Phys. Rev. D **87**, 083515 (2013).
[26] M. Archidiacono, N. Fornengo, C. Giunti, S. Hannestad, and A. Melchiorri, Phys. Rev. D **87**, 125034 (2013).
[27] J. A. Casas and A. Ibarra, Nucl. Phys. **B618**, 171 (2001).
[28] M. Blennow and E. Fernandez-Martinez, Phys. Lett. B **704**, 223 (2011).
[29] D. Notzold and G. Raffelt, Nucl. Phys. **B307**, 924 (1988).
[30] K. Kimura, A. Takamura, and H. Yokomakura, Phys. Lett. B **537**, 86 (2002); Phys. Rev. D **66**, 073005 (2002); A. Donini, K.-i. Fuki, J. López-Pavón, D. Meloni, and O. Yasuda, J. High Energy Phys. 08 (2009) 041.
[31] L. Stodolsky, Phys. Rev. D **36**, 2273 (1987); G. Raffelt, G. Sigl, and L. Stodolsky, Phys. Rev. Lett. **70**, 2363 (1993); M. J. Thomson, Phys. Rev. A **45**, 2243 (1992).
[32] K. Enqvist, K. Kainulainen, and M. Thomson, Nucl. Phys. **B373**, 498 (1992); B. H. J. McKellar and M. J. Thomson, Phys. Rev. D **49**, 2710 (1994).
[33] G. Sigl and G. Raffelt, Nucl. Phys. **B406**, 423 (1993).
[34] A. D. Dolgov, Phys. Rep. **370**, 333 (2002).
[35] A. D. Dolgov, S. H. Hansen, S. Pastor, and D. V. Semikoz, Astropart. Phys. **14**, 79 (2000).
[36] R. Foot and R. R. Volkas, Phys. Rev. D **55**, 5147 (1997).
[37] N. F. Bell, R. R. Volkas, and Y. Y. Y. Wong, Phys. Rev. D **59**, 113001 (1999).
[38] D. Gorbunov and M. Shaposhnikov, J. High Energy Phys. 10 (2007) 015.
[39] A. Atre, T. Han, S. Pascoli, and B. Zhang, J. High Energy Phys. 05 (2009) 030.
[40] O. Ruchayskiy and A. Ivashko, J. High Energy Phys. 06 (2012) 100.
[41] A. D. Dolgov, S. H. Hansen, G. Raffelt, and D. V. Semikoz, Nucl. Phys. **B580**, 331 (2000); A. D. Dolgov, S. H. Hansen, G. Raffelt, and D. V. Semikoz, Nucl. Phys. **B590**, 562 (2000).
[42] K. N. Abazajian and G. M. Fuller, Phys. Rev. D **66**, 023526 (2002); K. Abazajian, Phys. Rev. D **73**, 063506 (2006).
[43] T. Asaka, M. Laine, and M. Shaposhnikov, J. High Energy Phys. 01 (2007) 091.
[44] G. M. Fuller, C. T. Kishimoto, and A. Kusenko, arXiv:1110.6479.
[45] O. Ruchayskiy and A. Ivashko, J. Cosmol. Astropart. Phys. 10 (2012) 014.
[46] E. Di Valentino, A. Melchiorri, and O. Mena, arXiv:1304.5981.

PHYSICAL REVIEW D **90,** 065033 (2014)

$N_{\rm eff}$ in low-scale seesaw models versus the lightest neutrino mass

P. Hernández,[1,*] M. Kekic,[1,†] and J. Lopez-Pavon[2,3,‡]

[1]*IFIC (CSIC) and Departamento Física Teórica, Universidad de Valencia, Edificio Institutos Investigación, Apartado de Correos 22085, E-46071 Valencia, Spain*

[2]*SISSA, via Bonomea 265, 34136 Trieste, Italy*

[3]*INFN, sezione di Trieste, 34136 Trieste, Italy*

(Received 19 June 2014; published 25 September 2014)

We evaluate the contribution to $N_{\rm eff}$ of the extra sterile states in low-scale type I seesaw models (with three extra sterile states). We explore the full parameter space and find that at least two of the heavy states always reach thermalization in the early Universe, while the third one might not thermalize provided the lightest neutrino mass is below $\mathcal{O}(10^{-3}$ eV). Constraints from cosmology therefore severely restrict the spectra of heavy states in the range 1 eV–100 MeV. The implications for neutrinoless double beta decay are also discussed.

DOI: 10.1103/PhysRevD.90.065033 PACS numbers: 14.60.St, 98.80.Cq

I. INTRODUCTION

The simplest extension of the standard model (SM) that can account for the observed neutrino masses is a type I seesaw model [1] with $N \geq 2$ extra singlet Majorana fermions. The Majorana masses, that we globally denote as M, constitute a new scale of physics (the seesaw scale) which is presently unknown. Since the light neutrino masses are a combination of the Yukawa couplings, the electroweak scale and the seesaw scale, the latter can be arbitrary if the Yukawas are adjusted accordingly. As a result, the seesaw scale is presently unconstrained to lie anywhere above $\mathcal{O}$(eV) up to $\mathcal{O}(10^{15}$ GeV) [2]. The determination of this scale is one of the most important open questions in neutrino physics.

It is often assumed that the seesaw scale is very high, above the electroweak scale. However, in the absence of any other hint of new physics beyond the SM, the possibility that the seesaw scale could be at the electroweak scale or lower should be seriously considered. As far as naturalness goes, the model with a low scale is technically natural, since in the limit $M \to 0$, a global lepton number symmetry is recovered: neutrinos becoming Dirac particles by the pairing of the Majorana fermions.

The spectra of $N = 3$ type I seesaw models contain six Majorana neutrinos: the three lightest neutrinos, mostly active, and three heavier, mostly sterile. The coupling of the latter with the leptons, U_{as}, is strongly correlated with their masses (the naive seesaw scaling being $|U_{as}|^2 \propto M^{-1}$). The possibility that such neutrino sterile states could be responsible for any of the anomalies found in various experiments is of course very interesting, since it could open a new window into establishing the new physics of neutrino masses.

Models with extra light sterile neutrinos with masses in the range of $\mathcal{O}$(eV) could provide an explanation to the LSND/MiniBOONE [5,6] and reactor anomalies [7]. Sterile species in the $\mathcal{O}$(keV) range could still be valid candidates for warm dark matter [8–11]. The recent measurement of an x-ray signal [12,13] might be the first experimental indication of such possibility. Species in the $\mathcal{O}$(GeV) range could account for the baryon asymmetry in the Universe [14,15] (for a recent review see [16]).

There are important constraints on low-scale models from direct searches and rare processes such as $\mu \to e\gamma$ and μe conversion. Recent results can be found in [17–19]. The constraints are strongly dependent on M for $M \lesssim \mathcal{O}(100$ GeV).

It is well known that if light sterile neutrinos with significant active-sterile mixing exist they can contribute significantly to the energy density of the Universe. Mechanisms to reduce this contribution have been proposed, such as the presence of primordial lepton asymmetries [20] or new interactions [21,22], which however typically require new physics beyond that of the sterile species. The energy density of the extra neutrino species, ϵ_s, is usually quantified in terms of $\Delta N_{\rm eff}$ (when they are relativistic) defined by

$$\Delta N_{\rm eff} \equiv \frac{\epsilon_s}{\epsilon_\nu^0}, \tag{1}$$

where ϵ_ν^0 is the energy density of one SM massless neutrino with a thermal distribution [below $e^\pm$ annihilation it is $\epsilon_\nu^0 \equiv (7\pi^2/120)(4/11)^{4/3}T_\gamma^4$ at the photon temperature T_γ]. One fully thermal extra sterile state that decouples from the thermal bath being relativistic contributes $\Delta N_{\rm eff} \simeq 1$ when it decouples.

$N_{\rm eff}$ at big bang nucleosynthesis (BBN) strongly influences the primordial helium production. A recent analysis of BBN bounds [23] gives $N_{\rm eff}^{\rm BBN} = 3.5 \pm 0.2$.

*m.pilar.hernandez@uv.es
†Marija.Kekic@ific.uv.es
‡jlpavon@sissa.it

 © 2014 American Physical Society

$N_{\rm eff}$ also affects the anisotropies of the cosmic microwave background (CMB). Recent CMB measurements from Planck give $N_{\rm eff}^{\rm CMB} = 3.30 \pm 0.27$ [24], which includes WMAP-9 polarization data [25] and high multipole measurements from the South Pole Telescope [26] and the Atacama Cosmology Telescope [27]. Recent global analyses, including the BICEP2 results [28,29], seem to prefer larger values of $N_{\rm eff}^{\rm CMB}$ [30–32].

The contribution of extra sterile neutrinos to $N_{\rm eff}$ has been extensively studied in phenomenological models, where there is no correlation between masses and mixing angles [33–35]. For recent analyses of eV scale neutrinos, with and without lepton asymmetries, see [36–42]. In [43] we explored systematically the contribution to $N_{\rm eff}$ of the minimal type I seesaw models with just two extra singlets, $N = 2$. We found that whenever the two heavier states are below $\mathcal{O}(100\ {\rm MeV})$, they contribute too much energy/matter density to the Universe, while the possibility of having one state $\lesssim$ eV and another heavier than 100 MeV may not be excluded by cosmological and oscillation data constraints, but requires further scrutiny.

The purpose of this paper is to perform the same study in the next-to-minimal seesaw model where $N = 3$. This is the standard type I seesaw model with a low scale, and is also often referred to as the neutrino Minimal Standard Model (νMSM). This model has been extensively studied in the literature, concentrating on regions of parameter space where the lightest sterile state could be a warm dark matter particle, and the two heavier states could be responsible for the baryon asymmetry in the Universe [15]. What we add in this paper is a systematic study of the full parameter space to understand the constraints on the seesaw scale(s) from the modifications to the standard cosmology induced by the three heavy neutrino states. We will assume that primordial lepton asymmetries are negligible. Although the model in principle satisfies the Sakharov conditions to generate a lepton asymmetry, previous works indicate that significant lepton asymmetries can only be generated when at least two of the sterile states are heavy enough, $\mathcal{O}({\rm GeV})$, and extremely degenerate [44]. Here we will concentrate on studying the bounds from cosmology when such an extreme degeneracy of the sterile neutrino states is not present. We show that, in spite of the large parameter space, the thermalization of the sterile states in this model is essentially controlled by one parameter: the lightest neutrino mass.

The paper is organized as follows. In Sec. II we review the estimates of the thermalization rate of the sterile states as derived in [43], which allow us to efficiently explore the full parameter space of the model. In Sec. III we derive analytical bounds for the thermalization rate and in Sec. IV we correlate $\Delta N_{\rm eff}$ with the lightest neutrino mass. In Sec. V we present numerical results from solving the Boltzmann equations and finally in Sec. VI we analyze the impact on neutrinoless double beta decay. In Sec. VII we conclude.

II. THERMALIZATION OF STERILE NEUTRINOS IN 3 + 3 SEESAW MODELS

The model is described by the most general renormalizable Lagrangian including $N = 3$ extra singlet Weyl fermions, ν_R^i:

$$\mathcal{L} = \mathcal{L}_{\rm SM} - \sum_{\alpha,i} \bar{L}^\alpha Y^{\alpha i} \tilde{\Phi} \nu_R^i - \sum_{i,j=1}^{3} \frac{1}{2} \bar{\nu}_R^{ic} M_N^{ij} \nu_R^j + {\rm H.c.},$$

where Y is a 3×3 complex matrix and M_N a diagonal real matrix. The spectrum of this theory has six massive Majorana neutrinos, and the mixing is described in terms of six angles and six charge parity (CP) phases.

We assume that the eigenvalues of M_N are significantly larger than the atmospheric and solar neutrino mass splittings, which implies a hierarchy $M_N \gg Yv$ and therefore the seesaw approximation is good. A convenient parametrization in this case is provided by that of Casas-Ibarra [45], or its extension to all orders in the seesaw expansion as described in [46] (for an alternative see [47]). The mass matrix can be written as

$$\mathcal{M}_\nu = U^* {\rm Diag}(m_l, M_h) U^\dagger, \tag{2}$$

where $m_l = {\rm Diag}(m_1, m_2, m_3)$ and $M_h = {\rm Diag}(M_1, M_2, M_3)$. Denoting by a the active/light neutrinos and s the sterile/heavy species, the unitary matrix can be written as

$$U = \begin{pmatrix} U_{aa} & U_{as} \\ U_{sa} & U_{ss} \end{pmatrix}, \tag{3}$$

with

$$\begin{aligned} U_{aa} &= U_{\rm PMNS} \mathcal{H}, \\ U_{ss} &= \bar{\mathcal{H}}, \\ U_{sa} &= i \bar{\mathcal{H}} M_h^{-1/2} R m_l^{1/2}, \\ U_{as} &= i U_{\rm PMNS} \mathcal{H} m_l^{1/2} R^\dagger M_h^{-1/2}, \end{aligned} \tag{4}$$

where $U_{\rm PMNS}$ is a 3×3 unitary matrix and R is a generic 3×3 orthogonal complex matrix, while $\mathcal{H}$ and $\bar{\mathcal{H}}$ are defined by

$$\begin{aligned} \mathcal{H}^{-2} &= I + m_l^{1/2} R^\dagger M_h^{-1} R m_l^{1/2}, \\ \bar{\mathcal{H}}^{-2} &= I + M_h^{-1/2} R m_l R^\dagger M_h^{-1/2}. \end{aligned} \tag{5}$$

At leading order in the seesaw expansion, i.e. up to $\mathcal{O}(\frac{m_l}{M_h})$, $\mathcal{H} \simeq \bar{\mathcal{H}} \simeq 1$, and we recover the Casas-Ibarra parametrization. In this approximation $U_{\rm PMNS}$ is the light neutrino mixing matrix measured in oscillations.

Neutrino oscillation data fix two of the three eigenvalues in m_l and the three angles in $U_{\rm PMNS}$; however all the heavy

masses in M_h, the lightest neutrino mass in m_l, the three complex angles in R and the three CP violating phases in $U_{\rm PMNS}$ are presently unconstrained [48].

In [49] a simple estimate for the thermalization of one sterile neutrino in the early Universe, neglecting primordial lepton asymmetries, was given as follows. Assuming that the active neutrinos are in thermal equilibrium with a collision rate given by Γ_{ν_α}, the collision rate for the sterile neutrinos can be estimated to be

$$\Gamma_{s_j} \simeq \frac{1}{2}\sum_a \langle P(\nu_a \to \nu_{s_j})\rangle \times \Gamma_{\nu_\alpha}, \tag{6}$$

where $\langle P(\nu_\alpha \to \nu_{s_j})\rangle$ is the time-averaged probability $\nu_\alpha \to \nu_{s_j}$. This probability depends strongly on temperature because the neutrino index of refraction in the early Universe is modified by coherent scattering of neutrinos with the particles in the plasma [50]. Thermalization will be achieved if there is any temperature where this rate is higher than the Hubble expansion rate, i.e. $\Gamma_{s_j}(T) \geq H(T)$. In a radiation-dominated universe, $H(T) = \sqrt{\frac{4\pi^3 g_*(T)}{45}}\frac{T^2}{M_{\rm Planck}}$, with $g_*(T)$ being the number of relativistic degrees of freedom.

One can therefore define the function $f_{s_j}(T)$, which measures the sterile production rate of the species s_j in units of the Hubble expansion rate,

$$f_{s_j}(T) \equiv \frac{\Gamma_{s_j}(T)}{H(T)}. \tag{7}$$

It reaches a maximum at some temperature, $T_{\rm max}$ [49]. If $f_{s_j}(T_{\rm max}) \geq 1$, the sterile state will reach a thermal abundance at early times. We can estimate the contribution to $N_{\rm eff}$ as

$$N_{\rm eff} \simeq N_{\rm eff}^{\rm SM} + \sum_j (1 - \exp(-\alpha f_{s_j}(T^j_{\rm max}))), \tag{8}$$

at decoupling if they are still relativistic, where α is an $\mathcal{O}(1)$ numerical constant. Provided $f_{s_j}(T^j_{\rm max})$ is sufficiently larger than one, $N_{\rm eff}$ saturates to the number of thermalized species, up to exponentially small corrections.

In [43], this result was also derived from the Boltzmann equations [51–54], in the assumption of no primordial large lepton asymmetries. As shown in Appendix A, in spite of the complex 6×6 mixing, the thermalization of the sterile state j is roughly given by the sum of three 2×2 mixing contributions in agreement with the naive expectation of Eq. (6),

$$f_{s_j}(T) = \sum_{\alpha=e,\mu,\tau}\frac{\Gamma_{\nu_\alpha}(T)}{H(T)}\left(\frac{M_j^2}{2pV_\alpha(T) - M_j^2}\right)^2 |(U_{as})_{\alpha j}|^2, \tag{9}$$

where p is the momentum, $V_\alpha(T)$ is the potential induced by coherent scattering in the plasma [50] and $\Gamma_{\nu_\alpha}(T)$ is the scattering rate of the active neutrinos. Both V_α and Γ_α depend on the temperature since the number of scatters increases with T [10,55,56]. While the former varies only when the lepton states become populated, the latter depends significantly on the quark degrees of freedom and therefore changes significantly at the QCD phase transition. The quark contribution to Γ_{ν_α} is however rather uncertain; we therefore neglect this contribution, since this is a conservative assumption if we want to minimize thermalization: any contribution that will increase Γ_{ν_α} would help increase the thermalization rate.

The most complete calculation of Γ_{ν_α} has been presented in [56], where a full two-loop computation of the imaginary part of the neutrino self-energy was presented. The results for the leptonic contribution to $\Gamma_{\nu_\alpha}(T)$ can be accurately parametrized in terms of $C_\alpha(T)$ as

$$\Gamma_{\nu_\alpha} \simeq C_\alpha(T) G_F^2 T^4 p \tag{10}$$

that can be extracted from the numerical results of [56], recently made publicly available in Ref. [57].

For temperatures above the different lepton thresholds, the results can be approximated by
(τ) $T \gtrsim 180$ MeV: $C_{e,\mu,\tau} \simeq 3.43$ and $V_\alpha = AT^4 p$ for $\alpha = e,\mu,\tau$;
(μ) 20 MeV $\lesssim T \lesssim 180$ MeV: $C_{e,\mu} \simeq 2.65$, $C_\tau \simeq 1.26$, $V_e = V_\mu = AT^4 p$ and $V_\tau = BT^4 p$;
(e) $T \lesssim 20$ MeV: $C_e \simeq 1.72$, $C_{\mu,\tau} \simeq 0.95$, $V_e = AT^4 p$ and $V_\mu = V_\tau = BT^4 p$,
with

$$\begin{aligned} B &\equiv -2\sqrt{2}\left(\frac{7\zeta(4)}{\pi^2}\right)\frac{G_F}{M_Z^2}, \\ A &\equiv B - 4\sqrt{2}\left(\frac{7\zeta(4)}{\pi^2}\right)\frac{G_F}{M_W^2}. \end{aligned} \tag{11}$$

In Fig. 1 we show $C_\alpha(T)/\sqrt{g_*(T)}$ as a function of the temperature. We include the T dependent normalization

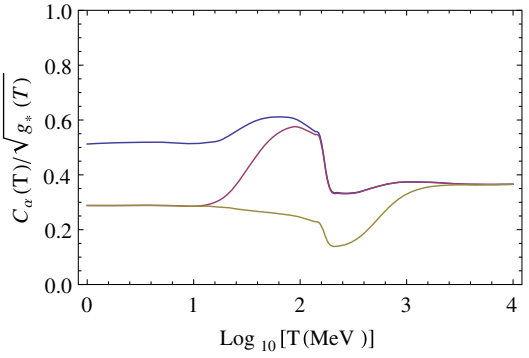

FIG. 1 (color online). Leptonic contribution to $C_\alpha(T)/\sqrt{g_*(T)}$ taken from Refs. [56,57] for $\alpha = e$ (top/blue), μ (middle/magenta), τ (bottom/yellow).

factor, $\sqrt{g_*(T)}$, coming from $H(T)$. Note that the dependence on the temperature of this factor is small.

Let $T_{\rm max}$ be the value of the temperature at which $f_{s_j}(T)$ is maximum [58]. For $p = 3.15T$, and neglecting the T dependence of $C_\alpha/\sqrt{g_*}$, $T_{\rm max}$ is bounded by

$$T^\tau_{\rm max} \equiv \left(\frac{M_j^2}{59.5|A|}\right)^{1/6} \leq T_{\rm max} \leq \left(\frac{M_j^2}{59.5|B|}\right)^{1/6}. \quad (12)$$

Thermalization will take place provided $f_{s_j}(T_{\rm max}) \geq 1$. In the next section we derive an analytical lower bound on this quantity, which can be translated therefore into a sufficient condition for thermalization.

III. ANALYTICAL BOUNDS

For a given set of mixing and mass parameters we have the following general lower bound for $f_{s_j}(T)$:

$$f_{\rm B}(T) \equiv {\rm Min}\left[\frac{C_\tau(T)}{\sqrt{g_*(T)}}\right] \frac{G_F^2 p T^4 \sqrt{g_*(T)}}{H(T)} \left(\frac{M_j^2}{2pV_e - M_j^2}\right)^2 \times \sum_{\alpha=e,\mu,\tau} |(U_{as})_{\alpha j}|^2 \leq f_{s_j}(T). \quad (13)$$

This results from the fact that $|V_e| \geq |V_\alpha|$ and $C_\alpha \geq C_\tau$ for all $\alpha = e, \mu, \tau$. The minimization of $C_\tau/\sqrt{g_*}$ as a function of T gets rid of the T dependence of this factor.

The function $f_{\rm B}(T)$ is maximized at $T^\tau_{\rm max}$, defined in Eq. (12). It then follows that

$$f_{\rm B}(T^\tau_{\rm max}) \leq f_{s_j}(T^\tau_{\rm max}) \leq f_{s_j}(T_{\rm max}). \quad (14)$$

In summary, taking the average momentum, $p = 3.15T$, $f_{s_j}(T_{\rm max})$ is bounded by

$$f_{s_j}(T_{\rm max}) \geq f_{\rm B}(T^\tau_{\rm max}) = \frac{\sum_\alpha |(U_{as})_{\alpha j}|^2 M_j}{3.25 \times 10^{-3}\ {\rm eV}}. \quad (15)$$

Using Eq. (4) in the Casas-Ibarra limit, the dependence on the parameters of the model in the above equation can be simplified to the following combination:

$$\sum_\alpha |(U_{as})_{\alpha j}|^2 M_j = \sum_\alpha (U_{\rm PMNS} m_l^{1/2} R)_{\alpha j} (R^\dagger m_l^{1/2} U^\dagger_{\rm PMNS})_{j\alpha} = (R^\dagger m_l R)_{jj} \equiv h_j. \quad (16)$$

Therefore the analytical lower bound does not depend on the angles and CP phases of the Pontecorvo-Maki-Nakagawa-Sakata (PMNS) matrix. It depends only on the undetermined Casas-Ibarra parameters and the light neutrino masses. The lower bound can be further simplified using

$$h_j = \sum_\alpha |R_{\alpha j}|^2 m_\alpha \geq |\sum_\alpha R^2_{\alpha j} m_\alpha| \geq |\sum_\alpha R^2_{\alpha j} m_1| = m_1, \quad (17)$$

where in the last step we have used the orthogonality of the R matrix and assumed a normal hierarchy of the light neutrinos (NH). The result for an inverted hierarchy (IH) is the same substituting $m_1 \to m_3$. Finally using Eqs. (16) and (17) in Eq. (15) we obtain

$$f_{s_j}(T_{\rm max}) \geq \frac{h_j}{3.25 \times 10^{-3}\ {\rm eV}} \geq \frac{m_1}{3.25 \times 10^{-3}\ {\rm eV}} \equiv \frac{m_1}{m_1^{\rm th}}, \quad (18)$$

which defines $m_1^{\rm th}$.

IV. LIGHTEST NEUTRINO MASS VERSUS THERMALIZATION

The thermalization of jth heavy sterile state will occur provided $f_{s_j}(T) \geq 1$ for some T. Therefore a sufficient condition is that $f_{s_j}(T_{\rm max}) \geq 1$ or using Eq. (18) $m_1 \geq m_1^{\rm th}$. From the analytical bound we therefore deduce that thermalization of the three states will occur if

$$m_1 \geq 3.25 \times 10^{-3}\ {\rm eV}, \quad (19)$$

for any value of the unconstrained parameters in R and the CP phases. We note that a more restrictive upper bound on the lightest neutrino mass was derived in [11,56] under the assumption that M_1 was a warm dark matter candidate in the keV range.

In Fig. 2 we show the contour plots of the minimum of $f_{s_1}(T_{\rm max})$ (varying the unconstrained parameters in R and the CP phases in the full range), as a function of m_1 and M_1. The three lines correspond to ${\rm Min}[f_{s_1}(T_{\rm max})] = 10^{-1}, 1, 10$. As expected the minimum is strongly correlated with m_1 and is roughly independent of M_1. Values of m_1 below the contour line at 1 correspond to nonthermalization; therefore we read

$$m_1 \leq \mathcal{O}(10^{-3}\ {\rm eV}), \quad (20)$$

for $M_1 \in [1\ {\rm eV}–100\ {\rm MeV}]$. The numerical bound is slightly stronger than the analytical bound given by

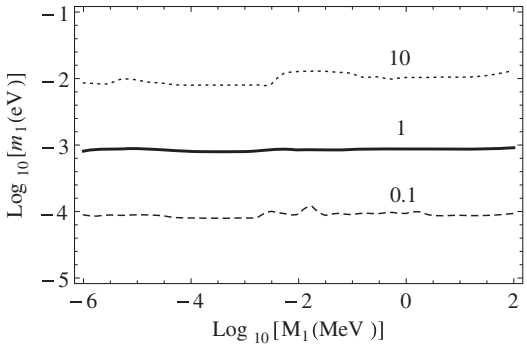

FIG. 2. Contours of ${\rm Min}[f_{s_1}(T_{\rm max})] = 0.1, 1, 10$ on the plane (M_1, m_1).

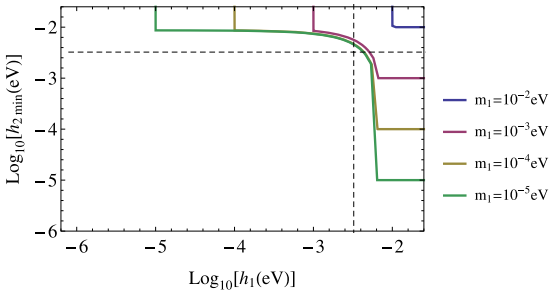

FIG. 3 (color online). Minimum of h_2 in bins of h_1 in the full allowed parameter space with fixed $m_1 = 10^{-[5-2]}$ eV. The dashed line corresponds to the analytical bound $m_1^{\rm th} = 3.25 \times 10^{-3}$ eV.

Eq. (19). Had we considered any other of the heavy states $j = 2, 3$ the results would be the same [i.e. the same minimum of $f_{s_j}(T_{\rm max})$ would be obtained for different values of the unconstrained parameters].

A less stringent (sufficient) condition for thermalization of the state j is

$$h_j \geq m_1^{\rm th} \tag{21}$$

as it follows from Eq. (18). It turns out that this condition is always satisfied for at least two of the three heavy neutrinos, independently of m_1 or the Casas-Ibarra parameters. In Fig. 3 we show the minimization of h_2 in the full parameter space within each bin of h_1, shown in the x-axis, for fixed values of m_1. Although either h_1 or h_2 can always be below the $m_1^{\rm th}$ line (shown as dashed line) if $m_1 \leq m_1^{\rm th}$, the other one is always significantly above it. The same pattern is observed with any pair of h_j. This shows that at most one of the sterile states might not thermalize, and to have one not thermal requires that $m_1 \leq m_1^{\rm th}$.

It is easy to see how h_j can reach its lower bound, m_1, without contradicting present neutrino data. One can always choose $R_{\alpha j} = 0$ for $\alpha \neq j$. For $j = 1$, the orthogonal matrix reduces to the form

$$R = \begin{pmatrix} 1 & 0 \\ 0 & R_{2\times 2} \end{pmatrix}, \tag{22}$$

where $R_{2\times 2}$ is an orthogonal two-dimensional matrix that depends on one complex angle. For $j = 2, 3$ the matrix is analogous with the appropriate permutation of the heavy states. The model therefore reduces in this limit to a $3 + 2 + 1$, where one sterile state is essentially decoupled. When $m_1 \leq m_1^{\rm th}$, the latter might thermalize or not depending on the unknown parameters, while the other two states always thermalize, as in the minimal $3 + 2$ model already considered in Ref. [43].

In the next section we evaluate the implications for $N_{\rm eff}$ in both cases.

V. $N_{\rm EFF}$ IN THE $3 + 3$ MODEL

A. $m_1 \geq m_1^{\rm th}$

In this case, the three sterile states thermalize, each of them contributing with $\Delta N_{\rm eff}^{(j)}(T_{d_j}) \approx 1$ at their decoupling temperature, T_{d_j} (provided they are still relativistic). This contribution gets diluted later on, due to the change of $g_*(T)$ between T_{d_j} and the active neutrino decoupling, $T_{\rm BBN}$, when BBN starts. The dilution factor is relevant only for masses larger than $M_j \gtrsim 1$ keV [43].

If they are still relativistic at T_W, we can therefore estimate

$$\Delta N_{\rm eff}^{\rm BBN} = \sum_j \left(\frac{g_*(T_{\rm BBN})}{g_*(T_{d_j})}\right)^{4/3}, \tag{23}$$

where the sum runs over the three heavier states.

For $M_j \geq \mathcal{O}(100)$ MeV, the contribution to the energy density could be significantly suppressed with respect to the estimate Eq. (23), because either they decay sufficiently early before BBN and/or become nonrelativistic at T_{d_j} and therefore get Boltzmann suppressed. Additional constraints will be at work in some regions of parameter space even for those larger masses, but they are likely to depend on the unknown mixing parameters, so we concentrate on the case where at least one of the three heavy neutrinos has a mass below this limit.

We consider in turn the following possibilities.

(i) For all j, $M_j \lesssim 100$ MeV

After recent measurements, the BBN constraints mentioned in the introduction give $\Delta N_{\rm eff}^{\rm BBN} \leq 0.9$ at 2σ. From the results of [43] in the $3 + 2$ model, we estimate that $M_j \lesssim 10$–100 keV would be excluded from BBN bounds in this case. For larger masses, dilution is sufficiently strong to avoid BBN bounds, but the contribution to the energy density after BBN is anyway too large. When they become nonrelativistic, their contribution to the energy density can be estimated to be [59]

$$\Omega_{s_j} h^2 = 10^{-2} M_j({\rm eV}) \Delta N_{\rm eff}^{(j){\rm BBN}}, \tag{24}$$

where $\Delta N_{\rm eff}^{(j){\rm BBN}}$ is estimated from the ratio of number densities of the jth state and one standard neutrino at BBN. If they do not decay before recombination, Planck constraint on $\Omega_m h^2$ would completely exclude such high masses. On the other hand, if they decay, they transfer this energy density to radiation. The case in which they decay at BBN or before (only for masses above 10 MeV or so) has been considered in detail in [60,61] and essentially BBN constraints, combined with direct search constraints [18,19,62], exclude the range 10–140 MeV. If they decay after BBN, they transfer the energy density mostly to the already decoupled light neutrinos, a contribution that can be parametrized in terms of $\Delta N_{\rm eff}$ which is enhanced with

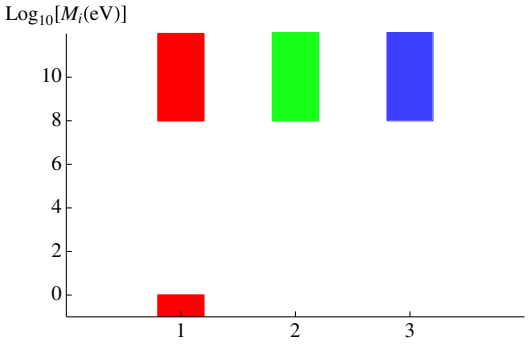

FIG. 4 (color online). Allowed spectra of the heavy states M_i for $m_1 \geq m_1^{\rm th}$.

respect to that at BBN, Eq. (23), by a factor $\propto \frac{M_j}{T_{\rm dec}^{(j)}}$, where $T_{\rm dec}^{(j)}$ is the decay temperature of the jth species. This temperature can be estimated by the relation $H(T_{\rm dec}^{(j)}) = \tau_{s_j}^{-1}$, where

$$\tau_{s_j}^{-1} \simeq \frac{G_F^2 M_j^5}{192\pi^3} \sum_\alpha |(U_{as})_{\alpha j}|^2 \tag{25}$$

(for M_j below any lepton or hadron threshold). We are not aware of a self-consistent global cosmological analysis of such a scenario. Assuming that CMB constraints on extra radiation $\Delta N_{\rm eff}$ roughly apply to it, the large mass region, still allowed by BBN due to dilution, is anyway excluded by CMB measurements, because the ratio $M_j/T_{\rm dec}^{(j)}$ is very large. Recent analyses on dark radiation from decays can be found in [63–65].

(i) $M_1, M_2 \lesssim 100$ MeV $\ll M_3$

In this case, the results of the $3+2$ model apply directly and the conclusion is the same as before: BBN constraints force the masses to be large to enhance dilution, but such heavy states contribute too much energy density either in the form of matter or extra radiation.

(i) $M_1 \lesssim 100$ MeV $\ll M_2, M_3$

In this case, any value of M_1 could be barely compatible with BBN constraints, since $\Delta N_{\rm eff} \leq 1$. CMB constraints would however force the state to be very light, sub-eV, which implies $\Delta N_{\rm eff} \simeq 1$ and therefore some tension with BBN. On the other hand, constraints from oscillations are important in this range [4].

The allowed ranges of the M_j are qualitatively depicted in Fig. 4.

B. $m_1 \leq m_1^{\rm th}$

If the lightest neutrino mass is below $m_1^{\rm th}$, one of the states might not thermalize [66], we will take it to be the lightest sterile state although it could be any other. As shown above, this can happen in a region of parameter space with effective decoupling of the first state. A more precise estimate of $\Delta N_{\rm eff}^{\rm BBN}$ is given from solving the Boltzmann equations reviewed in Appendix A. We consider two cases:

(i) The unknown mixing parameters (i.e. the Casas-Ibarra parameter of the matrix R and the CP phases) are fixed by minimizing $f_{s_1}(T_{\rm max})$ and $f_{s_2}(T_{\rm max})$ as a function of m_1 and M_1, and for fixed values of M_2 and M_3.

(ii) The unknown parameters correspond to those that satisfy $f_{s_1}(T_{\rm max}) = 10{\rm Min}[f_{s_1}(T_{\rm max})]$ (i.e. the lightest sterile state does not thermalize, but the thermalization rate is ten times larger than its minimum) and minimize $f_{s_2}(T_{\rm max})$.

In Fig. 5 we show the contribution $\sum_{j=2,3} \Delta N_{\rm eff}^{(j)\rm BBN}$ for the NH (IH) cases. It is approximately the same as that found in the $3+2$ model [67] and independent of m_1 and M_1. On the other hand, the contribution $\Delta N_{\rm eff}^{(1)\rm BBN}$ depends strongly on m_1 and it is roughly ten times larger in the second case than in the first, as expected from Fig. 2. Assuming that the contribution of the nonthermal state is negligible, the model is still strongly disfavored if $M_2, M_3 \lesssim 100$ MeV, as explained above. The case with $M_2 \lesssim 100$ MeV $\ll M_3$ could be barely compatible with BBN and CMB constraints if $M_2 \lesssim$ eV. The allowed ranges of the M_j are qualitatively depicted in Fig. 6.

When M_2, M_3 are above 100 MeV, the only contribution to $\Delta N_{\rm eff}$ would be that of the lighter state. In Fig. 7 we show the contour levels for $\Delta N_{\rm eff}^{(1)\rm BBN}$ as obtained from the Boltzmann equations from the ratio of energy (number) densities of the $j=1$ sterile state and one standard neutrino at BBN [see Eqs. (A18) and (A19) in the appendix], versus m_1 and M_1, assuming no lepton asymmetries. In the case of degenerate heavier states significant lepton asymmetries

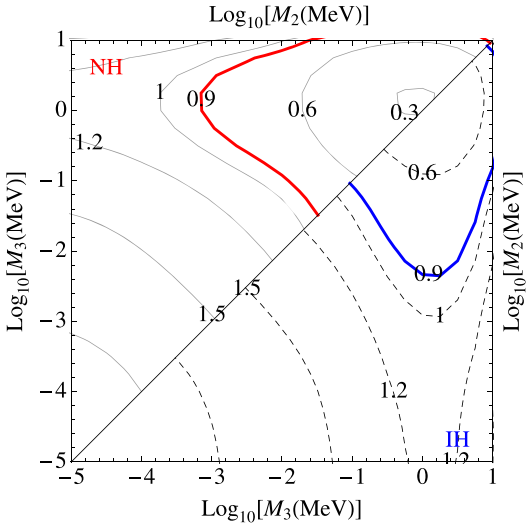

FIG. 5 (color online). $\sum_{j=2,3} \Delta N_{\rm eff}^{(j)\rm BBN}$ for $m_1 \leq m_1^{\rm th}$, as a function of M_2 and M_3. The thick lines correspond to present BBN bounds.

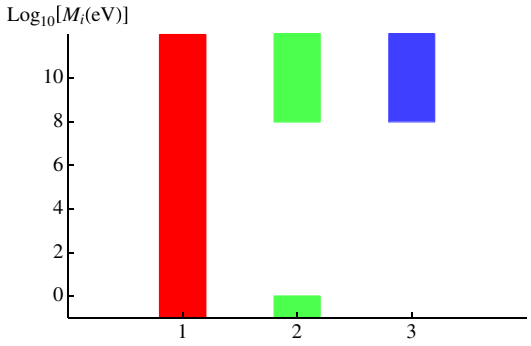

FIG. 6 (color online). Allowed spectra of the heavy states M_i for $m_1 \leq m_1^{\rm th}$. The unconstrained mass could be any $i = 1, 2, 3$.

can be produced [68], which can modify significantly the production of the lighter state [68–70]. We will explore systematically that region of parameter space in a future work, but here we consider only the nondegenerate case where asymmetries are not expected to be of relevance.

In the figure we also included the line, enclosing the shaded region, corresponding to $\Omega_{s_1} h^2 = \Omega_m h^2 = 0.1199$, which is the result from the PLANCK collaboration in a ΛCDM model [24]. In the shaded region the sterile state contributes too much to the matter density and therefore is excluded. Further constraints from Lyman-α and x rays can be found in the recent review [16], and based on the Pauli

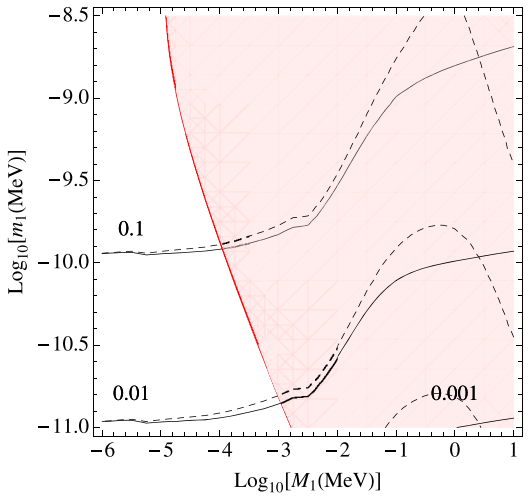

FIG. 7 (color online). Contour plots for $\Delta N_{\rm eff}^{(1)\rm BBN} = 10^{-1}, 10^{-2}, 10^{-3}$ defined by the ratio of the energy density of the $j = 1$ sterile state and one standard neutrino as a function of m_1 and M_1. The solid (dashed) lines correspond to the contours of the ratio of sterile to active number (energy) densities. The shaded region corresponds to $\Omega_{s_1} h^2 \geq 0.1199$ and the dashed straight line is roughly the one corresponding to decay at recombination. The heavier neutrino masses have been fixed to $M_{2,3} = 1$ GeV, 10 GeV and the unconstrained parameters have been chosen to minimize $f_1(T_{\rm max})$ and $f_2(T_{\rm max})$. The light neutrino spectrum has been assumed to be normal (NH).

exclusion principle and Liouville's theorem in [71]. The almost vertical dashed line corresponds to decay roughly at recombination, which means that in the region to the right of this curve, the $j = 1$ state decays before, and contributes as extra radiation, roughly $\Delta N_{\rm eff}^{(1)\rm BBN} \times \frac{M_1}{T_{\rm dec}^{(1)}}$, which is much larger than one in the whole plane and is therefore excluded.

We note that for M_1 in the keV range, where it could be a warm dark matter candidate, the allowed region requires $m_1 \lesssim \mathcal{O}(10^{-5}$ eV), which is in good agreement with the bound derived in [15].

We have also studied the case where it is the $j = 2$ state that does not reach thermalization, with $M_1 = 0.5$ eV, $M_3 = 1$ GeV. The contribution of the $j = 2$ state, $\Delta N_{\rm eff}^{(2)}$ is essentially the same as that shown in Fig. 7. In this case the contribution of the lighter state is $\Delta N_{\rm eff}^{(1)\rm BBN} \simeq 1$, because dilution is very small for such light masses.

All the results we have shown are for a normal hierarchy of the light neutrino spectrum, but the results for IH are almost identical if we exchange $m_1 \to m_3$.

VI. IMPACT ON NEUTRINOLESS DOUBLE BETA DECAY

In the $3 + 3$ seesaw models studied here the light and heavy neutrinos are Majorana particles and, therefore, they can contribute to lepton number violating processes such as the neutrinoless double beta ($\beta\beta0\nu$) decay. The spectra of Fig. 6, allowed if $m_1 \leq m_1^{\rm th}$, will have important implications for this observable for two reasons: (1) the contribution of the light neutrinos to the amplitude of this process, $m_{\beta\beta}$, depends strongly on the lightest neutrino mass and (2) sterile states with masses below 100 MeV could also contribute significantly to this amplitude. The contribution of states with masses well above 100 MeV would be generically subleading [72,73].

If the three heavy states are well above 100 MeV, $m_{\beta\beta}$ is the standard result for the three light Majorana neutrinos. It is shown by the well-known colored bands on Fig. 8 as a function of the lightest neutrino mass, for the two neutrino hierarchies. If one of the states, for example $j = 1$, is in the range [1 eV, 100 MeV], we have seen that it cannot have the thermal abundance which requires an upper bound on the lightest neutrino, $m_1 \leq 10^{-3}$ eV, shown by the vertical dashed grey line. In this case, the sterile state can give a relevant contribution to the amplitude of the process and $m_{\beta\beta}$ reads

$$m_{\beta\beta} = e^{i\alpha} m_1 c_{12}^2 c_{13}^2 + e^{i\beta} m_2 c_{13}^2 s_{12}^2 + m_3 s_{13}^2 + (U_{as})_{e4}^2 M_1. \tag{26}$$

The maximum value of the extra term (with the constraints that the corresponding sterile state does not thermalize, i.e. $f_{s_1}(T_{\rm max}) \leq 1$, and it does not contribute too much to the

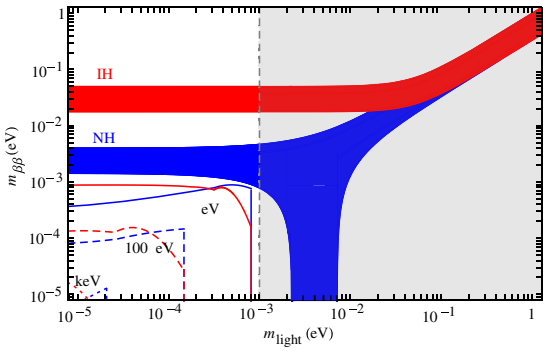

FIG. 8 (color online). $m_{\beta\beta}$ as a function of the lightest neutrino mass: contribution from the active neutrinos (red and blue regions) and the maximum contribution of the lightest sterile neutrino, for $M_1 = 1$ eV (solid), 100 eV (dashed), 1 keV (dotted), for NH (blue) and IH (red) restricting $\Omega_{s_1}h^2 \leq 0.12$ and $f_{s_1}(T_{\rm max}) \leq 1$, for $M_{2,3} \gg 100$ MeV, as a function of the lightest neutrino mass. The shaded region is ruled out for $M_1 \in [1\text{ eV}–100\text{ MeV}]$ by the thermalization bound on the lightest neutrino mass, $m_1 \leq 10^{-3}$ eV.

energy density, $\Omega_{s_1}h^2 \leq 0.12$) is shown by the lines for $M_1 = 1$ eV, 100 eV and 1 keV, as a function of the lightest neutrino mass, $m_{\rm light} = m_1(m_3)$ for NH (IH).

Figure 8 shows that the quasidegenerate light neutrino spectrum is ruled out for $M_1 \in [1\text{ eV}–100\text{ MeV}]$ and $M_{2,3} \gg 100$ MeV. The region of the parameter space in which a cancellation can occur in the active neutrino contribution is also excluded. It is remarkable that the thermalization bound on $m_{\rm light}$ is around two orders of magnitude stronger than the present constraint on the absolute neutrino mass scale from Planck [24]. On the other hand, we can also conclude that the contribution of the lightest sterile neutrino to the process is subleading and well below the (optimistic) sensitivity of the next-to-next generation of $\beta\beta0\nu$ decay experiments, 10^{-2} eV. This is so, independently of the light neutrino hierarchy.

Finally, there is a still plausible possibility of having a significant contribution to the $\beta\beta0\nu$ decay from a sub-eV thermal sterile neutrino which can satisfy the cosmological bounds. For example, if $f_{s_1}(T_{\rm max}) \geq 1$ with $M_1 \lesssim 1$ eV and $M_{2,3} \gg 100$ MeV, the lightest sterile neutrino could give a significant contribution to the process. However, for such a low M_1 scale, the constraints from neutrino oscillations are expected to be very relevant. Therefore, this case deserves a more careful analysis which should also face the possibility of explaining the neutrino anomalies. This would also apply to the scenario where $M_1 \leq 1$ eV, $1\text{ eV} \leq M_2 \leq 100$ MeV and $M_3 \gg 100$ MeV, if $m_1 \leq m_1^{\rm th}$. The two lighter states would contribute to $\beta\beta0\nu$. The contribution of M_2 would be similar to that of M_1 in Fig. 8, while that of M_1 would depend significantly on oscillation constraints.

VII. CONCLUSIONS

We have studied the thermalization of the heavy sterile neutrinos in the standard type I seesaw model with three extra singlets and a low scale, $\text{eV} \leq M_j \leq 100$ MeV. The production of the states in the early Universe occurs via nonresonant mixing (in the absence of large primordial asymmetries) and we have found that, independently of the unknown mixing parameters in the model, full thermalization is always reached for the three states if the lightest neutrino mass is above $\mathcal{O}(10^{-3}$ eV). Since they decouple early, while they are still relativistic, these states either violate BBN constraints on $\Delta N_{\rm eff}$ and/or contribute too much energy density to the Universe at later times, either in the form of cold dark matter (if they decay late enough) or in the form of dark radiation (if they decay earlier). Majorana masses would all need to be heavier than $\mathcal{O}(100$ MeV) to avoid cosmology constraints, or alternatively one of them could remain very light sub-eV, resulting in a milder tension with cosmology.

In contrast, if the lightest neutrino mass is below $\mathcal{O}(10^{-3}$ eV), one and only one of the sterile states might never thermalize, depending on the unknown parameters of the model, and therefore its mass is unconstrained. The other two states always thermalize and therefore their masses should be above $\mathcal{O}(100$ MeV) to avoid cosmological constraints. The scenario often referred to as the νMSM [15] falls in this category, where the nonthermalized state in the keV region could be a candidate for warm dark matter [8,11] and the heavier states could generate the baryon asymmetry [14]. In fact, a more stringent upper bound on m_1 had been previously derived from the requirement that $M_1 \sim$ keV and could be a warm dark matter candidate [15]. Alternatively, the tension with cosmology could also be minimized in this case if one of the two thermalized states is very light sub-eV and the other remains heavy.

Although the possibility of having one of the species in the sub-eV range could provide an interesting scenario to maybe explain the neutrino oscillation anomalies, the tension between cosmology and neutrino oscillation experiments is likely to be significant.

Finally, we have also studied the impact of the cosmological bounds extracted in this work on the $\beta\beta0\nu$ decay phenomenology. We have found that if one of the sterile neutrinos does not thermalize, the quasidegenerate light neutrino spectrum would be ruled out. The region of the parameter space in which a cancellation can take place in the active neutrino contribution is also excluded in this scenario. In addition, we have also shown that the contributions of sterile states with $M_1 \in [1\text{ eV}–100\text{ MeV}]$ are subleading and well beyond the sensitivity of the next-to-next generation of $\beta\beta0\nu$ decay experiments. However, a sub-eV thermal sterile state could give a contribution, in this scenario, within reach of the next-to-next generation of

$\beta\beta0\nu$ decay experiments, the constraints from neutrino oscillations playing a very important role.

ACKNOWLEDGMENTS

We thank M. Laine for providing us with data files with the numerical results of Ref. [56] in an easy-to-use format. We also thank A. Donini, E. Fernández-Martínez, O. Mena, S. Petcov and A.Vincent for useful discussions. This work was partially supported by Grants FPA2011-29678, PROMETEO/2009/116, CUP (CSD2008-00037), ITN INVISIBLES (Marie Curie Actions, PITN-GA-2011-289442) and the INFN program on "Astroparticle Physics." J. López-Pavón acknowledges NORDITA for the hospitality during the "News in Neutrino Physics" workshop, where part of this work was done. M. Kekic thanks the IFT-UAM/CSIC institute for hospitality while this work was done.

APPENDIX:

In the density matrix formalism [54], the kinetic equations have the usual form:

$$\dot{\rho} = -i[H,\rho] - \frac{1}{2}\{\Gamma, \rho - \rho_{\rm eq} I_A\}, \tag{A1}$$

where ρ is the 6×6 density matrix, H is the Hamiltonian describing the propagation of relativistic neutrinos in the plasma, Γ is the collision term that we take from Refs. [56,57] and $\rho_{\rm eq}$ is the active neutrino thermal density, i.e. the Fermi-Dirac distribution $\rho_{\rm eq} = \frac{1}{e^{E/T}+1}$, in the absence of a chemical potential. I_A is the projector on the active sector. The trace of the density matrix corresponds to the number density of neutrinos.

Rewriting Eq. (A1) in the form of active-sterile block matrices we get the following set of equations:

$$\dot{\rho}_A = -i(H_A\rho_A - \rho_A H_A + H_{AS}\rho_{AS}^\dagger - \rho_{AS}H_{AS}^\dagger) - \frac{1}{2}\{\Gamma_A, \rho_A - \rho_{\rm eq} I_A\}, \tag{A2}$$

$$\dot{\rho}_{AS} = -i(H_A\rho_{AS} - \rho_A H_{AS} + H_{AS}\rho_S - \rho_{AS}H_S) - \frac{1}{2}\Gamma_A\rho_{AS}, \tag{A3}$$

$$\dot{\rho}_S = -i(H_{AS}^\dagger\rho_{AS} - \rho_{AS}^\dagger H_{AS} + H_S\rho_S - \rho_S H_S). \tag{A4}$$

Assuming that $\Gamma_A \gg$ Hubble rate, we can approximate

$$\dot{\rho}_A = \dot{\rho}_{AS} = 0. \tag{A5}$$

This is the so-called "static approximation" [33,69,70].

The first equation implies $\rho_A = \rho_{\rm eq} I_A$, while the second equality implies

$$(\rho_{AS})_{ai} = (-(H_A - \tilde{H}_i I_A) + i\Gamma_A/2)^{-1}_{aa'}(H_{AS})_{a'j}((\rho_S)_{ji} - \rho_{\rm eq}\delta_{ji}), \tag{A6}$$

where we have made the approximation that $(H_S)_{ij} = \tilde{H}_i\delta_{ij}$, which is very good in the seesaw limit. Similarly we find

$$(\rho_{AS}^\dagger)_{ia} = ((\rho_S)_{ij} - \rho_{\rm eq}\delta_{ij})(H_{AS}^\dagger)_{ja'}(-(H_A - \tilde{H}_i I_A) - i\Gamma_A/2)^{-1}_{a'a}. \tag{A7}$$

Defining $\tilde{\rho}_S \equiv \rho_S - \rho_{\rm eq} I_S$, and after substituting ρ_{AS} and $\rho_{AS}^\dagger$ in Eq. (A4), we get the following equation:

$$\begin{aligned}(\dot{\rho}_S)_{ij} = &-i(\tilde{H}_i - \tilde{H}_j)(\rho_S)_{ij} \\ &- i(H_{AS}^\dagger)_{a'i}(-(H_A - \tilde{H}_j I_A) \\ &+ i\Gamma_A/2)^{-1}_{a'a}(H_{AS})_{ak}\tilde{\rho}_{kj} \\ &+ i\tilde{\rho}_{ik}(H_{AS}^\dagger)_{a'k}(-(H_A - \tilde{H}_i I_A) \\ &- i\Gamma_A/2)^{-1}_{a'a}(H_{AS})_{aj}.\end{aligned} \tag{A8}$$

It is clear that the equilibrium distribution for the sterile components is $\tilde{\rho}_{ii} = 0$ or $\rho_{ii} = \rho_{eq}\delta_{ii}$.

At this point it is necessary to solve the 3×3 system of differential equations (A8), but we can further simplify the problem if we assume that the dynamics of the different sterile components decouple from each other, which is the case provided their masses are sufficiently different. Since H_{AS} depends on temperature, if the sterile splittings are significantly different from each other, we will generically have that H_{AS} will be very suppressed unless the temperature-dependent effective mass is similar to one of the mass splittings. Let us suppose that this is the case. At high T all active-sterile mixings are very suppressed, until one splitting that associated to the sterile state s is reached; at this point only $(H_{AS})_{as}$ is non-negligible. Then only $(\rho_S)_{ss}$ changes significantly and can be described by

$$\begin{aligned}\dot{\rho}_{ss} &= -i\left(H_{AS}^\dagger\left\{\frac{1}{-(H_A - \tilde{H}_s) + i\Gamma_A/2} - \frac{1}{-(H_A - \tilde{H}_s) - i\Gamma_A/2}\right\}H_{AS}\right)_{ss}\tilde{\rho}_{ss} \\ &= -\left(H_{AS}^\dagger\left\{\frac{\Gamma_A}{(H_A - \tilde{H}_s)^2 + \Gamma_A^2/4}\right\}H_{AS}\right)_{ss}\tilde{\rho}_{ss},\end{aligned} \tag{A9}$$

where in the last step we have assumed that H_A, Γ_A commute, which again is a good approximation in the seesaw limit. This equation justifies Eq. (6), since the source term on the right of Eq. (A9) is the same as Γ_s in Eq. (6) if we neglect the term $\sim\Gamma_A^2$ in the denominator. We have checked that the result of solving the three coupled

equations or the three independent ones gives very similar results and the latter is obviously much faster.

Now we have to consider the evolution in an expanding universe, where the variation of the scale factor $a(t)$ depends on the Hubble expansion rate, which, in a radiation-dominated universe at temperature T, is given by

$$H(T) = \sqrt{\frac{8\pi G_N}{3}\left(\frac{\pi^2}{30}g_*(T)T^4 + \epsilon_s(T)\right)}, \tag{A10}$$

where g_* counts the relativistic degrees of freedom and we have included the contribution to the energy density of the sterile states, ϵ_s, which must be computed integrating the trace of the density matrix, ρ_S. As in Ref. [33] we introduce new variables:

$$x = \frac{a(t)}{a_{\rm BBN}}, \qquad y = x\frac{p}{T_{\rm BBN}}, \tag{A11}$$

where $a(t)$ is the cosmic scale factor, $T_{\rm BBN} \simeq 1$ MeV is the temperature of active neutrino decoupling and $a_{\rm BBN}$ the scale factor at this point. On the other hand, entropy conservation implies $g_{S*}(T)T^3a(t)^3 = \text{constant}$ (here g_{S*} refers to the relativistic degrees of freedom in equilibrium; it differs from g_* in the Hubble expansion only after light neutrino decoupling). This relation implies

$$x = \frac{T_{\rm BBN}}{T}\left(\frac{g_{S*}(T_{\rm BBN})}{g_{S*}(T)}\right)^{1/3}. \tag{A12}$$

We neglect the contribution of the sterile states to g_{S*}, because they decouple very early and therefore they give a small contribution.

The time derivative acting on any phase space distribution can be written as

$$\frac{d}{dt}f(t,p) = (\partial_t - Hp\partial_p)f(t,p) = Hx\partial_x f(x,y). \tag{A13}$$

Applied to Eq. (A1) this leads to

$$Hx\frac{\partial}{\partial x}\rho(x,y)\big|_y = -i[\hat{H},\rho(x,y)] - \frac{1}{2}\{\Gamma,\rho(x,y) - \rho_{\rm eq}(x,y)I_A\}, \tag{A14}$$

where

$$\rho_{\rm eq}(x,y) = \frac{1}{\exp\left[y(g_{S*}(T(x))/g_{S*}(T_{\rm BBN}))^{1/3}\right] + 1}, \tag{A15}$$

and for Eq. (A9) similarly

$$Hx\frac{\partial}{\partial x}\rho_{ss}(x,y)\big|_y = -\left(H_{AS}^\dagger\left\{\frac{\Gamma_A}{(H_A - \tilde{H}_s)^2 + \Gamma_A^2/4}\right\}H_{AS}\right)_{ss}\tilde{\rho}_{ss}(x,y). \tag{A16}$$

The equations are evolved from an initial condition at $x_i \to 0$, $\rho_{ss} = 0$, until active neutrino decoupling, $x_f = 1$ for fixed y. We define the effective number of additional neutrino species by

$$\Delta N_{\rm eff} = \frac{\epsilon_s}{\epsilon_\nu^0}, \tag{A17}$$

where ϵ_ν^0 is the energy density of one SM massless neutrino. For each additional neutrino we compute the contribution to $\Delta N_{\rm eff}$ from the solution of $\rho_{s_j s_j}(x_f,y)$ as

$$\Delta N_{\rm eff}^{(j)\rm BBN}|_{\rm energy} = \frac{\int {\rm d}y y^2 E(y)\rho_{s_j s_j}(x_f,y)}{\int {\rm d}y y^2 p(y)\rho_{\rm eq}(x_f,y)}, \tag{A18}$$

where $p(y) = \frac{y}{x_f}T_{\rm BBN}$ and $E(y) = \sqrt{p(y)^2 + M_j^2}$.

We can also define the ratio of number densities instead, which is more appropriate when they are not relativistic,

$$\Delta N_{\rm eff}^{(j)\rm BBN}|_{\rm number} = \frac{\int {\rm d}y y^2 \rho_{s_j s_j}(x_f,y)}{\int {\rm d}y y^2 \rho_{\rm eq}(x_f,y)}. \tag{A19}$$

The two correspond to the solid/dashed curves depicted in Fig. 7.

[1] P. Minkowski, Phys. Lett. **67B**, 421 (1977); M. Gell-Mann, P. Ramond, and R. Slansky, in *Supergravity*, edited by P. van Nieuwenhuizen and D. Freedman (North-Holland, Amsterdam, 1979), p. 315; T. Yanagida in *Proceedings of the Workshop on the Unified Theory and the Baryon Number in the Universe*, edited by O. Sawada and A. Sugamoto (KEK Report No. 79-18, Tsukuba, 1979), p. 95; R. N. Mohapatra and G. Senjanovic, Phys. Rev. Lett. **44**, 912 (1980).

[2] The range 10^{-10}–1 eV can be excluded from oscillation data [3,4], while a scale above 10^{15} GeV would require nonperturbative Yukawa couplings.

[3] A. de Gouvea, Phys. Rev. D **72**, 033005 (2005); A. de Gouvea, J. Jenkins, and N. Vasudevan, Phys. Rev. D **75**, 013003 (2007).

[4] A. Donini, P. Hernández, J. López-Pavón, and M. Maltoni, J. High Energy Phys. 07 (2011) 105.

[5] A. Aguilar-Arevalo *et al.* (LSND Collaboration), Phys. Rev. D **64**, 112007 (2001).

[6] A. A. Aguilar-Arevalo *et al.* (MiniBooNE Collaboration), Phys. Rev. Lett. **110**, 161801 (2013).

[7] G. Mention, M. Fechner, Th. Lasserre, Th. A. Mueller, D. Lhuillier, M. Cribier, and A. Letourneau, Phys. Rev. D **83**, 073006 (2011); P. Huber, Phys. Rev. C **84**, 024617 (2011); **85**, 029901 (2012).

[8] S. Dodelson and L. M. Widrow, Phys. Rev. Lett. **72**, 17 (1994).

[9] X.-D. Shi and G. M. Fuller, Phys. Rev. Lett. **82**, 2832 (1999).

[10] K. Abazajian, G. M. Fuller, and M. Patel, Phys. Rev. D **64**, 023501 (2001).

[11] T. Asaka, S. Blanchet, and M. Shaposhnikov, Phys. Lett. B **631**, 151 (2005).

[12] E. Bulbul, M. Markevitch, A. Foster, R. K. Smith, M. Loewenstein, and S. W. Randall, Astrophys. J. **789**, 13 (2014).

[13] A. Boyarsky, O. Ruchayskiy, D. Iakubovskyi, and J. Franse, arXiv:1402.4119.

[14] E. K. Akhmedov, V. A. Rubakov, and A. Y. Smirnov, Phys. Rev. Lett. **81**, 1359 (1998).

[15] T. Asaka and M. Shaposhnikov, Phys. Lett. B **620**, 17 (2005).

[16] L. Canetti, M. Drewes, T. Frossard, and M. Shaposhnikov, Phys. Rev. D **87**, 093006 (2013), and references therein.

[17] S. Antusch, C. Biggio, E. Fernandez-Martinez, M. B. Gavela, and J. Lopez-Pavon, J. High Energy Phys. 10 (2006) 084; A. Abada, C. Biggio, F. Bonnet, M. B. Gavela, and T. Hambye, J. High Energy Phys. 12 (2007) 061; S. Antusch, J. P. Baumann, and E. Fernandez-Martinez, Nucl. Phys. **B810**, 369 (2009); D. N. Dinh, A. Ibarra, E. Molinaro, and S. T. Petcov, J. High Energy Phys. 08 (2012) 125; 09 (2013) 023; R. Alonso, M. Dhen, M. B. Gavela, and T. Hambye, J. High Energy Phys. 01 (2013) 118; D. N. Dinh and S. T. Petcov, J. High Energy Phys. 09 (2013) 086.

[18] D. Gorbunov and M. Shaposhnikov, J. High Energy Phys. 10 (2007) 015.

[19] A. Atre, T. Han, S. Pascoli, and B. Zhang, J. High Energy Phys. 05 (2009) 030.

[20] R. Foot, M. J. Thomson, and R. R. Volkas, Phys. Rev. D **53**, R5349 (1996).

[21] S. Hannestad, R. S. Hansen, and T. Tram, Phys. Rev. Lett. **112**, 031802 (2014).

[22] B. Dasgupta and J. Kopp, Phys. Rev. Lett. **112**, 031803 (2014).

[23] R. Cooke, M. Pettini, R. A. Jorgenson, M. T. Murphy, and C. C. Steidel, arXiv:1308.3240 [Astrophys. J. (to be published)].

[24] P. A. R. Ade *et al.* (Planck Collaboration), Astron. Astrophys., doi:10.1051/0004-6361/201321591, 2014.

[25] G. Hinshaw *et al.* (WMAP Collaboration), Astrophys. J. Suppl. Ser. **208**, 19 (2013).

[26] Z. Hou *et al.*, Astrophys. J. **782**, 74 (2014).

[27] J. L. Sievers *et al.*, J. Cosmol. Astropart. Phys. 10 (2013) 060.

[28] P. A. R. Ade *et al.* (BICEP2 Collaboration), Phys. Rev. Lett. **112**, 241101 (2014).

[29] P. A. R. Ade *et al.* (BICEP2 Collaboration), Astrophys. J. **792**, 62 (2014).

[30] E. Giusarma, E. Di Valentino, M. Lattanzi, A. Melchiorri, and O. Mena, Phys. Rev. D **90**, 043507 (2014).

[31] M. Archidiacono, N. Fornengo, S. Gariazzo, C. Giunti, S. Hannestad, and M. Laveder, J. Cosmol. Astropart. Phys. 06 (2014) 031.

[32] J. Bergström, M. C. Gonzalez-Garcia, V. Niro, and J. Salvado, arXiv:1407.3806.

[33] A. D. Dolgov and F. L. Villante, Nucl. Phys. **B679**, 261 (2004).

[34] M. Cirelli, G. Marandella, A. Strumia, and F. Vissani, Nucl. Phys. **B708**, 215 (2005).

[35] A. Melchiorri, O. Mena, S. Palomares-Ruiz, S. Pascoli, A. Slosar, and M. Sorel, J. Cosmol. Astropart. Phys. 01 (2009) 036.

[36] S. Hannestad, I. Tamborra, and T. Tram, J. Cosmol. Astropart. Phys. 07 (2012) 025.

[37] E. Kuflik, S. D. McDermott, and K. M. Zurek, Phys. Rev. D **86**, 033015 (2012).

[38] A. Mirizzi, N. Saviano, G. Miele, and P. D. Serpico, Phys. Rev. D **86**, 053009 (2012).

[39] T. D. Jacques, L. M. Krauss, and C. Lunardini, Phys. Rev. D **87**, 083515 (2013).

[40] N. Saviano, A. Mirizzi, O. Pisanti, P. Serpico, G. Mangano, and G. Miele, Phys. Rev. D **87**, 073006 (2013).

[41] M. Archidiacono, N. Fornengo, C. Giunti, S. Hannestad, and A. Melchiorri, Phys. Rev. D **87**, 125034 (2013).

[42] A. Mirizzi, G. Mangano, N. Saviano, E. Borriello, C. Giunti, G. Miele, and O. Pisanti, Phys. Lett. B **726**, 8 (2013).

[43] P. Hernandez, M. Kekic, and J. Lopez-Pavon, Phys. Rev. D **89**, 073009 (2014).

[44] M. Shaposhnikov, J. High Energy Phys. 08 (2008) 008.

[45] J. A. Casas and A. Ibarra, Nucl. Phys. **B618**, 171 (2001).

[46] A. Donini, P. Hernández, J. López-Pavón, M. Maltoni, and T. Schwetz, J. High Energy Phys. 07 (2012) 161.

[47] M. Blennow and E. Fernandez-Martinez, Phys. Lett. B **704**, 223 (2011).

[48] There is an upper bound for the lightest neutrino mass but no lower bound exists at present.

[49] R. Barbieri and A. Dolgov, Phys. Lett. B **237**, 440 (1990); Nucl. Phys. **B349**, 743 (1991); K. Kainulainen, Phys. Lett. B **244**, 191 (1990).

[50] D. Notzold and G. Raffelt, Nucl. Phys. **B307**, 924 (1988).

[51] L. Stodolsky, Phys. Rev. D **36**, 2273 (1987); G. Raffelt, G. Sigl, and L. Stodolsky, Phys. Rev. Lett. **70**, 2363 (1993); M. J. Thomson, Phys. Rev. A **45**, 2243 (1992).

[52] K. Enqvist, K. Kainulainen, and M. Thomson, Nucl. Phys. **B373**, 498 (1992); B. H. J. McKellar and M. J. Thomson, Phys. Rev. D **49**, 2710 (1994).

[53] G. Sigl and G. Raffelt, Nucl. Phys. **B406**, 423 (1993).

[54] A. D. Dolgov, Phys. Rep. **370**, 333 (2002).
[55] K. N. Abazajian and G. M. Fuller, Phys. Rev. D **66**, 023526 (2002); K. Abazajian, Phys. Rev. D **73**, 063506 (2006).
[56] T. Asaka, M. Laine, and M. Shaposhnikov, J. High Energy Phys. 01 (2007) 091.
[57] Data files for the imaginary part of the neutrino self-energy have been made available in http://www.laine.itp.unibe.ch/neutrino-rate/.
[58] We note that $T_{\max}$ depends on M_j, but to simplify notation we skip the index j in this quantity.
[59] E. W. Kolb and M. S. Turner, Front. Phys. **69**, 1 (1990).
[60] A. D. Dolgov, S. H. Hansen, G. Raffelt, and D. V. Semikoz, Nucl. Phys. **B580**, 331 (2000); , **B590**, 562 (2000).
[61] O. Ruchayskiy and A. Ivashko, J. Cosmol. Astropart. Phys. 10 (2012) 014.
[62] O. Ruchayskiy and A. Ivashko, J. High Energy Phys. 06 (2012) 100.
[63] M. C. Gonzalez-Garcia, V. Niro, and J. Salvado, J. High Energy Phys. 04 (2013) 052.
[64] J. Hasenkamp and J. Kersten, J. Cosmol. Astropart. Phys. 08 (2013) 024.
[65] J. Hasenkamp, arXiv:1405.6736.
[66] There are always ranges of parameters where it does thermalize and in this case the same conclusions apply as in the previous section.
[67] The small differences with respect to the results in [43] are due to the more precise scattering rates Γ_α used here.
[68] M. Laine and M. Shaposhnikov, J. Cosmol. Astropart. Phys. 06 (2008) 031.
[69] R. Foot and R. R. Volkas, Phys. Rev. D **55**, 5147 (1997).
[70] N. F. Bell, R. R. Volkas, and Y. Y. Y. Wong, Phys. Rev. D **59**, 113001 (1999).
[71] A. Boyarsky, O. Ruchayskiy, and D. Iakubovskyi, J. Cosmol. Astropart. Phys. 03 (2009) 005.
[72] M. Blennow, E. Fernandez-Martinez, J. Lopez-Pavon, and J. Menendez, J. High Energy Phys. 07 (2010) 096.
[73] J. Lopez-Pavon, S. Pascoli, and C.-f. Wong, Phys. Rev. D **87**, 093007 (2013).

JHEP

Published for SISSA by Springer

Received: August 31, 2015
Accepted: September 15, 2015
Published: October 9, 2015

Leptogenesis in GeV-scale seesaw models

P. Hernández,[a] **M. Kekic,**[a] **J. López-Pavón,**[b] **J. Racker**[a] **and N. Rius**[a]

[a] *Instituto de Física Corpuscular, Universidad de Valencia and CSIC, Edificio Institutos Investigación, Apt. 22085, Valencia, E-46071 Spain*

[b] *SISSA and INFN Sezione di Trieste, via Bonomea 265, Trieste, 34136 Italy*

E-mail: m.pilar.hernandez@uv.es, marija.kekic@ific.uv.es, jacobo.lopezpavon@sissa.it, racker@cab.cnea.gov.ar, nuria.rius@ific.uv.es

Abstract: We revisit the production of leptonic asymmetries in minimal extensions of the Standard Model that can explain neutrino masses, involving extra singlets with Majorana masses in the GeV scale. We study the quantum kinetic equations both analytically, via a perturbative expansion up to third order in the mixing angles, and numerically. The analytical solution allows us to identify the relevant CP invariants, and simplifies the exploration of the parameter space. We find that sizeable lepton asymmetries are compatible with non-degenerate neutrino masses and measurable active-sterile mixings.

Keywords: Beyond Standard Model, Cosmology of Theories beyond the SM, Neutrino Physics, CP violation

ArXiv ePrint: 1508.03676

Open Access, © The Authors.
Article funded by SCOAP[3].

doi:10.1007/JHEP10(2015)067

JHEP10(2015)067

Contents

JHEP10(2015)067

1 Introduction

One of the interesting potential implications of (Majorana) neutrino masses is the generation of a matter-antimatter asymmetry in the Universe. It has been demonstrated that the generation of sizeable leptonic asymmetries, leptogenesis, is generic in extensions of the Standard Model that can account for neutrino masses [1]. In particular two new ingredients are essential for this mechanism to work: the existence of new weakly interacting particles that are not in thermal equilibrium sometime before the electroweak phase transition and the existence of new sources of CP violation.

Leptogenesis from the out-of-equilibrium decay of heavy Majorana fermions that appear in type I seesaw models [1] has been extensively studied (for a comprehensive review see e.g. [2]). The simplest version requires however relatively large Majorana masses $> 10^8$ GeV [3, 4] (or $> 10^6$ if flavour effects are included [5]), which imply that this scenario

would be very difficult to test experimentally. It is possible to have sizeable asymmetries for smaller masses if a large degeneracy exists, through resonant leptogenesis [6].

On the other hand, for Majorana masses in the GeV range, when the neutrino Yukawa couplings are small, another mechanism might be at work. In particular, the non-equilibrium condition takes place not in the decay, but in the production of the heavy sterile neutrinos. The small Yukawa couplings imply that some of the species might never reach thermal equilibrium and a lepton asymmetry can be generated at production and seed the baryon asymmetry in the Universe. This mechanism was first proposed by Akhmedov, Rubakov and Smirnov (ARS) in their pioneering work [7] and pursued, with important refinements in refs. [8, 9]. For a recent review and further references see [10]. In most of these works, the case of just two extra sterile species is considered, which is also the limiting case of the so-called νMSM where there are three species, but one of them plays the role of warm dark matter (WDM) and is almost decoupled, having no impact in the generation of the lepton asymmetry. When the mechanism involves just two species, it has been found that the observed baryon asymmetry is only possible if the two states are highly degenerate in mass. This however was not the conclusion of the ARS paper.

The purpose of this paper is to explore systematically the parameter space in the case of three sterile species (which encompass the one with two neutrinos) as regards the baryon asymmetry, in particular we do not want to restrict the parameter space to have a WDM candidate. The model has many free parameters (only 5 out of the 18 parameters are fixed by the measured light neutrino masses and mixings) and the exploration of the full parameter space is challenging. Only with the help of approximate analytical solutions to the kinetic equations this task is feasible. The analytical solutions furthermore allows us to identify the relevant CP invariants and to reach regions of parameter space where the equations become stiff and very difficult to deal with numerically.

The paper is organised as follows. In section 2 we present the model, which is essentially a generic type I seesaw model, establish the notation and discuss on general grounds what are the CP reparametrization and flavour invariants we expect to find in computing any CP violating quantity such as any putative lepton asymmetry. In section 3 we present the kinetic equations that describe the production of sterile neutrinos and solve them analytically via a perturbative expansion in the mixing angles up to the third order. In section 4 we compare the analytical and numerical solutions for several choices of the parameters, and identify the region of parameter space where the analytical solution accurately describes the numerical one. In section 5 we use the analytical solutions and perform a Monte Carlo scan (using the software package MultiNest [11, 12]) to find regions of parameter space that can reproduce the observed baryon asymmetry, and that are compatible with the measured neutrino masses and mixings. In section 6 we conclude.

2 Minimal model of neutrino masses

We will concentrate on the arguably simplest model of neutrino masses that includes three right-handed singlets. The Lagrangian is given by:

$$\mathcal{L} = \mathcal{L}_{\rm SM} - \sum_{\alpha,i} \bar{L}^{\alpha} Y^{\alpha i} \tilde{\Phi} N_R^i - \sum_{i,j=1}^{3} \frac{1}{2} \bar{N}_R^{ic} M^{ij} N_R^j + \text{h.c.},$$

JHEP10(2015)067

where Y is a 3×3 complex matrix and M a diagonal real matrix. The spectrum of this theory has six massive Majorana neutrinos, and the mixing is described in terms of six angles and six CP phases generically. One convenient parametrization for the problem at hand is in terms of the eigenvalues of the yukawa and majorana mass matrices together with two unitary matrices, V and W. In the basis where the Majorana mass is diagonal, $M = \mathrm{Diag}(M_1, M_2, M_3)$, the neutrino Yukawa matrix is given by:

$$Y \equiv V^\dagger \mathrm{Diag}(y_1, y_2, y_3) W. \tag{2.1}$$

Without loss of generality, using rephasing invariance, we can reduce the unitary matrices to the form:[1]

$$\begin{aligned} W &= U(\theta_{12}, \theta_{13}, \theta_{23}, \delta)^\dagger \mathrm{Diag}(1, e^{i\alpha_1}, e^{i\alpha_2}), \\ V &= \mathrm{Diag}(1, e^{i\phi_1}, e^{i\phi_2}) U(\bar{\theta}_{12}, \bar{\theta}_{13}, \bar{\theta}_{23}, \bar{\delta}), \end{aligned} \tag{2.2}$$

where[2]

$$U(\theta_1, \theta_2, \theta_3, \delta) \equiv \begin{pmatrix} \cos\theta_1 & \sin\theta_1 & 0 \\ -\sin\theta_1 & \cos\theta_1 & 0 \\ 0 & 0 & 1 \end{pmatrix} \begin{pmatrix} \cos\theta_2 & 0 & \sin\theta_2 e^{-i\delta} \\ 0 & 1 & 0 \\ -\sin\theta_2 e^{i\delta} & 0 & \cos\theta_2 \end{pmatrix} \begin{pmatrix} 1 & 0 & 0 \\ 0 & \cos\theta_3 & \sin\theta_3 \\ 0 & -\sin\theta_3 & \cos\theta_3 \end{pmatrix}. \tag{2.3}$$

Obviously not all the parameters are free, since this model must reproduce the light neutrino masses, which approximately implies the seesaw relation:

$$m_\nu \simeq -\frac{v^2}{2} Y \frac{1}{M} Y^T, \tag{2.4}$$

where $v = 246\,\mathrm{GeV}$ is the vev of the Higgs. On the other hand, the known neutrino masses and mixings do not give us enough information to determine the Majorana spectrum, not even the absolute scale. Very strong constraints can be derived from neutrino oscillation experiments for masses below the eV range [13–16]. Cosmology can exclude a huge window below 100 MeV [17–22], except maybe for one species that could be lighter provided the lightest active neutrino mass is below $\lesssim 3 \times 10^{-3}$eV [20, 21]. The GeV range is interesting because an alternative mechanism for lepton asymmetry generation could be at work [7–9]. Majorana neutrinos in this range are heavy enough to safely decay before Big Bang Nucleosynthesis, while they are light enough that they might have not reached thermal equilibrium by the time of the electroweak phase transition (EWPT), behaving as reservoirs of a putative lepton asymmetry.

Our goal in this paper is to explore the full parameter space of this model allowed by neutrino masses, as regards leptogenesis. An essential condition will be that at least one of the sterile neutrinos does not reach thermal equilibrium before the EWPT. This can be ensured assuming a large hierarchy in the yukawas [7]:

$$y_3 \ll y_1, y_2. \tag{2.5}$$

[1] Although we use the same notation for the mixing angles and phases of W as those in the usual PMNS matrix, they should not be confused.

[2] Note the unconventional ordering of the 2×2 rotation matrices in U.

JHEP10(2015)067

It is mandatory, however, to have an accurate analytical description, since the unconstrained parameter space is huge. We will solve the quantum kinetic equations in a perturbative expansion in the mixings in the next section. Since the lepton asymmetry is necessarily a CP-odd observable, on general grounds we can derive what are the expectations in terms of weak-basis CP invariants.

2.1 CP invariants

In [23], weak basis (WB) invariants sensitive to the CP violating phases which appear in leptogenesis, within the type I seesaw model, were derived. All of them should vanish if CP is conserved, and conversely the non-vanishing of any of these invariants signals CP violation. They must be invariant under the basis transformations:

$$\begin{aligned} \ell_L &\to W_L \ell_L, \\ N_R &\to W_R N_R \ . \end{aligned} \tag{2.6}$$

Defining $h \equiv Y^\dagger Y$, and $H_M \equiv M^\dagger M$, a subset of the invariants can be written as:

$$I_1 \equiv \mathrm{ImTr}[h H_M M^* h^* M], \tag{2.7}$$

$$I_2 \equiv \mathrm{ImTr}[h H_M^2 M^* h^* M], \tag{2.8}$$

$$I_3 \equiv \mathrm{ImTr}[h H_M^2 M^* h^* M H_M]. \tag{2.9}$$

Since the I_i are WB invariants, we can evaluate them in any basis. In the WB where the sterile neutrino mass matrix M is real and diagonal, one obtains:

$$I_1 = M_1 M_2 \Delta M_{21}^2 \mathrm{Im}(h_{12}^2) + M_1 M_3 \Delta M_{31}^2 \mathrm{Im}(h_{13}^2) + M_2 M_3 \Delta M_{32}^2 \mathrm{Im}(h_{23}^2), \tag{2.10}$$

$$\begin{aligned} I_2 = {} & M_1 M_2 (M_2^4 - M_1^4) \mathrm{Im}(h_{12}^2) + M_1 M_3 (M_3^4 - M_1^4) \mathrm{Im}(h_{13}^2) \\ & + M_2 M_3 (M_3^4 - M_2^4) \mathrm{Im}(h_{23}^2), \end{aligned} \tag{2.11}$$

$$I_3 = M_1^3 M_2^3 \Delta M_{21}^2 \mathrm{Im}(h_{12}^2) + M_1^3 M_3^3 \Delta M_{31}^2 \mathrm{Im}(h_{13}^2) + M_2^3 M_3^3 \Delta M_{32}^2 \mathrm{Im}(h_{23}^2), \tag{2.12}$$

where $\Delta M_{ij}^2 \equiv M_i^2 - M_j^2$ and, using the parametrization of eq. (2.1)

$$\mathrm{Im}(h_{ij}^2) = \mathrm{Im}[(Y^\dagger Y)_{ij}^2] = \sum_{\alpha,\beta} y_\alpha^2 y_\beta^2 \, \mathrm{Im}[W_{\alpha i}^* W_{\beta i}^* W_{\alpha j} W_{\beta j}] \ . \tag{2.13}$$

It is explicit in the above expression that such unflavoured invariants depend only on the CP phases of the sterile neutrino sector, which are encoded in the unitary matrix W: one Dirac-type phase, δ and two Majorana-type phases α_1, α_2. Not surprisingly, these invariants are the relevant ones in unflavoured leptogenesis, i.e., in the conventional computation of the CP asymmetry generated by heavy Majorana neutrino decay neglecting flavour effects.

The combinations of W matrix elements which appear in $\mathrm{Im}(h_{ij}^2)$ can be expressed in terms of the rephasing invariants defined in [24] as follows:

$$\mathrm{Im}[W_{\alpha i}^* W_{\beta i}^* W_{\alpha j} W_{\beta j}] = \frac{\mathrm{Im}[W_{\alpha i} W_{\beta i}^* W_{\alpha j}^* W_{\beta j} (W_{\alpha j} W_{\alpha i}^*)^2]}{|W_{\alpha i} W_{\alpha j}|^2} \ . \tag{2.14}$$

JHEP10(2015)067

Notice that $J_W \equiv \pm \mathrm{Im}[W_{\alpha i} W^*_{\beta i} W^*_{\alpha j} W_{\beta j}]$ is the Jarlskog invariant for the matrix W, while the quantities $\mathrm{Im}[(W_{\alpha j} W^*_{\alpha i})^2]$ determine the Majorana phases, $\alpha_{1,2}$. When considering processes, such as heavy neutrino oscillations, where the Majorana nature does not play a role, only the Dirac phase δ will be relevant and therefore we expect to find just the Jarlskog invariant of the matrix W.

Since there are six independent CP-violating phases, it is possible to construct three more independent WB invariants, which would complete the description of CP violation in the leptonic sector. One simple choice are those invariants obtained from I_i under the change of the matrix h by $\bar{h} \equiv Y^\dagger h_\ell Y$, with $h_\ell = \lambda_\ell \lambda_\ell^\dagger$, being λ_ℓ the charged lepton Yukawa couplings, i.e.,

$$\bar{I}_1 = \mathrm{Im}\mathrm{Tr}[Y^\dagger h_\ell Y H_M M^* Y^T h_\ell^* Y^* M]\,, \tag{2.15}$$

and analogously for $\bar{I}_2, \bar{I}_3$. The corresponding CP odd invariants are $\mathrm{Im}(\bar{h}^2_{ij})$, which in the basis where also the charged lepton Yukawa matrix is real and diagonal can be written as:

$$\mathrm{Im}(\bar{h}^2_{ij}) = \sum_{\alpha,\beta} \lambda^2_\alpha \lambda^2_\beta \,\mathrm{Im}[Y^*_{\alpha i} Y_{\alpha j} Y_{\beta j} Y^*_{\beta i}]\ . \tag{2.16}$$

The lepton number (L) violating part of the flavoured CP asymmetries in leptogenesis depends on the above combinations [25]:

$$\epsilon^{\not L}_{i\alpha} = \sum_{\beta,j} \mathrm{Im}[Y^*_{\alpha i} Y_{\alpha j} Y_{\beta j} Y^*_{\beta i}] \tilde{f}(M_i, M_j)\,, \tag{2.17}$$

where $\tilde{f}$ is an arbitrary function. Upon substitution of the neutrino Yukawa couplings as given in eq. (2.1) can be written as:

$$\epsilon^{\not L}_{i\alpha} = \sum_j \sum_{\beta,\delta,\sigma} y_\beta\, y_\delta\, y^2_\sigma\, \mathrm{Im}[W^*_{\beta i} V_{\beta\alpha} V^*_{\delta\alpha} W_{\delta j} W^*_{\sigma i} W_{\sigma j}] \tilde{f}(M_i, M_j)\ . \tag{2.18}$$

These asymmetries contain the additional rephasing invariants of the form $\mathrm{Im}[W^*_{\beta i} V_{\beta\alpha} V^*_{\delta\alpha} W_{\delta j}]$, which depend on the phases in the matrix $V(\bar{\delta}, \phi_1, \phi_2)$, showing that the flavoured CP asymmetries of leptogenesis are also sensitive to the CP phases in the V leptonic mixing matrix, besides those in W.

Alternatively, we choose to construct the WB invariants which will appear when the Majorana character of the sterile neutrinos is not relevant, i.e., L-conserving ones. These are given by:

$$\begin{aligned}
\bar{I}'_1 &\equiv \mathrm{Im}\mathrm{Tr}[h H^2_M \bar{h} H_M] \\
&= M_1^2 M_2^2 \Delta M^2_{21} \mathrm{Im}(h_{12}\bar{h}_{21}) + M_1^2 M_3^2 \Delta M^2_{31} \mathrm{Im}(h_{13}\bar{h}_{31}) \\
&\quad + M_2^2 M_3^2 \Delta M^2_{32} \mathrm{Im}(h_{23}\bar{h}_{32}),
\end{aligned} \tag{2.19}$$

$$\begin{aligned}
\bar{I}'_2 &\equiv \mathrm{Im}\mathrm{Tr}[h H^3_M \bar{h} H_M] \\
&= M_1^2 M_2^2 (M_2^4 - M_1^4) \mathrm{Im}(h_{12}\bar{h}_{21}) + M_1^2 M_3^2 (M_3^4 - M_1^4) \mathrm{Im}(h_{13}\bar{h}_{31}) \\
&\quad + M_2^2 M_3^2 (M_3^4 - M_2^4) \mathrm{Im}(h_{23}\bar{h}_{32}),
\end{aligned} \tag{2.20}$$

$$\begin{aligned}
\bar{I}'_3 &\equiv \mathrm{Im}\mathrm{Tr}[h H^3_M \bar{h} H^2_M] \\
&= M_1^4 M_2^4 \Delta M^2_{21} \mathrm{Im}(h_{12}\bar{h}_{21}) + M_1^4 M_3^4 \Delta M^2_{31} \mathrm{Im}(h_{13}\bar{h}_{31}) \\
&\quad + M_2^4 M_3^4 \Delta M^2_{32} \mathrm{Im}(h_{23}\bar{h}_{32})\,,
\end{aligned} \tag{2.21}$$

JHEP10(2015)067

where

$$\mathrm{Im}(h_{ij}\bar{h}_{ji}) = \sum_{\alpha,\beta} \lambda_\alpha^2 \,\mathrm{Im}[Y_{\alpha i} Y^*_{\alpha j} Y_{\beta j} Y^*_{\beta i}] \ . \tag{2.22}$$

The L-conserving CP asymmetry in leptogenesis via heavy neutrino decay, as well as the CP asymmetries encountered in leptogenesis through sterile neutrino oscillations, are sensitive to the above combinations of Yukawa couplings [25]:

$$\epsilon^L_{i\alpha} = \sum_{j,\beta} \mathrm{Im}[Y_{\alpha i} Y^*_{\alpha j} Y_{\beta j} Y^*_{\beta i}]\, f(M_i, M_j)\,, \tag{2.23}$$

where f is an arbitrary function, and can be written in terms of the rephasing invariants as:

$$\epsilon^L_{i\alpha} = -\sum_{j} \sum_{\beta,\delta,\sigma} y_\beta y_\delta y_\sigma^2 \,\mathrm{Im}[W^*_{\beta i} V_{\beta\alpha} V^*_{\delta\alpha} W_{\delta j} W_{\sigma i} W^*_{\sigma j}]\, f(M_i, M_j)\ . \tag{2.24}$$

Notice that the crucial difference between the L-violating and the L-conserving CP asymmetries is that in $\epsilon^L_{i\alpha}$ the combination of W matrix elements is such that all dependence on the Majorana phases $\alpha_{1,2}$ disappears, as expected.

In the approximation of neglecting $y_3 \ll y_1, y_2$, we obtain that $\mathrm{Im}[Y_{\alpha i} Y^*_{\alpha j} (Y^\dagger Y)_{ij}] = \sum_\beta \mathrm{Im}[Y_{\alpha i} Y^*_{\alpha j} Y_{\beta j} Y^*_{\beta i}]$ reduces to

$$\begin{aligned}
\mathrm{Im}[Y_{\alpha i} Y^*_{\alpha j} (Y^\dagger Y)_{ij}] = {} & y_1^2 y_2^2 (|V_{2\alpha}|^2 - |V_{1\alpha}|^2) \mathrm{Im}[W^*_{1i} W_{1j} W^*_{2j} W_{2i}] \\
& + y_1 y_2 \left\{ \left[y_2^2 |W_{2i}|^2 - y_1^2 |W_{1i}|^2 \right] \mathrm{Im}[W^*_{1j} V_{1\alpha} V^*_{2\alpha} W_{2j}] \right. \\
& \left. + \left[y_1^2 |W_{1j}|^2 \ - y_2^2 |W_{2j}|^2 \right] \mathrm{Im}[W^*_{1i} V_{1\alpha} V^*_{2\alpha} W_{2i}] \right\}\ ,
\end{aligned} \tag{2.25}$$

so in principle we expect that the lepton asymmetry will depend on ten CP invariants, namely $\mathrm{Im}[W^*_{1i} V_{1\alpha} V^*_{2\alpha} W_{2i}]$, with $i = 1, 2, 3$ and $\alpha = 1, 2, 3$ and J_W.

However, they are not all independent. In ref. [24] it has been shown that in the minimal seesaw there are only six independent CP invariants that can be made out of the matrices V, W. Two of them correspond to the Majorana phases of W, $\alpha_{1,2}$, which as we have argued before will not contribute in the limit of small sterile neutrino Majorana masses that we are considering. Other two are the equivalent of the Jarlskog invariants for the matrices V, W and therefore determine the Dirac phases, $\bar{\delta}, \delta$, respectively. The last two are of the form $\mathrm{Im}[W^*_{1i} V_{1\alpha} V^*_{2\alpha} W_{2i}]$, for two reference values of i, α, that fix the additional phases $\phi_{1,2}$. Moreover, it can be shown that since we are neglecting the Yukawa coupling y_3, the phase ϕ_2 of the matrix V does not appear in eq. (2.25), thus we are left with only three independent invariants.

The unitarity of the mixing matrices V, W implies that

$$\sum_\alpha V_{1\alpha} V^*_{2\alpha} = 0\,, \tag{2.26}$$

$$\sum_i W^*_{1i} W_{2i} = 0\,, \tag{2.27}$$

which allows to write the invariants $\mathrm{Im}[W^*_{1i} V_{1\alpha} V^*_{2\alpha} W_{2i}]$ for $\alpha = 2$ in terms of those with $\alpha = 1, 3$, and the invariants for $i = 2$ in terms of the corresponding ones with $i = 1, 3$. By

JHEP10(2015)067

exploiting the identities

$$\mathrm{Im}[W_{1i}^* V_{1\beta} V_{2\beta}^* W_{2i}] = \frac{\mathrm{Im}[(W_{1i}^* V_{1\alpha} V_{2\alpha}^* W_{2i})(V_{2\beta}^* V_{2\alpha} V_{1\alpha}^* V_{1\beta})]}{|V_{1\alpha} V_{2\alpha}|^2}, \tag{2.28}$$

we can write for instance one of the invariants with $\beta = 3$ in terms of the invariant with $\alpha = 1$ and the Jarlskog invariant for V, $\mathrm{Im}[V_{2\beta}^* V_{2\alpha} V_{1\alpha}^* V_{1\beta}] = \pm J_V$.

It is simpler, though, to write the results in terms of the following four invariants, even if only three are independent, expanded up to 3rd order in the small mixing angles $\theta_{ij}, \bar{\theta}_{ij}$:

$$\begin{aligned} I_1^{(2)} &= -\mathrm{Im}[W_{12}^* V_{11} V_{21}^* W_{22}] \simeq \theta_{12}\bar{\theta}_{12} \sin\phi_1, \\ I_1^{(3)} &= \mathrm{Im}[W_{12}^* V_{13} V_{23}^* W_{22}] \simeq \theta_{12}\bar{\theta}_{13}\bar{\theta}_{23} \sin(\bar{\delta} + \phi_1), \\ I_2^{(3)} &= \mathrm{Im}[W_{13}^* V_{12} V_{22}^* W_{23}] \simeq \bar{\theta}_{12}\theta_{13}\theta_{23} \sin(\delta - \phi_1), \\ J_W &= -\mathrm{Im}[W_{23}^* W_{22} W_{32}^* W_{33}] \simeq \theta_{12}\theta_{13}\theta_{23} \sin\delta. \end{aligned} \tag{2.29}$$

A generic expectation for the CP-asymmetry relevant for leptogenesis is

$$\Delta_{\mathrm{CP}} = \sum_{\alpha,k} |Y_{\alpha k}|^2 \, \Delta_\alpha, \tag{2.30}$$

with

$$\Delta_\alpha = \sum_i \epsilon_{i\alpha}^L = \sum_{i,j} \mathrm{Im}[Y_{\alpha i} Y_{\alpha j}^* (Y^\dagger Y)_{ij}] f(M_i, M_j). \tag{2.31}$$

Since the CP rephasing invariants are at least second order in the angles, we just need to take the diagonal elements in Δ_{CP}, to keep the result up to 3rd order. Then, in the limit $y_3 = 0$, we get:

$$\begin{aligned} \Delta_{\mathrm{CP}} = {} & y_1^2 y_2^2 (y_2^2 - y_1^2) \sum_{i,j} \mathrm{Im}[W_{1i}^* W_{1j} W_{2j}^* W_{2i}] f(M_i, M_j) \\ & + y_1 y_2 \Big((y_2^2 - y_1^2) \Big\{ I_1^{(2)} [g(M_1) - g(M_2)] + I_2^{(3)} [g(M_1) - g(M_3)] \Big\} \\ & - y_2^2 I_1^{(3)} [g(M_1) - g(M_2)] \Big) , \end{aligned} \tag{2.32}$$

where

$$g(M_i) \equiv y_1^2 [f(M_1, M_i) - f(M_i, M_1)] - y_2^2 [f(M_2, M_i) - f(M_i, M_2)] \ . \tag{2.33}$$

From the above definition of $g(M_i)$, it immediately follows that $g(M_1) - g(M_2) = (y_2^2 - y_1^2)[f(M_1, M_2) - f(M_2, M_1)]$, so Δ_{CP} simplifies to

$$\begin{aligned} \Delta_{\mathrm{CP}} = {} & y_1^2 y_2^2 (y_2^2 - y_1^2) \sum_{i,j} \mathrm{Im}[W_{1i}^* W_{1j} W_{2j}^* W_{2i}] f(M_i, M_j) \\ & + y_1 y_2 (y_2^2 - y_1^2) \Big\{ \Big[(y_2^2 - y_1^2) I_1^{(2)} - y_2^2 I_1^{(3)} \Big] [f(M_1, M_2) - f(M_2, M_1)] \\ & + I_2^{(3)} [g(M_1) - g(M_3)] \Big\} \ . \end{aligned} \tag{2.34}$$

We will see in the next section that this is precisely the yukawa and mixing angle dependence we will find when solving the kinetic equations, which is a strong crosscheck of the result.

JHEP10(2015)067

3 Perturbative solution of the Raffelt-Sigl equation

3.1 Sterile neutrino production

Our starting point is the Raffelt-Sigl formulation [26] of the kinetic equations that describe the production of sterile neutrinos in the early Universe. The density matrix is the expectation value of the one-particle number operator for momentum k: $\rho_N(k)$ for neutrinos, and $\bar{\rho}_N(k)$ for antineutrinos. We will assume that only sterile neutrinos and the lepton doublets are out of chemical equilibrium, but assume that all the particles are in kinetic equilibrium, using Maxwell-Boltzmann statistics:

$$\rho_a(k) = A_a \rho_{\rm eq}(k), \quad A_a = e^{\mu_a}; \qquad \rho_{\bar{a}}(k) = A_{\bar{a}} \rho_{\rm eq}(k), \quad A_{\bar{a}} = e^{-\mu_a}, \tag{3.1}$$

where $\rho_{\rm eq}(k) \equiv e^{-k_0/T}$, with $k_0 = |\mathbf{k}|$, and μ_a denotes the chemical potential normalised by the temperature. We will furthermore neglect spectator processes and the washout induced by the asymmetries in all the fields other than the sterile neutrinos and lepton doublets. We expect this approximation to give uncertainties of $\mathcal{O}(1)$ which for our purpose is good enough [27].

In [7], only the asymmetry in the sterile sector was considered, neglecting the feedback of the leptonic chemical potentials. In this case, the equations get the standard form

$$\dot{\rho}_N = -i\big[H, \rho_N\big] - \frac{1}{2}\big\{\Gamma, \rho_N - \rho_{\rm eq}\big\}, \tag{3.2}$$

and the analogous for $\bar{\rho}_N$ with $H \to H^*$, where H is the Hamiltonian (we neglect matter potentials for the time being but we will include them later on)

$$H \equiv W \Delta W^\dagger, \qquad \Delta \equiv {\rm Diag}\left(0, \frac{\Delta M^2_{12}}{2k_0}, \frac{\Delta M^2_{13}}{2k_0}\right). \tag{3.3}$$

Γ is the rate of production/annihilation of sterile neutrinos in the plasma, which is diagonal in the basis that diagonalises the neutrino Yukawa's:

$$\Gamma = {\rm Diag}(\Gamma_1, \Gamma_2, 0), \qquad \Gamma_i \propto y_i^2, \tag{3.4}$$

where we assume $y_3 = 0$. In deriving eq. (3.2) it is assumed that the particles involved in the production/annihilation of the sterile neutrinos are in full equilibrium (all chemical potentials vanish), and that kinematical effects of neutrino masses are negligible.

Note that only the matrix W appears in these equations and therefore any CP asymmetry generated can only be proportional to the invariant J_W which depends at third order on the mixing angles of W.

In [8] it was correctly pointed out that the asymmetries in the sterile sector will be modified by the leptonic chemical potentials that will be generated as soon as sterile neutrinos start to be produced. Including the evolution of the leptonic chemical potentials has two important consequences: new sources of CP violation become relevant and washout effects are effective. Leptons are fastly interacting through electroweak interactions in the plasma and therefore it is a good approximation to assume they are in kinetic equilibrium.

JHEP10(2015)067

An important question is what is the flavour structure of these chemical potentials. For $T \lesssim 10^9$ GeV the Yukawa interactions of the tau and muon are very fast, which implies that μ will be diagonal in the basis that diagonalises the charged lepton Yukawa matrix, since no other interaction changing flavour is in equilibrium before the heavy neutrinos are produced. Note however that this is not the basis where the neutrino Yukawas are diagonal, the two are related by the mixing matrix V. As a result, when the evolution of the lepton chemical potentials is taken into account, the CP phases of the matrix V become relevant.

Adapting the derivation of [26] to this situation, we find that the evolution of the CP-even and CP-odd parts of the neutrino densities: $\rho_\pm \equiv \frac{\rho_N \pm \bar{\rho}_N}{2}$ and the lepton chemical potentials , μ_α, to linear order in μ_α, ρ_-, satisfy in this case:

$$\begin{aligned}
\dot{\rho}_+ &= -i[H_{\rm re}, \rho_+] + [H_{\rm im}, \rho_-] - \frac{\gamma_N^a + \gamma_N^b}{2}\{Y^\dagger Y, \rho_+ - \rho_{\rm eq}\} \\
&\quad + i\gamma_N^b {\rm Im}[Y^\dagger \mu Y]\rho_{\rm eq} + i\frac{\gamma_N^a}{2}\big\{{\rm Im}[Y^\dagger \mu Y], \rho_+\big\}, \\
\dot{\rho}_- &= -i[H_{\rm re}, \rho_-] + [H_{\rm im}, \rho_+] - \frac{\gamma_N^a + \gamma_N^b}{2}\big\{Y^\dagger Y, \rho_-\big\} \\
&\quad + \gamma_N^b {\rm Re}[Y^\dagger \mu Y]\rho_{\rm eq} + \frac{\gamma_N^a}{2}\big\{{\rm Re}[Y^\dagger \mu Y], \rho_+\big\}, \\
\dot{\mu}_\alpha &= -\mu_\alpha\left(\gamma_\nu^b {\rm Tr}[YY^\dagger I_\alpha] + \gamma_\nu^a {\rm Tr}\big[{\rm Re}[Y^\dagger I_\alpha Y] r_+\big]\right) \\
&\quad + (\gamma_\nu^a + \gamma_\nu^b){\rm Tr}\big[{\rm Re}[Y^\dagger I_\alpha Y] r_-\big],
\end{aligned} \tag{3.5}$$

where $H_{\rm re} \equiv {\rm Re}[H]$, $H_{\rm im} \equiv {\rm Im}[H]$, I_α is the projector on flavour α and $\gamma_N^{a,b}, \gamma_\nu^{a,b}$ are the rates of production/annihilation of a sterile neutrino or a lepton doublet neglecting all masses, after factorizing the flavour structure in the Yukawas,

$$\gamma_{N(\nu)}^{a(b)} \equiv \frac{1}{2k_0}\sum_i \int_{\mathbf{p_1},\mathbf{p_2},\mathbf{p_3}} \rho_{\rm eq}(p_1)|\mathcal{M}_{N(\nu),i}^{(a(b))}|^2 (2\pi)^4 \delta(k + p_1 - p_2 - p_3), \tag{3.6}$$

where k is the momentum of the N or ν and $a(b)$ refer to the s-channel (t,u-channels) depicted in figure 1. In topology a the lepton and sterile neutrino are *both* in the initial or final state, while topology b corresponds to those diagrams where one is in the initial and other in the final state. Finally

$$r_\pm \equiv \frac{\sum_i \int_{\mathbf{p_1},\mathbf{p_2},\mathbf{p_3}} \rho_\pm(\mathbf{p_1})|\mathcal{M}_{\nu i}^{(a)}|^2 (2\pi)^4 \delta(k + p_1 - p_2 - p_3)}{\sum_i \int_{\mathbf{p_1},\mathbf{p_2},\mathbf{p_3}} \rho_{\rm eq}(\mathbf{p_1})|\mathcal{M}_{\nu i}^{(a)}|^2 (2\pi)^4 \delta(k + p_1 - p_2 - p_3)}\,. \tag{3.7}$$

A similar derivation can be found in [28] and we agree with their findings.

These equations reduce to those in eq. (3.2) in the limit $\mu \to 0$ with $\Gamma_i = y_i^2(\gamma_N^a + \gamma_N^b)$.

Most previous studies have assumed that the rates are dominated by the top quark scatterings. In this case, the rates are given (in the Boltzman approximation) by the well-known result [29, 30]

$$\gamma_{N,Q}^b = 2\gamma_{N,Q}^a = 2\gamma_{\nu,Q}^b = 4\gamma_{\nu,Q}^a = \frac{3}{16\pi^3}\frac{y_t^2 T^2}{k_0}. \tag{3.8}$$

JHEP10(2015)067

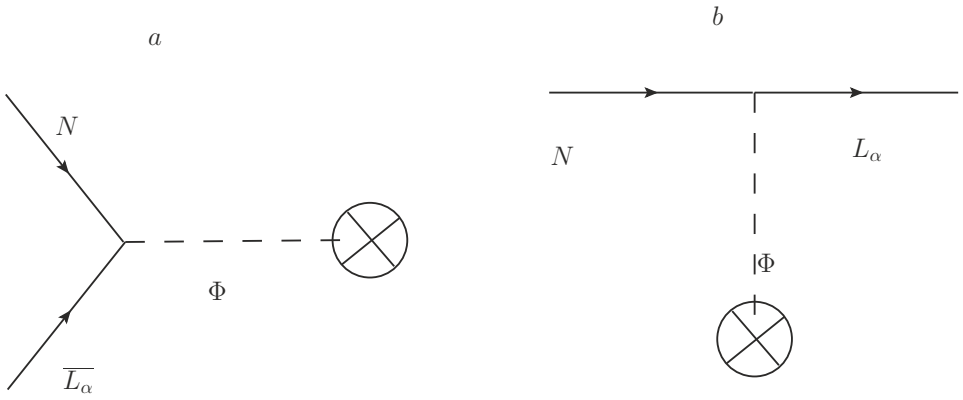

Figure 1. a, b topologies for annihilation/production of sterile neutrinos.

The factor of 2 difference between the rates of the N and the ν is due to the fact that the lepton is a doublet and the sterile neutrino is a singlet. Note that there is a non-linear term of the form $\mathcal{O}(\mu\rho_+)$, as first noted in [28]. More recently in [31], the equations have been written in terms of the $\mu_{B-L_\alpha/3}$ chemical potentials, however not all the chemical potentials (e.g. higgs and top quark) have been included. A full treatment including all chemical potentials will be postponed for a future work, but we expect that including these spectator effects will change the results by factors of $\mathcal{O}(1)$.

In [30, 32], it has been pointed out that the scattering processes $\bar{L}N \leftrightarrow WH$ get a strong enhancement from hard thermal loops and are actually the dominant scatterings. The results of [30, 32] however do not include the chemical potentials of spectators, so it is not clear how to include them consistently in the above equations. We will neglect these effects in the following. Note however that the lepton flavour structure of these and of the top quark scatterings is the same.

It is easy to see also that total lepton number is conserved as it should:

$$2\sum_\alpha \dot{\mu}_\alpha + \mathrm{Tr}[\dot{r}_-] = 0. \tag{3.9}$$

Two approximations are often used in solving these equations: 1) assume that the momentum dependence of $\rho_\pm$ follows that of $\rho_{\rm eq}$, i.e. kinetic equilibrium for the sterile states, which implies $r_\pm = \rho_\pm/\rho_{\rm eq}$ are constants and the integro-differential equations become just differential equations, 2) neglect the k_0 dependence of the rates by approximating

$$\langle k_0^{-1}\rangle \simeq \frac{T^{-1}}{2}. \tag{3.10}$$

The effect of these approximations has been studied numerically in [28] and the results do not differ too much. We will therefore adopt both approximations that simplify considerably the perturbative treatment.

JHEP10(2015)067

3.2 Lepton asymmetries in the sterile sector

We are going to solve these equations perturbing in the mixing angles up to third order. We first consider the simpler case, neglecting leptonic chemical potentials and considering in turn the evolution in a static Universe and in the expanding case.

3.2.1 Static Universe

We start with eq. (3.2) and assume $y_3 = 0$. In this case, neither H nor Γ depend on time. Defining $\rho_{Nij}/\rho_{\rm eq} \equiv a_{ij} + ib_{ij}$ and taking into account the hermiticity of ρ_N we change the matrix equation into a vector equation:

$$r \equiv (a_{11}, a_{22}, a_{12}, b_{12}, a_{13}, b_{13}, a_{23}, b_{23}, a_{33}). \tag{3.11}$$

At 0-th order the system of equations of eq. (3.2) can be rewritten as

$$\dot{r}^{(0)} = A_0 r^{(0)} + h_0, \tag{3.12}$$

with

$$h_0 \equiv (\Gamma_1 \rho_{\rm eq}, \Gamma_2 \rho_{\rm eq}, 0, \ldots .0), \tag{3.13}$$

and the matrix A_0 is constant and has a block structure:

$$A_0 \equiv \begin{pmatrix} (A_I)_{4\times 4} & 0 & 0 \\ 0 & (A_{II})_{4\times 4} & 0 \\ 0 & 0 & 0 \end{pmatrix}, \tag{3.14}$$

$$A_I \equiv \begin{pmatrix} -\Gamma_1 & 0 & 0 & 0 \\ 0 & -\Gamma_2 & 0 & 0 \\ 0 & 0 & -\frac{\Gamma_1+\Gamma_2}{2} & -\Delta_{12} \\ & & \Delta_{12} & -\frac{\Gamma_1+\Gamma_2}{2} \end{pmatrix}, \; A_{II} \equiv \begin{pmatrix} -\Gamma_1/2 & -\Delta_{13} & 0 & 0 \\ \Delta_{13} & -\Gamma_1/2 & 0 & 0 \\ 0 & 0 & -\frac{\Gamma_2}{2} & \Delta_{12}-\Delta_{13} \\ 0 & 0 & -(\Delta_{12}-\Delta_{13}) & -\frac{\Gamma_2}{2} \end{pmatrix}. \tag{3.15}$$

The matrix can be easily diagonalised and exponentiated so the general solution to the equation is

$$r^{(0)}(t) = e^{A_0 t} \int_0^t dx \; e^{-A_0 x} h_0. \tag{3.16}$$

At the next order we have to keep $\mathcal{O}(\theta_{ij})$ in the Hamiltonian and translate the matrix form into the vector form:

$$-i[H^{(1)}, \rho^{(0)}(t)] \to A_1 r^{(0)}. \tag{3.17}$$

The equation for the first order correction to the density is

$$\dot{r}^{(1)} = A_0 r^{(1)} + A_1 r^{(0)}(t). \tag{3.18}$$

JHEP10(2015)067

The solution at this order is therefore

$$r^{(1)}(t) = e^{A_0 t} \int_0^t dx e^{-A_0 x} A_1 r^{(0)}(x). \tag{3.19}$$

We can iterate this procedure to get the correction at order n:

$$\dot{r}^{(n)}(t) = A_0 r^{(n)}(t) + \sum_{i=1}^{n-1} A_i r^{(n-i)}(t), \tag{3.20}$$

with solution

$$r^{(n)}(t) = e^{A_0 t} \int_0^t dx e^{-A_0 x} \sum_{i=1}^{n-1} A_i r^{(n-i)}(x). \tag{3.21}$$

We can define the evolution operator

$$U_0(t,x) \equiv e^{A_0 t} e^{-A_0 x}, \tag{3.22}$$

so that the solution can be written as

$$r^{(n)}(t) = \int_0^t dx\ U_0(t,x) \sum_{i=1}^{n-1} A_i r^{(n-i)}(x). \tag{3.23}$$

As a first estimate of the leptonic asymmetry that can be generated, we are interested in $\Delta\rho_{33}$ since this is the sector that will never reach equilibrium (in the absence of mixing) and therefore can act as reservoir of the leptonic asymmetry until the electroweak phase transition [7].

One can easily compute the solution of the eq. (3.21) up to order $n = 3$, which is the first order that gives a non-vanishing result, as expected from general considerations on CP invariants. The result at finite t is not particularly illuminating but the limit $t \to \infty$ is rather simple:

$$\lim_{t\to\infty} \frac{\Delta\rho_{33}}{\rho_{\rm eq}} \equiv \lim_{t\to\infty} \frac{\rho_{N33} - \bar{\rho}_{N33}}{\rho_{\rm eq}} = 2J_W \frac{(\Gamma_1 - \Gamma_2)\Delta_{12}\Delta_{13}(\Delta_{12} - \Delta_{13})}{\left[\Delta_{13}^2 + \frac{\Gamma_1^2}{4}\right]\left[(\Delta_{12} - \Delta_{13})^2 + \frac{\Gamma_2^2}{4}\right]}. \tag{3.24}$$

A few comments are in order. We have not assumed any expansion in Γ_i in this expression, only in the mixing angles. According to general theorems the equations should reach a stationary solution if all the eigenvalues of the matrix $A_0 + A_1 + A_2 + \ldots$ are real and negative. However, because $\Gamma_3 = 0$, one of the eigenvalues of A_0 vanishes and it is lifted only at second order in perturbation theory, $\sim \theta_{i3}^2 \Gamma_i$, therefore we expect the perturbative expansion should break down for $t \sim \frac{1}{\theta_{i3}^2 \Gamma_i}$, which is the time scale of equilibration of the third state. On the other hand, if θ is small, the perturbative solution should be accurate for times $t \geq \Gamma_{1(2)}^{-1}$. Indeed this is precisely what we find comparing the perturbative and numerical solutions in figure 2.

The result is proportional to J_W which is the only CP rephasing invariant that can appear in this case. The result vanishes if any two of the masses or the yukawa's are degenerate, since the CP phase would be unphysical in this case.

JHEP10(2015)067

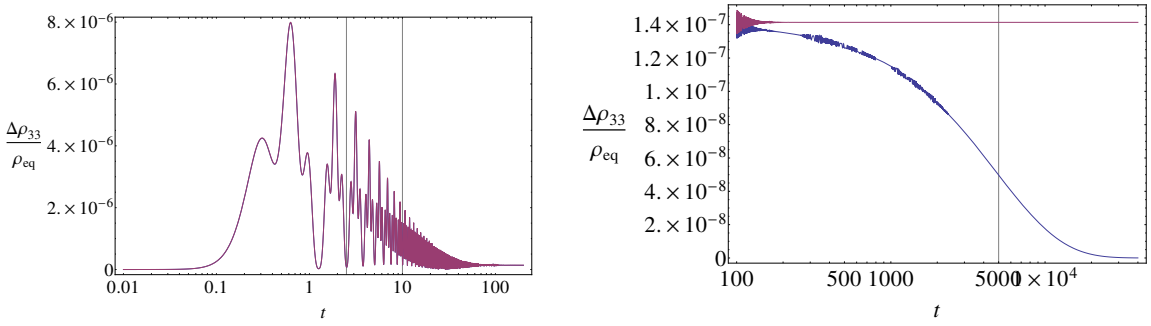

Figure 2. Comparison of numerical (blue) and perturbative (red) solution for $\Delta\rho_{33}$ as a function of time, in the case with no expansion of the Universe. The two curves are indistinguishable (left plot) until large times (right plot): the vertical line on the left plot corresponds to $(\theta_{31}^2\Gamma_1)^{-1}$, while those on the right one correspond to Γ_2^{-1} and Γ_1^{-1} respectively.

3.2.2 Expanding Universe

Let us turn now to the realistic case of an expanding Universe. As usual, we will consider the evolution as a function of the scale factor $x \equiv a$, in such a way that the Raffelt-Sigl equation becomes

$$\frac{d}{dt} \to xH_u(x)\frac{\partial}{\partial x}\rho(x,y)\Big|_{\text{fixed y}} = -i[H(x,y),\rho(x,y)] - \frac{1}{2}\{\Gamma(x),\rho(x,y)-\rho_{eq}(y)\}, \tag{3.25}$$

where $H_u(x)$ is the Hubble parameter, $H_u = \sqrt{\frac{4\pi^3 g_*(T)}{45}}\frac{T^2}{M_{\text{Planck}}}$, and $y \equiv \frac{p}{T}$. Assuming for simplicity a radiation dominated Universe with constant number of degrees of freedom, during the sterile evolution time we can assume $xT=$ constant that we can fix to be one. Therefore the scaling of the different terms is

$$H(x,y) \equiv xW\frac{\Delta M^2}{2y}W^\dagger, \qquad \Gamma_i(x) \equiv \frac{c_i}{x}, \qquad xH_u(x) \equiv \frac{1}{M_{\text{P}}^* x}, \tag{3.26}$$

where $M_P^* \equiv M_{\text{Planck}}\sqrt{\frac{45}{4\pi^3 g_*(T_0)}}$ and $g_*(T_0)$ is the number of relativistic degrees of freedom in the plasma during the sterile evolution.

Therefore the equation as function of x is:

$$\dot{\rho} = -ix^2[W\Delta W^\dagger,\rho] - \frac{1}{2}\{\gamma,\rho-\rho_{eq}\}, \tag{3.27}$$

where we have defined

$$\Delta_{ij} \equiv \frac{\Delta M_{ij}^2}{2y}M_P^*, \qquad \gamma_i \equiv c_i M_P^*. \tag{3.28}$$

The perturbative expansion works as in section 3.2.1, but now all the $A_n(x)$ are x-dependent: $A_n(x)$ with $n \geq 1$ scale like the Hamiltonian, ie. x^2, while $A_0(x)$ contains terms that scale with x^2 and others that do not depend on x. Fortunately, there is an important

JHEP10(2015)067

simplification in that $A_0(x)$ can be diagonalised by an x-independent matrix, therefore the path-ordered exponential can be easily evaluated. The result can be written in the same form of eq. (3.23), with the evolution operator given by

$$U_0(t,r) = e^{\int_0^t A_0(x)dx} e^{-\int_0^r A_0(y)dy}. \tag{3.29}$$

At third order in the mixings, after algebraic simplifications and partial integrations, the result can be given in terms of integrals of the form

$$J_n(\alpha_1,\beta_1,\ldots,\alpha_n,\beta_n,t) \equiv \int_0^t dx_1 e^{i\alpha_1 \frac{x_1^3}{3}+\beta_1 x_1} \int_0^{x_1} dx_2 e^{i\alpha_2 \frac{x_2^3}{3}+\beta_2 x_2} \ldots \int_0^{x_{n-1}} dx_n e^{i\alpha_n \frac{x_n^3}{3}+\beta_n x_n}, \tag{3.30}$$

where α_i are combinations of Δ_{ij} and β_i are combinations of γ_i. Up to third order in the perturbative expansion only integrals with $n \leq 3$ appear.

Since we are in a regime where $\gamma_i \ll |\Delta_{ij}|^{(1/3)}$, the integrands are highly oscillatory and hard to deal with numerically. To evaluate the integrals, we separate the integration interval $[0,t] = [0,t_0] + [t_0,t]$ with t_0 such that $t_0|\Delta_{ij}|^{1/3} \gg 1$ and $t_0\gamma_i \ll 1$:

$$J_n(\alpha_1,\beta_1,\ldots,\alpha_n,\beta_n,t) = J_n(\alpha_1,\beta_1,\ldots\alpha_n,\beta_n,t_0) + \Delta J_n(\alpha_1,\beta_1,\ldots\alpha_n,\beta_n,t_0,t). \tag{3.31}$$

To solve the integrals up to t_0 we can safely Taylor expand in β_i (which results in an expansion in $\gamma_{1,2}/|\Delta_{ij}|$) and write the integrals in terms of simpler integrals of the form:

$$J_{n\mathbf{k}}(\alpha_1,\ldots,\alpha_n,t) \equiv \int_0^t dx_1 x_1^{k_1}\ e^{i\frac{\alpha_1 x_1^3}{3}} \int_0^{x_1} dx_2 x_2^{k_2}\ e^{i\frac{\alpha_2 x_2^3}{3}} \ldots \int_0^{x_{n-1}} dx_n x_n^{k_n}\ e^{i\frac{\alpha_n x_n^3}{3}}, \tag{3.32}$$

up to third order in the β_i expansion we just need integrals with $n + \sum_i k_i \leq 3$. We can use the relation

$$\frac{d}{dx}\left[F_n(x)\right] = x^n e^{i\frac{\alpha x^3}{3}}, \tag{3.33}$$

with

$$F_n(\alpha,x) = -3^{\frac{n-2}{3}}(-i\alpha)^{-\frac{1+n}{3}}\ \Gamma\left[\frac{1+n}{3}, -\frac{1}{3}i\alpha x^3\right], \tag{3.34}$$

to evaluate immediately the one-dimensional integrals in terms of incomplete Γ functions. The integrals in the range $[t_0,t]$ can be approximated by the large t behaviour of the $J_{1n}(\alpha,t)$ functions, after resumming the Taylor series in β_i. Further details are presented in appendix A.

The finite t dependence of the asymmetry $\Delta\rho_{33}$ is rather complicated, but the asymptotic value is non-zero and rather simple:

$$\begin{aligned}\lim_{t\to\infty}\frac{\Delta\rho_{33}}{\rho_{\rm eq}} = &-J_W\gamma_1\gamma_2(\gamma_2-\gamma_1)\lim_{t\to\infty}\mathrm{Im}[J_{3\mathbf{0}}(\Delta_{12}-\Delta_{13},-\Delta_{12},\Delta_{13},t)\\ &+J_{3\mathbf{0}}(\Delta_{12}-\Delta_{13},\Delta_{13},-\Delta_{12},t)+J_{3\mathbf{0}}(\Delta_{13},-\Delta_{12},\Delta_{12}-\Delta_{13},t)\\ &+J_{3\mathbf{0}}(\Delta_{13},\Delta_{12}-\Delta_{13},-\Delta_{12},t)].\end{aligned} \tag{3.35}$$

JHEP10(2015)067

This can be simplified to

$$\lim_{t\to\infty}\frac{\Delta\rho_{33}}{\rho_{\rm eq}} = -J_W\frac{\gamma_1\gamma_2(\gamma_2-\gamma_1)}{(\Delta_{13}\Delta_{12}\Delta_{23})^{1/3}}{\rm Im}\left[I\left(\frac{\Delta_{12}}{\Delta_{23}},-\frac{\Delta_{13}}{\Delta_{23}}\right)+I\left(-\frac{\Delta_{12}}{\Delta_{13}},-\frac{\Delta_{23}}{\Delta_{13}}\right)\right], \tag{3.36}$$

where

$$I\left(\frac{\Delta_2}{\Delta_1},\frac{\Delta_3}{\Delta_1}\right)\equiv(\Delta_1\Delta_2\Delta_3)^{1/3}\int_0^\infty dx e^{i\frac{\Delta_1 x^3}{3}}\ J_{10}(\Delta_2,x)J_{10}(\Delta_3,x). \tag{3.37}$$

Comparing eq. (3.36) and eq. (3.24) we see that in the expanding case the asymmetry is cubic in γ_i and not linear. Note that the dependence on the yukawa's is precisely that expected from a flavour invariant CP asymmetry. In fact this is effectively the situation in the expanding case, because the asymmetry is generated at times $t \ll \gamma_i^{-1}$ and the dependence in the yukawa's in this regime is therefore perturbative. This is in contrast with the non-expanding case, where the asymmetry evolves all the way till $t \sim \gamma_i^{-1}$. To understand the reason behind this different behavior, it is useful to recall the definition of Δ_{ij} from eq. (3.28). Then, we see that $\Delta_{ij}x^3 \gg 1$ implies $\Delta M_{ij}^2/(4T) \gg T^2/M_P^* = H_u(T)$, therefore in this regime the sterile neutrino oscillations are much faster than the Hubble parameter and no asymmetry is produced anymore, since oscillations are averaged out. Thus in the expanding Universe the generation of the asymmetry occurs at $x \sim |\Delta_{ij}|^{-1/3} \ll \gamma_i^{-1}$.

Until now we have neglected the matter potentials, however given the suppression in three powers of γ of the leading result, there are corrections of same order coming from the potentials, and in fact they are numerically more important.

The equation including the potentials in the basis with diagonal neutrino Yukawas is:

$$\dot\rho = -ix^2[W\Delta W^\dagger,\rho] - i[v,\rho] - \frac{1}{2}\{\gamma,\rho-\rho_{eq}\}, \tag{3.38}$$

where

$$v_{ij} = \frac{y_i^2}{8}M_P^*\delta_{ij} \equiv v_i\delta_{ij}. \tag{3.39}$$

The result for the asymmetry including the potentials is given by:

$$\begin{aligned}\lim_{t\to\infty}\frac{\Delta\rho_{33}}{\rho_{\rm eq}} = J_W\lim_{t\to\infty}{\rm Re}\,[&z_1J_{30}(\Delta_{12}-\Delta_{13},-\Delta_{12},\Delta_{13},t)+z_2J_{30}(\Delta_{12}-\Delta_{13},\Delta_{13},-\Delta_{12},t)\\ &+z_2J_{30}(\Delta_{13},\Delta_{12}-\Delta_{13},-\Delta_{12},t)+z_3J_{30}(\Delta_{13},-\Delta_{12},\Delta_{12}-\Delta_{13},t)],\end{aligned} \tag{3.40}$$

with

$$\begin{aligned} z_1 &\equiv \gamma_1\gamma_2\Delta_v+\gamma_1v_2\Delta_\gamma+i\left(\frac{\gamma_1\gamma_2\Delta_\gamma}{2}-2\gamma_1v_2\Delta_v\right),\\ z_2 &\equiv \left[\gamma_1v_2-\gamma_2v_1+i\left(\frac{\gamma_1\gamma_2}{2}+2v_1v_2\right)\right]\Delta_\gamma,\\ z_3 &\equiv -\gamma_1\gamma_2\Delta_v-\gamma_2v_1\Delta_\gamma+i\left(\frac{\gamma_1\gamma_2\Delta_\gamma}{2}-2\gamma_2v_1\Delta_v\right). \end{aligned} \tag{3.41}$$

and $\Delta_v \equiv v_2 - v_1$ and $\Delta_\gamma \equiv (\gamma_2 - \gamma_1)$.

JHEP10(2015)067

The leading terms $\mathcal{O}(v^2\gamma)$ at asymptotic times $t \gg \gamma_{1,2}^{-1}$ are:

$$\lim_{t\to\infty}\frac{\Delta\rho_{33}}{\rho_{\rm eq}} = \frac{9y_t^6}{2048\pi^3}J_W\frac{y_1^2y_2^2(y_2^2-y_1^2)M_P^{*2}}{|\Delta M_{12}^2\Delta M_{13}^2\Delta M_{23}^2|^{1/3}}\kappa, \tag{3.42}$$

where

$$\begin{aligned}\kappa \equiv |\Delta_{12}\Delta_{13}\Delta_{23}|^{1/3}{\rm Im}\big[&J_{30}(\Delta_{12}-\Delta_{13},-\Delta_{12},\Delta_{13},t) - J_{30}(\Delta_{12}-\Delta_{13},\Delta_{13},-\Delta_{12},t)\\ &-J_{30}(\Delta_{13},\Delta_{12}-\Delta_{13},-\Delta_{12},t) + J_{30}(\Delta_{13},-\Delta_{12},\Delta_{12}-\Delta_{13},t)\big],\end{aligned} \tag{3.43}$$

depends only on the ratios of mass differences and/or the ordering of the states. This result is parametrically the same as the result of [7] if we neglect the dependence of κ on the mass differences and has the dependence on the yukawas expected from eq. (2.34).

Considering the naive seesaw scaling $y_i^2 \sim 2\frac{m_\nu M_i}{v^2}$, for $m_\nu \sim 1\,{\rm eV}$ and assuming no big hierarchies or degeneracies, i.e. $M_i^2 \sim \Delta M_{ij}^2 \sim M^2$, leads to

$$\lim_{t\to\infty}\frac{\Delta\rho_{33}}{\rho_{\rm eq}} \sim 2\times 10^{-7}J_W\left(\frac{m_\nu}{1\,{\rm eV}}\right)^3\left(\frac{M}{10\,{\rm GeV}}\right). \tag{3.44}$$

The asymmetry is highly sensitive to the light neutrino mass. Note that we have pushed the value to the limit, a light neutrino mass in the less constrained 0.1 eV range would imply three orders of magnitude suppression. The asymmetry grows linearly with the mass of the heavy steriles. However, for masses larger than $\sim$ 10–100 GeV lepton number violating transitions via the Majorana mass could washout further the asymmetry, an effect that requires a refinement of the formulation to be taken into account.

3.3 Lepton asymmetries in the active sector

The asymmetry generated ignoring the μ evolution depends only on the Dirac-type phase, δ, appearing in W as we have seen. However when the evolution of the leptonic chemical potentials is included, other phases contribute to the total lepton asymmetry. We will perform a perturbative expansion to third order in the mixings of both V and W matrices.

The result at finite $t \ll \theta_{i3}^2(\bar\theta_{i3}^2)\gamma_i^{-1}$ can be written in the form:

$${\rm Tr}[\mu](t) = \sum_{I_{\rm CP}} I_{\rm CP}A_{I_{\rm CP}}(t), \tag{3.45}$$

where all the four CP invariants appear, $I_{\rm CP} = \left\{J_W, I_1^{(2)}, I_1^{(3)}, I_2^{(3)}\right\}$, given in eqs. (2.29).

At finite t, the result for the functions $A_{I_{\rm CP}}$ is well approximated by

$$\begin{aligned}A_{I_1^{(2)}}(t) &= y_1y_2(y_2^2-y_1^2)\left(1-\frac{\gamma_N}{\bar\gamma_N}\right)\gamma_N^2G_1(t),\\ A_{I_1^{(3)}}(t) &= -y_1y_2(y_2^2-y_1^2)\left(1-\frac{\gamma_N}{\bar\gamma_N}\right)\gamma_N^2G_2(t),\\ A_{I_2^{(3)}}(t) &= y_1y_2\left(1-\frac{\gamma_N}{\bar\gamma_N}\right)\gamma_NG_3(t),\\ A_{J_W}(t) &= \gamma_1\gamma_2\left(1-\frac{\gamma_N}{\bar\gamma_N}\right)G_{41}(t) - \frac{\gamma_N}{2\bar\gamma_N}G_{42}(t),\end{aligned} \tag{3.46}$$

JHEP10(2015)067

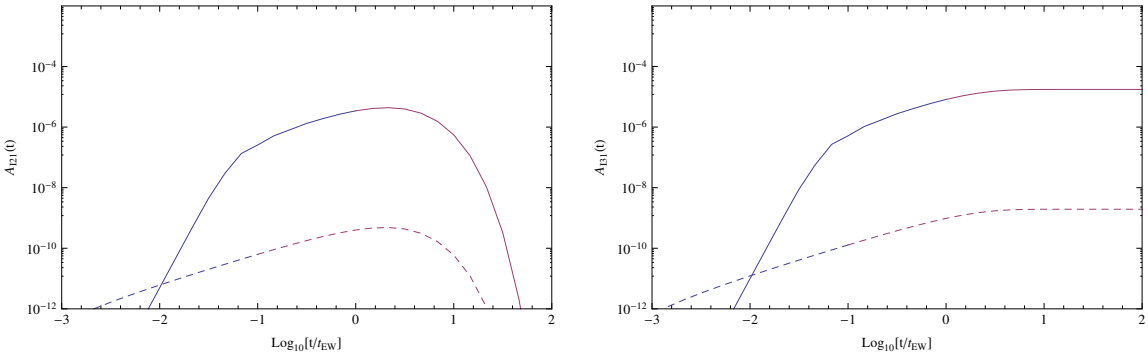

Figure 3. Functions $A_{I_1^{(2)}}(t)$ (left) and $A_{I_1^{(3)}}(t)$ (right) assuming the rates are dominated by top quark scattering, and taking $y_2/\sqrt{2} = y_1 = 10^{-7}$, for two choices of $\Delta M_{12}^2 = 1\,\mathrm{GeV}^2$ (dashed) and $\Delta M_{12}^2 = 10^{-6}\,\mathrm{GeV}^2$ (solid). $t_{\rm EW}$ is the electroweak phase transition time, corresponding to $T_{\rm EW} \simeq 140\mathrm{GeV}$.

where $\gamma_N \equiv \gamma_N^a + \gamma_N^b$ and $\bar{\gamma}_N \equiv \frac{2\gamma_N^a + 3\gamma_N^b}{2}$, while

$$G_1(t) \equiv \left(e^{-\bar{\gamma}_2 t} - e^{-\bar{\gamma}_1 t}\right) \mathrm{Re}\left[iJ_{20}(\Delta_{12}, -\Delta_{12}, t) + 2\Delta_v J_{201}(\Delta_{12}, -\Delta_{12}, t)\right] + \frac{1}{2}\sum_{k=1}^{2}(-1)^k e^{-\bar{\gamma}_k t}\mathrm{Re}\left[J_{210}(\Delta_{12}, -\Delta_{12}, t)\left(-2\Delta_v + i(2\bar{\gamma}_k - \gamma_1 - \gamma_2)\right)\right], \tag{3.47}$$

and

$$G_2(t) = G_1(t)|_{\bar{\gamma}_1 = 0}\,, \tag{3.48}$$

where we have defined $\bar{\gamma}_i \equiv y_i^2 \bar{\gamma}_N$ and $\Delta_v \equiv v_2 - v_1$, and the result for $G_3(t), G_{41}(t), G_{42}(t)$ are lengthier and reported in the appendix B. These results would get modified for $\gamma_i t \gg 1$ had we included the non-linear terms that modify the rate of thermalisation at large times. In these equations there is an implicit expansion up to third order in $\gamma_i(v_i)/\Delta^{1/3}$ when $\Delta^{1/3} t \gg 1$, while the terms $\gamma_i(v_i)t$ are resumed.

In figure 3 we plot the functions $A_{I_1^{(2)}}(t)$ and $A_{I_1^{(3)}}(t)$, which depend only on one neutrino mass difference. We show two physical situations: one with very degenerate neutrinos and the other with no strong degeneracies.

These two invariants are the only ones relevant for the scenario that has been considered in most previous studies, where it has been assumed that only two sterile neutrinos have a role in generating the lepton asymmetry (see for instance [33] for a very recent analysis). This is the situation in the limit of complete decoupling of N_3, ensured by the condition $\theta_{i3} = 0$, implying that only the invariants $I_1^{(2)}$ and $I_1^{(3)}$ survive. In [8] an approximate analytical solution was obtained, expanding in the yukawa's, under the assumption that $|\Delta_{12}|^{-1/3} \ll t_{\rm EW} \ll \bar{\gamma}_i^{-1}$. In this limit, the result of eqs. (3.46) and (3.47) can be simplified to

$$\mathrm{Tr}[\mu](t_{\rm EW}) \simeq -\left((y_2^2 - y_1^2) I_1^{(2)} - y_2^2 I_1^{(3)}\right) y_1 y_2 (y_2^2 - y_1^2) \left(1 - \frac{\bar{\gamma}_N}{\gamma_N}\right) \gamma_N^3 \frac{\mathrm{Im}[J_{20}(\Delta_{12}, -\Delta_{12}, \infty)]}{T_{\rm EW}}. \tag{3.49}$$

JHEP10(2015)067

Comparing with eq. (2.34), we see that the dependence on the yukawa's is again that expected from a flavour invariant CP asymmetry. Using

$$\mathrm{Im}[J_{20}(\Delta_{12},-\Delta_{12},\infty)] = -2\left(\frac{2}{3}\right)^{1/3}\frac{\pi^{3/2}}{\Gamma[-1/6]}\frac{\mathrm{sign}(\Delta_{12})}{|\Delta_{12}|^{2/3}}, \tag{3.50}$$

and $\bar{\gamma}_N = \frac{4}{3}\gamma_N$, and assuming the naive seesaw relations $y_1^2 = 2\frac{\sqrt{\Delta_{\rm sol}}M_1}{v^2}$, $y_2^2 = 2\frac{\sqrt{\Delta_{\rm atm}}M_2}{v^2}$ we find:

$$\mathrm{Tr}[\mu](t_{\rm EW}) \simeq 10^{-2}(I_1^{(2)} - I_1^{(3)})\frac{\sqrt{M_1 M_2^{7/3}}}{\mathrm{GeV}^{5/3}}\left(\frac{M_2^2}{|\Delta M_{12}^2|}\right)^{2/3}, \tag{3.51}$$

while for $y_1^2 = y_2^2/2 = 10^{-14}$ (that would correspond to light neutrino masses in the eV range and heavy ones in the GeV range) we would have

$$\mathrm{Tr}[\mu](t_{\rm EW}) \simeq 7\times 10^{-10}\frac{I_1^{(2)} - 2I_1^{(3)}}{|\Delta M_{12}^2(\mathrm{GeV}^2)|^{2/3}}. \tag{3.52}$$

Even if the CP invariants are of $\mathcal{O}(1)$, the asymmetry is too small unless there is a significant degeneracy between the two states [8]. It is important however to realise that the naive seesaw scaling is too naive and a full exploration of parameter space is necessary.

In figure 4 we plot the functions $A_{I_2^{(3)}}(t)$ and $A_{J_W}(t)$. They depend on the two neutrino mass differences, so we show three examples here: one in which there are no degeneracies, one where there are two almost degenerate states, and the case where the three states are almost degenerate. As in the previous case we see a large enhancement when only one of the mass differences is small and a further enhancement when the two are small compared to the absolute scale. In the case of A_{J_W} we find that there is a significant difference in the regime $\Delta_{ij}^{1/3}t \ll 1$ if we plot $A_{J_W}(t)$ truncated to the terms of $\mathcal{O}(y_i^6)$. As we will see in the next section, the latter is much closer to the numerical result. The reason for this difference is that at small times, $\Delta^{1/3}t \ll 1$, only some terms of order $\mathcal{O}(y_i^8)$ are kept in eqs. (3.46), while there is a strong cancellation if all had been included. Note however that this effect is only important at times where the asymmetry is suppressed and seems to affect only A_{J_W}.

It is interesting to note that even though the dependence on the yukawas of the functions $A_{I_{\rm CP}}(t)$ is different (fourth or sixth order), the maxima for all cases are roughly of the same order of magnitude. Note, however, that in the limit $t \gg \gamma_i^{-1}$, only the contribution of two invariants, J_W and $I_1^{(3)}$, survive:

$$\begin{aligned}\lim_{t\to\infty}\mathrm{Tr}[\mu](t) \simeq & -\frac{\gamma_N}{2\bar{\gamma}_N}\lim_{t\to\infty}\left[\frac{\Delta\rho_{33}(t)}{\rho_{\rm eq}}\right]_{\text{eq. (3.41)}} \\ & -\frac{2^{4/3}\pi^{3/2}}{3^{1/3}\Gamma\left[-\frac{1}{6}\right]}I_1^{(3)}\frac{y_1 y_2(y_2^2-y_1^2)}{|\Delta_{12}|^{2/3}}\left(1-\frac{\gamma_N}{\bar{\gamma}_N}\right)\gamma_N^2,\end{aligned} \tag{3.53}$$

where we kept only the leading terms $\mathcal{O}(y^4)$ proportional to $I_1^{(3)}$ and we have used the result of eq. (3.50).

JHEP10(2015)067

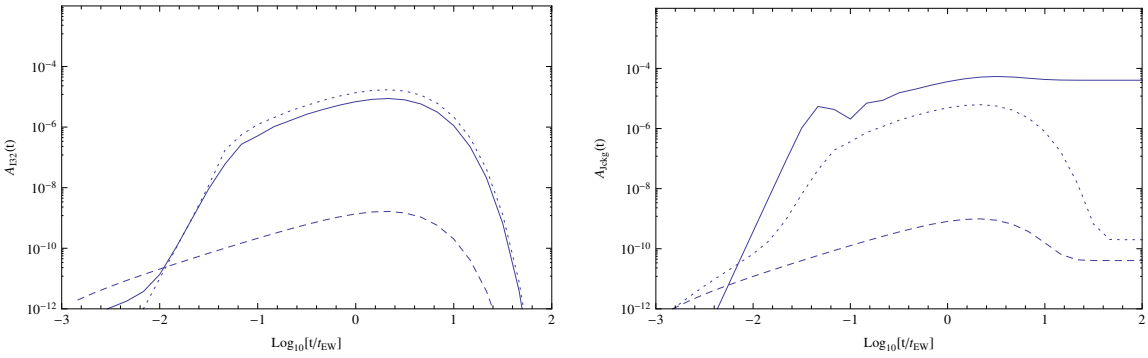

Figure 4. Functions $A_{I_2^{(3)}}(t)$ (left) and $A_{J_W}(t)$ (right) assuming the rates are dominated by top quark scattering, and taking $y_2/\sqrt{2} = y_1 = 10^{-7}$, for three choices of $[\Delta M_{12}^2, \Delta M_{13}^2] = [1, 2], [10^{-6}, 2]$ and $[10^{-6}, 2 \times 10^{-6}]$ in GeV^2 (dashed, dotted and solid). t_{EW} is the electroweak phase transition time, corresponding to $T_{\mathrm{EW}} \simeq 140\mathrm{GeV}$.

The first term in this expression corresponds to the expectation of [7], ie. the final asymmetry is proportional to that stored in the third sterile state, eq. (3.40), while the second term was missing in the simplified treatment of [7]. Note that they depend on different CP invariants.

4 Numerical solution

In order to check the accuracy of the analytical solutions presented in the previous section, we have solved the differential equations numerically. As shown in [28], the momentum dependence does not change significantly the results so we will consider the average-momentum approximation.

In figures 5–6 we compare the analytical and numerical solutions for the functions $A_{I_{\mathrm{CP}}}(t)$ in the highly degenerate case (the values of the mixing angles are of $\mathcal{O}(10^{-2})$). In order to isolate the appropriate invariant we make the following choices:

- Case 1: $\theta_{i3} = \bar{\theta}_{i3} = 0$ isolates $I_1^{(2)}$,
- Case 2: $\theta_{i3} = \bar{\theta}_{12} = 0$ isolates $I_1^{(3)}$,
- Case 3: $\theta_{12} = \bar{\theta}_{i3} = 0$ isolates $I_2^{(3)}$,
- Case 4: $\bar{\theta}_{ij} = 0$ isolates I_{J_W}.

The numerical results normalised by the corresponding CP invariant are shown together with the predictions of the previous section. In the case of J_W, we plotted the function A_{J_W} keeping only the terms of $\mathcal{O}(y^6)$ that is more accurate at small t and the full function at large t. The agreement in all cases is quite good. The differences observed at large t come from the non-linear terms in the equations. We also show the numerical results of the equations without them and find a very good agreement also at large t. Note that the approximation works well in the regime $\gamma t \gg 1$, that is in the strong washout regime of the fast modes.

JHEP10(2015)067

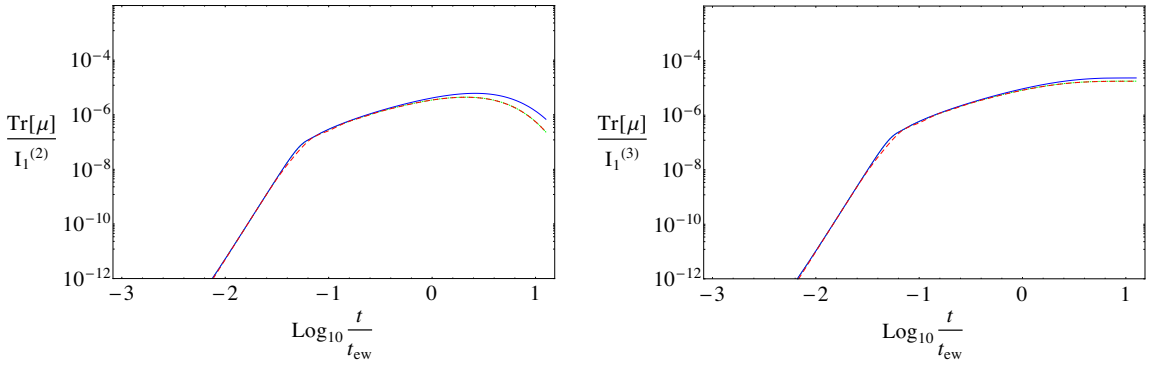

Figure 5. Left: full numerical solution (solid blue) and numerical solution neglecting non-linear terms (dotted green) for case 1, normalised to the invariant $I_1^{(2)}$, compared with the prediction, $A_{I_1^{(2)}}(t)$ (dashed red). Right: same for case 2 normalised to the invariant $I_1^{(3)}$ compared to $A_{I_1^{(3)}}(t)$. The parameters are the same as in figure 3 for the degenerate case.

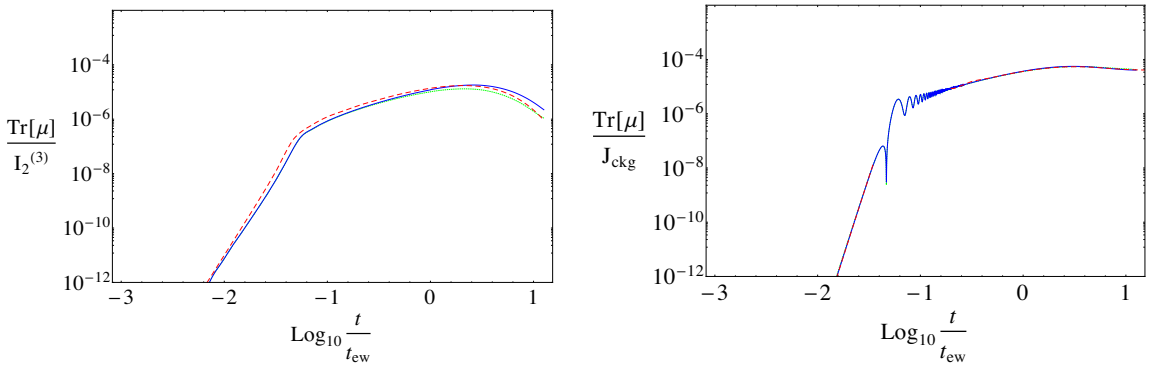

Figure 6. Left: full numerical solution (solid blue) and numerical solution neglecting non-linear terms (dotted green) for case 3, normalised to the invariant $I_2^{(3)}$, compared with the prediction, $A_{I_2^{(3)}}(t)$ (dashed red). Right: same for case 4 normalised to the invariant J_W compared to $A_{J_W}(t)$. The parameters are the same as in figure 4 for the double degenerate case.

Numerically it is very hard to go to regimes where the ratios $\gamma/|\Delta|^{1/3}$ become very small, since the system becomes stiff. On the other hand, there is no reason why the perturbative solution is not accurate in such regime. We will therefore assume this to be the case in the following section and use the perturbative solution to perform a scan of parameter space.

5 Baryon asymmetry

The observed baryon asymmetry is usually quoted in terms of the abundance, which is the number-density asymmetry of baryons normalised by the entropy. After Planck this quantity is known to per cent precision [34]:

$$Y_B^{\rm exp} \simeq 8.6(1) \times 10^{-11}. \tag{5.1}$$

JHEP10(2015)067

The lepton asymmetries in the left-handed (LH) leptons generated in the production of the sterile neutrinos are efficiently transferred via sphaleron processes [35] to the baryons. The baryon asymmetry is given by

$$Y_B = \frac{28}{79} Y_{B-L}. \tag{5.2}$$

Since we have neglected spectator processes in the transport equations, the $B-L$ asymmetry is related to the chemical potentials computed in the previous sections by the relation

$$Y_{B-L} = -\frac{90}{\pi^4 g_*} \mathrm{Tr}[\mu], \tag{5.3}$$

where $g_* = 106.75$ (which ignores the contribution to the entropy of the sterile states). Our estimate for the baryon asymmetry is therefore

$$Y_B \simeq 3 \times 10^{-3}\ \mathrm{Tr}[\mu(t)]|_{t_{\rm EW}}\,. \tag{5.4}$$

We have performed a first scan of the full parameter space of the model. Given the theoretical uncertainties mentioned in different sections of the paper, we have considered as interesting the points that can explain the baryon asymmetry within a factor of 5. For this we have used the analytical solutions, even though in some regions of parameter space they will not be precise, since they are based on a perturbative expansion on the mixing angles of the matrices V and W. We have considered however a few cases where the angles are not small and we find that the analytical solutions differ from the numerical ones only in some global numerical factor of a few (ie. safely within our factor of 10 uncertainty), but the time dependence is very similar.

Even with an analytical expression the exploration of the large parameter space is a challenge. We have used the package Multinest [11, 12] to perform a scan on the Casas-Ibarra parameters [36], where the Yukawa matrix is written as

$$Y = -iU^*_{\rm PMNS}\sqrt{m_{\rm light}}R(z_{ij})^T\sqrt{M}\frac{\sqrt{2}}{v}. \tag{5.5}$$

$m_{\rm light}$ is a diagonal matrix of the light neutrino masses and R is a complex orthogonal matrix that depends on three complex angles z_{ij}. We fix the light neutrino masses and mixings to the present best fit points in the global analysis of neutrino oscillation data of ref. [37] and leave as free parameters: three complex angles, the three phases of the PMNS matrix, the lightest neutrino mass as well as the heavy Majorana masses that are allowed to vary in the range $M_i \in [0.1, 100]\,\mathrm{GeV}$. In total thirteen free parameters.

The scan searches for minima of the quantity $|\log_{10}|Y_B(t_{\rm EW})/Y_B^{\rm exp}||$ (in the range ≤ 1.5) and the MultiNest algorithm is optimised to sample properly when there are several maxima. For the determination of Y_B we use the analytical results of the previous sections, for which the CP invariants are computed directly from the matrix elements of the V, W matrices that can be easily calculated by diagonalising the Yukawa mass matrix obtained in the Casas-Ibarra parametrization. Since the mechanism to work requires that at least one of the modes does not get to equilibrium before the electroweak phase transition we

JHEP10(2015)067

restrict the search to the range where one of the yukawa eigenvalues, y_3, is much smaller than the others and the following conditions are satisfied

$$y_3 \leq 0.01\text{Min}[y_1, y_2], \qquad \sum_{i=1,2} \Gamma_i \left(|V_{i3}|^2 + |W_{i3}|^2\right) \leq 0.01 H_u(T_{\rm EW}). \tag{5.6}$$

Furthermore, since the kinetic equations neglect lepton number violating effects in the rates, we impose additionally the constraint

$$\left(\frac{M_i}{T_{\rm EW}}\right)^2 \Gamma_i \ll H_u(T_{\rm EW}). \tag{5.7}$$

We first consider a case where one of the sterile neutrinos is effectively decoupled from baryon number generation, that we can assume to be N_3. This can be achieved with the choice of parameters:

$$m_{3(1)} = 0, \qquad z_{i3} = 0, \qquad R(z_{ij}) \to R(z_{ij})(P), \tag{5.8}$$

for the IH(NH), where P is the $123 \to 312$ permutation matrix (only necessary for the NH). With this choice, only the terms corresponding to the CP invariants $I_1^{(2)}$ and $I_1^{(3)}$ contribute. This case is the one that has been considered in most previous works on the subject [8, 9, 28, 31, 38], where the number of parameters is reduced to six: only one complex angle, two PMNS CP phases and two Majorana neutrino masses are relevant.

It is believed that a large degeneracy of the two sterile neutrinos is needed to obtain the correct baryon asymmetry. In figure 7 we show the result of the scan under the conditions of eq. (5.8) on the plane $\Delta M_{12} \equiv M_2 - M_1$ versus M_1 for normal and inverted orderings of the light neutrinos. The different colours correspond to values of $Y_B > 1/5, 1, 5 \times Y_B^{\rm exp}$ (blue,green,red). Successful leptogenesis is possible in a larger range of parameter space for IH than for NH. In the range shown our results agree reasonably well with those in ref. [39] for the IH, while the range for NH looks a bit smaller. We see that there are a significant number of points for which the degeneracy is mild for the IH. We have analysed more carefully some of these points by solving the full numerical equations. We find that even though these points correspond to cases where the angles in V, W are not small, the analytical and numerical solution agree very well and have the same t dependence as shown in figure 8. Note that the numerical solution is difficult at large times for non-degenerate solutions and the standard methods that we use fail. An optimised numerical method is needed to solve the stiffness problem and this will be studied elsewhere. It is very interesting to correlate the baryon asymmetry with observables that could be in principle measured such as the Dirac CP phase of the PMNS matrix, the amplitude of neutrinoless double beta decay or the active-sterile mixings that control the probability for the heavy sterile states to be observed in accelerators or in rare decays of heavy mesons. The effective mass entering the $0\nu\beta\beta$ decay is given by

$$m_{\beta\beta} = \sum_{i=1}^{3} U_{ei}^2 m_i + \sum_{i=1}^{3} U_{e(i+3)}^2 M_i \frac{\mathcal{M}^{0\nu\beta\beta}(M_i)}{\mathcal{M}^{0\nu\beta\beta}(0)}, \tag{5.9}$$

JHEP10(2015)067

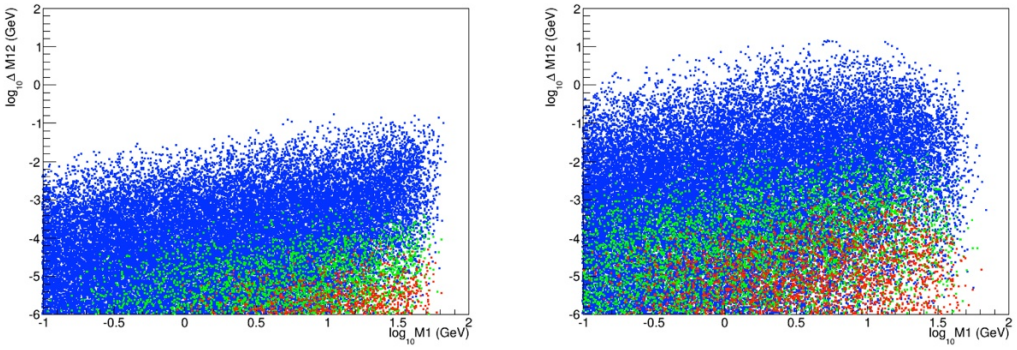

Figure 7. Points on the plane $\Delta M = M_2 - M_1$ versus M_1 for which $Y_B > 1/5 \times Y_B^{\rm exp}$ (blue), $Y_B > Y_B^{\rm exp}$ (green) and $Y_B > 5 \times Y_B^{\rm exp}$ (red) for NH (left) and IH (right), with only two sterile neutrino species.

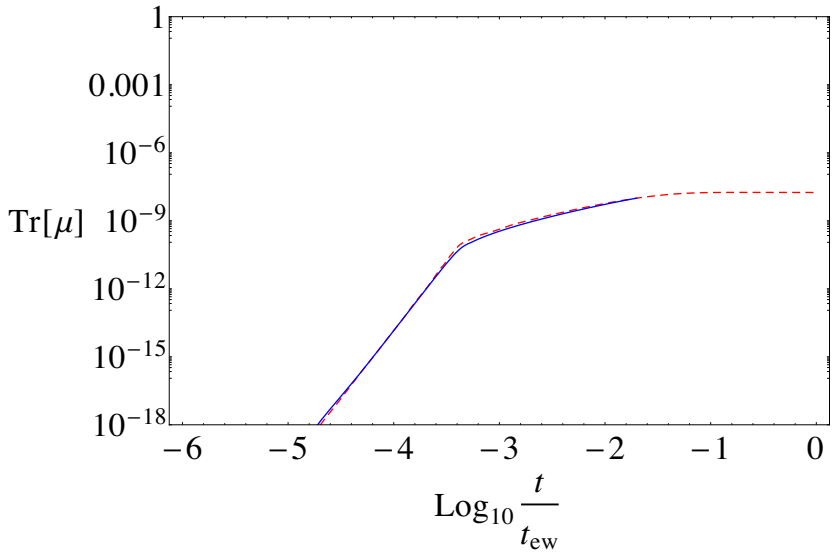

Figure 8. Comparison of the analytical (red-dashed) and numerical (blue-solid) solution for one of the points with mild degeneracy and $Y_B \geq Y_B^{\rm exp}$, corresponding to $\log_{10}(M_1(GeV)) = 0.9$ and $\log_{10}(\Delta M(GeV)) = -0.92$ and yukawa couplings $y_1 = 1.3 \times 10^{-6}, y_2 = 9.8 \times 10^{-9}$.

where $\mathcal{M}^{0\nu\beta\beta}$ are the Nuclear Matrix Elements (NMEs) defined in [40].[3] The first term corresponds to the standard light neutrino contribution and the second is the contribution from the heavy states. U_{ei} with $i \geq 4$ is the active-sterile neutrino mixing.

In figure 9 we show the results for the active-sterile mixing as function of the sterile mass and compare them with present direct bounds and the prospects of SHiP [43] and LBNE near detector [44]. We show the result for M_1 but the one for M_2 is almost identical. We see that most of the parameter space for successfull baryogenesis is not excluded by present constraints and that the active-sterile mixings tend to be larger for the IH. A

[3]The results for the NMEs computation in the interacting shell model [41, 42] are available in appendix A of [40].

JHEP10(2015)067

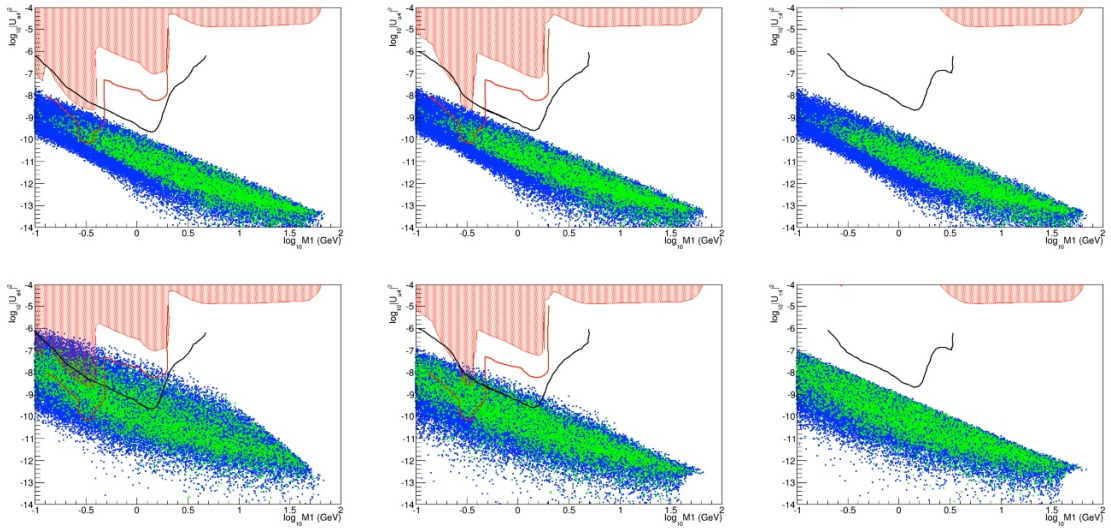

Figure 9. Points on the plane $|U_{e4}|^2$(left), $|U_{\mu 4}|^2$(middle), $|U_{\tau 4}|^2$(right) versus M_1 for which Y_B is in the range $[1/5-1]\times Y_B^{\rm exp}$ (blue) and $[1-5]\times Y_B^{\rm exp}$ (green) for NH (up) and IH (down), with only two sterile neutrino species. The red bands are the present constraints [45], the solid black line shows the reach of the SHiP experiment [43] and the solid red line is the reach of LBNE near detector [44].

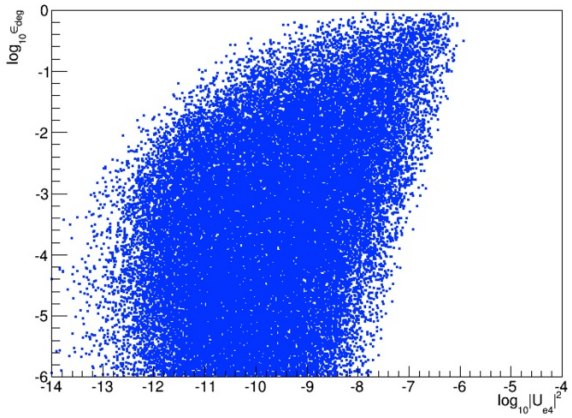

Figure 10. Points on the plane $\epsilon_{\rm deg}=\frac{|M_2-M_1|}{M_2+M_1}$ versus $|U_{e4}|^2$ for which the asymmetry is in the range $[1/5,5]\times Y_B^{\rm exp}$ in the range explored for IH.

sizeable region in the range of the GeV could be explored in the future experiment SHiP in the case of the IH and by LBNE near detectors. It is interesting to note that the less degenerate solutions can not have very small active-sterile mixing, as shown in figure 10, where we plot the points on the plane $\epsilon_{\rm deg}\equiv|M_2-M_1|/(M_2+M_1)$ versus the active-sterile mixing in the electron flavour. The degeneracy can be lifted to some extent at the expense of larger yukawa couplings which also imply larger mixings.

We have looked for direct correlations of the baryon asymmetry with the phases of the PMNS matrix. We have found that the distribution on the Dirac phase and the Majorana

JHEP10(2015)067

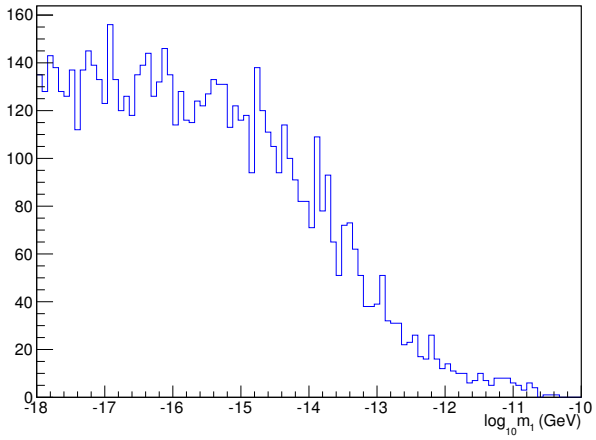

Figure 11. Distribution of m_1 for points that satisfy $Y_B > Y_B^{\rm exp}$ for the NH.

phase are flat. This is due to the fact that the complex angle can provide the necessary CP violation, even if the PMNS phases would vanish. The same is true for the effective mass of neutrinoless double beta decay, which depends on the Majorana phase. A dedicated scan is needed to quantify how the putative measurement of various observables could constrain the lepton asymmetry. This will be done elsewhere.

In the general case, N_3 is also relevant and the main difference with respect to the previous situation is that there is a significantly enlarged parameter space where degeneracy is not necessary. This was already found in refs. [46] for some points of parameter space. In figure 12 we show the points on the plane $(\Delta M_{12}, M_1)$ for the general case. The active-sterile mixings are shown in figure 13. These mixings can be larger in this case, specially in the case of the NH. The SHiP prospects are therefore more promising in this context. As in the $N = 2$ case there is no direct connection between the asymmetry and the PMNS CP phases. On the other hand, the lightest neutrino mass is non-zero in this case, but the requirement that one yukawa needs to be significantly smaller than the others, eq. (5.6), implies that the lightest neutrino mass must be small. In figure 11 we show the distribution of this quantity for those points that satisfy $Y_B \geq Y_B^{\rm exp}$ in the case of NH (the IH being very similar).

6 Conclusions

We have studied the mechanism of leptogenesis in a low-scale seesaw model that is arguably the simplest extension of the Standard Model that can account for neutrino masses. For Majorana neutrino masses in the GeV range, sizeable lepton asymmetries can be generated in the production of these states some of which never reach thermal equilibrium before the electroweak phase transition. Lepton asymmetries are efficiently transferred to baryons via sphaleron processes. This mechanism was proposed in [7, 8] and studied in many works, but a full exploration of parameter space in the general case of three neutrinos

JHEP10(2015)067

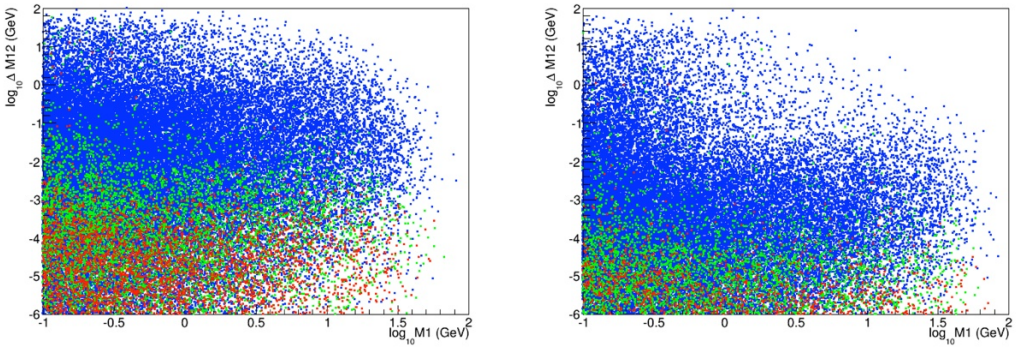

Figure 12. Points on the plane $\Delta M = M_2 - M_1$ versus M_1 for which $Y_B > 1/5 \times Y_B^{\rm exp}$ (blue), $Y_B > Y_B^{\rm exp}$ (green) and $Y_B > 5 \times Y_B^{\rm exp}$ (red) for NH (left) and IH (right), in the general case with three neutrinos.

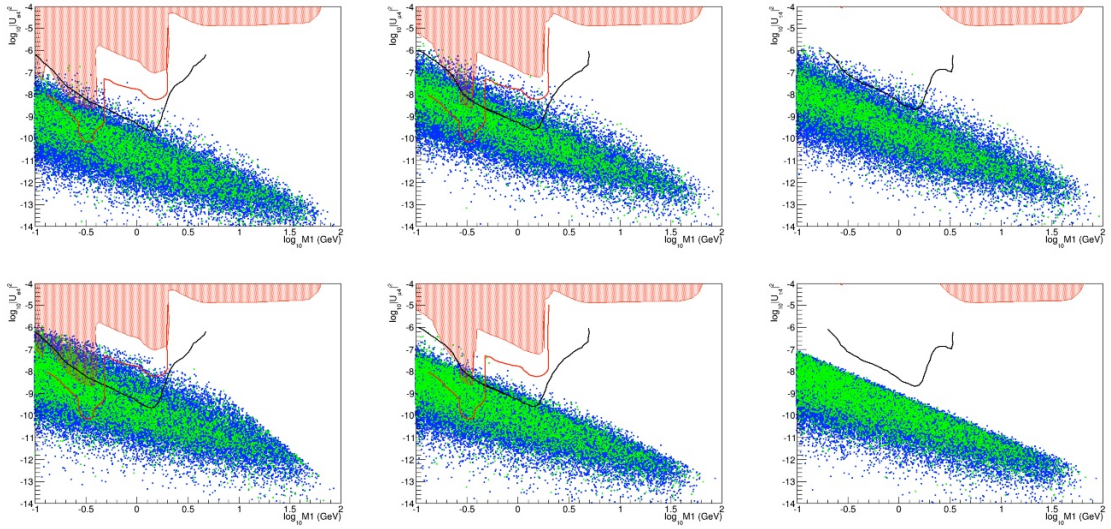

Figure 13. Points on the plane $|U_{e4}|^2$(left), $|U_{\mu 4}|^2$(middle), $|U_{\tau 4}|^2$(right) versus M_1 for which Y_B is in the range $[1/5, 1] \times Y_B^{\rm exp}$ (blue) and $[1 - 5] \times Y_B^{\rm exp}$ (green) for NH (up) and IH (down), with three sterile species. The red bands are the present constraints, the solid black line shows the reach of the SHiP experiment [43] and the solid red line is the reach of LBNE near detector [44].

is lacking. To this aim we have developed an accurate analytical approximation to the quantum kinetic equations which works both in the weak and strong washout regimes of the fast modes (there is always a slow mode that does not reach thermal equilibrium before the EW phase transition). It relies on a perturbative expansion in the mixing angles of the two unitary matrices that diagonalise the Yukawa matrix. This analytical approximation allows us to identify the relevant CP invariants, and explore with confidence the regime of non-degenerate neutrino masses which is very challenging from the numerical point of view. We have used this analytical solution to scan the full parameter space using the MultiNest package to identify the regions where the baryon asymmetry is within an order of magnitude of the experimental value. We have performed first a scan in the simpler

JHEP10(2015)067

setting where one of the sterile neutrino decouples, which reduces the parameter space, and is the approximation that has been considered in most previous works on the subject, for example in the so-called νMSM. Although baryon asymmetries tend to be larger in the case of highly degenerate neutrinos, we find solutions with a very mild degeneracy that also correlate with a larger active-sterile mixing. These non-degenerate solutions appear for an inverted ordering of the light neutrinos. On the other hand we do not observe a direct correlation with other observables, such as the PMNS CP phases nor the neutrinoless double beta decay amplitude.

We have also performed a scan in the full parameter space, with the only requirement that one of the yukawa matrix eigenvalues is very small, and that one mode will not reach equilibrium before the electroweak transition, for the washout not to be complete. The main difference with the simpler case of two neutrinos is that the parameter space with successfull baryogenesis is significantly enlarged, in particular as regards non-degenerate spectra. Also the active-sterile mixings can reach larger values, particularly in the normal hierarchy case, improving the chances of future experiments such as SHiP or LBNE to find the GeV sterile neutrinos. There is much less difference in this case between normal and inverted neutrino orderings and also no direct correlation with the PMNS phases. On the other hand, the requirement of a small yukawa eigenvalue implies that the lightest neutrino mass cannot be large.

A number of refinements are needed to improve the precision of the determination of the baryon asymmetry. First a more precise determination of the scattering rates of the sterile neutrinos is required. Most previous studies, and this one, have included only top-quark scatterings, but it has been pointed out recently that gauge scatterings are also very important. A correct treatment of these processes in the kinetic equations is necessary. Also the kinetic equations neglect effects of $\mathcal{O}((M_i/T)^2)$. Such effects are not so small for masses in the GeV near the electroweak phase transition and their effect should be quantified. Finally, spectator processes and the asymmetries of fields other than the sterile neutrinos and LH leptons have not been taken into account in the kinetic equations. A proper treatment could easily bring corrections of $\mathcal{O}(1)$. Finally, a more ambitious scan of parameter space should define more accurately the limits of eq. (5.6) for successfull baryogenesis. These effects will be studied in the future.

Acknowledgments

We wish to thank R. Ruiz de Austri, J. Martín-Albo and J.M. Martí for their help with the used software, and D. Bödeker, V. Domcke, M. Drewes and M. Laine for useful discussions. This work was partially supported by grants FPA2011-29678, FPA2014-57816-P, PROMETEOII/2014/050, CUP (CSD2008-00037), ITN INVISIBLES (Marie Curie Actions, PITN-GA-2011-289442), the INFN program on Theoretical Astroparticle Physics (TASP) and the grant 2012CPPYP7 (*Theoretical Astroparticle Physics*) under the program PRIN 2012 funded by the Italian Ministry of Education, University and Research (MIUR). PH acknowledges the support of the Aspen Center for Physics (National Science

JHEP10(2015)067

Foundation grant PHY-1066293), where this work was completed. MK thanks Fermilab for hosting her while part of this work was done.

A Results for the perturbative integrals

A.1 One dimensional integrals

We just need them up to $\mathcal{O}(\beta/\alpha)^2$:

$$J_1(\alpha_1,\beta_1,t) \simeq J_{10}(\alpha_1,t_0)+\beta_1 J_{11}(\alpha_1,t_0)+\frac{\beta_1^2}{2}J_{12}(\alpha_1,t_0)+\Delta J_1(\alpha_1,\beta_1,t,t_0), \tag{A.1}$$

with

$$\begin{aligned}\Delta J_1(\alpha_1,\beta_1,t,t_0) &= \sum_n \frac{\beta_1^n}{n!}J_{1n}(\alpha_1,t,t_0) \simeq i\sum_n \frac{\beta_1^n}{n!}\left(\frac{e^{i\frac{\alpha_1 t_0^3}{3}}}{\alpha_1 t_0^{2-n}}-\frac{e^{i\frac{\alpha_1 t^3}{3}}}{\alpha_1 t^{2-n}}\right)+\mathcal{O}(t^{-4},t_0^{-4})\\ &= i\left(\frac{e^{i\frac{\alpha_1 t_0^3}{3}+\beta_1 t_0}}{\alpha_1 t_0^2}-\frac{e^{i\frac{\alpha_1 t^3}{3}+\beta_1 t}}{\alpha_1 t^2}\right).\end{aligned} \tag{A.2}$$

We can factor out the α dependence and define:

$$J_{10}(\alpha,t)=\frac{1}{|\alpha|^{1/3}}\Big(\mathrm{Re}\big[J_{10}(1,t|\alpha|^{1/3})\big]+i\mathrm{sign}(\alpha)\mathrm{Im}\big[J_{10}(1,t|\alpha|^{1/3})\big]\Big). \tag{A.3}$$

A.2 Two dimensional integrals

We just need them up to $\mathcal{O}(\beta/\alpha)$:

$$\begin{aligned}J_2(\alpha_1,\beta_1,\alpha_2,\beta_2,t) \simeq\ & J_{200}(\alpha_1,\alpha_2,t_0)+\beta_1 J_{210}(\alpha_1,\alpha_2,t_0)+\beta_2 J_{201}(\alpha_1,\alpha_2,t_0)\\ &+\Delta J_2(\alpha_1,\beta_1,\alpha_2,\beta_2,t,t_0),\end{aligned} \tag{A.4}$$

where if $\sum_i \alpha_i \neq 0$:

$$\begin{aligned}\Delta J_2(\alpha_1,\beta_1,\alpha_2,\beta_2,t,t_0) =\ & \left(J_1(\alpha_2,\beta_2,t_0)+i\frac{e^{i\frac{\alpha_2 t_0^3}{3}+\beta_2 t_0}}{\alpha_2 t_0^2}\right)\Delta J_1(\alpha_1,\beta_1,t,t_0)\\ & -i\left(i\frac{e^{i\frac{\sum_i \alpha_i t_0^3}{3}+\sum_i \beta_i t_0}}{\alpha_2\sum_i \alpha_i t_0^4}-i\frac{e^{i\frac{\sum_i \alpha_i t^3}{3}+\sum_i \beta_i t}}{\alpha_2\sum_i \alpha_i t^4}\right),\end{aligned} \tag{A.5}$$

and for those terms where $\sum_i \alpha_i = 0$

$$\begin{aligned}\Delta J_2(\alpha_1,\beta_1,\alpha_2,\beta_2,t,t_0) =\ & \left(J_1(\alpha_2,\beta_2,t_0)+i\frac{e^{i\frac{\alpha_2 t_0^3}{3}+\beta_2 t_0}}{\alpha_2 t_0^2}\right)\Delta J_1(\alpha_1,\beta_1,t,t_0)\\ & -\frac{i}{\alpha_2}\left(\int_{t_0}^{t}\frac{e^{\sum_i \beta_i x}}{x^2}\right).\end{aligned} \tag{A.6}$$

JHEP10(2015)067

We can factorize the α-dependence:

$$J_{200}(-\alpha,\alpha,t) = \frac{1}{|\alpha|^{2/3}}\Big(\mathrm{Re}\big[J_{200}(-1,1,t|\alpha|^{1/3})\big] + i\ \mathrm{sign}(\alpha)\mathrm{Im}\big[J_{200}(-1,1,t|\alpha|^{1/3})\big]\Big),$$
$$J_{201}(-\alpha,\alpha,t) = \frac{1}{|\alpha|}\Big(\mathrm{Re}\big[J_{201}(-1,1,t|\alpha|^{1/3})\big] + i\ \mathrm{sign}(\alpha)\mathrm{Im}\big[J_{201}(-1,1,t|\alpha|^{1/3})\big]\Big),$$
$$J_{210}(-\alpha,\alpha,t) = \frac{1}{|\alpha|}\Big(\mathrm{Re}\big[J_{210}(-1,1,t|\alpha|^{1/3})\big] + i\mathrm{sign}(\alpha)\mathrm{Im}\big[J_{210}(-1,1,t|\alpha|^{1/3})\big]\Big), \quad (A.7)$$

and reduce the integrals to the basic ones.

A.3 Three dimensional integrals

We need the integrals up to $\mathcal{O}(\beta/\alpha)^0$ in this case. We can use the relation:

$$J_{\mathbf{30}}(\alpha_1,\alpha_2,\alpha_3,t) = J_{10}(\alpha_1,t)J_{200}(\alpha_2,\alpha_3,t) - \int_0^t dx\ e^{\frac{i\alpha_2 x^3}{3}} J_{10}(\alpha_1,x)J_{10}(\alpha_3,x). \quad (A.8)$$

Since $\sum_i \alpha_i = 0$ for the cases of interest, we can rewrite the result in terms of some basic integrals, I_1 and I_2:

$$J_{200}(\alpha_1,\alpha_2,t) = \frac{1}{|\alpha_1\alpha_2|^{1/3}} I_1\big(|\alpha_2/\alpha_1|,\mathrm{sign}(\alpha_2),\mathrm{sign}(\alpha_1),t|\alpha_1|^{1/3}\big), \quad (A.9)$$

and

$$\int_0^t dx\ e^{\frac{i\alpha_2 x^3}{3}} J_{10}(\alpha_1,x)J_{10}(\alpha_3,x) = \frac{I_2\big(|\alpha_1/\alpha_2|,\mathrm{sign}(\alpha_1),\mathrm{sign}(\alpha_3),\mathrm{sign}(\alpha_2),t|\alpha_2|^{1/3}\big)}{|\alpha_1\alpha_2\alpha_3|^{1/3}}, \quad (A.10)$$

where

$$I_1(r,s_1,s_2,t) \equiv \int_0^t dx\ e^{is_2x^3/3} J_{10}(s_1,r^{1/3}x), \quad (A.11)$$
$$I_2(r,s_1,s_2,s_3,t) \equiv \int_0^t dx\ e^{is_3x^3/3} J_{10}(s_1,r^{1/3}t)J_{10}(s_2,(-s_3/s_2-s_1/s_2r)^{1/3}t). \quad (A.12)$$

B Pertubative results for the invariants J_W and $I_2^{(3)}$

The finite t perturbative results proportional to the invariants J_W are given by the following expressions (we have used the property $\gamma_i \propto v_i$ to simplify them):

$$A_{J_W}(t) = \gamma_1\gamma_2\left(1-\frac{\gamma_N}{\bar\gamma_N}\right)G_{41}(t) - \frac{\gamma_N}{2\bar\gamma_N}G_{42}(t), \quad (B.1)$$

where

$$G_{41}(t) \equiv \sum_{k=1}^{2}(-1)^k\ e^{-\bar\gamma_k t}\Bigg\{ \sum_{i<j}\mathrm{Re}\Big[a_{ij}J_{20}(\Delta_{ij},-\Delta_{ij},t_0)+b_{ij}J_{201}(\Delta_{ij},-\Delta_{ij},t_0)+c_{ij}^{(k)}(t)J_{210}(\Delta_{ij},-\Delta_{ij},t_0)\Big]\Bigg\}, \quad (B.2)$$

JHEP10(2015)067

with

$$
\begin{aligned}
&a_{12}=i, \qquad b_{12}=2\Delta_v, \qquad c_{12}^{(k)}=-\Delta_v+\frac{i}{2}(2\bar{\gamma}_k-\gamma_1-\gamma_2),\\
&a_{13}=-i, \qquad b_{13}=2v_1, \qquad c_{13}^{(k)}=-v_1-\frac{i}{2}(2\bar{\gamma}_k-\gamma_1),\\
&a_{23}=i, \qquad b_{23}=-2v_2, \qquad c_{23}^{(k)}=v_2+\frac{i}{2}(2\bar{\gamma}_k-\gamma_2),
\end{aligned}
$$

and $\Delta_v \equiv v_2 - v_1$, $\Delta_\gamma \equiv (\gamma_2 - \gamma_1)$.

$$
\begin{aligned}
G_{42}(t) \equiv \mathrm{Re}\Big[&d_1 J_{30}(\Delta_{12}-\Delta_{13},-\Delta_{12},\Delta_{13},t)+d_2 J_{30}(\Delta_{12}-\Delta_{13},\Delta_{13},-\Delta_{12},t)\\
&+d_3 J_{30}(\Delta_{13},\Delta_{12}-\Delta_{13},-\Delta_{12},t)+d_4 J_{30}(\Delta_{13},-\Delta_{12},\Delta_{12}-\Delta_{13},t)\\
&+d_5 J_{30}(\Delta_{12},-\Delta_{12}+\Delta_{13},-\Delta_{13},t)+d_6 J_{30}(\Delta_{12},-\Delta_{13},-\Delta_{12}+\Delta_{13},t)\Big],
\end{aligned}
\tag{B.3}
$$

with

$$
\begin{aligned}
d_1 &= z_1 + i\frac{\gamma_1}{2}\big[2\Delta_v + i\Delta_\gamma\big]\big[2v_2 - i(2\bar{\gamma}_2-\gamma_2)\big]e^{-\bar{\gamma}_2 t},\\
d_2 &= z_2 + i\frac{\Delta_\gamma}{2}\big[-2v_1 + i\gamma_1\big]\big[2v_2 - i(2\bar{\gamma}_2-\gamma_2)\big]e^{-\bar{\gamma}_2 t},\\
d_3 &= z_2 - i\frac{\Delta_\gamma}{2}\big[2v_2 + i\gamma_2\big]\big[2v_1 + i\big(2\bar{\gamma}_1-\gamma_1\big)\big]e^{-\bar{\gamma}_1 t},\\
d_4 &= z_3 + i\frac{\gamma_2}{2}\big[2\Delta_v - i\Delta_\gamma\big]\big[2v_1 + i(2\bar{\gamma}_1-\gamma_1)\big]e^{-\bar{\gamma}_1 t},\\
d_5 &= \frac{\gamma_1}{2}\big(2v_2 + i\gamma_2\big)\Big[e^{-\bar{\gamma}_1 t}(2i\Delta_v + 2\bar{\gamma}_1 - \gamma_1 - \gamma_2) - e^{-\bar{\gamma}_2 t}(2i\Delta_v + 2\bar{\gamma}_2 - \gamma_1 - \gamma_2)\Big],\\
d_6 &= -\frac{\gamma_2}{2}\big(2v_1 - i\gamma_1\big)\Big[e^{-\bar{\gamma}_1 t}(2i\Delta_v + 2\bar{\gamma}_1 - \gamma_1 - \gamma_2) - e^{-\bar{\gamma}_2 t}(2i\Delta_v + 2\bar{\gamma}_2 - \gamma_1 - \gamma_2)\Big].
\end{aligned}
\tag{B.4}
$$

On the other hand, for the invariant $I_2^{(3)}$

$$
A_{I_2^{(3)}}(t) = y_1 y_2 \left(1 - \frac{\gamma_N}{\bar{\gamma}_N}\right)\gamma_N G_3(t), \tag{B.5}
$$

$$
\begin{aligned}
G_3(t) \equiv \sum_{k=1}^{2}(-1)^k\, e^{-\bar{\gamma}_k t}\Bigg\{ &\sum_{i<j}\mathrm{Re}\Big[a'_{ij}J_{20}(\Delta_{ij},-\Delta_{ij},t_0)+b'_{ij}(t)J_{201}(\Delta_{ij},-\Delta_{ij},t_0)\\
&+c'^{(k)}_{ij}(t)J_{210}(\Delta_{ij},-\Delta_{ij},t_0)\Big]+\mathrm{Re}\Big[w_1 J_{30}(\Delta_{12},-\Delta_{12}+\Delta_{13},-\Delta_{13},t)\\
&+w_2 J_{30}(\Delta_{12},-\Delta_{13},-\Delta_{12}+\Delta_{13},t)\Big]\Bigg\},
\end{aligned}
\tag{B.6}
$$

JHEP10(2015)067

with

$$w_1 = \frac{1}{2}\left[2v_2\gamma_1 + i\gamma_1\gamma_2\right], \qquad w_2 = \frac{1}{2}\left[-2v_1\gamma_2 + i\gamma_1\gamma_2\right], \tag{B.7}$$

and

$$\begin{aligned}
a'_{12} &= i\gamma_2, & b'_{12} &= 2\gamma_2 v_2 - v_1\gamma_2 - v_2\gamma_1, & c'^{(k)}_{12} &= \frac{1}{2}\gamma_2\Big(-2\Delta_v + i(2\bar{\gamma}_k - \gamma_2 - \gamma_1)\Big),\\
a'_{13} &= -i\gamma_1, & b'_{13} &= 2\gamma_1 v_1, & c'^{(k)}_{13} &= -\frac{1}{2}\gamma_1\Big(2v_1 + i(2\bar{\gamma}_k - \gamma_1)\Big),\\
a'_{23} &= i\gamma_2, & b'_{23} &= -2\gamma_2 v_2, & c'^{(k)}_{23} &= \frac{1}{2}\gamma_2\Big(2v_2 + i(2\bar{\gamma}_k - \gamma_2)\Big).
\end{aligned}$$

Open Access. This article is distributed under the terms of the Creative Commons Attribution License (CC-BY 4.0), which permits any use, distribution and reproduction in any medium, provided the original author(s) and source are credited.

References

[1] M. Fukugita and T. Yanagida, *Baryogenesis Without Grand Unification*, *Phys. Lett.* **B 174** (1986) 45 [INSPIRE].

[2] S. Davidson, E. Nardi and Y. Nir, *Leptogenesis*, *Phys. Rept.* **466** (2008) 105 [arXiv:0802.2962] [INSPIRE].

[3] S. Davidson and A. Ibarra, *A Lower bound on the right-handed neutrino mass from leptogenesis*, *Phys. Lett.* **B 535** (2002) 25 [hep-ph/0202239] [INSPIRE].

[4] T. Hambye, Y. Lin, A. Notari, M. Papucci and A. Strumia, *Constraints on neutrino masses from leptogenesis models*, *Nucl. Phys.* **B 695** (2004) 169 [hep-ph/0312203] [INSPIRE].

[5] J. Racker, M. Peña and N. Rius, *Leptogenesis with small violation of $B - L$*, *JCAP* **07** (2012) 030 [arXiv:1205.1948] [INSPIRE].

[6] A. Pilaftsis and T.E.J. Underwood, *Resonant leptogenesis*, *Nucl. Phys.* **B 692** (2004) 303 [hep-ph/0309342] [INSPIRE].

[7] E.K. Akhmedov, V.A. Rubakov and A.Yu. Smirnov, *Baryogenesis via neutrino oscillations*, *Phys. Rev. Lett.* **81** (1998) 1359 [hep-ph/9803255] [INSPIRE].

[8] T. Asaka and M. Shaposhnikov, *The νMSM, dark matter and baryon asymmetry of the Universe*, *Phys. Lett.* **B 620** (2005) 17 [hep-ph/0505013] [INSPIRE].

[9] M. Shaposhnikov, *The νMSM, leptonic asymmetries and properties of singlet fermions*, *JHEP* **08** (2008) 008 [arXiv:0804.4542] [INSPIRE].

[10] L. Canetti, M. Drewes, T. Frossard and M. Shaposhnikov, *Dark Matter, Baryogenesis and Neutrino Oscillations from Right Handed Neutrinos*, *Phys. Rev.* **D 87** (2013) 093006 [arXiv:1208.4607] [INSPIRE].

[11] F. Feroz and M.P. Hobson, *Multimodal nested sampling: an efficient and robust alternative to MCMC methods for astronomical data analysis*, *Mon. Not. Roy. Astron. Soc.* **384** (2008) 449 [arXiv:0704.3704] [INSPIRE].

[12] F. Feroz, M.P. Hobson and M. Bridges, *MultiNest: an efficient and robust Bayesian inference tool for cosmology and particle physics*, *Mon. Not. Roy. Astron. Soc.* **398** (2009) 1601 [arXiv:0809.3437] [INSPIRE].

JHEP10(2015)067

[13] A. de Gouvêa, W.-C. Huang and J. Jenkins, *Pseudo-Dirac Neutrinos in the New Standard Model*, *Phys. Rev.* **D 80** (2009) 073007 [arXiv:0906.1611] [INSPIRE].

[14] A. de Gouvêa and W.-C. Huang, *Constraining the (Low-Energy) Type-I Seesaw*, *Phys. Rev.* **D 85** (2012) 053006 [arXiv:1110.6122] [INSPIRE].

[15] A. Donini, P. Hernández, J. López-Pavón and M. Maltoni, *Minimal models with light sterile neutrinos*, *JHEP* **07** (2011) 105 [arXiv:1106.0064] [INSPIRE].

[16] A. Donini, P. Hernández, J. López-Pavón, M. Maltoni and T. Schwetz, *The minimal* $3+2$ *neutrino model versus oscillation anomalies*, *JHEP* **07** (2012) 161 [arXiv:1205.5230] [INSPIRE].

[17] A.D. Dolgov, S.H. Hansen, G. Raffelt and D.V. Semikoz, *Cosmological and astrophysical bounds on a heavy sterile neutrino and the KARMEN anomaly*, *Nucl. Phys.* **B 580** (2000) 331 [hep-ph/0002223] [INSPIRE].

[18] A.D. Dolgov, S.H. Hansen, G. Raffelt and D.V. Semikoz, *Heavy sterile neutrinos: Bounds from big bang nucleosynthesis and SN1987A*, *Nucl. Phys.* **B 590** (2000) 562 [hep-ph/0008138] [INSPIRE].

[19] O. Ruchayskiy and A. Ivashko, *Restrictions on the lifetime of sterile neutrinos from primordial nucleosynthesis*, *JCAP* **10** (2012) 014 [arXiv:1202.2841] [INSPIRE].

[20] P. Hernández, M. Kekic and J. López-Pavón, *Low-scale seesaw models versus* $N_{\rm eff}$, *Phys. Rev.* **D 89** (2014) 073009 [arXiv:1311.2614] [INSPIRE].

[21] P. Hernández, M. Kekic and J. López-Pavón, $N_{\rm eff}$ *in low-scale seesaw models versus the lightest neutrino mass*, *Phys. Rev.* **D 90** (2014) 065033 [arXiv:1406.2961] [INSPIRE].

[22] M. Drewes and B. Garbrecht, *Experimental and cosmological constraints on heavy neutrinos*, arXiv:1502.00477 [INSPIRE].

[23] G.C. Branco, T. Morozumi, B.M. Nobre and M.N. Rebelo, *A Bridge between CP-violation at low-energies and leptogenesis*, *Nucl. Phys.* **B 617** (2001) 475 [hep-ph/0107164] [INSPIRE].

[24] E.E. Jenkins and A.V. Manohar, *Rephasing Invariants of Quark and Lepton Mixing Matrices*, *Nucl. Phys.* **B 792** (2008) 187 [arXiv:0706.4313] [INSPIRE].

[25] L. Covi, E. Roulet and F. Vissani, *CP violating decays in leptogenesis scenarios*, *Phys. Lett.* **B 384** (1996) 169 [SISSA-66-96-EP] [IC-96-73] [hep-ph/9605319] [INSPIRE].

[26] G. Sigl and G. Raffelt, *General kinetic description of relativistic mixed neutrinos*, *Nucl. Phys.* **B 406** (1993) 423 [INSPIRE].

[27] E. Nardi, Y. Nir, J. Racker and E. Roulet, *On Higgs and sphaleron effects during the leptogenesis era*, *JHEP* **01** (2006) 068 [hep-ph/0512052] [INSPIRE].

[28] T. Asaka, S. Eijima and H. Ishida, *Kinetic Equations for Baryogenesis via Sterile Neutrino Oscillation*, *JCAP* **02** (2012) 021 [arXiv:1112.5565] [INSPIRE].

[29] M.A. Luty, *Baryogenesis via leptogenesis*, *Phys. Rev.* **D 45** (1992) 455 [INSPIRE].

[30] D. Besak and D. Bödeker, *Thermal production of ultrarelativistic right-handed neutrinos: Complete leading-order results*, *JCAP* **03** (2012) 029 [arXiv:1202.1288] [INSPIRE].

[31] B. Shuve and I. Yavin, *Baryogenesis through Neutrino Oscillations: A Unified Perspective*, *Phys. Rev.* **D 89** (2014) 075014 [arXiv:1401.2459] [INSPIRE].

JHEP10(2015)067

[32] I. Ghisoiu and M. Laine, *Right-handed neutrino production rate at $T > 160\,GeV$*, *JCAP* **12** (2014) 032 [arXiv:1411.1765] [INSPIRE].

[33] A. Abada, G. Arcadi, V. Domcke and M. Lucente, *Lepton number violation as a key to low-scale leptogenesis*, arXiv:1507.06215 [INSPIRE].

[34] PLANCK collaboration, P.A.R. Ade et al., *Planck 2013 results. XVI. Cosmological parameters*, *Astron. Astrophys.* **571** (2014) A16 [arXiv:1303.5076] [INSPIRE].

[35] V.A. Kuzmin, V.A. Rubakov and M.E. Shaposhnikov, *On the Anomalous Electroweak Baryon Number Nonconservation in the Early Universe*, *Phys. Lett.* **B 155** (1985) 36 [INSPIRE].

[36] J.A. Casas and A. Ibarra, *Oscillating neutrinos and $\mu \to e, \gamma$*, *Nucl. Phys.* **B 618** (2001) 171 [hep-ph/0103065] [INSPIRE].

[37] M.C. Gonzalez-Garcia, M. Maltoni and T. Schwetz, *Updated fit to three neutrino mixing: status of leptonic CP-violation*, *JHEP* **11** (2014) 052 [arXiv:1409.5439] [INSPIRE].

[38] L. Canetti and M. Shaposhnikov, *Baryon Asymmetry of the Universe in the νMSM*, *JCAP* **09** (2010) 001 [arXiv:1006.0133] [INSPIRE].

[39] T. Asaka and S. Eijima, *Direct Search for Right-handed Neutrinos and Neutrinoless Double Beta Decay*, *Prog. Theor. Exp. Phys.* **2013** (2013) 113B02 [arXiv:1308.3550] [INSPIRE].

[40] M. Blennow, E. Fernandez-Martinez, J. López-Pavón and J. Menendez, *Neutrinoless double beta decay in seesaw models*, *JHEP* **07** (2010) 096 [arXiv:1005.3240] [INSPIRE].

[41] E. Caurier, G. Martinez-Pinedo, F. Nowacki, A. Poves and A.P. Zuker, *The Shell model as unified view of nuclear structure*, *Rev. Mod. Phys.* **77** (2005) 427 [nucl-th/0402046] [INSPIRE].

[42] E. Caurier, J. Menendez, F. Nowacki and A. Poves, *The Influence of pairing on the nuclear matrix elements of the neutrinoless $\beta\beta$ decays*, *Phys. Rev. Lett.* **100** (2008) 052503 [arXiv:0709.2137] [INSPIRE].

[43] S. Alekhin et al., *A facility to Search for Hidden Particles at the CERN SPS: the SHiP physics case*, arXiv:1504.04855 [INSPIRE].

[44] LBNE collaboration, C. Adams et al., *The Long-Baseline Neutrino Experiment: Exploring Fundamental Symmetries of the Universe*, arXiv:1307.7335 [INSPIRE].

[45] A. Atre, T. Han, S. Pascoli and B. Zhang, *The Search for Heavy Majorana Neutrinos*, *JHEP* **05** (2009) 030 [arXiv:0901.3589] [INSPIRE].

[46] M. Drewes and B. Garbrecht, *Leptogenesis from a GeV Seesaw without Mass Degeneracy*, *JHEP* **03** (2013) 096 [arXiv:1206.5537] [INSPIRE].

JHEP10(2015)067

JHEP

Published for SISSA by Springer

Received: July 5, 2016
Revised: July 28, 2016
Accepted: August 15, 2016
Published: August 26, 2016

Testable baryogenesis in seesaw models

P. Hernández,[a] **M. Kekic,**[a] **J. López-Pavón,**[b] **J. Racker**[a] **and J. Salvado**[a]

[a] *Instituto de Física Corpuscular, Universidad de Valencia and CSIC, Edificio Institutos Investigación, Catedrático José Beltrán 2, 46980 Spain*

[b] *INFN, Sezione di Genova, via Dodecaneso 33, 16146 Genova, Italy*

E-mail: m.pilar.hernandez@uv.es, marija.kekic@ific.uv.es, jacobo.lopez.pavon@ge.infn.it, juandiego.racker@gmail.com, jor.salvado@gmail.com

Abstract: We revisit the production of baryon asymmetries in the minimal type I seesaw model with heavy Majorana singlets in the GeV range. In particular we include "washout" effects from scattering processes with gauge bosons, Higgs decays and inverse decays, besides the dominant top scatterings. We show that in the minimal model with two singlets, and for an inverted light neutrino ordering, future measurements from SHiP and neutrinoless double beta decay could in principle provide sufficient information to predict the matter-antimatter asymmetry in the universe. We also show that SHiP measurements could provide very valuable information on the PMNS CP phases.

Keywords: Cosmology of Theories beyond the SM, CP violation, Neutrino Physics, Beyond Standard Model

ArXiv ePrint: 1606.06719

Open Access, © The Authors.
Article funded by SCOAP[3].

doi:10.1007/JHEP08(2016)157

JHEP08(2016)157

Contents

1 Introduction

It is well known that minimal extensions of the Standard Model that accommodate massive neutrinos, such as the type I seesaw models, could also explain the observed matter-antimatter asymmetry in the universe [1]. The two new ingredients that make this possible are the existence of new particles that are not in thermal equilibrium sometime before the electroweak phase transition ($T_{EW} \simeq 140$GeV) and the presence of new CP-violating interactions of these particles.

Two basic scenarios have been shown to work. In the first one, the heavy Majorana singlets decay out of equilibrium generating a lepton asymmetry that sphaleron processes recycle into a baryonic one. These neutrinos have masses well above the electroweak scale, typically $M \gtrsim 10^8 - 10^9$ GeV [2, 3] and $M \gtrsim 10^6$ GeV when $B - L$ is almost conserved [4], while in resonant leptogenesis masses in the TeV scale are possible [5]. For a comprehensive review and references of this very well studied scenario see ref. [6]. In the second scenario, the heavy Majorana singlets have masses below the electroweak scale, and therefore their Yukawa couplings are small enough that one or more of these states might not reach thermal equilibrium by the time the electroweak phase transition takes place. A lepton (and baryon) asymmetry can be generated when the states are being produced, i.e. at freeze-in. The sterile states get populated via Yukawa interactions, but the coherence between collisions is essential to produce a CP asymmetry, via the interference of CP-odd and CP-even phases. This is why this mechanism is often referred-to as baryogenesis from neutrino oscillations. It was first proposed by Akhmedov, Rubakov and Smirnov (ARS) in their pioneering work [7] and pursued, with important refinements in references [8, 9]. A list of recent references is [10–15].

In [15], we studied this second scenario and explored the available phase space for successful leptogenesis in the minimal models with two or three extra singlets, $N = 2, 3$.

JHEP08(2016)157

In particular we considered an accurate analytical approximation, where we could identify the relevant CP invariants, and that helped us explore the full parameter space. The case with $N = 2$ is effectively equivalent to the popular νMSM [8], which is a $N = 2+1$ model, where the lighter neutrino plays the role of dark matter and decouples from the problem in the generation of the baryon asymmetry. The original ARS scenario on the other hand required the interplay of all the three species. The analytical approximation of [15] allowed to clarify these different scenarios.

The purpose of this paper is twofold. First, we will refine our previous study in various aspects. In [15] (like in most previous works) the collision terms only included the dominant top quark scatterings. As has been known for sometime [16, 17], scatterings off gauge bosons, as well as the resumed decays and inverse decay processes, are also very important. These rates have been computed in [17, 18] in the limit of vanishing leptonic chemical potentials. In the generation of lepton asymmetries, it is very important however to include the effect of the latter, since these will tend to washout the asymmetry. In section 2 we derive new kinetic equations including all the scattering processes considered in [17, 18], that we have re-evaluated in the presence of small leptonic chemical potentials. Furthermore Fermi-Bose statistics is consistently used through-out.

The second important improvement concerns our scans of parameter space. In our previous study we speeded-up the scan using the analytical approximation. This forced us to avoid some regions in parameter space, to ensure that the approximation was good enough. We have now optimized significantly the numerical solution of the kinetic equations, in particular addressing the stiffness problem. The analytical approximation is no longer needed, and therefore the ad hoc constraints on parameter space are avoided. We use a Bayesian approach to extract posterior probabilities on the relevant observables of the model, from a prediction of the measured baryon asymmetry, using the Multinest package. In section 3, we present the results of these scans of parameter space.

In the second part of the paper, we address the question: to what extent it would be possible to predict quantitatively the baryon asymmetry, within the minimal model $N = 2$, if the heavy neutrino states would be discovered in future experiments, such as SHiP. In section 4, we derive approximate analytical formulae valid in the range within SHiP reach, which demonstrate the complementarity of the different measurements: mixings and masses of the extra states from direct searches, neutrinoless double beta decay and the CP phase measurable in neutrino oscillations. The numerical study confirms these expectations and allows us to answer the question in the affirmative if nature is kind enough to provide us with positive signals at SHiP and an inverted neutrino ordering. Furthermore we show how such SHiP measurements could constrain the CP-violating phases of the PMNS matrix.

2 Kinetic equations

The Lagrangian of the model is given by:

$$\mathcal{L} = \mathcal{L}_{SM} - \sum_{\alpha,i} \bar{L}^{\alpha} Y^{\alpha i} \tilde{\Phi} N_R^i - \sum_{i,j=1}^{3} \frac{1}{2} \bar{N}_R^{ic} M^{ij} N_R^j + h.c.,$$

JHEP08(2016)157

where Y is a 3×3 complex matrix and M a symmetric matrix. One convenient parametrization is in terms of the eigenvalues of the Y and M matrices, together with two unitary matrices, V and W. In the basis where the Majorana mass is diagonal, $M = \mathrm{Diag}(M_1, M_2, M_3)$, the neutrino Yukawa matrix is given by:

$$Y \equiv V^\dagger \mathrm{Diag}(y_1, y_2, y_3) W. \tag{2.1}$$

Without loss of generality, using rephasing invariance, we can reduce the unitary matrices to the form:

$$\begin{aligned} W &= U\left(\phi_{12}, \phi_{13}, \phi_{23}, d\right)^\dagger \mathrm{Diag}\left(1, e^{i\alpha_1}, e^{i\alpha_2}\right), \\ V &= \mathrm{Diag}\left(1, e^{i\beta_1}, e^{i\beta_2}\right) U\left(\bar{\phi}_{12}, \bar{\phi}_{13}, \bar{\phi}_{23}, \bar{d}\right), \end{aligned} \tag{2.2}$$

where[1]

$$U(\alpha,\beta,\gamma,\delta) \equiv \begin{pmatrix} \cos\alpha & \sin\alpha & 0 \\ -\sin\alpha & \cos\alpha & 0 \\ 0 & 0 & 1 \end{pmatrix} \begin{pmatrix} \cos\beta & 0 & \sin\beta e^{-i\delta} \\ 0 & 1 & 0 \\ -\sin\beta e^{i\delta} & 0 & \cos\beta \end{pmatrix} \begin{pmatrix} 1 & 0 & 0 \\ 0 & \cos\gamma & \sin\gamma \\ 0 & -\sin\gamma & \cos\gamma \end{pmatrix}. \tag{2.3}$$

Obviously not all the parameters are free, since this model must reproduce the light neutrino masses, which approximately implies the seesaw relation:

$$m_\nu \simeq -\frac{v^2}{2} Y \frac{1}{M} Y^T, \tag{2.4}$$

where $v = 246\,\mathrm{GeV}$ is the vev of the Higgs. A very convenient parametrization that takes this constraint into account is the Casas-Ibarra one [19], where the Yukawa matrix can be written in terms of the light neutrino masses and mixings as

$$Y = -i U^*_{\mathrm{PMNS}} \sqrt{m_{\mathrm{light}}}\, R(z_{ij})^T \sqrt{M} \frac{\sqrt{2}}{v}, \tag{2.5}$$

where m_{light} is a diagonal matrix of the light neutrino masses, $U_{\mathrm{PMNS}}(\theta_{12}, \theta_{13}, \theta_{23}, \delta, \phi_1, \phi_2)$ is the PMNS matrix that describes the light neutrino mixing, M is the diagonal matrix of the heavy neutrino masses, and R is a complex orthogonal matrix, that depends generically on one (three) complex angle(s) z_{ij} for $N = 2$ ($N = 3$).

The kinetic equations that describe the production of sterile neutrinos in the early Universe have been studied in many previous works, see for example [11–13]. In this work we have rederived these equations with the following refinements with respect to our previous work [15]:

- Fermi-Dirac or Bose-Einstein statistics is kept throughout
- Collision terms include $2 \leftrightarrow 2$ scatterings at tree level with top quarks and gauge bosons, as well as $1 \leftrightarrow 2$ scatterings including the resummation of scatterings mediated by soft gauge bosons as obtained in refs. [16–18]

[1] Note the unconventional ordering of the 2×2 rotation matrices in U.

JHEP08(2016)157

- Leptonic chemical potentials are kept in all collision terms to linear order
- Include spectator processes

As usual we assume that all the spectator particles are in kinetic equilibrium. On the other hand, we neglect the effects of the top quark and Higgs chemical potentials. These effects are expected to be smaller than the effect of thermal masses in $2 \leftrightarrow 2$ processes that we are neglecting. Note that, in contrast with the effects of the lepton chemical potential, the former do not bring in any new flavour structure.

The starting point to derive the equations is the Raffelt-Sigl formalism [20], where the sterile neutrino density satisfies the equation:

$$\frac{d\rho_N(k)}{dt} = -i[H, \rho_N(k)] - \frac{1}{2}\left\{\Gamma^a_N, \rho_N\right\} + \frac{1}{2}\left\{\Gamma^p_N, 1-\rho_N\right\}, \tag{2.6}$$

where

$$H \equiv \frac{M^2}{2k_0} + V_N(k), \quad V_N(k) \equiv \frac{T^2}{8k_0} Y^\dagger Y, \tag{2.7}$$

and $\Gamma^a_N(k)$ and $\Gamma^p_N(k)$ are the annihilation and production rates of the sterile neutrinos.

The result can be written as

$$\begin{aligned}
\Gamma^p_{Nij} &= Y^\dagger_{i\alpha}\rho_F\left(\frac{k_0}{T} - \mu_\alpha\right)\gamma_N(k,\mu_\alpha)Y_{\alpha j}, \\
\Gamma^a_{Nij} &= Y^\dagger_{i\alpha}\left(1 - \rho_F\left(\frac{k_0}{T} - \mu_\alpha\right)\right)\gamma_N(k,\mu_\alpha)Y_{\alpha j},
\end{aligned} \tag{2.8}$$

where $\rho_F(y) = (\exp y + 1)^{-1}$ is the Fermi-Dirac distribution and μ_α is the leptonic chemical potential normalised by the temperature. γ_N contain the contributions from all $2 \to 2$ processes that produce an N:

$$\bar{Q}t \to \bar{l}N;\ tl \to QN;\ \bar{Q}l \to \bar{t}N;\ Wl \to \bar{\phi}N;\ l\phi \to WN;\ W\phi \to \bar{l}N, \tag{2.9}$$

and $1 \leftrightarrow 2$ processes: $\phi \to \bar{l}N$ including resummed soft-gauge interactions. All these contributions have been computed for vanishing leptonic chemical potential in [10, 17, 18]. We have followed their methods including the effects of a lepton chemical potential to linear order.

Defining

$$\gamma_N(k,\mu_\alpha) \simeq \gamma^{(0)}_N(k) + \gamma^{(2)}_N(k)\mu_\alpha, \tag{2.10}$$

and

$$\gamma^{(1)}_N \equiv \gamma^{(2)}_N - \frac{\rho'_F}{\rho_F}\gamma^{(0)}_N, \tag{2.11}$$

with $\rho'_F(y) \equiv \frac{d\rho_F(y)}{dy}$, the functions $\gamma^{(i)}_N$ get contributions from quark (Q), gauge scattering (V) and the $1 \to 2$ resummed processes (LPM):

$$\gamma^{(i)}_N = \gamma^{(i)}_{LPM} + y_t^2\gamma^{(i)}_Q + (3g^2 + g'^2)\left(\gamma^{(i)}_V + \gamma^{(i)}_{IR}\log\left(\frac{1}{3g^2+g'^2}\right)\right). \tag{2.12}$$

JHEP08(2016)157

The functions $\gamma^{(i)}_{Q,V}$ depend only on the ratio k_0/T, while $\gamma^{(i)}_{LPM}$ has non-trivial temperature dependence due to the runnings of the coupling constants.[2] In figure 1 the three functions are plotted, where the two lines labeled LPM curve correspond to two temperatures 10^4 GeV and 10^{10} GeV, while

$$\gamma^{(0)}_{IR} = 2\gamma^{(1)}_{IR} = \frac{T^2}{256\pi k_0}\frac{\rho_B}{\rho_F}, \quad \gamma^{(2)}_{IR} = \gamma^{(0)}_{IR}\frac{\rho'_F}{\rho_F} + \gamma^{(1)}_{IR}, \tag{2.13}$$

where $\rho_B(y) = (\exp y - 1)^{-1}$ is the Bose-Einstein distribution.

Inserting these functions in the kinetic equation we get:

$$\begin{aligned}\frac{d\rho_N}{dt} &= -i[H,\rho_N] - \frac{\gamma^{(0)}_N}{2}\left\{Y^\dagger Y, \rho_N - \rho_F\right\} + \gamma^{(1)}_N \rho_F Y^\dagger \mu Y \\ &\quad -\frac{\gamma^{(2)}_N}{2}\left\{Y^\dagger \mu Y, \rho_N\right\},\end{aligned} \tag{2.14}$$

where $\mu \equiv \mathrm{Diag}(\mu_\alpha)$. The equation for the antineutrino (opposite helicity state) density is the same but changing $\mu \to -\mu$ and $Y \to Y^*$.

It is often useful to consider instead the evolution of the CP conserving and violating combinations:

$$\rho_\pm \equiv \frac{\rho_N \pm \rho_{\bar{N}}}{2}. \tag{2.15}$$

The equations for these combinations are:

$$\begin{aligned}\dot{\rho}_+ &= -i[H_{\rm re},\rho_+] + [H_{\rm im},\rho_-] - \frac{\gamma^{(0)}_N}{2}\left\{\mathrm{Re}\left[Y^\dagger Y\right], \rho_+ - \rho_F\right\} \\ &\quad + i\gamma^{(1)}_N \mathrm{Im}\left[Y^\dagger \mu Y\right]\rho_F - i\frac{\gamma^{(2)}_N}{2}\left\{\mathrm{Im}\left[Y^\dagger \mu Y\right], \rho_+\right\} - i\frac{\gamma^{(0)}_N}{2}\left\{\mathrm{Im}\left[Y^\dagger Y\right], \rho_-\right\}, \\ \dot{\rho}_- &= -i[H_{\rm re},\rho_-] + [H_{\rm im},\rho_+] - \frac{\gamma^{(0)}_N}{2}\left\{\mathrm{Re}\left[Y^\dagger Y\right], \rho_-\right\} \\ &\quad + \gamma^{(1)}_N \mathrm{Re}\left[Y^\dagger \mu Y\right]\rho_F - \frac{\gamma^{(2)}_N}{2}\left\{\mathrm{Re}\left[Y^\dagger \mu Y\right], \rho_+\right\} - i\frac{\gamma^{(0)}_N}{2}\left\{\mathrm{Im}\left[Y^\dagger Y\right], \rho_+ - \rho_F\right\}.\end{aligned} \tag{2.16}$$

Finally we need the equations that describe the evolution of the leptonic chemical potentials. This is obtained from the equation that describes the evolution of the conserved charges in the absence of neutrino Yukawas, that is the $\frac{B}{3} - L_\alpha$ numbers. These numbers can only be changed by the same out of equilibrium processes that produce the sterile neutrinos:

$$\frac{dn_{B/3-L_\alpha}}{dt} = \frac{1}{2}\int_p \left\{\Gamma^a_l(p), \rho_l(p,\mu)\right\}_{\alpha\alpha} - \frac{1}{2}\int_p \left\{\Gamma^p_l(p), 1 - \rho_l(p,\mu)\right\}_{\alpha\alpha}. \tag{2.17}$$

[2] For the details of the calculation see [18].

JHEP08(2016)157

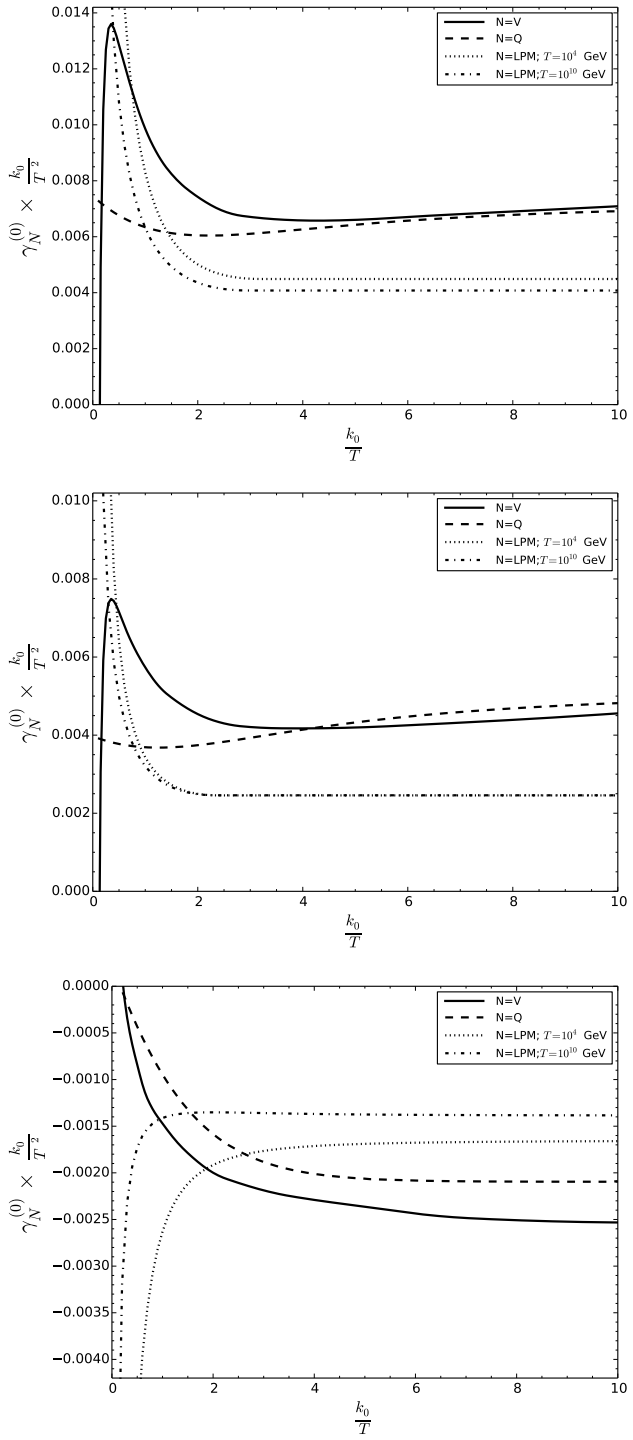

Figure 1. $\gamma_V^{(i)} k_0/T^2$ (solid), $\gamma_Q^{(i)} k_0/T^2$ (dashed), $\gamma_{LPM}^{(i)}(k_0) k_0/T^2$ for $T = 10^4\,\mathrm{GeV}$ (dotted) and $\gamma_{LPM}^{(i)}(k_0) k_0/T^2$ for $T = 10^{10}\,\mathrm{GeV}$ (dash-dotted) as a function of k_0/T.

JHEP08(2016)157

where $\int_p \equiv \int \frac{d^3p}{(2\pi)^3}$. Since $(\rho_l)_{\alpha\alpha} = \rho_F\left(\frac{p_0}{T} - \mu_\alpha\right)$, it is possible to relate the integrated rates of these equations to those of the sterile neutrinos and their densities:

$$\begin{aligned}\dot{n}_{B/3-L_\alpha} = -2\int_k \Bigg\{ & \frac{\gamma_N^{(0)}}{2}\left(Y\rho_N Y^\dagger - Y^*\rho_{\bar{N}}Y^T\right)_{\alpha\alpha} \\ & + \mu_\alpha\left(\frac{\gamma_N^{(2)}}{2}\left(Y\rho_N Y^\dagger + Y^*\rho_{\bar{N}}Y^T\right)_{\alpha\alpha} - \gamma_N^{(1)}\mathrm{Tr}\left[YY^\dagger I_\alpha\right]\rho_F\right)\Bigg\}, \end{aligned} \tag{2.18}$$

or in terms of $\rho_\pm$:

$$\begin{aligned}\dot{n}_{B/3-L_\alpha} = -2\int_k \Big\{ & \gamma_N^{(0)}\mathrm{Tr}\left[\rho_-\mathrm{Re}\left(Y^\dagger I_\alpha Y\right) + i\rho_+\mathrm{Im}\left(Y^\dagger I_\alpha Y\right)\right] \\ & + \mu_\alpha\left(\gamma_N^{(2)}\mathrm{Tr}\left[\rho_+\mathrm{Re}\left(Y^\dagger I_\alpha Y\right)\right] - \gamma_N^{(1)}\mathrm{Tr}\left[YY^\dagger I_\alpha\right]\rho_F\right)\Big\}, \end{aligned} \tag{2.19}$$

where I_α is the projector on flavour α, and we have neglected terms of $\mathcal{O}(\mu\rho_-)$.

The relation between the leptonic chemical potentials and the approximately conserved charges, $B/3 - L_\alpha$, is given for $T \leq 10^6$ GeV by [21]

$$\mu_\alpha = -\sum_\beta C_{\alpha\beta}\mu_{B/3-L_\beta}, \quad C_{\alpha\beta} = \frac{1}{711}\begin{pmatrix} 221 & -16 & -16 \\ -16 & 221 & -16 \\ -16 & -16 & 221 \end{pmatrix}, \tag{2.20}$$

where we have defined $\mu_{B/3-L_\beta}$ by the relation:

$$n_{B/3-L_\alpha} \equiv -2\mu_{B/3-L_\alpha}\int_k \rho_F' = \frac{1}{6}\mu_{B/3-L_\alpha}T^3. \tag{2.21}$$

Introducing finally the expansion of the universe and changing variables to the scale factor $x = a$ and $y = ka$, the time derivatives of the distribution functions change to:

$$\begin{aligned}\frac{d\rho_N(T,k)}{dt} &\to xH_u(x)\frac{\partial\rho_N(x,y)}{\partial x}\bigg|_{\text{y fixed}} \\ \frac{dn_{B/3-L_\alpha}}{dt} &\to -2xH_u(x)\frac{d\mu_{B/3-L_\alpha}}{dx}\int_k \rho_F', \end{aligned} \tag{2.22}$$

where $H_u(x) = \sqrt{\frac{4\pi^3 g_*(T)}{45}}\frac{T^2}{M_{\text{Planck}}}$ is the Hubble expansion parameter. Assuming a radiation dominated universe with constant number of relativistic degrees of freedom $g_*(T_0) \simeq 106.75$ for $T_0 \geq T_{EW}$, then $xT=$ constant that we can fix to one.

2.1 Momentum averaging

In principle the equations should be solved for all momenta of the sterile neutrinos, but it is a good approximation [10] to assume $\rho_\pm(x,y) = r_\pm(x)\rho_F(y)$, with $r_\pm(x)$ independent of momentum. This allows to integrate explicitly over y and we get the momentum-averaged

JHEP08(2016)157

equations:

$$
\begin{aligned}
xH_u\frac{dr_+}{dx} &= -i[\langle H_{\rm re}\rangle, r_+] + [\langle H_{\rm im}\rangle, r_-] - \frac{\langle\gamma_N^{(0)}\rangle}{2}\Big\{{\rm Re}\left[Y^\dagger Y\right], r_+ - 1\Big\} \\
&\quad + i\langle\gamma_N^{(1)}\rangle{\rm Im}\Big[Y^\dagger\mu Y\Big] - i\frac{\langle\gamma_N^{(2)}\rangle}{2}\Big\{{\rm Im}\Big[Y^\dagger\mu Y\Big], r_+\Big\} - i\frac{\langle\gamma_N^{(0)}\rangle}{2}\Big\{{\rm Im}\Big[Y^\dagger Y\Big], r_-\Big\}, \\
xH_u\frac{dr_-}{dx} &= -i[\langle H_{\rm re}\rangle, r_-] + [\langle H_{\rm im}\rangle, r_+] - \frac{\langle\gamma_N^{(0)}\rangle}{2}\Big\{{\rm Re}\Big[Y^\dagger Y\Big], r_-\Big\} \\
&\quad + \langle\gamma_N^{(1)}\rangle{\rm Re}\Big[Y^\dagger\mu Y\Big] - \frac{\langle\gamma_N^{(2)}\rangle}{2}\Big\{{\rm Re}\Big[Y^\dagger\mu Y\Big], r_+\Big\} - i\frac{\langle\gamma_N^{(0)}\rangle}{2}\Big\{{\rm Im}\Big[Y^\dagger Y\Big], r_+ - 1\Big\}, \\
xH_u\frac{d\mu_{B/3-L_\alpha}}{dx} &= \frac{\int_k\rho_F}{\int_k\rho_F'}\Big\{\langle\gamma_N^{(0)}\rangle{\rm Tr}\Big[r_-{\rm Re}\Big(Y^\dagger I_\alpha Y\Big) + ir_+{\rm Im}\Big(Y^\dagger I_\alpha Y\Big)\Big] \\
&\quad + \mu_\alpha\Big(\langle\gamma_N^{(2)}\rangle{\rm Tr}\Big[r_+{\rm Re}\Big(Y^\dagger I_\alpha Y\Big)\Big] - \langle\gamma_N^{(1)}\rangle{\rm Tr}\left[YY^\dagger I_\alpha\right]\Big)\Big\}, \\
\mu_\alpha &= -\sum_\beta C_{\alpha\beta}\mu_{B/3-L_\beta},
\end{aligned}
\tag{2.23}
$$

where

$$
\langle(\ldots)\rangle \equiv \frac{\int_y(\ldots)n_F(y)}{\int_y n_F(y)} \tag{2.24}
$$

and $\frac{\int_k\rho_F}{\int_k\rho_F'} = -\frac{9\xi(3)}{\pi^2}$.

The equation for $r_N = \rho_N/\rho_F$ and $r_{\bar N} = \rho_{\bar N}/\rho_F$ are equivalently

$$
\begin{aligned}
xH_u\frac{dr_N}{dx} &= -i[\langle H\rangle, r_N] - \frac{\langle\gamma_N^{(0)}\rangle}{2}\Big\{Y^\dagger Y, r_N - 1\Big\} + \langle\gamma_N^{(1)}\rangle Y^\dagger\mu Y - \frac{\langle\gamma_N^{(2)}\rangle}{2}\Big\{Y^\dagger\mu Y, r_N\Big\}, \\
xH_u\frac{dr_{\bar N}}{dx} &= -i[\langle H^*\rangle, r_{\bar N}] - \frac{\langle\gamma_N^{(0)}\rangle}{2}\left\{Y^TY^*, r_{\bar N} - 1\right\} - \langle\gamma_N^{(1)}\rangle Y^T\mu Y^* + \frac{\langle\gamma_N^{(2)}\rangle}{2}\left\{Y^T\mu Y^*, r_{\bar N}\right\}, \\
xH_u\frac{d\mu_{B/3-L_\alpha}}{dx} &= \frac{\int_k\rho_F}{\int_k\rho_F'}\left\{\frac{\langle\gamma_N^{(0)}\rangle}{2}\Big(Yr_NY^\dagger - Y^*r_{\bar N}Y^T\Big)_{\alpha\alpha}\right. \\
&\quad \left. + \mu_\alpha\left(\frac{\langle\gamma_N^{(2)}\rangle}{2}\Big(Yr_NY^\dagger + Y^*r_{\bar N}Y^T\Big)_{\alpha\alpha} - \langle\gamma_N^{(1)}\rangle{\rm Tr}\Big[YY^\dagger I_\alpha\Big]\right)\right\}, \\
\mu_\alpha &= -\sum_\beta C_{\alpha\beta}\mu_{B/3-L_\beta}.
\end{aligned}
\tag{2.25}
$$

The momentum averaged rates are:

$$
\langle\gamma_N^{(i)}\rangle = A_i\left[c_{LPM}^{(i)} + y_t^2c_Q^{(i)} + (3g^2+g'^2)\left(c_V^{(i)} + \log\left(\frac{1}{3g^2+g'^2}\right)\right)\right], \tag{2.26}
$$

with

$$
A_0 = 2A_1 = -4A_2 \equiv \frac{4\pi^2}{3\xi(3)}\frac{T}{3072\pi}, \tag{2.27}
$$

and the coefficients are given in the table 1.

JHEP08(2016)157

i	$c^{(i)}_{LPM}(T_1)$	$c^{(i)}_{LPM}(T_2)$	$c^{(i)}_{Q}$	$c^{(i)}_{V}$
0	4.22	2.65	2.52	3.17
1	3.56	2.80	3.10	3.83
2	4.77	2.50	2.27	2.89

Table 1. Coefficients in the momentum averaged rates. The LPM ones have been evaluated at $T_1 = 10^4\,\mathrm{GeV}$ and $T_2 = 10^{10}\,\mathrm{GeV}$.

For the couplings g, g' we evaluate them at the scale πT:

$$\frac{1}{g(\pi T)^2} = \frac{1}{g(M_z)^2} + \frac{19}{48\pi^2}\ln\left(\frac{\pi T}{M_z}\right), \tag{2.28}$$

$$\frac{1}{g'(\pi T)^2} = \frac{1}{g'(M_z)^2} + \frac{41}{48\pi^2}\ln\left(\frac{M_z}{\pi T}\right), \tag{2.29}$$

while the top Yukawa running is obtained numerically from the one loop renormalization group equations.

In figure 2 we compare the time evolution of the asymmetry that we obtain with the new equations and the old equations of [15] that only included top scattering processes and Maxwell-Boltzmann statistics. As expected the larger scattering rates induce a larger asymmetry at short times, but also a stronger washout at late times.

In [15], we identified four independent CP rephasing invariants that can contribute to this asymmetry in the general case with $N = 3$ as:

$$I^{(2)}_1 = -\mathrm{Im}\left[W^*_{12}V_{11}V^*_{21}W_{22}\right], \tag{2.30}$$

$$I^{(3)}_1 = \mathrm{Im}\left[W^*_{12}V_{13}V^*_{23}W_{22}\right], \tag{2.31}$$

$$I^{(3)}_2 = \mathrm{Im}\left[W^*_{13}V_{12}V^*_{22}W_{23}\right], \tag{2.32}$$

$$J_W = -\mathrm{Im}\left[W^*_{23}W_{22}W^*_{32}W_{33}\right], \tag{2.33}$$

where V, W are the matrices parametrizing the neutrino Yukawa matrix, eq. (2.1). In the minimal scenario with $N = 2$ only the first two invariants can contribute. We considered a convenient analytical approximation, based on a perturbative expansion in the mixing angles of these matrices, that allowed us to solve the differential equations analytically, neglecting non-linear terms. It is straightforward to apply the same method to the new equations. As an example we give the result for the asymmetry when only the CP invariant $I^{(2)}_1$ survives (i.e. for $\phi_{i3} = \bar{\phi}_{i3} = 0$). Defining

$$\Delta_{ij} \equiv \frac{\Delta M^2_{ij}}{2y}M^*_P, \quad \Delta_v = \left(y^2_2 - y^2_1\right)\frac{M^*_P}{8y}, \quad \gamma^{(i)} \equiv \langle\gamma^{(i)}_N\rangle\frac{M^*_P}{T}, \tag{2.34}$$

with $M^*_P \equiv M_{\mathrm{Planck}}\sqrt{\frac{45}{4\pi^3 g_*(T_0)}}$, and neglecting the running of the couplings, the result is

$$\sum_\alpha \mu_{B/3-L_\alpha}(t) = \frac{2}{3}\left(\frac{9\xi(3)}{\pi^2}\right)^2 I^{(2)}_1 y_1 y_2 (y^2_2 - y^2_1)\frac{(\gamma^{(0)})^2\gamma^{(1)}}{\bar{\gamma}}G_1(t), \tag{2.35}$$

JHEP08(2016)157

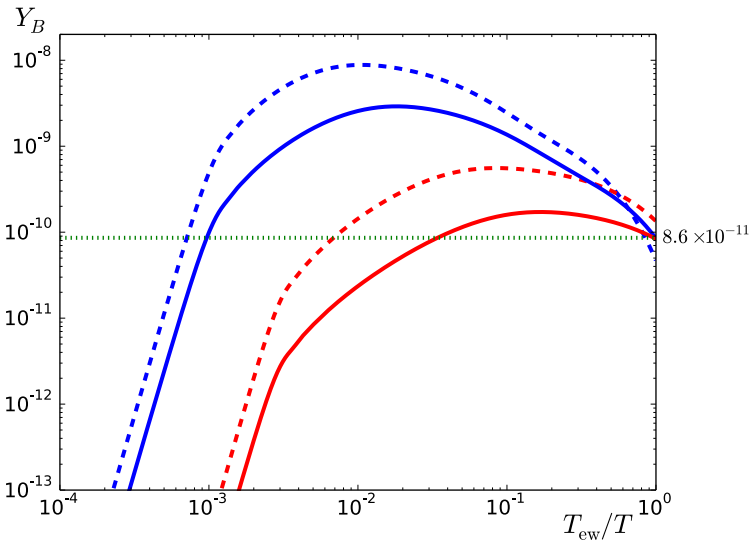

Figure 2. Time evolution of the baryon asymmetry for two different choices of parameters. First set (blue curves): $z = 0.81 + 3.22i, \phi_1 = 1.21, \delta = 2.07, M_1 = 9.683$ GeV, $M_2 = 9.677$ GeV; second set (red curves): $z = 0.88 - 0.35i, \phi_1 = 1.65, \delta = -2.07, M_1 = 0.754$ GeV, $M_2 = 0.750$ GeV, using the equations that only take into account quark scattering (solid) and those in eqs. (2.25) (dashed).

where

$$\bar{\gamma} \equiv \sqrt{\left(\gamma^{(0)} + \frac{221}{711}\frac{9\xi(3)}{\pi^2}\gamma^{(1)}\right)^2 + \frac{1024}{505521}\left(\frac{9\xi(3)}{\pi^2}\right)^2 \frac{y_2^2 y_1^2}{\left(y_2^2 - y_1^2\right)^2}\left(\gamma^{(1)}\right)^2}, \tag{2.36}$$

and

$$\begin{aligned} G_1(t) \equiv & \left(e^{-\Gamma_+ t} - e^{-\Gamma_- t}\right) \mathrm{Re}\left[iJ_{200}(\Delta_{12}, -\Delta_{12}, t) + 2\Delta_v J_{201}\left(\Delta_{12}, -\Delta_{12}, t\right)\right] \\ & + \frac{1}{2}\sum_{\sigma=\pm} \sigma e^{-\Gamma_\sigma t} \mathrm{Re}\left[J_{210}\left(\Delta_{12}, -\Delta_{12}, t\right)\left(-2\Delta_v + i\left(2\Gamma_\sigma - \left(y_2^2 + y_1^2\right)\gamma_N^{(0)}\right)\right)\right], \end{aligned} \tag{2.37}$$

$$\Gamma_\pm \equiv \frac{y_1^2 + y_2^2}{2}\left(\gamma^{(0)} + \frac{9\xi(3)}{\pi^2}\frac{221}{711}\gamma^{(1)}\right) \mp \frac{y_2^2 - y_1^2}{2}\bar{\gamma}. \tag{2.38}$$

The integrals are

$$J_{2nm}(\alpha, -\alpha, t) \equiv \int_0^t dx_1\, x_1^n\, e^{i\frac{\alpha x_1^3}{3}} \int_0^{x_1} dx_2\, x_2^m\, e^{-i\frac{\alpha x_2^3}{3}}. \tag{2.39}$$

Figure 3 shows the analytical result compared with the numerical solution to the equation for sufficiently small mixing angles.

2.2 Baryon asymmetry

The observed baryon asymmetry is usually quoted in terms of the abundance, which is the number-density asymmetry of baryons normalised to the entropy density. After Planck

JHEP08(2016)157

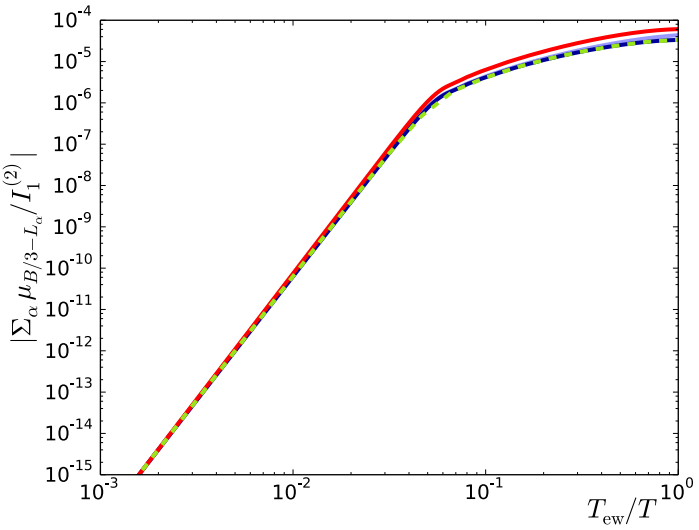

Figure 3. Assuming parameters for which only the simplest invariant, $I_1^{(2)}$ is non-vanishing, comparison of the analytical result of eq. (2.35) (dashed), the full numerical one (red), the numerical one neglecting the variation of the running of the couplings (blue) and that neglecting also non-linear terms (green). The parameters have been chosen as $M_1 = 1\,\text{GeV}$, $M_2 - M_1 = 10^{-3}\,\text{GeV}$, and $(y_1, y_2) = (10^{-7}, \sqrt{2} \times 10^{-7})$, and sufficiently small V, W mixings.

this quantity is known to per cent precision [22]:

$$Y_B^{\rm exp} \simeq 8.65(8) \times 10^{-11}. \tag{2.40}$$

The baryon abundance is related to that of $B - L$ by [23, 24]

$$Y_B \simeq \frac{28}{79} Y_{B-L}, \tag{2.41}$$

and

$$Y_{B-L} = \sum_\alpha \frac{n_{B/3-L_\alpha}}{s}, \quad n_{B/3-L_\alpha} = \frac{T^3}{6}\mu_{B/3-L_\alpha}, \quad s = \frac{2\pi^2}{45} g_* T^3, \tag{2.42}$$

where we take $g_* = 106.75$ (which ignores the contribution to the entropy of the sterile states). Our estimate for the baryon asymmetry is therefore

$$Y_B \simeq 1.3 \times 10^{-3} \sum_\alpha \mu_{B/3-L_\alpha}. \tag{2.43}$$

3 Numerical results

The numerical solution of the kinetic equations is challenging, because in most part of the parameter space, they are stiff since the oscillation time is much shorter than the collision one. In [15] we performed an exploration of the parameter space viable for leptogenesis for the models $N = 2, 3$ employing the perturbative analytical approximation. This required to constrain certain regions of parameter space where the perturbative solution could fail. We

JHEP08(2016)157

want to improve on this scan by going beyond the perturbative estimate of the asymmetry and using the full numerical solution of the equations.

We have solved eqs. (2.25) using the publicly available code SQuIDS [25, 26]. The code is designed to solve the evolution of a generic density matrix in the interaction picture. The interaction picture is useful because it removes the short time scale, i.e. the oscillation scale, from the numerical integration, but fast oscillatory coefficients then appear in the terms involving the off-diagonal elements of the density matrix. In order to optimize the code, at some large enough time, we switch to a fully decoherent evolution (when the exponents of all the oscillatory terms are larger than 10^5). The decoherent evolution is already included in the last version of the SQuIDs code [26]. Using this approximation the solution speeds up the computation by a factor more than a hundred and the result agrees with the full solution with a relative error smaller than $O(1\%)$.

Using these optimizations we get a computational time for the full numerical solution of order minutes, which allows us to do a Bayesian parameter estimation from the log-likelihood:

$$\log \mathcal{L} = -\frac{1}{2}\left(\frac{Y_B(t_{\rm EW}) - Y_B^{\rm exp}}{\sigma_{Y_B}}\right)^2 . \tag{3.1}$$

For this, we use a nested sampling algorithm implemented in the public package MultiNest [27–29] and the Markov Chain sample analysis tool GetDist [30] to get the posterior probabilities. The number of random starting points is 5000.

The scan is performed using the Casas-Ibarra parameters of eq. (2.5). We fix the light neutrino masses and mixings to the present best fit points in the global analysis of neutrino oscillation data of ref. [31] for each of the neutrino orderings (normal, NH, and inverted, IH), and leave as free parameters: the complex angle(s) of the R matrix, the CP phases of the PMNS matrix, the lightest neutrino mass as well as the heavy Majorana masses. For $N = 2$ these are six independent parameters, while for $N = 3$, there are thirteen free parameters.

In this work we consider the simplest case of $N = 2$, which can be obtained from the $N = 3$ model in the limit where one of the sterile neutrinos is effectively decoupled, that we can assume without loss of generality to be N_3. This can be achieved with the choice of parameters:

$$m_{3(1)} = 0, z_{i3} = 0, \;\; R(z_{ij}) \to R(z_{ij})(P) \tag{3.2}$$

for the IH(NH), where P is the $123 \to 312$ permutation matrix (only necessary for the NH).

This is then the model that has been considered in most previous works on the subject [8–10, 13, 32], where the number of constrained parameters is reduced to six: only one complex angle in R, $z \equiv \theta + i\gamma$, two CP phases, δ and ϕ_1 in the PMNS matrix, and two Majorana neutrino masses, M_1, M_2.

Figures 4 and 5 show, for IH and NH, the posterior probabilities of the spectrum of the two relevant states, M_1, M_2, the active-sterile mixings of the first heavy state $|U_{\alpha 4}|^2$ (those of the second state are almost identical), the neutrinoless double beta decay effective mass $|m_{\beta\beta}|$ and the baryon asymmetry Y_B. An important consideration are the priors. We have considered flat priors in all the Casas-Ibarra parameters except the masses where we assume

JHEP08(2016)157

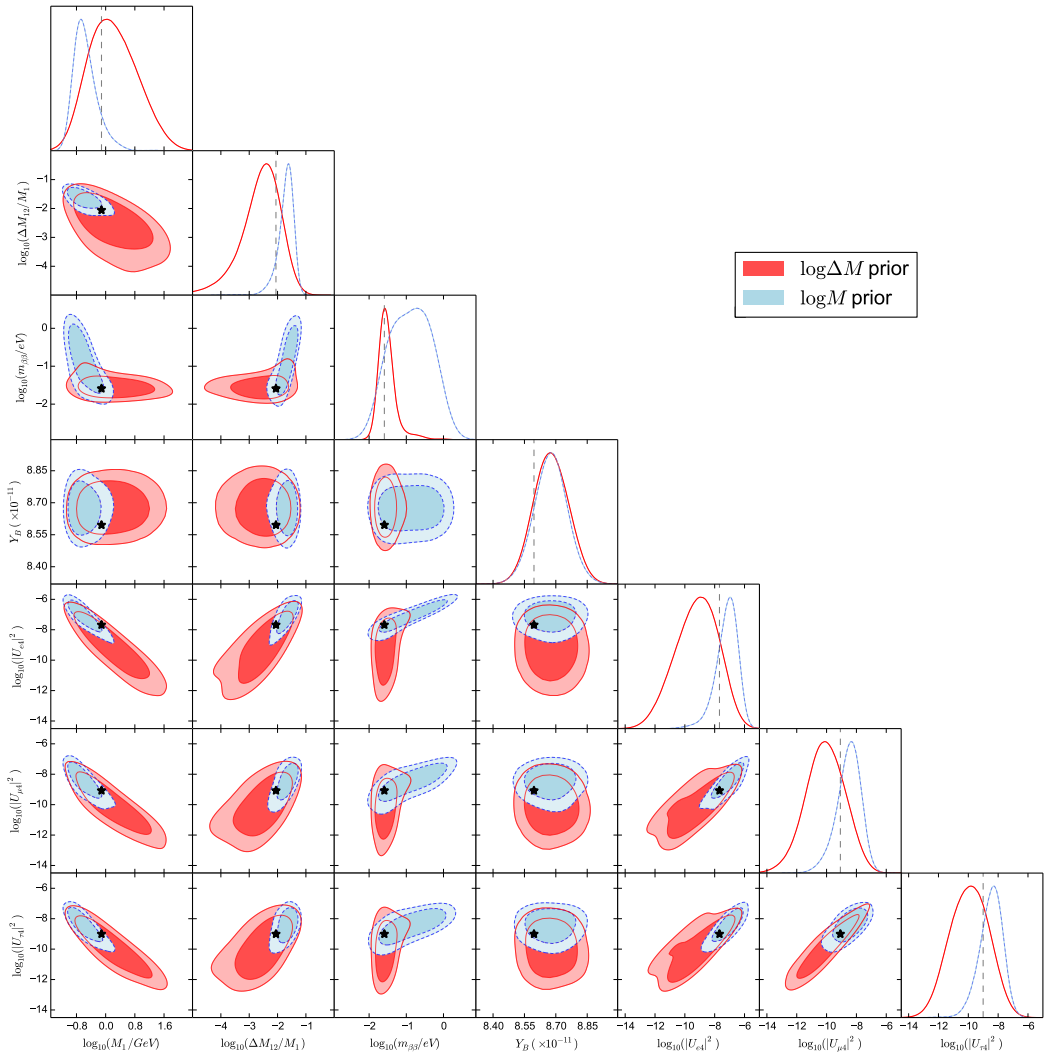

Figure 4. Triangle plot with 1D posterior probabilities and 2D 68% and 90% probability contours in the $N = 2$ scenario for IH. The parameters shown are the observables M_1, $\Delta M_{12}/M_1 = (M_2 - M_1)/M_1$, $m_{\beta\beta}$, Y_B, and the three mixings with the first of the heavy states $|U_{\alpha 4}|^2$ for $\alpha = e, \mu, \tau$. The blue and red contours correspond respectively to the assumption of a flat prior in $\log_{10} M_1$ and $\log_{10} M_2$ and to a flat prior in $\log_{10} M_1$ and $\log_{10}(\Delta M_{12})$. The star is the test point used for the SHiP study of the next section.

a flat prior in $\log_{10}\left(\frac{M_1}{\text{GeV}}\right)$, within the range $M_1 \in [0.1\text{GeV}, 10^2\text{GeV}]$, and two possibilities: 1) a flat prior also in $\log_{10}\left(\frac{M_2}{GeV}\right)$ in the same range or 2) a flat prior in $\log_{10}\left(\frac{|M_2-M_1|}{\text{GeV}}\right)$ in the range $M_2 - M_1 \in [10^{-8}\text{GeV}, 10^2\text{GeV}]$. The two different colours (light blue and red) in figure 4 correspond to the two options. The significant differences between the two posteriors show the effect of allowing or not for fine-tuning in the degeneracy of the two heavy states. Even though the contours are typically larger if more fine-tuning is allowed, we find interesting solutions with a mild degeneracy, which tend to imply smaller M_1, M_2, larger values of the active-sterile mixing parameters and a sizeable non-standard

JHEP08(2016)157

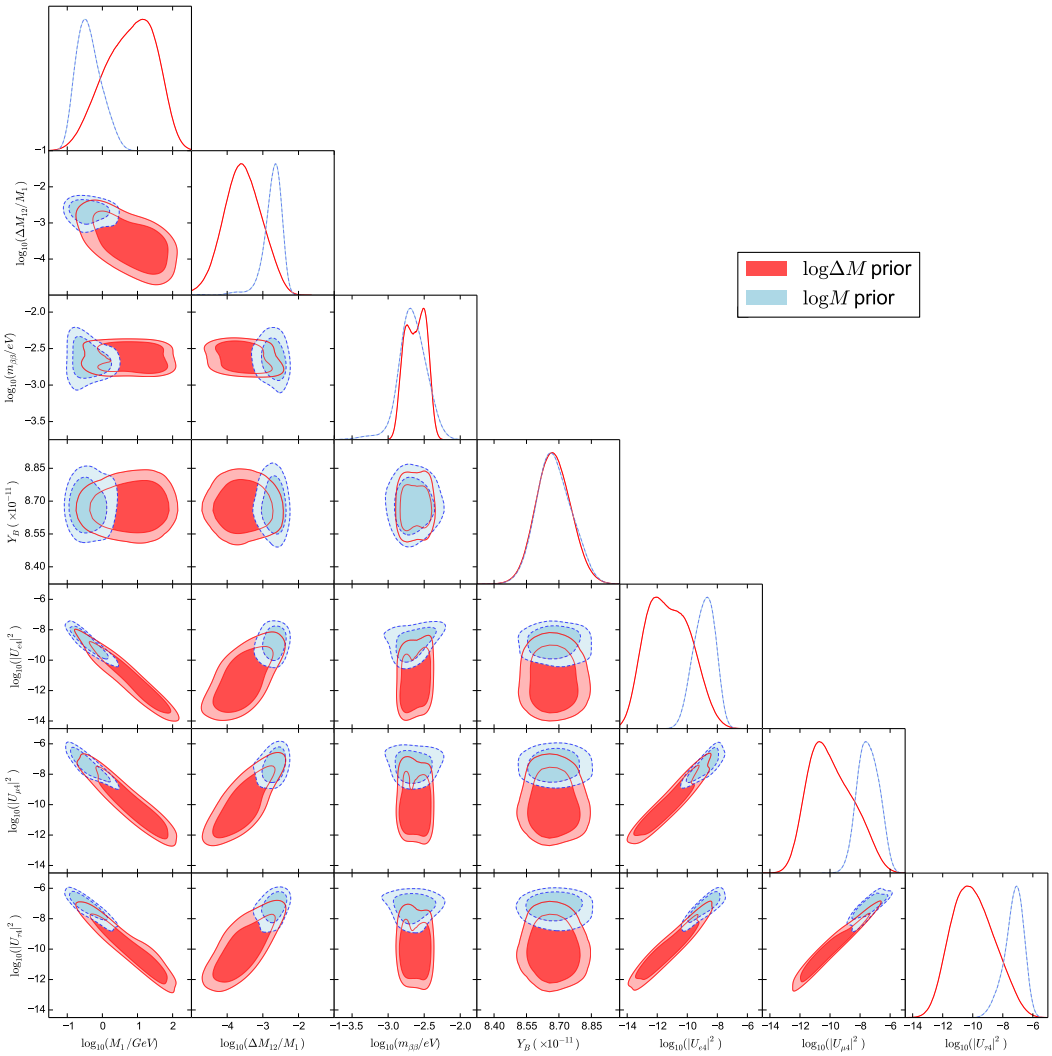

Figure 5. Triangle plot with 1D posterior probabilities and 2D 68% and 90% probability contours in the $N = 2$ scenario for NH. The parameters shown are the observables M_1, $\Delta M_{12}/M_1 = (M_2 - M_1)/M_1$, $m_{\beta\beta}$, Y_B, and the three mixings with the first of the heavy states $|U_{\alpha 4}|^2$ for $\alpha = e, \mu, \tau$. The blue and red contours correspond respectively to the assumption of a flat prior in $\log_{10} M_1$ and $\log_{10} M_2$ and to a flat prior in $\log_{10} M_1$ and $\log_{10}(\Delta M_{12})$.

contribution to neutrinoless double beta decay, which obviously imply much better chances of testability. Figures 6 zoom in the most interesting results from this study: the mild level of fine-tuning of the blue contours (neither a strong degeneracy is required, nor a very large deviation from the naive seesaw scaling of the mixings), correlated with a relatively large mixing, and a sizeable amplitude for neutrinoless double beta decay. We will come back to this point in the next section.

In table 2 we show the 68% probability ranges for the relevant parameters as extracted from the 1D posterior probabilities, for the two neutrino orderings and the two prior choices. The ranges for the mixings of the second heavy state, $|U_{\alpha 5}|^2$, are basically the same.

JHEP08(2016)157

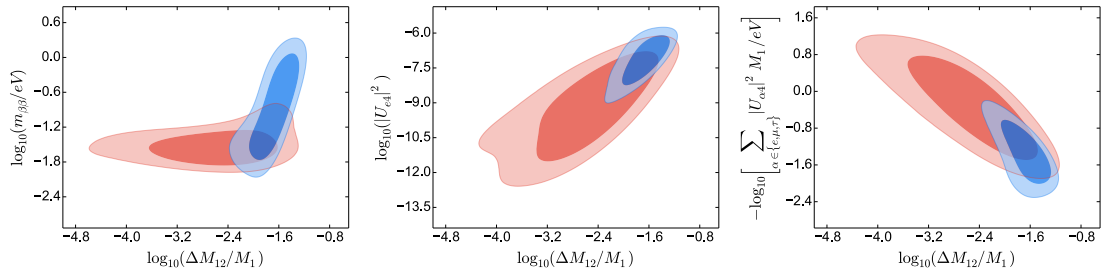

Figure 6. Posterior probabilities for the amplitude of neutrinoless double beta decay (left), electron mixing (middle) and $\sum_{\alpha=e,\mu,\tau}|U_{\alpha4}|^2 M_1$ (right) versus the mass degeneracy.

NO	Prior	M_1(GeV)	ΔM_{12}(GeV)	$\lvert U_{e4}\rvert^2$	$\lvert U_{\mu4}\rvert^2$	$\lvert U_{\tau4}\rvert^2$	$m_{\beta\beta}$(eV)
IH	M	$-0.55^{+0.16}_{-0.38}$	$-2.23^{+0.22}_{-0.19}$	$-7.2^{+0.9}_{-0.4}$	$-8.5^{+1.0}_{-0.6}$	$-8.5^{+0.8}_{-0.7}$	-0.84 ± 0.55
	ΔM	$0.23^{+0.68}_{-0.82}$	$-2.36^{+0.71}_{-0.51}$	$-9.2^{+1.7}_{-1.4}$	$-10.1^{+1.5}_{-1.2}$	$-9.9^{+1.4}_{-1.2}$	$-1.48^{+0.15}_{-0.28}$
NH	M	$-0.39^{+0.31}_{-0.42}$	-3.1 ± 0.4	$-8.9^{+0.8}_{-0.7}$	-7.4 ± 0.7	$-7.3^{+0.7}_{-0.5}$	-2.66 ± 0.20
	ΔM	$0.8^{+0.82}_{-0.66}$	-2.76 ± 0.62	$-11.2^{1.4}_{-1.6}$	$-9.9^{+1.3}_{-1.8}$	$-10.0^{+1.3}_{-1.6}$	-2.62 ± 0.14

Table 2. For the minimal model $N = 2$: 68% posterior probability ranges of $\log_{10}$(param) assuming flat prior in $\log_{10}(M_2(\text{GeV}))$ (M) or $\log_{10}(\Delta M_{12}(\text{GeV}))$ (ΔM).

In figures 7 we zoom in the probability plots for the heavy neutrino mixings versus mass and compare them with present [33, 34] and future constraints from DUNE [35], SHiP [36] and FCC [37]. Constraints from Big Bang Nucleosynthesis are very restrictive in the low mass range, particularly below the pion threshold [38, 39]. In ref. [15] similar figures were shown from a scan of parameter space assuming only flat priors in $\log_{10} M_1$ and $\log_{10}|M_2 - M_1|$. We note that the regions we show here are the result of a full numerical treatment, that avoids any constraint in parameter space and successfully explain the baryon asymmetry within its small 1% uncertainty. The most important addition is however that of the blue contours that use flat priors in $\log_{10} M_1$ and $\log_{10} M_2$, and therefore avoid too large fine-tuning. These solutions point to a region of parameter space within SHiP reach as the most probable one. It is interesting that the sensitivity of SHiP and DUNE to the e or μ channels will cover to a large extent the blue regions. When a larger degree of degeneracy in the masses is allowed (red regions), the right baryon asymmetry can be obtained also for larger masses, up to 10-100 GeV, but this high mass region will be harder to test experimentally (for recent work see also [40]).

In the $N = 3$ case, there are 13 unknown parameters and the exploration of parameter space is significantly more challenging. This case will be considered elsewhere.

4 Predicting the baryon asymmetry in the minimal $N = 2$ model

A very relevant question is whether the baryon asymmetry could be predicted in this scenario if the heavy sterile neutrinos are within reach of future experiments, such as the

JHEP08(2016)157

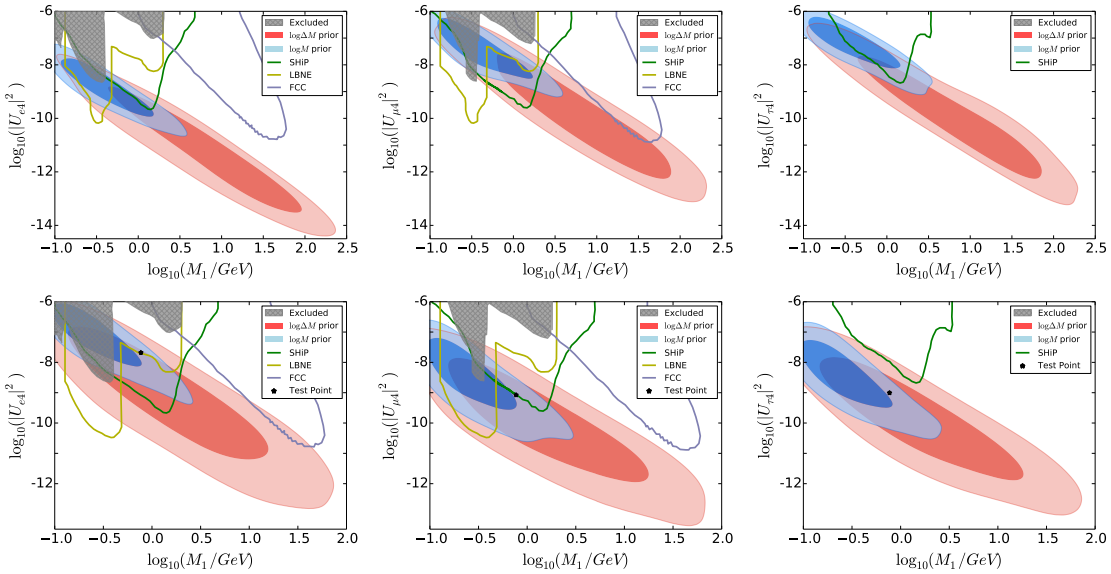

Figure 7. Comparison of the posterior probability contours at 68% and 90% on the planes mixings with e, μ, τ versus masses, with the present (shaded region) and future constraints from DUNE, FCC and SHiP for NH (up) y IH (down).

SHiP experiment. We will analyse this question in the simplest case $N = 2$ where the number of unknown parameters is minimal. Obviously the situation for the $N = 3$ case will be much more difficult.

The SHiP experiment will be capable of detecting heavy neutrinos in the few GeV range provided their mixings are sufficiently large. In particular significantly larger than what the naive seesaw scaling $|U_{ai}|^2 \sim m_i/M_i$ would suggest. In the Casas-Ibarra parametrization of eq. (2.5), this implies that the entries of the R matrix need to be significantly larger than one, and therefore the imaginary part of the complex angle needs to be sizeable.

In order to understand the dependence of Y_B on the different parameters, it is useful to consider the perturbative results of [15]. The CP asymmetries responsible for the baryon number generation, Δ_{CP}, in the weak washout regime, can be generically written as

$$\Delta_{CP} = \sum_{\alpha,k} |Y_{\alpha k}|^2 \, \Delta_\alpha, \tag{4.1}$$

with

$$\Delta_\alpha = \sum_{i,j} \mathrm{Im}\left[Y_{\alpha i} Y^*_{\alpha j} \left(Y^\dagger Y \right)_{ij} \right] f(M_i, M_j). \tag{4.2}$$

For the $N = 2$ case, when $\phi_{i3} = 0$ and $y_3 = 0$, this quantity can be written as [15]

$$Y_B = \Delta_{CP} = y_1 y_2 \left(y_2^2 - y_1^2 \right) \left(\left(y_2^2 - y_1^2 \right) I_1^{(2)} + y_2^2 I_1^{(3)} \right) g(M_2, M_1), \tag{4.3}$$

where the invariants $I_1^{(2),(3)}$ are defined in eq. (2.33). This is indeed the dependence obtained from the solution of the kinetic equations in the perturbative approximation obtained in [15], in the weak washout limit. For our new kinetic equations, the perturbative result

JHEP08(2016)157

is shown in eq. (2.35) (where only the $I_1^{(2)}$ contribution has been kept). We can read from eq. (2.35) in the limit of weak washout, $\Gamma_\pm t \ll 1$, and using eq. (2.43):

$$g(M_2, M_1) = 1.3 \times 10^{-3} \times 2 \left(\frac{2}{3}\right)^{\frac{4}{3}} \frac{\pi^{3/2}}{\Gamma(-1/6)} \left(\frac{9\xi(3)}{\pi^2}\right)^2 \frac{(\gamma^{(0)})^2 \gamma^{(1)}}{M_P^{*2/3} T_{EW}} \frac{\text{sign}(\Delta M_{12}^2)}{|\Delta M_{12}^2|^{2/3}}. \quad (4.4)$$

In contrast with eq. (2.35), this approximation fails at large times since it is valid only for $\Gamma_\pm t \ll 1$. It typically overestimates the asymmetry, but should give qualitatively the right dependence on the parameters.

What we need however are the expressions in terms of the Casas-Ibarra parameters. The relations are typically very complicated, but we can identify a few small parameters and perturb in them:

$$\mathcal{O}(\epsilon) : r \equiv \sqrt{\frac{\Delta m^2_{\text{sol}}}{\Delta m^2_{\text{atm}}}} \sim \theta_{13} \sim e^{-\frac{\gamma}{2}}, \quad (4.5)$$

where γ, assumed positive, is the imaginary part of the complex angle of the R matrix that needs to be large to avoid the naive seesaw scaling of the active-sterile mixings.[3] Defining

$$A \equiv \frac{e^{2\gamma}\sqrt{\Delta m^2_{\text{atm}}}}{4}, \quad (4.6)$$

the result for the heavy-light mixing for IH can be written as

$$\begin{aligned}
|U_{e4}|^2 M_1 \simeq |U_{e5}|^2 M_2 \simeq\ & A\Big[(1+\sin\phi_1 \sin 2\theta_{12})(1-\theta_{13}^2) + \frac{1}{2} r^2 s_{12}(c_{12}\sin\phi_1 + s_{12}) + \mathcal{O}(\epsilon^3)\Big], \\
|U_{\mu 4}|^2 M_1 \simeq |U_{\mu 5}|^2 M_2 \simeq\ & A\Big[\Big(1 - \sin\phi_1 \sin 2\theta_{12}\left(1 + \frac{1}{4}r^2\right) + \frac{1}{2} r^2 c_{12}^2\Big) c_{23}^2 \\
& + \theta_{13}(\cos\phi_1 \sin\delta - \sin\phi_1 \cos 2\theta_{12} \cos\delta) \sin 2\theta_{23} \\
& + \theta_{13}^2 (1 + \sin\phi_1 \sin 2\theta_{12}) s_{23}^2 + \mathcal{O}(\epsilon^3)\Big], \\
|U_{\tau 4}|^2 M_1 \simeq |U_{\tau 5}|^2 M_2 \simeq\ & A\Big[\Big(1 - \sin\phi_1 \sin 2\theta_{12}\left(1 + \frac{1}{4}r^2\right) + \frac{1}{2} r^2 c_{12}^2\Big) s_{23}^2 \\
& - \theta_{13}(\cos\phi_1 \sin\delta - \sin\phi_1 \cos 2\theta_{12} \cos\delta) \sin 2\theta_{23} \\
& + \theta_{13}^2 (1 + \sin\phi_1 \sin 2\theta_{12}) c_{23}^2 + \mathcal{O}(\epsilon^3)\Big].
\end{aligned} \quad (4.7)$$

The result for NH is:

$$\begin{aligned}
|U_{e4}|^2 M_1 \simeq |U_{e5}|^2 M_2 \simeq\ & A\Big[r s_{12}^2 - 2\sqrt{r}\theta_{13}\sin(\delta+\phi_1) s_{12} + \theta_{13}^2 + \mathcal{O}\Big(\epsilon^{5/2}\Big)\Big], \\
|U_{\mu 4}|^2 M_1 \simeq |U_{\mu 5}|^2 M_2 \simeq\ & A\Big[s_{23}^2 - \sqrt{r}\ c_{12}\sin\phi_1 \sin 2\theta_{23} + r c_{12}^2 c_{23}^2 \\
& + 2\sqrt{r}\ \theta_{13}\sin(\phi_1+\delta) s_{12} s_{23}^2 - \theta_{13}^2 s_{23}^2 + \mathcal{O}\Big(\epsilon^{5/2}\Big)\Big], \\
|U_{\tau 4}|^2 M_1 \simeq |U_{\tau 5}|^2 M_2 \simeq\ & A\Big[c_{23}^2 + \sqrt{r} c_{12}\sin\phi_1 \sin 2\theta_{23} + r c_{12}^2 s_{23}^2 \\
& + 2\sqrt{r}\ \theta_{13}\sin(\phi_1+\delta) s_{12} c_{23}^2 - \theta_{13}^2 c_{23}^2 + \mathcal{O}\Big(\epsilon^{5/2}\Big)\Big].
\end{aligned} \quad (4.8)$$

[3] Note that γ can also be negative, but there is an approximate symmetry $\gamma \to -\gamma$, that would lead to very similar results by expanding in $e^{-\frac{|\gamma|}{2}}$ in this case.

JHEP08(2016)157

Note that the mixings depend exponentially on γ and are inversely proportional to the heavy masses, but this dependence drops in any ratio.

At leading order (LO) in the ϵ expansion, we see that for IH, the ratio of the electron and muon mixings is independent of γ and heavy masses and depends exclusively on the Majorana CP phase of the PMNS matrix, ϕ_1:

$$\text{IH}: \quad \frac{|U_{e4}|^2}{|U_{\mu 4}|^2} \simeq \frac{1}{c_{23}^2}\frac{1+\sin\phi_1 \sin 2\theta_{12}}{1-\sin\phi_1 \sin 2\theta_{12}} + \mathcal{O}(\epsilon). \tag{4.9}$$

This is important because the CP asymmetry strongly depends on this phase as we will see below, therefore for the IH, the putative measurement of the masses and the mixings of these states in SHiP for example, would allow in principle to fix simultaneously γ and ϕ_1. For NH on the other hand the SHiP measurement would only provide information on γ but not on ϕ_1 nor any other phase, at this order:

$$\text{NH}: \quad \frac{|U_{e4}|^2}{|U_{\mu 4}|^2} \simeq 2r\frac{s_{12}^2}{s_{23}^2} + \mathcal{O}\Big(\epsilon^{3/2}\Big). \tag{4.10}$$

The mixings to taus are at this order the same as those to muons.

The leading order however is not precise enough. For IH, it is clear from eq. (4.9) that depending on the value of ϕ_1 a significant suppression of the leading terms in the numerator or denominator can take place, therefore at this point the NLO corrections are relevant and these bring a new undetermined parameter, δ, as can be seen from eqs. (4.7), which is the CP phase that can be measured in neutrino oscillations! In this case, the measurement of the ratio of mixings at SHiP cannot resolve ϕ_1 and δ simultaneously and a degeneracy between these two phases remains. We will come back to this interesting observation in the following section. Clearly the δ phase could be determined in future neutrino oscillation experiments.

At leading order in the ϵ expansion, the CP asymmetry in this regime can be approximated by

$$\begin{aligned}
\left|\frac{\Delta_{CP}}{g(M_1,M_2)}\right|_{IH} &= e^{4\gamma}\,\frac{(\Delta m^2_{\text{atm}})^{3/2}}{4v^6} M_1M_2(M_1+M_2)\Big[(\sin 2\theta\cos 2\theta_{12} - \cos\phi_1\cos 2\theta\sin 2\theta_{12})\times \\
&\quad \left(\sin^2 2\theta_{23} + (4+\cos 4\theta_{23})\sin\phi_1\sin 2\theta_{12}\right) + \mathcal{O}(\epsilon)\Big], \\
\left|\frac{\Delta_{CP}}{g(M_1,M_2)}\right|_{NH} &= e^{4\gamma}\,\frac{(\Delta m^2_{\text{atm}})^{3/2}}{4v^6} M_1M_2(M_1+M_2)\left[\frac{\sqrt{r}}{2}\sin 4\theta_{23}c_{12}\cos(\phi_1-2\theta)\right. \\
&\quad + r\Big(\sin^2 2\theta_{23}\left[c_{12}^2\sin 2(\phi_1-\theta) + (2+\cos 2\theta_{12})\sin 2\theta\right] - 2\Big) \\
&\quad \left. + \sqrt{r}\,\theta_{13}\,s_{12}(1+\cos^2 2\theta_{23})\cos(\delta+\phi_1-2\theta) + \mathcal{O}(\epsilon^2)\right],
\end{aligned} \tag{4.11}$$

where in the case of NH we have included NLO corrections because the LO cancel for maximal atmospheric mixing. We see that for both neutrino orderings, it depends strongly on the real part of the Casas-Ibarra angle θ, which does not affect any other of the observables above. In particular, independently of the value of ϕ_1, there is always a value of

JHEP08(2016)157

θ that can make the asymmetry vanish. For instance for the IH result the value can be approximated by

$$\text{IH}: \quad \tan 2\theta \simeq \cos\phi_1 \tan 2\theta_{12}, \tag{4.12}$$

therefore the uncertainty in θ forbids to set a lower bound on the asymmetry, although an upper bound can be derived. Therefore even if the sterile states would be discovered at SHiP and their mixings to electrons and muons accurately measured, the asymmetry can only be predicted up to this angle.

Furthermore as we have seen in order to explain the baryon asymmetry in the $N = 2$ case, a significant level of degeneracy between the two states is needed. The dependence on this quantity enters in the function $g(M_1, M_2)$. Although we have not found a detailed study of the expected uncertainty in the invariant mass at SHiP, given the momentum resolution for muons and pions quoted in [41], we expect that this uncertainty could be better than 1%. If the degeneracy cannot be measured, a large uncertainty in the CP asymmetry will result also from this unknown.

Interestingly neutrinoless double beta decay also depends on both unknowns: θ and ΔM_{12}. The effective neutrino mass in neutrinoless double beta is given approximately by [42, 43]

$$\begin{aligned} |m_{\beta\beta}|_{IH} \simeq \sqrt{\Delta m^2_{\rm atm}} \Bigg| & c_{13}^2 \left(c_{12}^2 + e^{2i\phi_1} s_{12}^2 \left(1 + \frac{r^2}{2}\right)\right) \\ & - f(A)\, e^{2i\theta} e^{2\gamma} (c_{12} - i e^{i\phi_1} s_{12})^2 (1 - 2 e^{i\delta} s_{23}\theta_{13}) \frac{(0.9\,\text{GeV})^2}{4M_1^2} \left(1 - \left(\frac{M_1}{M_1 + \Delta M_{12}}\right)^2\right)\Bigg|, \end{aligned} \tag{4.13}$$

$$\begin{aligned} |m_{\beta\beta}|_{NH} \simeq \sqrt{\Delta m^2_{\rm atm}} \Bigg| & e^{2i\phi_1} c_{13}^2 s_{12}^2 r + e^{-2i\delta} s_{13}^2 \\ & - f(A)\, e^{2i\theta} e^{2\gamma} s_{12} \left(r s_{12} e^{2i\phi_1} - 2i\sqrt{r}\theta_{13} e^{-i\delta}\right) \frac{(0.9\,\text{GeV})^2}{4M_1^2} \left(1 - \left(\frac{M_1}{M_1 + \Delta M_{12}}\right)^2\right)\Bigg|, \end{aligned} \tag{4.14}$$

where the two lines in each amplitude correspond respectively to the light and heavy contributions. $f(A)$ depends on the nucleus under consideration. For ^{48}Ca, ^{76}Ge, ^{82}Se, ^{130}Te and ^{136}Xe, $f(A) \approx 0.035$, 0.028, 0.028, 0.033 and 0.032, respectively [44, 45]. Since $f(A)$ is very small we have neglected $\mathcal{O}(\epsilon^2)$ effects in the heavy contribution.

Note that the non-standard contribution from the heavy states is very sensitive to the mass degeneracy. Furthermore the interference between the light and heavy contributions is very sensitive to the angle θ, and it is precisely in the region around 1 GeV where the heavy and light contributions can be comparable, and can effectively interfere [43, 46, 47]. There is therefore the possibility that neutrinoless double beta decay could provide the missing information to predict the baryon asymmetry.

On the left plot of figure 8 we show $|m_{\beta\beta}|$ as a function of the angle θ for IH and some choice of parameters that are within the range of SHiP and assumed known. $|m_{\beta\beta}|$ has been computed exactly using the nuclear matrix elements for ^{76}Ge from ref. [44].The bands are the standard 3ν contributions to $|m_{\beta\beta}|$ for NH/IH. If the uncertainty in $|m_{\beta\beta}|$ could be better than the spread within the standard IH region, a determination of θ could result from this measurement. On the right plot we show the dependence of Y_B (computed

JHEP08(2016)157

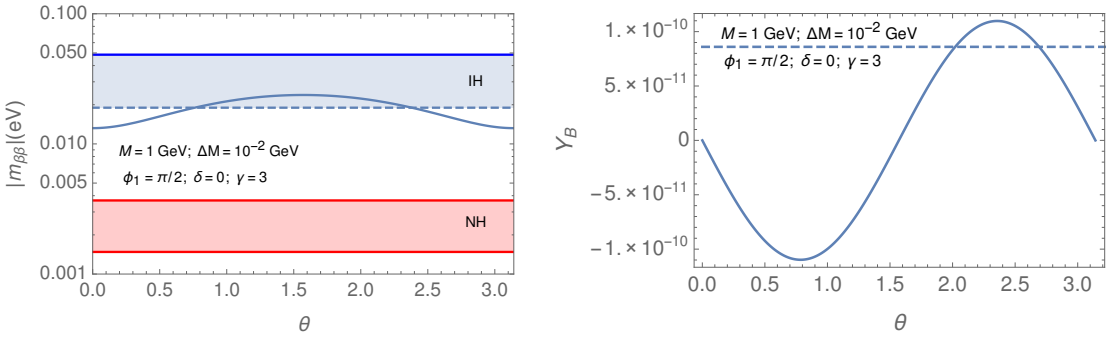

Figure 8. Left: dependence of $m_{\beta\beta}$ on θ for IH and $M_1 = 1\text{GeV}, \Delta M_{12} = 10^{-2}\,\text{GeV}$, $\phi_1 = \frac{\pi}{2}$, $\delta = 0$ and $\gamma = 3$. The red band is the standard 3ν expectation for NH and the blue one that for the IH. The dashed line would be the standard 3ν contribution for the chosen value of ϕ_1. Right: Y_B versus θ for the same parameters. The dashed line is the experimental value of Y_B.

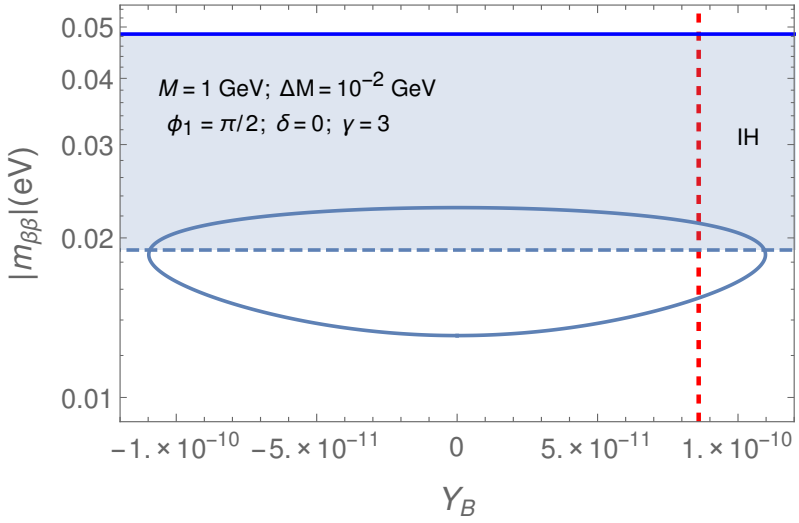

Figure 9. Correlation of $|m_{\beta\beta}|$ and Y_B when the parameters that could in principle be measured at SHiP are fixed and the neutrino ordering is inverted. The band is the standard 3ν expectation. The vertical dashed line is the measured Y_B, and the horizontal one corresponds to the 3ν expectation for $\phi_1 = \frac{\pi}{2}$.

exactly) on the same angle. In figure 9 we show the correlation between $|m_{\beta\beta}|$ and Y_B as we vary θ. Ideally a precise determination of $|m_{\beta\beta}|$ could predict the baryon asymmetry up to a global sign. In practice, this would require a very good control of the nuclear matrix elements which is very challenging.

As a proof of principle we have studied the posterior probabilities for a hypothetical measurement of SHiP of M_1 and M_2 and their respective couplings to electrons and muons for IH. The point chosen is indicated by a star in figure 4. We did not look for a very special nor optimal point, simply that it was within the range of SHiP and could explain the baryon asymmetry. The corresponding triangle plots are shown in figure 10 for two values of the

JHEP08(2016)157

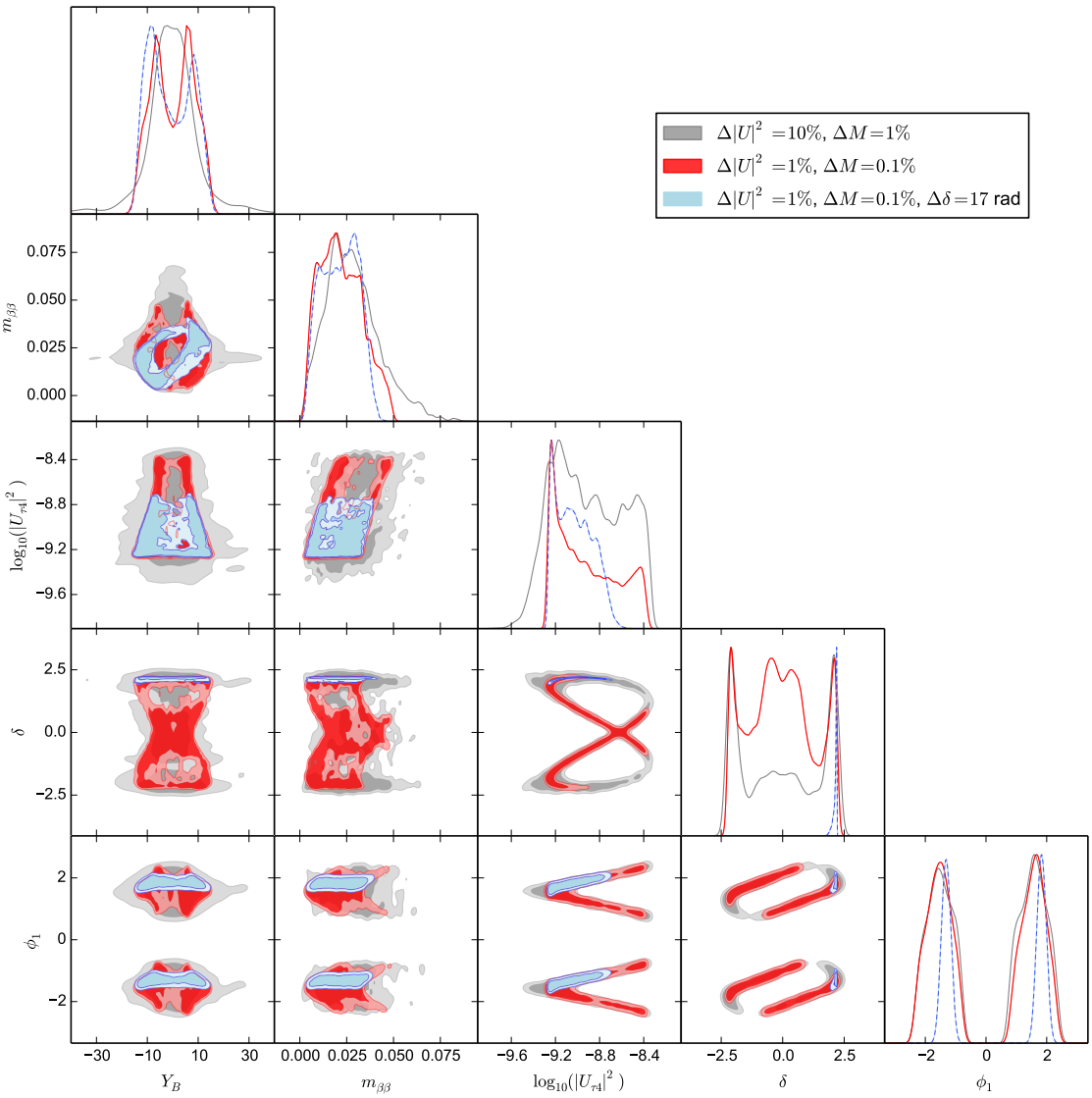

Figure 10. Triangle plot with 1D posterior probabilities and 2D 68% and 90% probability contours in the $N = 2$ scenario for IH, assuming a putative measurement of SHiP of the two masses M_1, M_2 and their mixings to electrons and muons. We assume uncertainties of $1\%, 10\%$ for the masses and mixings in the grey contours and $0.1\%, 1\%$ in the red ones. An additional posterior probability in light blue is shown for a combination of SHiP and a measurement of the phase δ in DUNE or HyperK. The parameters shown are the observables Y_B, $|m_{\beta\beta}|$, $|U_{\tau 4}|^2$, δ and ϕ_1.

assumed errors in this experiment: relative errors on masses and mixings of $(1\%, 10\%)$ and the much more optimistic $(0.1\%, 1\%)$. We furthermore considered a combination of SHiP, with the more optimistic errors, with a determination of δ in future neutrino oscillation experiments such as HyperK and DUNE. We have assumed $\sigma_\delta \simeq 10^\circ$ as derived from the studies in references [48, 49]. The $|m_{\beta\beta}|$ versus Y_B plot is zoomed in in figure 11.

Clearly the determination of δ results in a more clear correlation between $|m_{\beta\beta}|$ and Y_B. In fact the resulting width of the contour can be understood from the propagation of

JHEP08(2016)157

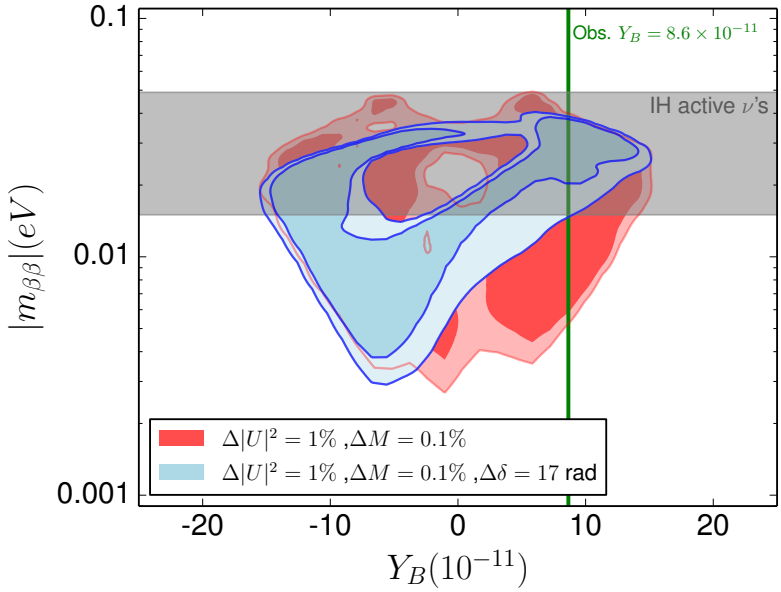

Figure 11. Posterior probabilities in the $|m_{\beta\beta}|$ vs Y_B plane from a putative measurement at SHiP, assuming $0.1\%, 1\%$ uncertainties in the masses and mixings (red) or the latter with an additional measurement of δ in DUNE and HyperK (blue). The grey band is the standard 3ν expectation.

the error in δ on the determination of ϕ_1. This is shown in figure 12, where we compare the posterior probability with the three curves obtained in the following way: 1) fixing the parameters to those of the test point and changing only θ (solid line), 2) the same as 1) except δ which is fixed to $\delta_{\rm test} - \sigma_\delta$, and correspondingly ϕ_1, γ tuned to keep the mixings unchanged. There are two solutions for ϕ_1 and the two dashed lines correspond to the two values (see figure 13), according to the analytical approximate formulae. The region encompassed by these lines is roughly similar to the 68% and 90% regions.

For NH, the expectations are much more pessimistic, since the SHiP measurement would have a hard time to pin down ϕ_1, even if δ is known, and therefore two unknowns ϕ_1, θ would remain. They could be determined in principle from a measurement of Y_B and $|m_{\beta\beta}|$ but not from one single measurement and therefore the baryon asymmetry will be very difficult to predict in this case. The measurement of $|m_{\beta\beta}|$ for NH would nevertheless be futuristic since the value would be roughly a factor 10 smaller, which is beyond the reach of the next generation of neutrinoless double beta decay experiments.

5 $U_{\rm PMNS}$ phases from SHiP and neutrinoless double beta decay

We have seen that the ratios of electron and muon mixings that could be measured at SHiP could give very interesting information of the phases of the PMNS matrix. We stress that this is independent of whether the baryon asymmetry can be explained or not. This relies on the fact that the mixings are large enough so that they can be discovered at SHiP. In this case, the ratio of the electron to muon mixings are dominantly controlled by the phases of the PMNS mixing matrix, as can be seen in eqs. (4.7) and (4.8).

JHEP08(2016)157

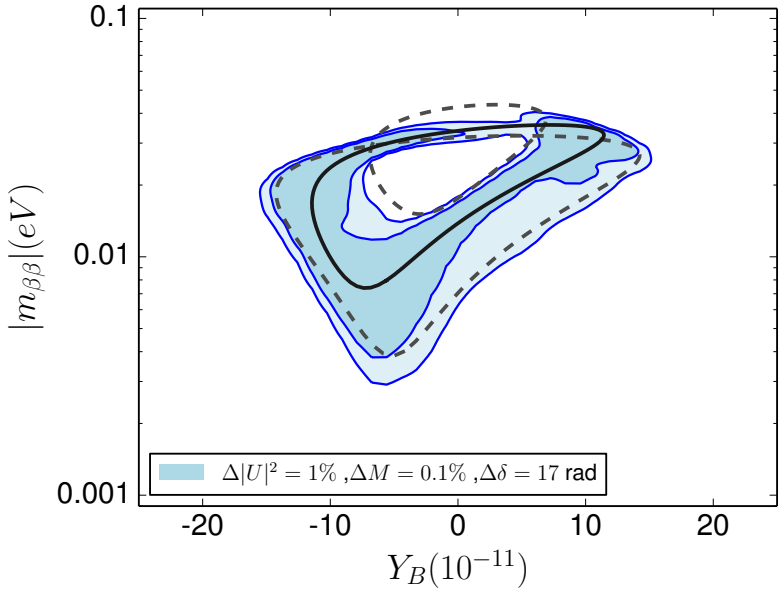

Figure 12. Posterior probabilities in the $|m_{\beta\beta}|$ vs Y_B plane from a putative measurement at SHiP, assuming $0.1\%, 1\%$ uncertainty and an additional measurement of δ in DUNE and HyperK, together with the contours obtained by changing θ and every other parameter fixed to the test point values (solid line) or with $\delta = \delta_{\rm test} - \sigma_\delta$ and ϕ_1, γ in each case tuned to keep $|U_{e4}|^2$, $|U_{\mu 4}|^2$ fixed. There are two solutions for ϕ_1 and these correspond to the two dashed lines.

In figure 13, we compare the correlation expected on the (ϕ_1, δ) plane from a putative measurement of this ratio using the analytical formulae of eqs. (4.7) for the test point of the previous section, to the posterior probabilities obtained with the most competitive SHiP uncertainties assumed in the previous section. Clearly the analytical formulae work very well and demonstrate the potential of SHiP in constraining the CP violating phases of the mixing matrix.

This has the following interesting consequence. If neutrinoless double beta decay could be measured with sufficient precision and the effect of the unknown θ would be small (this would happen for example in a more degenerate situation or for larger heavy masses which suppress the heavy contribution to neutrinoless double beta decay), the combination of this measurement with that at SHiP could provide information on the phase δ. Quantifying what is the reach of the combination of SHiP and neutrinoless double beta decay on δ is very interesting and deserves a dedicated study.

Reversely, if a measurement of δ could be obtained from neutrino oscillation measurements, a putative measurement of SHiP could provide a more precise prediction of the neutrinoless double beta decay amplitude if the neutrino ordering is inverted. This would be an extra motivation for improving the nuclear matrix element determination.

The possibility of measuring also the tau mixing at SHiP could help to resolve the degeneracy. Figure 14 shows the isocurves of $|U_{e4}|^2/|U_{\mu 4}|^2$ and $|U_{e4}|^2/|U_{\tau 4}|^2$ in the (ϕ_1, δ) plane. The test point we used did not have sensitivity to the tau mixing according to the expectations for SHiP, but if this measurement could be improved this would also be useful to reduce the (δ, ϕ_1) degeneracy.

JHEP08(2016)157

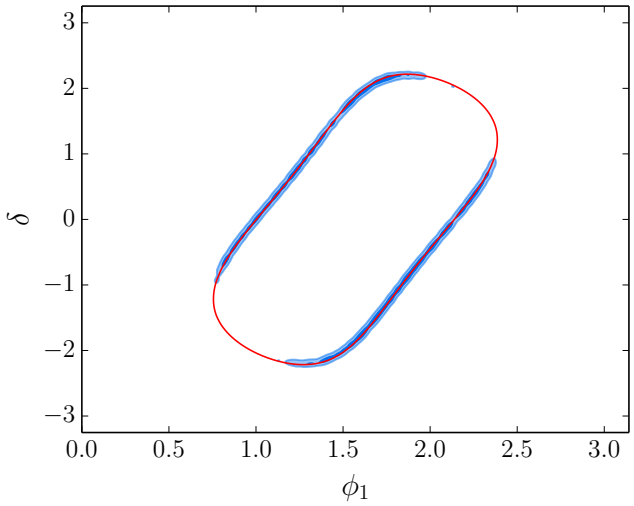

Figure 13. Posterior probabilities from a SHiP measurement of the masses and mixings with e, μ on the plane (ϕ_1, δ) compared with the result of the analytical ratio (red line) derived from eqs. (4.7) for parameters in the test point.

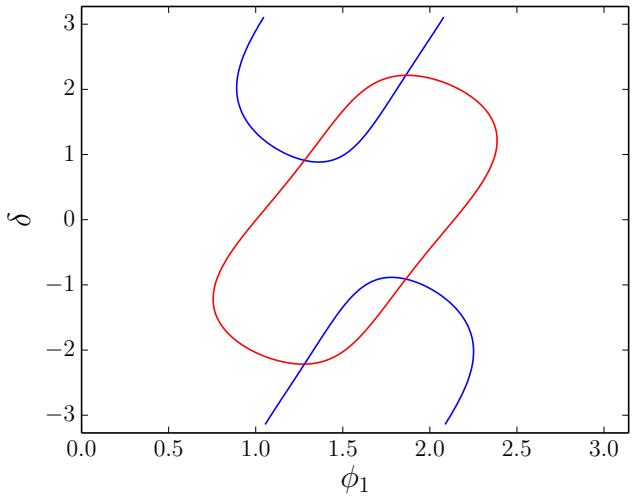

Figure 14. Isocurves for the ratios $|U_{e4}|^2/|U_{\mu 4}|^2$ (red) and $|U_{e4}|^2/|U_{\tau 4}|^2$ (blue) derived from eqs. (4.7).

6 Conclusions

We have studied the production of the matter-antimatter asymmetry in low-scale $\mathcal{O}$(GeV) seesaw models. We have improved our previous study [15] by including the washout processes from gauge interactions and Higgs decays and inverse decays, quantum statistics in the computation of all rates, as well as spectator processes. This together with a more efficient numerical treatment of the equations have allowed us to perform the first bayesian exploration of the full parameter space that explains the observed baryon asymmetry in the context of the minimal model, where only two singlets play a role in the generation of the baryon asymmetry.

JHEP08(2016)157

We have demonstrated that successful baryogenesis is possible with a mild heavy neutrino degeneracy, and more interestingly that these less fine-tuned solutions prefer smaller masses $M_i \leq 1\text{GeV}$, which is the target region of SHiP, and significant non-standard contributions to neutrinoless double beta decay. We have also demonstrated the complementarity of future putative measurements from SHiP, neutrinoless double beta decay and searches for leptonic CP violation in neutrino oscillations, in the quantitative prediction of the baryon asymmetry within the minimal model. If singlets with masses in the GeV range would be discovered in SHiP and the neutrino ordering is inverted, the possibility to predict the baryon asymmetry (maybe up to a sign) looks in principle viable, in contrast with previous beliefs. Unrelated to whether the baryon asymmetry is explained or not, we have also shown that a measurement of the electron and muon mixings of heavy species within SHiP range could precisely determine, in the minimal model, a combination of the two phases of the U_{PMNS} matrix.

Acknowledgments

We warmly thank N. Rius for useful discussions and earlier collaboration. This work was partially supported by grants FPA2014-57816-P, PROMETEOII/2014/050, and the European projects H2020-MSCA-ITN-2015//674896-ELUSIVES and H2020-MSCA-RISE-2015. PH acknowledges the support of the Munich Institute for Astro- and Particle Physics (MIAPP) of the DFG cluster of excellence Origin and Structure of the Universe to participate in the workshop *Why is there more matter than antimatter in the Universe*, where this work was first presented prior to publication [50].

Open Access. This article is distributed under the terms of the Creative Commons Attribution License (CC-BY 4.0), which permits any use, distribution and reproduction in any medium, provided the original author(s) and source are credited.

References

[1] M. Fukugita and T. Yanagida, *Baryogenesis Without Grand Unification*, *Phys. Lett.* **B 174** (1986) 45 [INSPIRE].

[2] S. Davidson and A. Ibarra, *A Lower bound on the right-handed neutrino mass from leptogenesis*, *Phys. Lett.* **B 535** (2002) 25 [hep-ph/0202239] [INSPIRE].

[3] T. Hambye, Y. Lin, A. Notari, M. Papucci and A. Strumia, *Constraints on neutrino masses from leptogenesis models*, *Nucl. Phys.* **B 695** (2004) 169 [hep-ph/0312203] [INSPIRE].

[4] J. Racker, M. Pena and N. Rius, *Leptogenesis with small violation of B-L*, *JCAP* **07** (2012) 030 [arXiv:1205.1948] [INSPIRE].

[5] A. Pilaftsis and T.E.J. Underwood, *Resonant leptogenesis*, *Nucl. Phys.* **B 692** (2004) 303 [hep-ph/0309342] [INSPIRE].

[6] S. Davidson, E. Nardi and Y. Nir, *Leptogenesis*, *Phys. Rept.* **466** (2008) 105 [arXiv:0802.2962] [INSPIRE].

[7] E.K. Akhmedov, V.A. Rubakov and A.Yu. Smirnov, *Baryogenesis via neutrino oscillations*, *Phys. Rev. Lett.* **81** (1998) 1359 [hep-ph/9803255] [INSPIRE].

JHEP08(2016)157

[8] T. Asaka and M. Shaposhnikov, *The nuMSM, dark matter and baryon asymmetry of the universe*, *Phys. Lett.* **B 620** (2005) 17 [hep-ph/0505013] [INSPIRE].

[9] M. Shaposhnikov, *The nuMSM, leptonic asymmetries and properties of singlet fermions*, *JHEP* **08** (2008) 008 [arXiv:0804.4542] [INSPIRE].

[10] T. Asaka, S. Eijima and H. Ishida, *Kinetic Equations for Baryogenesis via Sterile Neutrino Oscillation*, *JCAP* **02** (2012) 021 [arXiv:1112.5565] [INSPIRE].

[11] L. Canetti, M. Drewes, T. Frossard and M. Shaposhnikov, *Dark Matter, Baryogenesis and Neutrino Oscillations from Right Handed Neutrinos*, *Phys. Rev.* **D 87** (2013) 093006 [arXiv:1208.4607] [INSPIRE].

[12] M. Drewes and B. Garbrecht, *Leptogenesis from a GeV Seesaw without Mass Degeneracy*, *JHEP* **03** (2013) 096 [arXiv:1206.5537] [INSPIRE].

[13] B. Shuve and I. Yavin, *Baryogenesis through Neutrino Oscillations: A Unified Perspective*, *Phys. Rev.* **D 89** (2014) 075014 [arXiv:1401.2459] [INSPIRE].

[14] A. Abada, G. Arcadi, V. Domcke and M. Lucente, *Lepton number violation as a key to low-scale leptogenesis*, *JCAP* **11** (2015) 041 [arXiv:1507.06215] [INSPIRE].

[15] P. Hernández, M. Kekic, J. López-Pavón, J. Racker and N. Rius, *Leptogenesis in GeV scale seesaw models*, *JHEP* **10** (2015) 067 [arXiv:1508.03676] [INSPIRE].

[16] A. Anisimov, D. Besak and D. Bödeker, *Thermal production of relativistic Majorana neutrinos: Strong enhancement by multiple soft scattering*, *JCAP* **03** (2011) 042 [arXiv:1012.3784] [INSPIRE].

[17] D. Besak and D. Bödeker, *Thermal production of ultrarelativistic right-handed neutrinos: Complete leading-order results*, *JCAP* **03** (2012) 029 [arXiv:1202.1288] [INSPIRE].

[18] I. Ghisoiu and M. Laine, *Right-handed neutrino production rate at $T > 160$ GeV*, *JCAP* **12** (2014) 032 [arXiv:1411.1765] [INSPIRE].

[19] J.A. Casas and A. Ibarra, *Oscillating neutrinos and $\mu \to e\gamma$*, *Nucl. Phys.* **B 618** (2001) 171 [hep-ph/0103065] [INSPIRE].

[20] G. Sigl and G. Raffelt, *General kinetic description of relativistic mixed neutrinos*, *Nucl. Phys.* **B 406** (1993) 423 [INSPIRE].

[21] E. Nardi, Y. Nir, E. Roulet and J. Racker, *The Importance of flavor in leptogenesis*, *JHEP* **01** (2006) 164 [hep-ph/0601084] [INSPIRE].

[22] Planck collaboration, P.A.R. Ade et al., *Planck 2015 results. XIII. Cosmological parameters*, arXiv:1502.01589 [INSPIRE].

[23] J.A. Harvey and M.S. Turner, *Cosmological baryon and lepton number in the presence of electroweak fermion number violation*, *Phys. Rev.* **D 42** (1990) 3344 [INSPIRE].

[24] M. Laine and M.E. Shaposhnikov, *A Remark on sphaleron erasure of baryon asymmetry*, *Phys. Rev.* **D 61** (2000) 117302 [hep-ph/9911473] [INSPIRE].

[25] C.A. Argüelles Delgado, J. Salvado and C.N. Weaver, *A Simple Quantum Integro-Differential Solver (SQuIDS)*, *Comput. Phys. Commun.* **196** (2015) 569 [arXiv:1412.3832] [INSPIRE].

[26] https://github.com/jsalvado/SQuIDS.

JHEP08(2016)157

[27] F. Feroz and M. Hobson, *Multimodal nested sampling: an efficient and robust alternative to MCMC methods for astronomical data analysis*, *Mon. Not. Roy. Astron. Soc.* **384** (2008) 449 [arXiv:0704.3704] [INSPIRE].

[28] F. Feroz, M. Hobson and M. Bridges, *MultiNest: an efficient and robust Bayesian inference tool for cosmology and particle physics*, *Mon. Not. Roy. Astron. Soc.* **398** (2009) 1601 [arXiv:0809.3437] [INSPIRE].

[29] F. Feroz, M.P. Hobson, E. Cameron and A.N. Pettitt, *Importance Nested Sampling and the MultiNest Algorithm*, arXiv:1306.2144 [INSPIRE].

[30] https://github.com/cmbant/getdist.

[31] M.C. Gonzalez-Garcia, M. Maltoni and T. Schwetz, *Updated fit to three neutrino mixing: status of leptonic CP-violation*, *JHEP* **11** (2014) 052 [arXiv:1409.5439] [INSPIRE].

[32] L. Canetti and M. Shaposhnikov, *Baryon Asymmetry of the Universe in the NuMSM*, *JCAP* **09** (2010) 001 [arXiv:1006.0133] [INSPIRE].

[33] A. Atre, T. Han, S. Pascoli and B. Zhang, *The Search for Heavy Majorana Neutrinos*, *JHEP* **05** (2009) 030 [arXiv:0901.3589] [INSPIRE].

[34] F.F. Deppisch, P.S. Bhupal Dev and A. Pilaftsis, *Neutrinos and Collider Physics*, *New J. Phys.* **17** (2015) 075019 [arXiv:1502.06541] [INSPIRE].

[35] LBNE collaboration, C. Adams et al., *The Long-Baseline Neutrino Experiment: Exploring Fundamental Symmetries of the Universe*, arXiv:1307.7335 [INSPIRE].

[36] S. Alekhin et al., *A facility to Search for Hidden Particles at the CERN SPS: the SHiP physics case*, arXiv:1504.04855 [INSPIRE].

[37] FCC-EE STUDY TEAM collaboration, A. Blondel, E. Graverini, N. Serra and M. Shaposhnikov, *Search for Heavy Right Handed Neutrinos at the FCC-ee*, in proceedings of the *37th International Conference on High Energy Physics (ICHEP 2014)* (2016) [arXiv:1411.5230] [INSPIRE].

[38] A.D. Dolgov, S.H. Hansen, G. Raffelt and D.V. Semikoz, *Heavy sterile neutrinos: Bounds from big bang nucleosynthesis and SN1987A*, *Nucl. Phys.* **B 590** (2000) 562 [hep-ph/0008138] [INSPIRE].

[39] O. Ruchayskiy and A. Ivashko, *Restrictions on the lifetime of sterile neutrinos from primordial nucleosynthesis*, *JCAP* **10** (2012) 014 [arXiv:1202.2841] [INSPIRE].

[40] S. Antusch, E. Cazzato and O. Fischer, *Displaced vertex searches for sterile neutrinos at future lepton colliders*, arXiv:1604.02420 [INSPIRE].

[41] SHIP collaboration, M. Anelli et al., *A facility to Search for Hidden Particles (SHiP) at the CERN SPS*, arXiv:1504.04956 [INSPIRE].

[42] A. Ibarra, E. Molinaro and S.T. Petcov, *Low Energy Signatures of the TeV Scale See-Saw Mechanism*, *Phys. Rev.* **D 84** (2011) 013005 [arXiv:1103.6217] [INSPIRE].

[43] J. López-Pavón, E. Molinaro and S.T. Petcov, *Radiative Corrections to Light Neutrino Masses in Low Scale Type I Seesaw Scenarios and Neutrinoless Double Beta Decay*, *JHEP* **11** (2015) 030 [arXiv:1506.05296] [INSPIRE].

[44] M. Blennow, E. Fernandez-Martinez, J. López-Pavón and J. Menendez, *Neutrinoless double beta decay in seesaw models*, *JHEP* **07** (2010) 096 [arXiv:1005.3240] [INSPIRE].

JHEP08(2016)157

[45] A. Ibarra, E. Molinaro and S.T. Petcov, *TeV Scale See-Saw Mechanisms of Neutrino Mass Generation, the Majorana Nature of the Heavy Singlet Neutrinos and $(\beta\beta)_{0\nu}$-Decay*, *JHEP* **09** (2010) 108 [arXiv:1007.2378] [INSPIRE].

[46] M. Mitra, G. Senjanović and F. Vissani, *Neutrinoless Double Beta Decay and Heavy Sterile Neutrinos*, *Nucl. Phys.* **B 856** (2012) 26 [arXiv:1108.0004] [INSPIRE].

[47] J. López-Pavón, S. Pascoli and C.-f. Wong, *Can heavy neutrinos dominate neutrinoless double beta decay?*, *Phys. Rev.* **D 87** (2013) 093007 [arXiv:1209.5342] [INSPIRE].

[48] DUNE collaboration, R. Acciarri et al., *Long-Baseline Neutrino Facility (LBNF) and Deep Underground Neutrino Experiment (DUNE)*, arXiv:1512.06148 [INSPIRE].

[49] HYPER-KAMIOKANDE PROTO-COLLABORATION collaboration, K. Abe et al., *Physics potential of a long-baseline neutrino oscillation experiment using a J-PARC neutrino beam and Hyper-Kamiokande*, *PTEP* **2015** (2015) 053C02 [arXiv:1502.05199] [INSPIRE].

[50] https://users.ph.tum.de/ga24wax/2016_W3_slides/Hernandez_slides.pdf.

JHEP08(2016)157